

**SERI/TP-211-3643
UC Category: 270
DE90000318**

**Annual Report
Photovoltaic Program Branch
FY 1989**

K. A. Summers, Editor

March 1990

Prepared under Task No. PV940101

Solar Energy Research Institute

A Division of Midwest Research Institute

1617 Cole Boulevard
Golden, Colorado 80401-3393

Prepared for the
U.S. Department of Energy
Contract No. DE-AC02-83CH10093

NOTICE

This report was prepared as an account of work sponsored by an agency of the United States government. Neither the United States government nor any agency thereof, nor any of their employees, makes any warranty, express or implied, or assumes any legal liability or responsibility for the accuracy, completeness, or usefulness of any information, apparatus, product, or process disclosed, or represents that its use would not infringe privately owned rights. Reference herein to any specific commercial product, process, or service by trade name, trademark, manufacturer, or otherwise does not necessarily constitute or imply its endorsement, recommendation, or favoring by the United States government or any agency thereof. The views and opinions of authors expressed herein do not necessarily state or reflect those of the United States government or any agency thereof.

Printed in the United States of America
Available from:
National Technical Information Service
U.S. Department of Commerce
5285 Port Royal Road
Springfield, VA 22161

Price: Microfiche A01
Printed Copy A 3

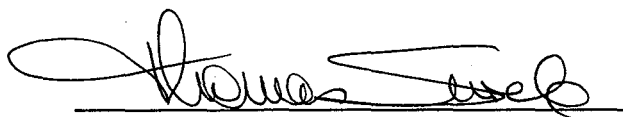
Codes are used for pricing all publications. The code is determined by the number of pages in the publication. Information pertaining to the pricing codes can be found in the current issue of the following publications which are generally available in most libraries: *Energy Research Abstracts (ERA)*; *Government Reports Announcements and Index (GRA and I)*; *Scientific and Technical Abstract Reports (STAR)*; and publication NTIS-PR-360 available from NTIS at the above address.

PREFACE

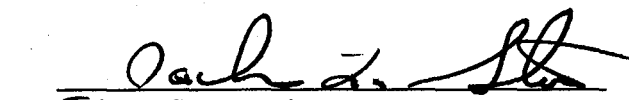
This report summarizes the progress of the Photovoltaic (PV) Program Branch of the Solar Energy Research Institute (SERI) from October 1, 1988, through September 30, 1989. The branch is responsible for the management of the subcontracted portion of SERI's PV Advanced Research and Development Project. In fiscal year (FY) 1989, this included nearly 50 subcontracts with a total annualized funding of approximately \$13.1 million. Approximately two-thirds of the subcontracts were with universities, at a total funding of nearly \$4 million. The six technical sections of the report cover the main areas of the subcontracted program: Amorphous Silicon Research Project, Polycrystalline Thin Films, Crystalline Silicon Materials Research, High-Efficiency Concepts, New Ideas Program, and University Participation Program. Technical summaries of each of the subcontracted programs provide a discussion of approaches, major accomplishments in FY 1989, and future research directions.

Approved for

SOLAR ENERGY RESEARCH INSTITUTE



Thomas Surek, Manager
Photovoltaic Program Branch


Jack L. Stone, Director
Solar Electric Research Division

Notice: This publication was reproduced from camera-ready copy submitted by the individual subcontractors.

SUMMARY

The Photovoltaics (PV) Program Branch of the Solar Energy Research Institute (SERI) is responsible for managing the subcontracted portion of SERI's Photovoltaic Advanced Research and Development (PV AR&D) Project. In fiscal year (FY) 1989, this included nearly 50 subcontracts, with a total annualized funding of \$13.1 million. Research was conducted in the following task areas: the Amorphous Silicon Research Project (ASRP), Polycrystalline Thin Films, Crystalline Silicon Materials Research, High-Efficiency Concepts, the New Ideas Program, and University Participation Program. Major program redirections in FY 1989 involved the issuance of competitive solicitations in five of the six task areas, while subcontracts under the sixth area (Crystalline Silicon) involved second-year funding on a FY 1988 solicitation. With the exception of the University Participation Program, awards on these solicitations were planned with FY 1990 funds.

Amorphous Silicon Research Project (ASRP)

The objectives of the research in amorphous silicon are to improve and to understand the optoelectronic properties of amorphous-silicon-based alloy materials and to improve the conversion efficiency and stability of single-junction and multijunction solar cells and submodules. The research is directed toward achieving FY 1990 goals, which are 10% efficiency area for single-junction and 13% efficiency for multijunction submodules of 900 cm² area.

The technical plan of the ASRP is divided into two principal activities: (1) multidisciplinary research activities and (2) fundamental research activities. Multidisciplinary activities involve government/industry cost-shared programs made up of broad-based research teams, located at individual companies' facilities, performing directed research that covers starting materials to demonstrations of proof-of-concept cells and submodules. Fundamental research activities involve basic, higher-risk, and supporting research at universities and research laboratories that aids industry in advancing the technology base. Cost-shared multidisciplinary programs address issues concerning single-junction and multijunction cells. Research is also performed to advance the conversion efficiency and the stability of small-area cells and of larger submodules, with areas of at least 900 cm², fabricated plasma-enhanced chemical vapor deposition. Stability issues encompass both intrinsic aspects, such as light-induced effects, and extrinsic aspects, diffusion or corrosion as a result of the environment. Efficiency improvement involves work on better light trapping, higher conductivity of interconnectors, and minimizing area losses due to interconnections.

Polycrystalline Thin Films

The objective of the Polycrystalline Thin Films Program is to develop thin-film, flat-plate modules that meet the Department of Energy's (DOE's) long-term goals of reasonable efficiencies (15%-20%), very low cost (near \$50/m²), and long-term reliability (30 yr). The approach relies on developing solar cells based on highly light-absorbing compound semiconductors such as CuInSe₂ and CdTe and their alloys. These semiconductors are fabricated as thin films (1-3 μm thick) with minimal material and processing costs.

Polycrystalline devices require continued development to achieve 15%-20% conversion efficiencies. Two strategies are being used: development of single-junction cells and an innovative effort on two-junction cascade cells. Improvement of the single-junction technologies has been steady and reliable. This strategy remains the major focus of the task. Potentially achievable module efficiencies exceed 15% at costs under \$50/m².

Developing scalable, low-cost fabrication methods is important in providing industry with a foundation for future large-area, high-throughput commercial processes. Within the SERI program, methods for fabricating polycrystalline cells include, for CuInSe₂, an electrochemical/selenization method, a reactive-sputtering and hybrid sputtering/evaporation method, and evaporation; for CdTe, close-spaced sublimation evaporation, electrodeposition, metal-organic chemical vapor deposition, and spraying.

Crystalline Silicon Materials Research

The emphasis of the SERI Silicon Materials Research Program is to develop a coordinated effort between Industry, University, and SERI to study basic mechanisms pertaining to kinetics of defects and synergistic effects related to defect-impurity interactions. Of particular interest is to identify the effects of post-growth processing on photovoltaic properties of low-cost silicon and methods for passivation of electrically active defects in silicon.

Although solar cells fabricated on low-cost silicon substrates have already demonstrated efficiencies exceeding 15%, the technology to commercially produce cells of such high efficiency on low-cost substrates does not exist. Some of the reasons for lack of such a technology are related to inadequate understanding of the role of high concentrations of defects and impurities on cell performance. Furthermore, it is not well understood how characteristics of silicon, containing defects/impurities, change under various thermal processes, thereby making it difficult to design cell fabrication processes which can ameliorate the deleterious effects of defects/impurities.

High-Efficiency Concepts

The objective of the High-Efficiency Concepts Task is to evaluate and develop advanced PV technologies capable of energy conversion efficiencies in excess of 20% for flat-plate configurations and 30% for concentrator systems. Because of the demonstrated performance of crystalline III-V semiconductors, the task has become synonymous with III-V compound semiconductor research.

SERI's program of research in High-Efficiency Concepts has approached the terrestrial photovoltaic goals from the direction of first demonstrating the feasibility of exceeding these efficiency targets to assure that production engineering trade-offs between performance and cost can be accommodated. Recent advancements by the community researching high-efficiency technologies provide a high level of confidence that the efficiency goals can readily be met.

Research supported by this program benefits future development efforts by strengthening the understanding of basic mechanisms that affect uniformity of doping, composition, and

thickness over large area wafers, from wafer to wafer and from run to run. Efficient utilization of source materials and evaluation of potentially superior sources (cost, purity, control, safety, and other factors) are also important topics for research. Continued improvement in cell efficiency is also a critical factor in reaching cost-effectiveness for the technology.

The basic issues that form the focus of research supported under this program have been summarized. Technology for deposition of III-V compound semiconductors by potentially low-cost processes which provide excellent uniformity, purity, and crystallographic quality is clearly the key factor for achieving the near-term PV program goals from the high efficiency path. Research on characterization of materials and cells; analysis of loss mechanisms in cells; demonstration of improved cell designs; and improvements in the monitoring, control, and safety of the processes also contribute greatly to the technology base.

New Ideas Program

The objective of the New Ideas Program is to identify new PV materials, device configurations, and concepts, and to conduct preliminary research and development in the areas that show the most promise. Subcontracted research in this task that shows significant potential is transferred into the appropriate major task area within the DOE PV Program for continued support.

The New Ideas Program provides public solicitations for new and innovative research ideas that are relevant under the PV AR&D guidelines to perform high-risk, long-term, and potentially high-payoff research and development. These solicitations for new and innovative research ideas are submitted by universities, businesses, and non-profit organizations. Subcontracts are awarded to study the most promising concepts associated with these solicitations. These subcontracts are reviewed, and successful concepts are selected for renewal with a second year of funding.

University Participation Program

The objective of this program is to maximize the contribution of universities to the future of PV technology by focusing on the traditional needs and strengths of that community. Thus, it provides a forum in which the university researchers identify research topics critical to the advancement of PV technology with minimal influence from the current programmatic interests.

The selected participants are then permitted to pursue the proposed basic and applied research ideas in an environment designed to foster creativity by limiting requirements for delivery of reports, samples, and achievement of specific goals. Reporting is limited to annual reports and journal publications. Research symposia organized by the participants are held periodically and are open to all students, program participants, and outside researchers. The intent of the initiative is to provide continuity of funding over a minimum three-year period which will allow universities to build and to support interdisciplinary teams with specialized expertise which can be applied to furthering the

technology base of PV. Such a program is expected to attract the most highly qualified university research teams to the DOE National PV Program. The University Participation Program also supports the PV industry through technology transfer which occurs not only by publication of research results in the technical literature, but also through enhanced student awareness of PV technology and education of future professionals.

Technology Transfer

The prompt and effective transfer of research results is a key element in the PV Program Branch's overall strategy. In addition to close working relationships with industrial and academic communities through subcontracts, such as the unique government/industry partnership in amorphous silicon, the primary means of information transfer are through subcontractor reports and review meetings. These reports are made available to the entire PV community, and the review meetings are open to all relevant outside interests as well as to subcontractors. Frequent discussions with university and industry researchers and utility planners assist task managers in assessing future research needs and directions. During FY 1989, over 470 researchers participated in various review meetings, conferences, and workshops organized or co-organized by the PV Program Branch. The participants included subcontractors, SERI in-house researchers, invited individuals from outside the program (including the international PV community), and PV Program Branch personnel. The meetings were: (1) the 9th PV AR&D Project Review; (2) the Amorphous Silicon Review; (3) the Polycrystalline Thin Films Review; (4) the High Efficiency Concepts Workshop; and (5) the PV Module Performance and Reliability Workshop. These meetings are just an example of the extensive SERI cooperation with DOE, other laboratories, the private sector, and international groups to foster enhanced opportunities for further development of PV science and technology. Other significant examples include participating in Sandia's Crystalline PV Technology Review, hosting the Interagency Power Group Meeting, and supporting numerous professional societies and meetings. With DOE and Sandia, we also participated in visits to several utilities to discuss their potential interest in PV technology.

TABLE OF CONTENTS

		<u>Page</u>
1.0	Introduction	1
1.1	Background	1
1.2	Key Accomplishments	3
1.2.1	Amorphous Silicon	3
1.2.2	Polycrystalline Thin Films	5
1.2.3	Crystalline Silicon Materials Research	6
1.2.4	High-Efficiency Concepts	6
1.2.5	New Ideas	7
1.2.6	University Participation	7
1.3	Technology Transfer	8
1.4	Conclusions	9
2.0	Amorphous Silicon Research Project	10
	Research on Amorphous Silicon-Based Thin Film Photovoltaic Devices; <i>ARCO Solar, Inc.</i>	12
	Research on Stable High-Efficiency Large-Area Amorphous Silicon-Based Submodules; <i>Chronar Corporation</i>	18
	Research on High-Efficiency, Multiple-Gap, Multijunction Amorphous Silicon-Based Alloy Thin Film Solar Cells; <i>Energy Conversion Devices, Inc.</i>	23
	Research on the Material Properties of Device Quality Amorphous Silicon Deposited at High Deposition Rates Using Higher Order Silanes; <i>Glasstech Solar, Inc.</i>	26
	Characterization and Comparison of Optically Transparent and Conducting Films; <i>Harvard University</i>	29
	Structural and Electronic Studies of a-SiGe:H Alloys; <i>Harvard University</i>	32
	Photochemical Vapor Deposition of Amorphous Silicon Alloy Materials and Devices; <i>Institute of Energy Conversion, University of Delaware</i>	35
	Amorphous Silicon Deposition Research with In Situ Diagnostics; <i>Jet Propulsion Laboratory</i>	41
	Diagnostics of Glow Discharges Used to Produce Hydrogenated Amorphous Silicon Films; <i>National Institute of Standards and Technology</i>	47

TABLE OF CONTENTS (continued)

		<u>Page</u>
	Research on Stable, High-Efficiency, Large-Area, Amorphous Silicon Based Submodules; <i>Solarex Thin Film Division</i>	50
	Studies on the Relative Effects of Charged and Neutral Defects in Hydrogenated Amorphous Silicon; <i>University of North Carolina</i> . .	56
	Investigations of the Origins of Light-Induced Changes in Hydrogenated Amorphous Silicon; <i>University of Oregon</i>	60
	Structure of Amorphous Silicon Alloy Films; <i>Washington University</i>	64
	Research on the Structural and Electronic Properties of Amorphous Silicon Alloys; <i>Xerox PARC</i>	70
3.0	Polycrystalline Thin Films	76
	Polycrystalline Thin Film Cadmium Telluride Solar Cells; <i>Ametek Applied Materials Laboratory</i>	78
	High-Efficiency CuInSe ₂ and CuInGaSe ₂ Based Cells and Materials Research; <i>Boeing Aerospace and Electronics</i>	81
	Investigations of CuInSe ₂ Thin Films and Contacts; <i>California Institute of Technology</i>	85
	Analysis of Loss Mechanisms in Polycrystalline Thin Film Solar Cells; <i>Colorado State University</i>	93
	High-Efficiency Cadmium and Zinc Telluride Based Thin Film Solar Cells; <i>Georgia Institute of Technology</i>	98
	Fundamentals of Polycrystalline Thin Film Materials and Devices; <i>Institute of Energy Conversion</i>	104
	High Efficiency CuInSe ₂ and CuInSe ₂ -Alloy Cells; <i>International Solar Electric Technology</i>	110
	High-Efficiency, Large-Area CdTe Panels; <i>Photon Energy, Inc.</i>	115
	Novel Thin Film CuInSe ₂ Fabrication; <i>University of Arkansas</i>	121
	Alternative Fabrication Techniques for High-Efficiency CuInSe ₂ and CuInSe ₂ -Alloy Films and Cells; <i>University of Illinois</i>	128

TABLE OF CONTENTS (continued)

		<u>Page</u>
	Thin Film Cadmium Telluride, Zinc Telluride, and Mercury Zinc Telluride Solar Cells; <i>University of South Florida</i>	133
4.0	Crystalline Silicon Materials Research	136
	Basic Studies of Point Defects and Their Influence on Solar Cell Related Electronic Properties of Crystalline Silicon; <i>Duke University</i>	137
	Impurity and Defect Characterization in Silicon; <i>Georgia Institute of Technology</i>	143
	Passivation and Gettering Studies in Solar Cell Silicon; <i>The University at Albany</i>	147
	The Effectiveness and Stability of Impurity/Defect Interaction and Their Impact on Minority Carrier Time; <i>North Carolina State University</i>	159
5.0	High-Efficiency Concepts	164
	High-Efficiency, Thin-Film GaAs and Ternary III-V Solar Cells; <i>Kopin Corporation</i>	165
	Basic Studies of III-V High-Efficiency Cell Components; <i>Purdue University</i>	170
	Research on Semiconductors for High-Efficiency Solar Cells; <i>Rensselaer Polytechnic Institute</i>	176
	Gallium Arsenide Based Ternary Compounds and Multibandgap Solar Cell Research; <i>Spire Corporation</i>	180
	Advanced High-Efficiency Concentrator Cells; <i>Varian Research Center</i>	185
6.0	New Ideas Program	190
	The Avalanche Heterostructure and Superlattice Solar Cells; <i>Georgia Tech Research Institute</i>	191
	Low-Cost Technique for Producing CdZnTe Devices for Cascade Cell Application; <i>International Solar Electric Technology</i>	198
	Hydrogen Radical Enhanced Growth of Solar Cells; <i>Rensselaer Polytechnic Institute</i>	201

TABLE OF CONTENTS (continued)

		<u>Page</u>
7.0	University Participation Program	204
	Rapid Liquid Phase Epitaxy; <i>Brown University</i>	205
	Improvement of Bulk and Epitaxial III-V Semiconductors for Solar Cells by Creation by Creation of Denuded Recombination Zones; <i>Carnegie-Mellon University</i>	211
	New Approaches for High-Efficiency Solar Cells: Role of Strained Layer Superlattices; <i>North Carolina State University</i>	217
	Fundamental Studies of Defect Generation in Amorphous Silicon Alloys Grown by Remote Plasma-Enhanced Chemical-Vapor Deposition (Remote PECVD); <i>North Carolina State University</i>	223
	Ion-Assisted Deposition Doping of p-CdTe; <i>Stanford University</i>	229
	Defects and Photocarrier Processes in Hydrogenated Amorphous Silicon Alloys; <i>Syracuse University</i>	233
	Low Temperature MOCVD Processes for High Efficiency Solar Cells; <i>University of Southern California</i>	239
	Electronic Processes in Thin Film PV Materials; <i>University of Utah</i>	245
8.0	List of Active Subcontracts	251
9.0	Photovoltaic Program Branch FY 1989 Bibliography	257
	Subcontractor Reports and Publications	257
	Photovoltaic Program Branch Reports and Publications	267

1.0 INTRODUCTION

This report reviews subcontracted research and development activities under SERI's Photovoltaic Advanced Research and Development (PV AR&D) Project from October 1, 1988, to September 30, 1989.

1.1 Background

The PV AR&D Project, under the U.S. Department of Energy's (DOE) National Photovoltaics (PV) Program, sponsors high-risk, potentially high-payoff research and development in photovoltaic energy technology. The aim is to provide a technology base from which the private sector can choose options for further development and competitive application in U.S. electrical markets. The Solar Energy Research Institute (SERI) project is responsible for most of the materials research and some of the module research performed under the National PV Program. Implementation of this program is based on cooperative research partnerships among the federal government, private industries, universities, and electric utilities, as outlined in the Program's "Five-Year Research Plan."

SERI's specific PV activities include the management of subcontracted R&D projects as well as internal research. The primary research activities are conducted in advanced photovoltaic material technologies, including amorphous silicon thin-film materials; polycrystalline thin films, such as copper indium diselenide, cadmium telluride, and their alloys; and high-efficiency crystalline cells, including silicon and gallium arsenide and their alloys. Transferring the R&D results to private industry in a timely and effective manner is a major objective of SERI's PV AR&D Project.

Subcontracted R&D is a significant part of the PV AR&D Project; more than 50% of the project's budget is allocated yearly to subcontracts. In fiscal year (FY) 1989, this included nearly 50 subcontracts with a total annualized funding of approximately \$13.1 million. Cost-sharing by industry subcontractors added over \$6 million to the subcontracted research program. Approximately two-thirds of the subcontracts were with universities, with a total funding of nearly \$4 million. In addition to the materials research activities listed above, subcontracted research is conducted under both the New Ideas and the University Participation programs. Table 1-1 shows how the subcontract budget is distributed among the various task areas for FY 1989 and prior years. Figure 1-1 shows the distribution of subcontract funds by business category. Management of the subcontracted PV program is the responsibility of the Photovoltaic (PV) Program Branch. Table 1-2 identifies branch personnel according to their respective task areas.

This report summarizes the R&D activities of the subcontracted PV program. The research is described under the following headings: Amorphous Silicon Research Project (Section 2.0), Polycrystalline Thin Films (Section 3.0), Crystalline Silicon Materials Research (Section 4.0), High-Efficiency Concepts (Section 5.0), New Ideas Program (Section 6.0), and University Participation Program (Section 7.0). The reports in each section are preceded by a brief overview of the task objectives and approaches as well as some of the key developments of FY 1989. The overviews are followed by technical summaries of each of the subcontracted efforts in FY 1989. These sections were provided by the subcontractors themselves or were derived from various project reports submitted by the subcontractors. Section 8.0 provides a list of active subcontracts in FY 1989, and a list of major subcontractor reports is given in Section 9.0.

Table 1-1. SERI Photovoltaic Program Branch Subcontract Budget History*

Task Area	FY 1978-FY 1987 (\$M)	FY 1988 (\$M)	FY 1989 (\$M)
Amorphous Silicon Thin Films	52.5	6.7	7.7
Polycrystalline Thin Films	34.9	2.2	3.7
High-Efficiency Concepts (III-V)	27.6	3.0	2.0
Crystalline Silicon	21.5	0.6	0.6
New Ideas	17.5 ^b	0.1	0.4
University Participation Program	3.5	1.3	0.9
Total	157.5	12.2	15.3

Includes approximately 15% for program management, fees, etc.

^bIncludes \$9 million for photoelectrochemical cell research.

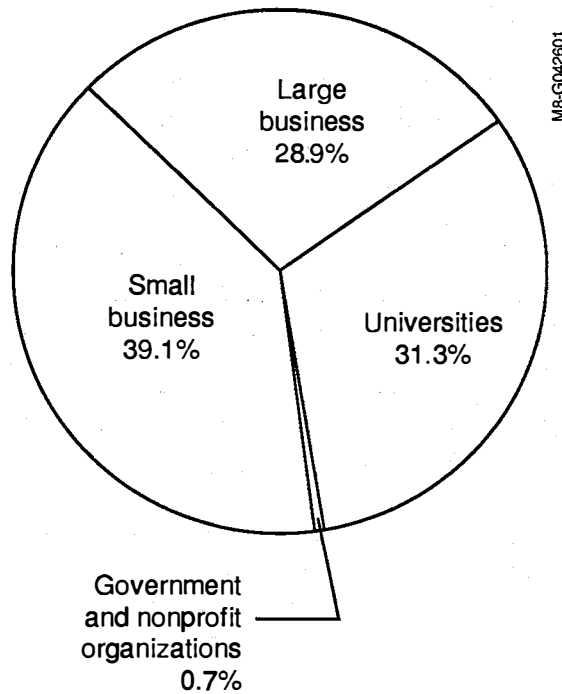


Figure 1-1. Distribution of FY 1989 subcontract funds by business category

Table 1-2. SERI PV Program Branch Personnel

Task Area	Contact Name	Telephone*
PV Program Branch	Thomas Surek, Manager	231-1371
	Kathy Summers, Admin. Assist.	231-1395
	Thomas S. Basso	231-7035
Amorphous Silicon Research Project	William Wallace	(202) 586-7307
	Werner Luft, Acting Manager	231-1823
	Byron Stafford	231-7126
High-Efficiency Concepts, Crystalline Silicon Materials, and University Program	John Benner, Manager	231-1396
	Cecile Leboeuf	231-1066
	Bhushan Sopori	231-1383
Polycrystalline Thin Films	Kenneth Zweibel, Manager	231-7141
	Richard Mitchell	231-1379
	Harin Ullal	231-1841
New Ideas Program	Richard Mitchell, Manager	231-1379

*Area code (303); FTS number 327-xxxx.

1.2 Key Accomplishments

1.2.1 Amorphous Silicon Research Project

Four companies were awarded contracts in 1987 under the second government/industry 50% cost-shared partnership for amorphous silicon research: namely, ARCO Solar, Chronar Corporation, Energy Conversion Devices, Inc., and Solarex Corporation. The primary goal of this three-year, nearly \$36 million program (cost shared 50% by the industrial partners) is to achieve 10% efficiency for single-junction and 13% for multijunction submodules having an area of about 900 cm². The key accomplishments during the third year of that joint program are described below.

Upon completion of the current three-year program (in the FY 1990 time frame), research priorities will be devoted to all-amorphous silicon, two-terminal multijunction cells and modules. For that purpose, a new three-year Government/Industry Partnership Program will be started in the February - March 1990 time frame with funding from the FY 1990 budget. The principal objectives of this research are: 1) to conduct research on semiconductor materials and non-semiconductor materials to enhance two-terminal, multijunction, thin-film, large-area, all-amorphous-silicon-alloy device performance, 2) to develop high-efficiency, *stable*, *reproducible*, and *low-cost* multijunction PV modules (of at least 900 cm² in area) based on all-amorphous materials; 3) to demonstrate in FY 1993 stable 12% (AM 1.5) aperture-area solar conversion efficiency for different-bandgap modules; and 4) to demonstrate in FY 1993 stable 10% (AM 1.5) aperture-area solar conversion efficiency for same-bandgap modules.

- o _ ARCO Solar achieved aperture-area efficiencies for amorphous silicon modules with white back reflectors of 9.4% for 844 cm² and 8.4% for 3,970 cm². For semitransparent amorphous silicon modules without the current gain due to the back reflected light, the corresponding efficiencies are 9.1% and 7.6%, respectively. Stand-alone CIS modules achieved 11.2% and 9.1% efficiency over 938 cm² and 3,970 cm² areas, respectively. Preliminary demonstration of 1 x 4-ft, size four-terminal tandem modules with an air gap separating the two module circuits gave a 10.5% aperture-area efficiency. Chronar has fabricated 1.1 m² single-junction amorphous silicon modules with 4.4% efficiency, as verified by SERI.
- o _ In addition to the government/industry program, progress has been made in the fundamental research on amorphous silicon. Glasstech Solar, Inc. has produced single-junction, 1 cm² cells of 9.7% efficiency in which the intrinsic layer was deposited at a rate of 2-nm/s from disilane. Solarex has fabricated single-junction and triple-junction submodules with aperture-area (>900 cm²) efficiencies of 9.1% and 7.0%, respectively.
- o _ A. Gallagher of the National Institute for Standards and Technology has found the surface reaction probability in silane, disilane, and silane/germanium discharge deposition to be in the range of 0.3 to 0.4. These results have led to the recognition that the key film-quality growth characteristic is the radical surface diffusion before incorporation in the film, combined with preferential incorporation in atomic-scale valleys.
- o _ The Jet Propulsion Laboratory has deposited a-C:H and a-SiC:H films by electron cyclotron resonance microwave plasma chemical vapor deposition. The ECR-deposited a-SiC:H films have a slightly higher optical bandgap than RF-deposited films. The deposition rate as a function of hydrogen dilution demonstrates that hydrogen etching plays an important role in a-SiC:H film deposition by ECR (CVD).
- o _ R. Gordon of Harvard University has developed fluorine-doped zinc oxide produced by atmospheric pressure CVD. The highest electrical conductivity (1200 S/cm) and light transmission were found for films containing 0.5 atomic percent fluorine deposited at 450°C.
- o _ David Cohen, University of Oregon, unambiguously confirmed that there is a significant deleterious role of carbon impurities in amorphous silicon films. Samples were prepared with a modulated carbon profile and then characterized by drive-level capacitance profiling in the annealed and light-soaked states.
- o _ Excellent agreement has been obtained on multijunction cell efficiency measurements between SERI, Energy Conversion Devices, and Solarex. While the measurement techniques and equipment may vary, agreement within 3% has been achieved on the same multijunction cells measured at the three different locations.
- o _ Extensive studies¹ of amorphous germanium films deposited by plasma-enhanced CVD at Harvard University have confirmed that the optoelectronic properties are poor. It

appears the preparation conditions need to be adjusted to enhance surface bombardment during deposition.

- o Xerox developed a chemical equilibrium model for plasma-enhanced CVD of amorphous silicon films. Studies from the incorporation of arsenic and phosphorus impurities indicate that chemical reactions at the growth surface rather than kinetic reactions in the plasma determine the impurity incorporation.
- o Xerox demonstrated that the rate of defect creation is dependent on the thermal history of the amorphous silicon film and cannot be directly the result of the specific hydrogen bonding structure (e.g., dihydride).
- o The Institute of Energy Conversion at the University of Delaware demonstrated a bandgap-graded device with 40% quantum efficiency at 800 nm using a "front-loaded" SiGe alloy 40 nm thick. A device model incorporating spatially dependent mobilities was developed to analyze the performance of bandgap-graded devices.

1.2.2 Polycrystalline Thin Films

Significant progress has been made in FY 1989 in the subcontracted research in polycrystalline thin films. The key accomplishments in both CdTe and CuInSe₂ solar cells and modules are listed below:

- o SERI issued a competitive request for proposals (RFP) to develop CuInSe₂ and CdTe submodules in cost-shared programs with industry. The proposals are being evaluated for three-year contracts to begin in spring 1990. Multiple subcontracts are expected, with SERI's share to be about \$500K-\$1M annually for each.
- o ARCO Solar has fabricated a large-area, 4-ft² CuInSe₂ module with a power output of 33.75 W. The aperture area efficiency for this module is 8.47%, and it has a $I_{sc} = 2.46$ A, $V_{oc} = 23.035$ V, and $FF = 0.6$. SERI tested two of ARCO Solar's CuInSe₂ modules outdoors a full year under open-circuit and load conditions. Very minimal changes in module output (about 3%-4%) have been observed. This is the first such test conducted on CuInSe₂ by an independent research group and is very promising in terms of assuring the reliability of CuInSe₂. ARCO Solar has achieved an active area efficiency of 13.05% on a laboratory cell, which has been verified by SERI.
- o Photon Energy has fabricated large-area CdS/CdTe modules by a potentially low-cost spraying method. SERI has verified a module output of 6.1 W and efficiency of 7.3% (aperture area) on a near 1-ft², monolithically interconnected submodule consisting of 27 cells in series. A "live" 4-ft² prototype module has also been delivered to SERI, and a production line for manufacturing an annual megawatt of these panels is presently being debugged. Recent outdoor testing of CdTe submodules at SERI indicates no change in performance after four months of exposure to natural sunlight.
- o Continued progress has been made by Ametek in improving their single-junction, total-area efficiency to 11.2% for thin film n-i-p CdTe solar cells. The thin film CdTe is deposited by a potentially low-cost electrodeposition method. Unencapsulated n-i-p cells have been tested for over 4000 hours under 1-sun illumination and load at 70°C

with no degradation. Encapsulated prototype submodules have passed similar tests, including one in which they were submerged underwater for a week.

- o _ International Solar Electric Technology (ISET) has developed a proprietary process to solve an adhesion problem they have encountered at the Mo/CuInSe₂ interface. Peeling of the CuInSe₂ films has been identified as a technological barrier for selenized CuInSe₂ devices. ISET has submitted a patent covering their new process, which could be of general import to the entire CIS community.
- o _ University of Illinois achieved 8.1% for a CuInSe₂ cell made by a hybrid co-evaporation, co-sputtering approach. This innovative method combines the best aspects of these two physical vapor depositions and could have low-cost potential.

1.2.3 Crystalline Silicon Materials Research

SERI has actively worked with subcontractors in several research areas and facilitated interactions among subcontracts as well as with the industry. Development of a basic facility for optical processing and availability of SERI expertise for hydrogenation have led to formation of a nucleus for a collaborative program.

Major accomplishments of this program are:

- o _ Formation of hydrogen damage and associated defect structure has been identified. A back-side hydrogenation technique has been developed for defect passivation of solar cells.
- o _ Efficiency of dislocations as sinks for point defects has been determined for commercial low-cost silicon.
- o _ Diffusion of hydrogen in silicon has been modelled using experimental data.
- o _ Influence of dissolved oxygen on minority carrier lifetime in silicon was studied.
- o _ A technique for fabrication of optically reflecting low-resistivity ohmic contacts on silicon has been developed.

1.2.4 High-Efficiency Concepts

A solicitation entitled, "Fundamental Research in Materials and Structures for Ultra-High-Efficiency Solar Cells," was released in October 1989. The intent of this procurement was to focus the efforts of the High-Efficiency Concepts Program on the establishment of a fundamental understanding and background data needed for development of viable high-efficiency PV technologies for large-scale, cost-effective terrestrial application in the mid-1990s. Proposals addressed one or more of the following topics: growth of III-V compounds and alloys; solar cell design, fabrication and evaluation; evaluation of new growth techniques and operating regimes; evaluation of new materials; and evaluation of characterization techniques. Awards will be made in April 1990.

- o _ Researchers at Purdue University have established the importance of bandgap narrowing in heavily doped, p-type GaAs and its implications for heterojunction device design. This result is important to the entire III-V PV research community, and helps device designers to predict the behavior of heavily doped films. In another effort by Purdue in collaboration with Spire Corporation, a record efficiency was achieved (23.8%) in GaAs solar cells grown by molecular beam epitaxy.
- o _ The efficiency of monolithic multijunction GaAs-based cells exceeded that of single-junction cells for the first time this year. Varian Associates achieved a record efficiency (27.6%) in a two-terminal, monolithic, multijunction cell (AlGaAs/GaAs) measured under one-sun illumination, beating the single-junction record (24.8%) held by Spire Corporation.
- o _ Researchers at Kopin Corporation achieved a record efficiency of 21.5% in a 4-cm², thin-film GaAs solar cell, up from a previous record of 20.7% last year.

1.2.5 New Ideas Program

- o _ A competitive solicitation for Letters of Interest (LOI) was issued in FY 1988 to over 800 interested research facilities. These included Universities, industries, and nonprofit organizations. We received 92 responding LOIs for the Phase I evaluation under this solicitation. The evaluation of these seven-page proposals identified 24 proposals that were in the competitive range. Those organizations were issued an RFP at the end of FY 1988. The proposals received in response to this RFP will be evaluated during FY 1989, and multiple subcontracts will be awarded, with research starting in FY 1990.
- o _ Researchers at ISET achieved Cu doping of ZnTe deposited by the two-step electrodeposition process with repeatable resistivities of 0.1 to 1.0 ohm-cm. These Cu-doped films have a high optical transmission which is required for use as a transparent back contact in the top cell of four-terminal devices.
- o _ Stanford University fabricated a record efficiency of 22.3% (8.252 aperture-area, AM 1.5, one-sun illumination, SERI-measured). This cell had a high resistivity base, and a textured front with a lightly doped, phosphorous-diffused emitter.

1.2.6 University Participation Program

This year, a competitive procurement was held in the University Participation Program for PV research, resulting in four new awards. Awardees and their principal investigators are:

- o _ North Carolina State University, S. Bedair and N. El-Masry
- o _ North Carolina State University, G. Lucovsky
- o _ University of Utah, P.C. Taylor
- o _ Stanford University, R.H. Bube

In each case, research began immediately, and graduate students are already in place to initiate these new programs. Summer awards should significantly enhance the rate of progress relative to September awards because both principal investigators and students

have increased levels of effort during the summer to get each program off to an effective start.

- o_ Two of the programs which were previous awardees (1986) that were not successful in this solicitation were extended until mid-1990 to allow gradual phaseout and completion of doctoral degrees for students supported in this program.
- o_ Over 25 students supported by this program have completed their Ph.D. work since 1986. Several of these students have gone to work in the PV industry.

1.3 Technology Transfer

The prompt and effective transfer of research results is a key element in the PV Program Branch's overall strategy. In addition to close working relationships with industrial and academic communities through subcontracts, such as the unique government/industry partnership in amorphous silicon, the primary means of information transfer is through subcontractor reports and review meetings. These reports are made available to the entire PV community, and the review meetings are open to all relevant outside interests as well as to subcontractors. During FY 1989, over 40 subcontractor reports were widely distributed. Frequent discussions with university and industry researchers and utility planners assisted task managers in assessing future research needs and directions. Branch staff has made nearly 50 site visits to subcontractor facilities in FY 1989 to review research progress. The following is a list of some key FY 1989 accomplishments in the area of technology transfer.

- o_ Over 470 researchers participated in various review meetings, conferences, and workshops organized or co-organized by the PV Program branch. The participants included subcontractors, SERI in-house researchers, invited individuals from outside the program (including the international PV community), and PV Program Branch personnel. The meetings were: (1) the 9th PV AR&D Project Review; (2) the Amorphous Silicon Review; (3) the Polycrystalline Thin Films Review; (4) the High-Efficiency Concepts Workshop; and (5) the PV Module Performance and Reliability Workshop. These meetings are just an example of the extensive SERI cooperation with DOE, other laboratories, the private sector, and international groups to foster enhanced opportunities for further development of PV science and technology. Other significant examples include participating in Sandia's Crystalline PV Technology Review, hosting the Interagency Power Group Meeting, and supporting numerous professional societies and meetings.
- o_ PV Program branch staff organized a tour of the U.S. PV industry for DOE in November and December 1988. DOE, SERI, and Sandia National Laboratories participated in the tour, which included flat-plate crystalline silicon, flat-plate thin-film, and concentrator PV companies. A report of the tour, published in February 1989 by SERI, was widely distributed to decision makers in the public and private sectors. The findings from the tour will form the basis for potential new initiative in PV technology.
- o_ SERI subcontractors and in-house researchers participated in an assessment of the DOE National PV Program by DOE's Office of Energy Research, Office of Program Analysis during the August-to-December time frame. Of the 129 presentations given to

17 panels of expert reviewers, 90 were based on research supported by SERI's PV AR&D Project. Forty-nine of the presentations were by SERI subcontractors. The results of this review are being evaluated and will be used in FY 1990 program plans.

1.4 Conclusions

More than 50% of SERI's PV AR&D Project involves subcontracted research with industry, universities, and nonprofit laboratories. Significant technical advances were made in all areas of the subcontracted PV program during FY 1989. Research progress was assessed through site visits, task review meetings, and topical workshops. That progress is expected to continue during FY 1990, to help achieve the long-term goals of the DOE National PV Program.

2.0 AMORPHOUS SILICON RESEARCH PROJECT

Werner Luft (Acting Manager), Byron Stafford,
and William Wallace

The objectives of this research in amorphous silicon are to improve and understand the optoelectronic properties of amorphous-silicon-based alloy materials and to improve the conversion efficiency and stability of single-junction and multijunction solar cells and submodules. The research is directed toward achieving the FY 1990 goals, which are 10% efficiency for single-junction and 13% for multijunction submodules of 900-cm² area.

The technical plan of the Amorphous Silicon Research Project (ASRP) is divided into two principal activities: (1) multidisciplinary research and (2) fundamental research. The multidisciplinary research activities comprise the government/industry cost-shared programs that have broad-based research teams located at the facilities of the individual companies. These teams perform directed research that covers aspects from starting materials to demonstration of proof-of-concept cells and submodules. Fundamental research, on the other hand, involves basic, higher-risk, and supporting research at universities and research laboratories that aids industry by advancing the technology base. Cost-shared multidisciplinary programs address issues concerning single-junction and multijunction devices. Research is also performed to advance the conversion efficiency and the stability of both small-area cells and large (900-cm² and up) submodules fabricated by plasma-enhanced CVD. The stability encompasses both intrinsic aspects, such as the light-induced effect, and extrinsic aspects, such as diffusion or corrosion as a result of the environment. The efficiency improvement involves work on improving light trapping, achieving higher conductivity of interconnectors, and minimizing area losses due to interconnections.

After the successful completion of the first government/industry program conducted from FY 1984 through FY 1987, the best single-junction a-Si cells had efficiencies as high as 11.7% and single-junction a-Si submodules had efficiencies up to 7.9%.

A three-year government/industry program was started in FY 1987 with participation by ARCO Solar, Inc.; Chronar Corporation; Energy Conversion Devices, Inc.; and Solarex Corporation. Emphasis of this second program is placed on amorphous silicon multijunction technology, with the major goals being the achievement by 1990 of efficiencies of: (1) 18% for multijunction cells (1 cm²), (2) 13% for multijunction submodules (900 cm²), and (3) 10% for single-junction submodules (900 cm²). Stability criteria, namely less than 5% degradation after the equivalent exposure to 2 months of insolation, are associated with the efficiency goals. The status of this program, now in its third year, is as follows.

ARCO Solar has achieved SERI-measured, aperture-area efficiencies of 9.3% for a single-junction, amorphous silicon, 844 cm² submodule and 11.3% for an amorphous silicon/copper-indium-diselenide stacked, four-terminal, 900-cm², 55-cell submodule. The best a-Si/CIS 4-cm² tandem cell measured by ARCO Solar is 15.6%, whereas the best value measured by SERI on a different tandem cell is 14.5% (13.1%) measured at SERI and for a 4-ft² module 8.5% (aperture-area) efficiency. The highest CIS cell measured by ARCO is 14.1% in efficiency. For a 40-cm² submodule, Solarex achieved 9.5% (aperture area) efficiency for single-junction amorphous silicon and 8.5% (aperture-area) for triple-junction a-Si/a-Si/a-SiGe.

A new three-year Government/Industry Partnership Program will start in the February - March 1990 time frame with funding from the FY 1990 budget. The principal objectives of this research are: (1) to conduct research on semiconductor materials and non-semiconductor materials to enhance two-terminal, multijunction, thin-film, large-area, all-amorphous-silicon-alloy device performance; (2) to develop high-efficiency, *stable*, *reproducible*, and *low-cost* multijunction photovoltaic modules based on all-amorphous materials; (3) to demonstrate in FY 1993 stable 12% (AM 1.5) aperture-area solar conversion efficiency for different-bandgap modules; and (4) to demonstrate in FY 1993 stable 10% (AM 1.5) aperture-area solar conversion efficiency for same-bandgap modules. The modules will be at least 900 cm² in area and consist of at least two integrally stacked devices using all-amorphous-silicon-alloy materials.

In addition to the government/industry programs, fundamental research involves work on the light-induced effect, material deposition rates, alternative deposition methods, amorphous-silicon-based alloy materials, material and plasma characterization, and modeling. Summaries of these studies follow.

Title: Research on Amorphous Silicon-Based Thin Film Photovoltaic Devices

Organization: ARCO Solar, Inc., Camarillo, California

Contributors: K. W. Mitchell, principal investigator;
C. Eberspacher, D. Tanner, and D. Willett

Objective

The primary goal of this contract, which began July 1987, is to develop stable, 13% efficient multijunction thin film modules using thin film silicon:hydrogen alloy (TFS) for the high band gap circuit and a copper indium diselenide (CIS) device for the low band gap circuit. TFS and CIS were selected because they are the leading thin film materials at present and because they have a near-ideal band gap match of 1.7 eV and 1.0 eV, respectively. Modeling calculations indicate practical, achievable efficiencies in the range of 20% for this combination [1].

Approaches

The issues are divided into four major tasks: (1) the materials and device physics of TFS and CIS junctions; (2) process development for large area coating to achieve the requisite electronic quality thin films; (3) the optimization of device configuration and optical coupling for tandem modules; and (4) process development for module patterning and encapsulation. These are described in more detail below.

The purpose of the first task is to fabricate, analyze, and model test structures in order to improve device performance. For TFS junctions, where the device structure is glass/ZnO/*p*-Si:C:H/*i-n* Si:H/ZnO, areas of investigation are: (1) control of the front and back ZnO texture, thickness, and electro-optical properties; (2) investigation of the extrinsic doping and grading of the *p*-Si:C:H layer; and (3) optimization of the Si:H *i*-layer thickness and electronic quality. For the bottom CIS cell structure, ZnO/thin CdS/CuInSe₂/Mo/glass, the technical issues are short-circuit current (J_{sc}) or V_{oc} improvements. For example, work on ZnO properties for CIS extend beyond those described above for TFS to include minimizing free carrier optical absorption through improvements to the electron doping and transport properties. The CdS junction formation work emphasizes uniform deposition of thin CdS layers and the passivation of electronic shunts.

The uniformity of the CIS layer, which is important to the development of high efficiency devices, is addressed in the second task, large area thin film processing. Large area processing of the layers involves identification and control of the relevant process control parameters such as source material control and deposition and thermal uniformity. The characterization of defects due to substrate quality, process contamination, growth flaws, and non-uniformities is critical. Identification of those defects that reduce cell and module performance provides focus to efforts to eliminate or passivate these defects.

Maximizing tandem module performance requires optimization of device configuration and optical coupling between the TFS and CIS circuits. This has been

approached both experimentally and theoretically by varying the thicknesses of the TFS front and back ZnO and the TFS *i*-layer, and then measuring its resulting optical transmission and effect on the TFS-filtered CIS spectral response and short-circuit current. Models have been developed to describe the spectral response of semitransparent TFS, stand-alone CIS, and TFS-filtered CIS devices.

The fourth research task, process development for module patterning and encapsulation, focuses on laser and mechanical scribing techniques. A major research problem is the debris and layer damage introduced by laser processing. Alignment of sequential, reproducible, straight scribes over 128 cm length requires significant development. Close tolerances between scribes to minimize loss of active module area and reduction of the interconnect contact resistance are also necessary. Finally, process development of module encapsulation and edge sealing/framing compatible with the TFS and CIS submodule circuits to provide environmentally durable packaging is required. Indoor environmental chamber and outdoor exposure tests are carried out to support this activity.

In-house optical and scanning electron microscopy, Auger analysis, X-ray diffraction, electro-optical film and device characterization, and other analytic facilities are used to guide the above research efforts.

Progress

Work during Phase 1 (July 1987-August 1988) focused on developing the basic film deposition, junction formation, and patterning techniques necessary to fabricate high efficiency cells and submodules. Work during Phase 2 (September 1988-February 1990) focuses more specifically on exploring large area (4140 cm² = 32.2x128.6 cm) processing.

The individual TFS and CIS cell efficiencies have increased significantly (Table 1). A 3.9 cm², 10.8% efficient semitransparent TFS cell results from a high 17.1 mA/cm² J_{sc}. Without conventional metal back optical reflectors, this high current is achieved through increased light trapping using textured ZnO layers. For the CIS cell, the ZnO/thin CdS window layer promotes both a high 41 mA/cm² J_{sc} and a high 508 mV V_{oc}, resulting in a world record 14.1% CIS cell efficiency. An optimum grid electrode design will further improve efficiency to 14.9% by reducing front ZnO series resistance and improving fill factor from 0.68 to 0.72.

Results for nominal 1x1 ft and 1x4 ft TFS and CIS modules are summarized in Table 2. TFS modules with white back reflectors have achieved record aperture efficiencies of 9.4% for 844 cm² and 8.4% for 3970 cm². For semitransparent TFS modules without the current gain due to the back reflected light, the efficiencies are 9.1% and 7.6% for 843 and 3970 cm² areas. In parallel, improvements in stand-alone CIS module performance have been dramatic, achieving 11.2% and 9.1% efficiencies over 938 and 3916 cm² aperture areas respectively. The uniform performance of 1x4 ft CIS modules is demonstrated in Fig. 1, which shows the V_{oc} mapping of a 53-cell, 1x4 ft module cut into five segments. The individual cell V_{oc}'s vary only ±4% across a finished 3900 cm² submodule.

The 4-terminal tandem cell efficiency of 15.6% (Table 3) exceeds the Phase 1 goal of 14%. The 30x30 cm tandem module efficiency of 12.3% (Table 4) also exceeds the Phase 1 goal of 9.5% and is rapidly approaching the primary project goal of 13%. Preliminary demonstration of 1x4 ft size tandem modules with an air gap separating the two module circuits gives 41.4 watts or 10.5% aperture efficiency

over an aperture area of about 3900 cm² (Table 5).

Stability continues to be a significant performance factor for TFS. Long-term outdoor losses of 15-20% are not uncommon for prototype single junction devices. TFS submodules are susceptible to electrical shunting due to debris and contamination resulting from laser patterning, inadequate substrate cleanliness, and contamination from static charge and atmospheric particulates. The presence of these shunts not only reduces initial module performance but also increases performance degradation upon outdoor exposure. Both opaque modules with metal back electrodes and semitransparent modules with ZnO front and back electrodes exhibit a decrease in dark shunt resistance with outdoor exposure. After outdoor exposure, module power losses are large (up to 35%) for low initial shunt resistances compared to less than 15% power loss for less shunted modules [2].

Initial outdoor exposure testing of CIS laminated modules shows promising stability. Two CIS submodules, placed separately under open-circuit and resistive loads at the SERI outdoor PV test site, show little change over the 12-month initial period of testing [3]. For a 10.4%, 840 cm² tandem module, a 14% performance loss is observed after 19 months of outdoor exposure at ARCO Solar. All of this loss is attributable to the TFS circuit.

Discussion

Significant progress has been made in cell and submodule performance for both TFS and CIS thin film technologies. Transfer of cell results to large areas has been demonstrated. CIS progress in particular has been outstanding with the achievement of a 14.1% efficient cell and 11.2% efficient 938 cm² and 9.1% efficient 3916 cm² modules.

The next period will emphasize continued development and characterization of 3900 cm² aperture area tandem modules to demonstrate 13% efficiencies, development of environmentally durable packaging for these large area submodules, and performance improvements and characterization of test structures and 30x30 cm submodules. Recent publications are listed below [4-10].

References

1. Mitchell, K.W., "Detailed Modeling of Thin Film Polycrystalline and Thin Film Silicon:Hydrogen Alloy Multiple Junction Solar Cells," *Technical Digest of the International PVSEC-1*, Kobe, Japan, 1984, pp. 691-694.
2. Mitchell, K.W., "Perspectives on Thin Film Module Development," DOE/SERI Amorphous Silicon Subcontractors' Review Meeting, Golden, CO, June 19-20, 1989.
3. Private communication with Laxmi Mrig, Solar Energy Research Institute, Golden, CO (1989).
4. Ermer, J., C. Fredric, K. Pauls, D. Pier, K. Mitchell, C. Eberspacher, and K. Kushiya, "Recent Progress in Large Area CuInSe₂ Submodules," *Proc. 4th International Photovoltaic Science and Engineering Conf.*, Sydney, Australia, Feb. 14-17, 1989, pp. 475-480.
5. Mitchell, K., C. Eberspacher, J. Ermer, K. Pauls, D. Pier, and D. Tanner, "Single and Tandem Junction CuInSe₂ Technology," *Proc. 4th International Photovoltaic Science and Engineering Conf.*, Sydney, Australia, Feb. 14-17, 1989, pp. 889-896.
6. Mitchell, K., C. Eberspacher, and K. Pauls, "Status of CuInSe₂ Photovoltaic

Technology," International Symposium on Uses of Selenium and Tellurium, Banff, Alberta, Canada, May 8, 1989.

7. Mitchell, K.W., C. Eberspacher, J. Ermer, K. Pauls, D. Pier, and D. Tanner, "Progress on High Efficiency Thin Film Cells and Submodules," SERI 9th Photovoltaic Advanced Research and Development Project Review Meeting, Lakewood, CO, May 24-26, 1989, and for publication in *Solar Cells*.
8. Mitchell, K.W., C. Eberspacher, J. Ermer, K. Pauls, D. Pier, and D. Tanner, "High Efficiency Si:H/CuInSe₂ Thin Film Cells and Submodules," DOE/SERI Amorphous Silicon Subcontractors' Review Meeting, Golden, CO, June 19-20, 1989.
9. Mitchell, K.W., C. Eberspacher, J. Ermer, K. Pauls, and D. Pier, "Status of CuInSe₂ Cells and Submodules," *Proceedings of the Polycrystalline Thin Film Program Meeting*, Lakewood, CO, Aug. 16-18, 1989, SERI Technical Report SERI/CP-211-3550, pp. 199-205.
10. Mitchell, K.W., "Copper Indium Diselenide: Towards 20% Efficiency," *Commission of the European Communities 9th E.C. Photovoltaic Solar Energy Conf.*, Freiburg, Federal Republic of Germany, Sept. 25-29, 1989, pp. 292-293.

Table 1. TFS and CIS cell performance.†

	Eff. (%)	J _{sc} (mA/cm ²)	V _{oc} (mV)	FF
Semitransparent TFS	10.8	17.1	867	0.72
Stand-Alone CIS	14.1	41.0	508	0.68

Table 2. TFS and CIS module performance.†

	Power (W)	Area‡ (cm ²)	Eff. (%)	I _{sc} (mA)	V _{oc} (V)	FF
Back Reflector TFS	7.9	844	9.4	277	42.8	0.67
	33.2	3970	8.4	1140	47.3	0.61
Semitransparent TFS	7.7	843	9.1	262	43.5	0.68
	30.2	3970	7.6	1030	47.2	0.62
Stand-Alone CIS	10.5	938	11.2	641	25.5	0.64
	35.8	3916	9.1	2540	23.5	0.60

† Measured at ASTM air mass 1.5, global 100 mW/cm², 25°C. ‡ Aperture area.

Table 3. 4-terminal tandem cell performance.†

4 cm ² Cell	Eff. (%)	J _{sc} (mA/cm ²)	V _{oc} (mV)	FF
Semitransparent TFS	10.3	16.4	871	0.72
Filtered CIS	5.3	17.9	432	0.68
Tandem	15.6			
Stand-Alone CIS	12.4	41.2	455	0.66

Table 4. 4-terminal tandem submodule performance.†

30x30 cm Module	Power (W)	Area‡ (cm ²)	Eff. (%)	I _{sc} (mA)	V _{oc} (V)	FF
Semitransparent TFS	7.69	843	9.1	262	43.5	0.68
Filtered CIS	2.66	843	3.2	228	19.2	0.61
Tandem	10.35		12.3			
Stand-Alone CIS	7.62	844	9.0	611	21.2	0.59

Table 5. 4-terminal tandem submodule performance.†

32x128 cm Module	Power (W)	Area‡ (cm ²)	Eff. (%)	I _{sc} (mA)	V _{oc} (V)	FF
Semitransparent TFS	30.2	3970	7.6	1030	47.2	0.62
Filtered CIS	11.2	3883	2.9	810	20.8	0.59
Tandem	41.4		10.5			
Stand-Alone CIS	31.6	3883	8.1	2380	23.1	0.57

† Measured at ASTM air mass 1.5, global 100 mW/cm², 25°C. ‡ Aperture area.

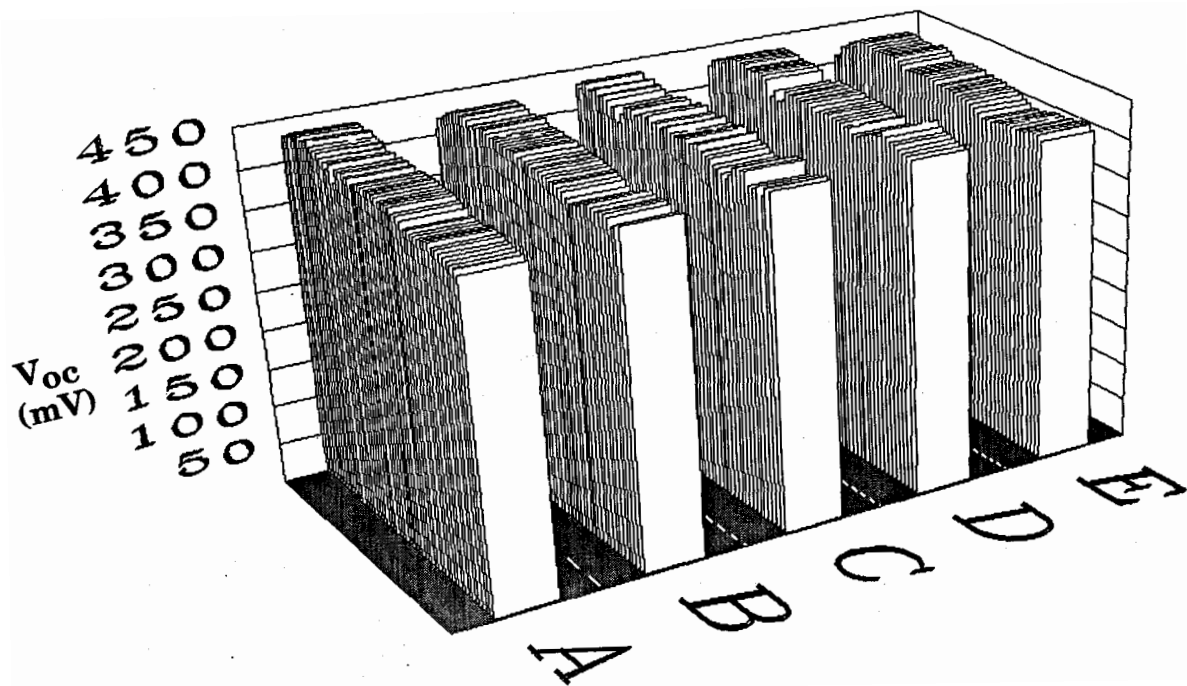


Fig. 1. V_{oc} map of 1x4 ft CIS module.

Title: Research on Stable, High Efficiency, Large Area, Amorphous Silicon Based Submodules

Organization: Chronar Corporation, Princeton, New Jersey 08542

Contributors: A.E. Delahoy, program manager and principal investigator; F.J. Kampas, principal investigator (until 5/89); F.B. Ellis, Jr., H. Schade, T. Tonon, and H.A. Weakliem

Objectives

The primary objective of this subcontract is to develop same bandgap amorphous silicon p-i-n/p-i-n tandem junction photovoltaic submodules ($\geq 900\text{cm}^2$) having an aperture area efficiency of at least 9%. A further objective is to demonstrate 8% tandem submodules that degrade by no more than 5% under standard light soaking conditions.

Approach

Chronar's approach to the attainment of these objectives is based on the following distinctive technologies: a) in-house deposition of $\text{SiO}_2/\text{SnO}_2$ by APCVD onto soda lime glass to provide the substrate for subsequent a-Si:H deposition, b) single chamber r.f. glow discharge deposition of the a-Si:H p-i-n layers with the discharge confined to an inner "box carrier" that holds the substrates, c) laser scribing of the three films (SnO_2 , a-Si:H, Al) with real-time scribe tracking to minimize area losses. We further consider it important to examine the consequences of using an alternative transparent conductor, and have selected ZnO for this purpose.

Results

Continued optimization of the a-Si:H component of tandem cells resulted in the achievement of 8.7% conversion efficiency for a 1 cm^2 cell. The J-V curve for this cell is shown in Fig. 1. The cell featured carbon-graded p-layers, a 100 \AA TiO_x interstack recombination layer to improve the fill factor [1-3], and a modified transitional i-layer in the second stack [1,2].

The i-layer of fully fabricated p-i-n structures was studied by two techniques, namely current collection in thick p-i-n devices, and current deep level transient spectroscopy (DLTS) in standard devices. In the first technique, photocurrent-voltage data taken on a p-i-n device with a $10\text{ }\mu\text{m}$ i-layer and a semitransparent Ti contact allowed the determination of both electron and hole mobility-lifetime products in a very direct fashion [4]. It was also observed that the current-voltage curve under uniformly absorbed light was almost identical to that obtained for electron transport alone, and very different from that obtained for hole transport. This demonstrates that for two carrier transport in a-Si:H, the carrier with the longer drift length determines the photocurrent.

Using current DLTS, based on short-circuit current transients after repetitive excitation of p-i-n devices by light, we observed in all samples low and high temperature peaks at about 130K and 320K [5]. The latter peak corresponds to a trap depth of 0.8 eV; we assign this peak to dangling bonds, and its magnitude increases with light soaking. The former peak (trap depth 0.3 eV) decreases with light soaking. We argue that the increase in dangling bond density results in a smaller shift of the quasi fermi level into the tail states, which in turn results in decreased trapping (upon excitation) and hence a lower DLTS signal for the low temperature peak [6].

In the area of transparent conductors, a comprehensive study of the deposition of silicon dioxide as a diffusion barrier between soda lime glass and fluorine doped tin oxide was completed [7]. Figure 2 shows how effective this barrier is - for 500nm tin oxide films only about 10nm of silicon dioxide are needed to obtain a factor of 10 increase in tin oxide conductivity.

Of considerable significance was the successful development of high quality, Al-doped films of zinc oxide by magnetron sputtering. Conductivities of 2500 S cm^{-1} were achieved, corresponding to a sheet resistance of 5.4 ohms/sq. for a film thickness of $0.75 \mu\text{m}$. A visible transmission of about 90% was achieved. It was discovered that the fabrication of efficient p-i-n cells on zinc oxide is a non-trivial problem, and means had to be developed to reduce the zinc oxide/p-layer contact resistance. Once this had been accomplished, 9% efficient cells were successfully fabricated on glass/tin oxide substrates overcoated with zinc oxide (see Fig. 3). The ability to employ a transparent conductor other than tin oxide opens up many avenues for future research, including studies of the influence of the transparent conductor on V_{oc} , FF, and stability. Indeed, we have some preliminary data indicating that improved photostability can be achieved through the use of zinc oxide rather than tin oxide as the substrate for a-Si:H deposition.

Best results so far for tandem junction submodule efficiency are 7.0% aperture area efficiency (SERI-verified) for a 1 ft.sq. submodule, and 6.2% aperture area efficiency for a 1' x 3' submodule [1]. The former submodule employed a 60 \AA TiO_x recombination layer and generated an average V_{oc} per cell of 1.67V. In order to realize the full potential performance of the a-Si:H on a given panel it has been found necessary to treat the panel in various ways after fabrication to remove shunt-type defects [1,2].

Regarding photostability, we have demonstrated the ability to fabricate tandem junction devices whose stabilized power output after prolonged light soaking exceeds that of single junction devices by about 10% [1-3]. Outdoor exposure tests performed by SERI on a Chronar 1' x 1' glass-glass encapsulated tandem submodule have shown quite acceptable long-term performance (see Fig. 4).

Conclusions

It has been clearly demonstrated that tandem junction cells can provide a higher stabilized power output than single junction cells. Further increase of the stabilized submodule efficiency depends on the increase of current through optical enhancement, the increase of voltage through the development of new p-layers (perhaps using trimethylboron), improved a-Si:H uniformity, more stable i-layer material, increased active area, and reduced IR losses in the transparent conductor. Work is on-going in all of these areas [3]. The use of zinc oxide as the substrate for a-Si:H deposition appears promising.

References

1. A.E. Delahoy et al., Annual Technical Progress Report for the period March 16, 1988 March 15, 1989 (Phase II), SERI Subcontract No. ZB-7-06003-1.
2. A.E. Delahoy, Recent Developments in Amorphous Silicon Photovoltaic Research and Manufacturing at Chronar Corporation, SERI PV AR&D 9th. Review Meeting, Lakewood, CO, May 1989, and to be published in Solar Cells.
3. A.E. Delahoy, J. Kalina, C. Kothandaraman, and T. Tonon, Advanced Technology Amorphous Silicon Photovoltaic Modules, Proc. 9th E.C. Photovoltaic Solar Energy Conference (W. Palz, G.T. Wrixon, P. Helm, Eds.) Kluwer Academic Publishers, Dordrecht, 1989, p.599.
4. R.S. Crandall, K. Sadlon, J. Kalina, and A.E. Delahoy, Direct Measurement of the Mobility-Lifetime Product of Holes and Electrons in an Amorphous Silicon p-i-n Cell, Mat. Res. Soc. Symp. Proc. Vol. 149, MRS 1989, p.423.
5. J. Kalina, H. Schade, and A.E. Delahoy, Correlation Between Fill Factors of Amorphous Silicon Solar Cells and their I-layer Densities of States as Determined by DLTS, SERI PV AR&D 9th. Review Meeting, Lakewood, CO, May 1989, and to be published in Solar Cells.
6. J. Kalina, A.E. Delahoy, and H. Schade, Correlation between Fill Factors in a-Si:H P-I-N Solar Cells and Densities of States in Their I-layers, Proc. 9th E.C. Photovoltaic Solar Energy Conference (W. Palz, G.T. Wrixon, P. Helm, Eds.) Kluwer Academic Publishers, Dordrecht, 1989, p.84.
7. F.B. Ellis, Jr., and J. Houghton, Chemical Vapor Deposition of Silicon Dioxide Barrier Layers for Conductivity Enhancement of Tin Oxide Films, J. Mater. Res., 4(4), 863 (1989).

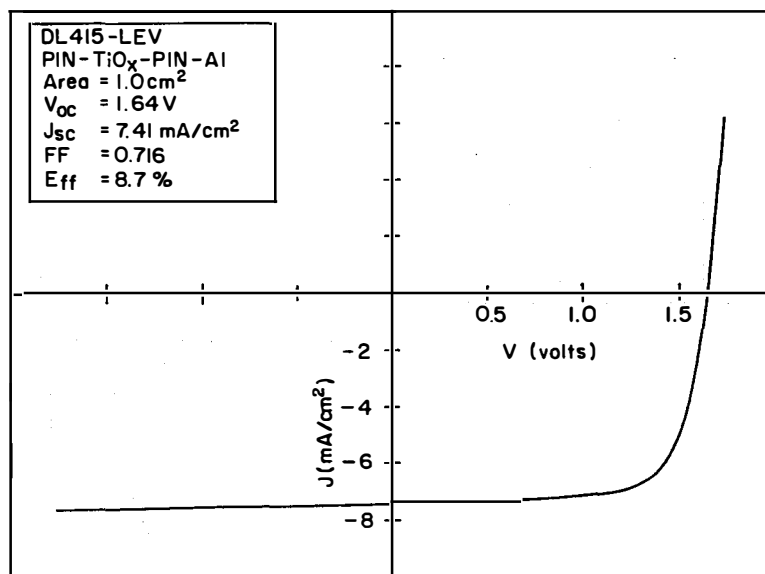


Fig. 1. J-V curve for a 8.7% 1cm² tandem cell.

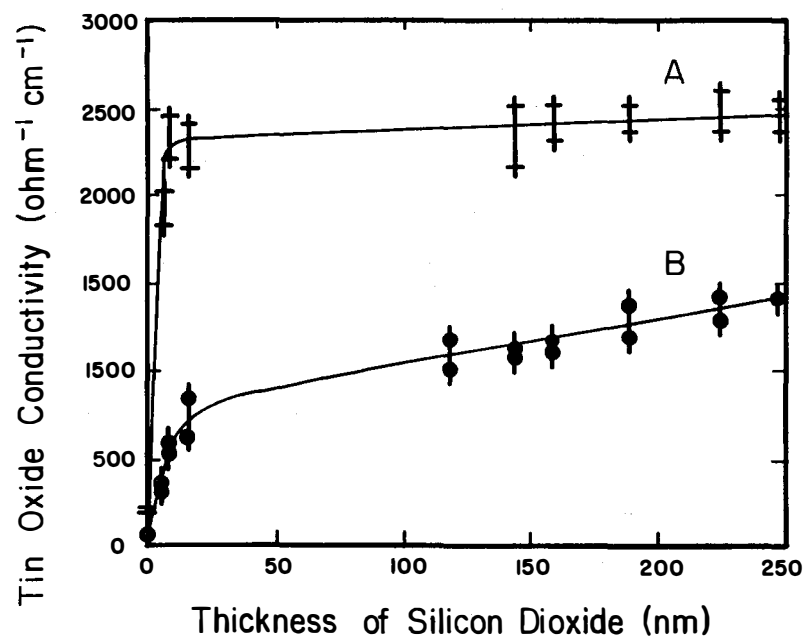


Fig. 2. Conductivity of tin oxide as a function of the silicon dioxide thickness. Curve A: 480-510 nm thick tin oxide deposited with a fluorocarbon flow rate of 250 cc/min. Curve B: 80-90 nm thick tin oxide deposited with a fluorocarbon flow rate of 110 cc/min.

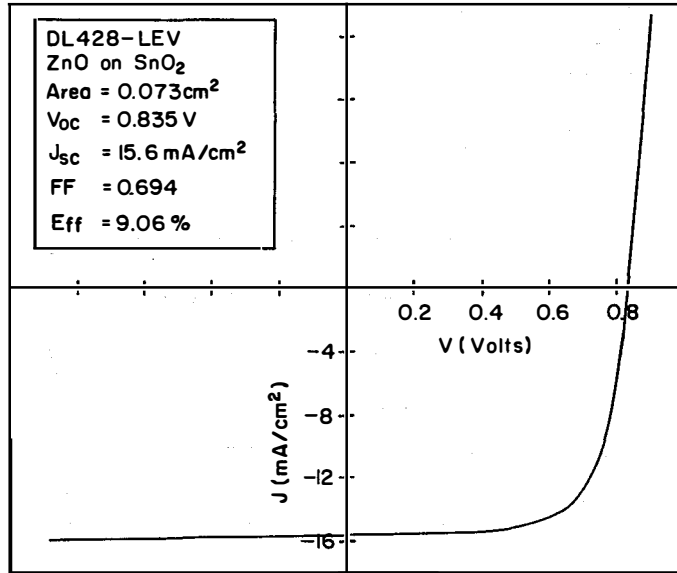


Fig. 3. Successful use of SnO₂/ZnO as a substrate for a-Si:H cell deposition

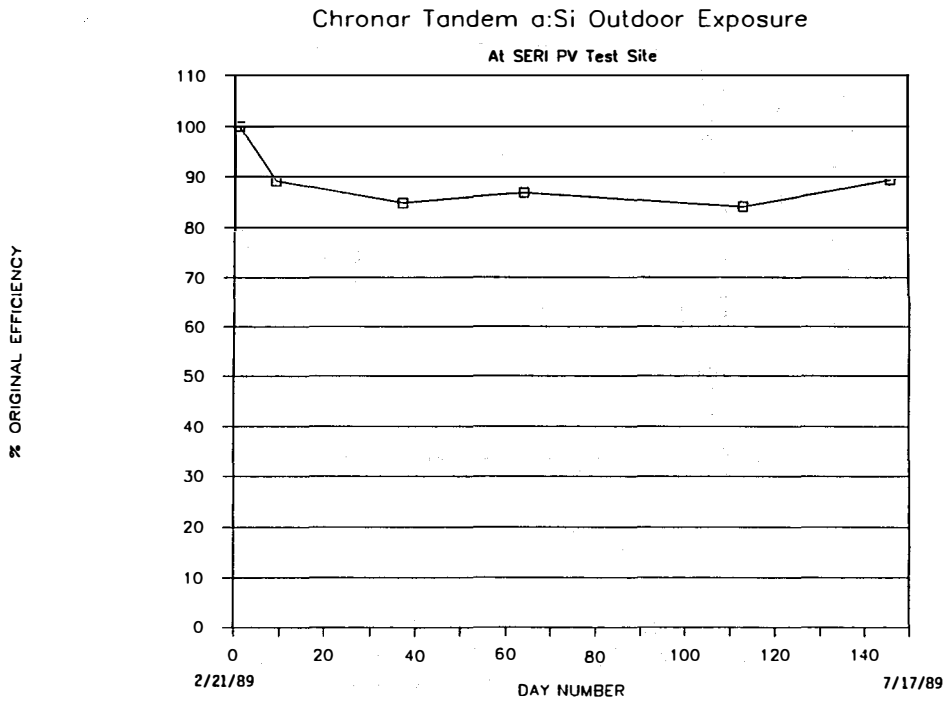


Fig. 4. Long term outdoor performance of a 1' x 1' glass-glass encapsulated tandem submodule.

Title: Research on High-Efficiency, Multiple-Gap, Multi-Junction Amorphous Silicon-Based Alloy Thin Film Solar Cells

Organization: Energy Conversion Devices, Inc., Troy, Michigan

Contributors: S. Guha, principal investigator, A. Banerjee, C. Bernotaitis, J. Burdick, E. Chen, T. Glatfelter, G. Hammond, M. Hopson, T. Laarman, M. Lycette, R. Mohr, P. Nath, A. Pawlikiewicz, I. Rosenstein, R. Ross, D. Wolf, J. Yang, and K. Younan.

The research program is directed toward advancing the understanding of amorphous silicon-based alloys and their use in small area, multijunction, multi-band gap solar cells. The principal objectives are (1) to develop a broad scientific base for the chemical, structural, optical, and electronic properties of amorphous silicon-based alloys; (2) to determine the optimum properties of alloy materials as they relate to high-efficiency cells; (3) to determine the optimum device configuration for multijunction cells; and (4) to demonstrate by February 1990 the proof-of-concept, multijunction amorphous silicon alloy-based solar cells having an efficiency of 16% under standard AM1.5 global insolation conditions and having an area of at least 1 cm².

Approach/Present Tasks

ECD has been using rf glow-discharge decomposition approach to deposit amorphous silicon alloy materials (a-Si:H:F, a-Si:Ge:H:F). In order to obtain high efficiency with good stability, a multijunction triple cell configuration has been used in which different band gap materials are used to capture the wide spectrum of solar photons. The different band gap materials are being optimized for incorporation in the cells. Novel cell designs are also being investigated to obtain higher efficiency with good stability. The tasks of the subcontract relate to materials, single-junction cell and multijunction cell research.

Status/FY 1989 Accomplishments

In order to obtain high efficiency multijunction a-Si alloy solar cells, the following requirements have to be fulfilled: 1. Optimized back reflector to facilitate light trapping, 2. Suitable antireflection coating, 3. High quality doped layer, 4. High quality narrow band gap material, 5. Optimized device design and 6. Optimum matching of cells. All these areas have been investigated during the current year. Some of the highlights are detailed below.

In our solar cell structure, we use an ITO film as the antireflection coating. The quantum efficiency of our solar cells at 400 nm is typically 60%. The loss is partly due to reflection from the single-layer ITO; absorption in the p-layer also reduces the quantum efficiency.

Using a two-layer antireflection coating and a microcrystalline p-SiC layer, we have improved the blue response significantly. The best results obtained to date is a quantum efficiency of 77% at 400 nm. Initial optimization studies with triple-cell structures showed significant enhancement in cell efficiency. A base line cell efficiency of 12.4% was found to go up to 13.15% when the two-layer antireflection coating was incorporated. Further optimizations are in progress.

We have also investigated the effect of Ge content on tandem cell performance. Since with more incorporation of germanium in a cell the open circuit voltage and the fill factor decrease whereas the short circuit current increases, it is possible to obtain high efficiency with a range of Ge content. The best results obtained for tandem and triple cells are shown in Table 1. The highest efficiency obtained with a tandem cell is 13% and with a triple cell it is 13.7%. The devices incorporate a profiled band gap intrinsic layer for the bottom cells as developed in our laboratories.

Table I. J-V parameters of high-efficiency multijunction devices measured under global AM1.5 illumination at 25°C.

Structure	Jsc (mA/cm ²)	Voc (Volts)	FF	Active Area (cm ²)	Eff (%)
1.75/1.70	8.91	1.846	.721	.249	11.9
1.75/1.55	10.48	1.709	.725	.244	13.0
1.75/1.50	11.03	1.653	.713	.249	13.0
1.75/1.45	11.35	1.632	.702	.250	13.0
1.75/1.40	11.90	1.635	.666	.250	13.0
1.75/1.70/1.40	7.66	2.545	.701	.248	13.7

Device simulation studies have been carried out to investigate performance tradeoffs between triple and tandem configurations. The simulation involves the numerical solution of coupled Poisson's and Continuity equations developed in our group. The results demonstrate unambiguously for any given narrow band gap material that triple cell structures give superior performance to tandem cells both in terms of efficiency and stability.

Finally, we have fabricated a triple-junction module with an aperture area of 840 cm². The module uses a-Si:Ge alloy in the bottom cell. The module has been measured at SERI to give a world record performance of 8.4% conversion efficiency.

References

1. J. Yang, R. Ross, T. Glatfelter, R. Mohr, and S. Guha, Improvement on Narrow Bandgap Amorphous Silicon Based Alloys and Multi-Junction Solar Cells, Proc. PVSEC 4, Sydney, Australia, 1989.
2. S. Guha, Advances In High-Efficiency, Multiple-Gap, Multijunction Amorphous Silicon-Based Alloy Thin-Film Solar Cells, MRS Spring Meeting, San Diego, CA, 1989.
3. J. Yang, R. Ross, T. Glatfelter, R. Mohr, and S. Guha, Amorphous Silicon-Germanium Alloy Solar Cells with Profiled Band Gaps, MRS Spring Meeting, San Diego, CA, 1989.
4. S. Guha, J. Yang, A. Pawlikiewicz, T. Glatfelter, R. Ross, and S.R. Ovshinsky, Band Gap Profiling for Improving the Efficiency of Amorphous Silicon Alloy Solar Cells, Appl. Phys. Lett., 1989.
5. S. Guha, J. Yang, A. Pawlikiewicz, R. Ross, T. Glatfelter, J. Burdick, and A. Banerjee, Progress in High-Efficiency, Multiple-Gap, Multijunction Amorphous Silicon-Based Alloy Thin-Film Solar Cells, SERI Amorphous Silicon Subcont. Review Meeting, Golden, CO, 1989.
6. A. Pawlikiewicz and S. Guha, Numerical Modeling of Amorphous Silicon Based p-i-n Solar Cells, IEEE Transactions on Electron Devices, Special Issue on Photovoltaics, Materials and Technology, accepted for publication.
7. S. Guha, Semiannual Subcontract Progress Report, SERI, Subcontract No. ZB-7-06003-4, August 1989.

Title: Research on the Material Properties of Device Quality Amorphous Silicon Deposited at High Deposition Rates Using Higher Order Silanes

Organization: Glasstech Solar, Inc., Wheat Ridge, CO

Contributors: H. Chatham, Program Manager; P.K. Bhat, Principal Investigator; D. Shen, C.E. Matovich, and A. Benson

Objectives

The major objectives of this research during FY 1989 were to obtain improvements in the material properties of intrinsic amorphous silicon (a-Si:H) films deposited from disilane at high deposition rates (up to 2 nm/s) and to demonstrate an a-Si:H p-i-n device with the intrinsic layer deposited from disilane at a rate of at least 2 nm/s having an AML5 efficiency of at least 9% over an area of 1 cm². The objectives of the current phase of research (commencing in the last few months of FY 1989) are to (1) demonstrate a p-i-n device with the intrinsic layer deposited at a rate of at least 2 nm/s having an efficiency of at least 10% (June 1990) and (2) to demonstrate a single or tandem junction p-i-n device with the intrinsic layer(s) deposited at 2 nm/s having an AML5 efficiency of at least 10% after 200 h of equivalent AML5 illumination (June 1991).

Approach

The general approach undertaken during FY 1989 was to focus on improving the properties of intrinsic materials deposited at high deposition rates and to optimize the performance of devices fabricated with these intrinsic layers. High quality intrinsic materials were deposited at high rates using 110 MHz disilane discharges.

Significant Results

1. Amorphous Silicon Materials Research

We have studied the influence of discharge excitation frequency over the range 13.56-110 MHz on the properties of materials deposited from disilane discharges.¹ The major conclusion of this work is that there are no significant changes in the material properties with increasing frequency other than those due to the associated increase in the deposition rate (from ~0.6 nm/s at 13.56 MHz to ~ 1.5 nm/s at 110 MHz for a constant power density of 40 mW/cm³).

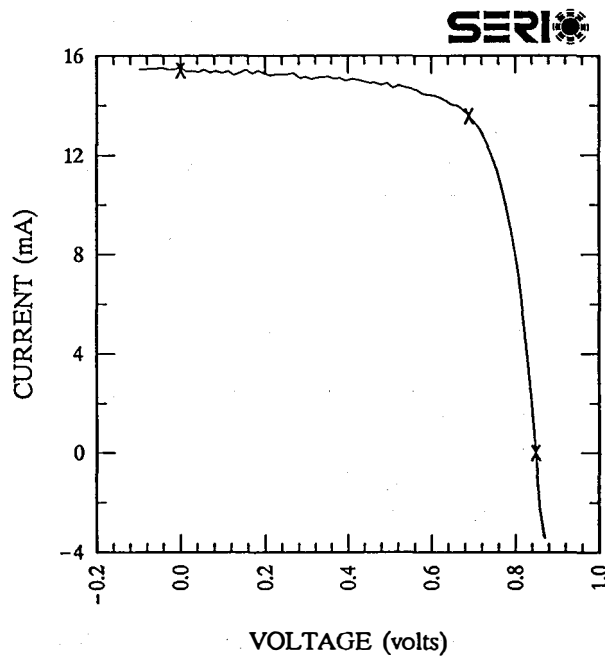
2. Amorphous Silicon Solar Cell Research

Device research during FY1989 was focused on achieving an efficiency of 9% for devices fabricated at 2 nm/s from disilane. This goal was achieved in April 1989 by using devices fabricated by depositing the intrinsic layer from 110 MHz disilane discharges. The performance of the best device delivered to SERI is displayed in Fig. 1. This device fulfilled final contract requirements for Phase II of this project. We have also

demonstrated that high deposition devices fabricated using 110 MHz intrinsic layers were superior to those fabricated using 13.56 MHz intrinsic layers. Since the intrinsic layer properties are similar, we suspect that the improvements in device performance are associated with improvements in the p/i interface.

GSI,a-Si, 20A/sec,Disilane, global

Sample: 89RD627C-1 Temperature = 25.0°C
 Apr. 12, 1989 10:10 am Area = 1.011 cm²



$V_{oc} = 0.8495$ volts	$I_{sc} = 15.42$ mA
$J_{sc} = 15.26$ mA/cm ²	$P_{max} = 9.38$ mW
Fill factor = 71.59 %	$I_{max} = 13.59$ mA
Efficiency = 9.3 %	$V_{max} = 0.6904$ V

Figure 1 I-V curve for an amorphous silicon p-i-n device fabricated with the intrinsic layer deposited at a rate of 2 nm/s from disilane

Recent work has focused on further improving this efficiency by improving the open current voltage (V_{oc}) and short circuit current density (J_{sc}). We have replaced diborane (B_2H_6) with trimethylboron ($B(CH_3)_3$) as the p layer doping gas which has allowed some improvement in the V_{oc} . Optimization of the p layer and intrinsic layer deposition temperature has resulted in the fabrication of devices with higher V_{oc} . The performance characteristics of the best of these devices is displayed in Table I.

Table I. Performance Characteristics of a-Si:H p-i-n solar cell fabricated using a $B(CH_3)_3$ p layer and 110 MHz disilane intrinsic layer.

V_{oc} (V)	J_{sc} (mA/cm ²)	Fill Factor	Efficiency (%)	Thickness (nm)	Deposition Rate (nm/s)
0.887	15.5	0.70	9.6	645	2.1

Further improvements must come from increasing the current density through reduction of optical losses and improvements in the intrinsic layer absorption as well as from improving the interface characteristics. Materials deposited at high deposition rates typically have low absorption relative to those deposited at low rates due to the increase in the amount of hydrogen in the film.

We are continuing to work on improving the quality of the intrinsic layer, in particular the intrinsic layer absorption, using methods such as hydrogen dilution, dc bias, and other techniques. Achievement of the final goals of this project will require use of the tandem cell structures, using high deposition rate intrinsic a-Si:H in the bottom cell and a narrow band gap SiGe alloy in the top cell. Thus, work will also focus on achieving high deposition rate a-SiGe material of high quality.

References

H. Chatham and P.K. Bhat, Final Technical Report for SERI Subcontract # AB-70-06001-2 (1989).

Title: Characterization and Comparison of Optically Transparent and Conducting Films

Organization: Department of Chemistry, Harvard University, Cambridge, Massachusetts

Contributors: R. G. Gordon, principal investigator; J. Hu, C. Giunta, and J. Musher.

Transparent conducting materials are essential components of thin-film solar cells, in which they serve as front-surface electrodes. In tandem cells, back surface electrodes also need to be transparent. Finally, some designs for highly reflective back contacts also call for a transparent conducting layer. The compositions of these transparent conducting layers are usually based on oxides of tin, indium and/or zinc, and are hence referred to as transparent conducting oxides (TCO). In addition to having low electrical resistance and low optical absorption, the structure of a TCO must minimize reflection losses. The TCO must also resist degradation during cell fabrication and use. Finally, the method for making the TCO must be inexpensive and safe.

Objectives

The general objectives are to improve the performance of TCO materials and the methods for their production. We aim to reduce their electrical resistance, optical absorption and reflection losses, and to avoid degradation of the materials. For the production method, the prime consideration is to deposit the TCO layers at a high rate with relatively simple apparatus.

Approaches Taken

During the present contract period, we have concentrated our attention primarily on fluorine-doped zinc oxide, since zinc metal is much less expensive than tin or indium. Also, zinc is much more abundant in the earth's crust, than is tin or indium, so that even large-scale use of solar cells would not lead to any shortage of zinc. Also, zinc is widely distributed on earth, and is mined in many countries, so continuity of supply is assured in any kind of political situation. In contrast, tin is mined in large quantities in only a few countries. Another advantage of zinc oxide is its greater stability toward hydrogen plasmas used to deposit amorphous silicon solar cells.

As a preparation method, we chose chemical vapor deposition (CVD), since for many materials, the highest deposition rates have been achieved using CVD. When operated at atmospheric pressure, CVD requires only simple equipment which is commercially available and capable of large-area coating.

Discovery of Electrically Conductive Fluorine-doped Zinc Oxide

Pure zinc oxide has low electrical conductivity. By partial reduction, nonstoichiometric (oxygen-deficient) zinc oxide can be prepared with high electrical conductivity, which is, however, unstable. Group III elements (boron, aluminum or indium) have been added to

zinc oxide to produce more stable, highly conductive films. However, out-diffusion of these group III dopants into amorphous silicon could produce uncontrolled doping of the amorphous silicon during deposition or use of the cell. We discovered that fluorine can also be used to dope zinc oxide to high electrical conductivity. Fluorine is an ideal dopant for zinc oxide, since it is known to be electrically inactive, or even beneficial, in hydrogenated amorphous silicon. An additional benefit of the fluorine doped zinc oxide is its higher electron mobility, which results in greater transparency.

The fluorine-doped zinc oxide is produced by CVD from diethyl zinc, ethanol and hexafluoropropylene at atmospheric pressure, in the temperature range 375° to 450°C. The highest electrical conductivity and light transmission are found for films deposited at the highest temperatures (450°C), and containing about 0.5 atomic percent fluorine. Figure 1 shows some typical results for the electrical conductivity as a function of fluorine content. The optical and electrical properties of these films can be understood in terms of electron scattering produced by both ionized impurities (fluorine) and grain boundaries between the crystallites. Visible and infrared reflection and transmission spectra for a typical film are shown in Figure 2, along with theoretical curves fit to the data. More details of our results for the new fluorine-doped zinc oxide material may be found in our final technical report for SERI subcontract XX-8-18148-1.

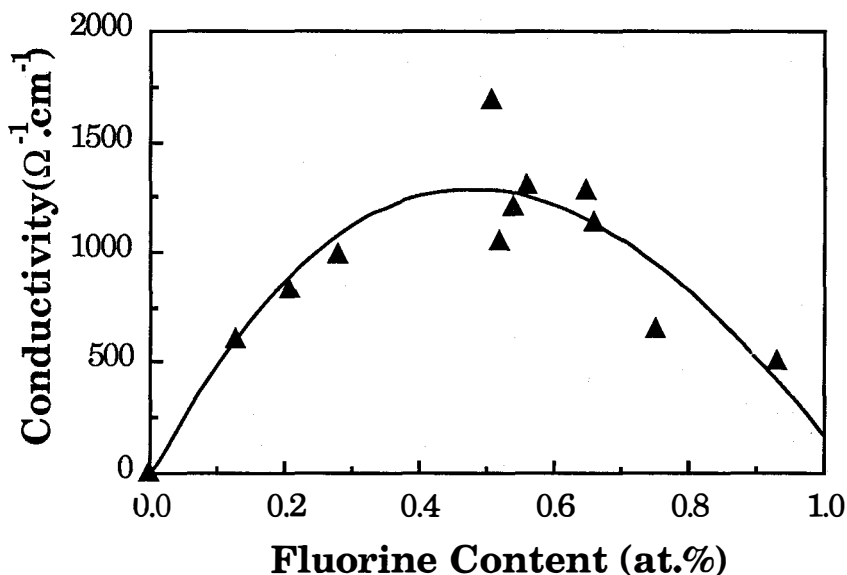


Fig. 1. Conductivity as a function of fluorine content for fluorine-doped zinc oxide films deposited at 400°C.

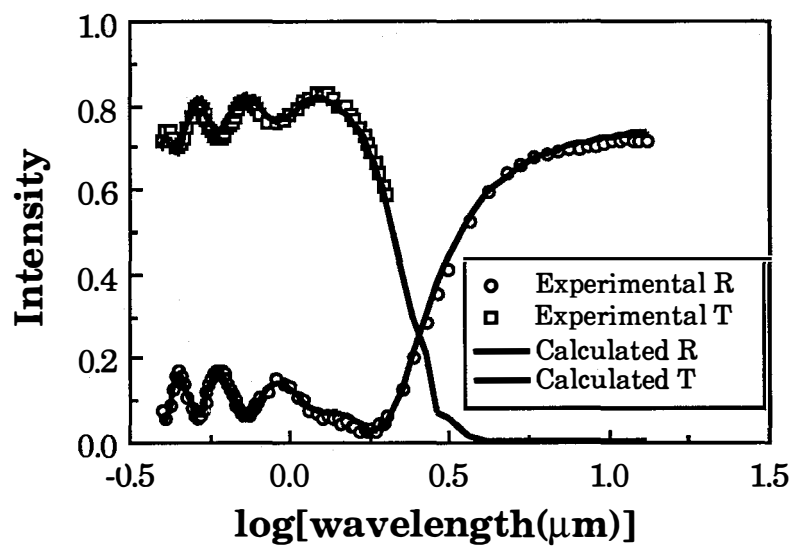


Fig 2. Typical experimental and calculated spectra. The film was deposited at 400°C from diethyl zinc, ethanol and hexafluoropropylene with concentrations of $2.60 \times 10^{-5} \text{ mol} \cdot \text{l}^{-1}$, $1.54 \times 10^{-3} \text{ mol} \cdot \text{l}^{-1}$ and $5.79 \times 10^{-5} \text{ mol} \cdot \text{l}^{-1}$.

Title: Structural and Electronic Studies of a-SiGe:H Alloys

Organization: Division of Applied Sciences, Harvard University, Cambridge, MA

Contributors: William Paul, principal investigator

Objectives

The principal objectives of this research have been (1) to carry out a detailed study of the structural, electrical and optical properties of a-Ge:H, the end-component of the a-Si_{1-x}Ge_x:H alloy series, in order to determine the values of deposition parameters optimizing the properties relevant to photovoltaic devices, (2) to continue to deposit films of a-Si:H and a-Ge:H by photo-chemical-vapor deposition, in order to augment the study of films produced by glow discharge, and to see if insight into deposition processes is available from study of this method, (3) to continue a collaboration with Professor Richard Norberg of Washington University to prepare films of a-Si and a-Ge containing deuterium, so that the Norberg laboratory can study deuteron magnetic resonances (DMR), which may be interpreted to give information on the microstructure of films on a 100 Å scale, (4) to continue a collaboration with Dr. M. L. Theye of the Laboratoire d'Optique, University of Paris, to explore low photon energy absorption spectra determined either by photothermal deflection spectroscopy (PDS) or steady-state photoconductivity (PC), (5) to carry out a collaboration with Professor I. Chamboleyron of the University of Campinas to compare the properties of a-Ge:H prepared by reactive sputtering (Campinas) and plasma-enhanced CVD (Harvard), and (6) to carry out a collaboration with Professor J. Chen of Boston College to study the electron spin resonance spectra of hydrogenated amorphous semiconductors.

Approach

The films required were prepared by r.f. glow discharge, reactive sputtering and photo-CVD. The measurements made included conductivity *versus* temperature, optical absorption in the sub-band-gap region of the spectrum, optical vibrational absorption in the infrared region, photoconductivity spectra, photoluminescence spectra, Raman spectra, gas evolution, transmission and scanning electron microscopy, Rutherford backscattering, differential scanning calorimetry and deuteron and electron magnetic resonance.

Discussion

Progress has been made on all of these projects. The investigation of a-Ge:H, the present principal focus of our work, has involved systematic variation of preparation parameters such as R.F. power, substrate temperature, nature of the substrate material, dilution of GeH₄ by H₂, dilution of GeH₄ by He, dilution of GeH₄ by GeF₄ and H₂, and on the electrical basis of the substrate platform. Conclusions from the structural, electrical and optical characterizations have been published (1). Our several collaborative efforts have all led to new results, and two of them to new publications (2). The collaboration with Professor Norberg has been especially productive this year, and has provided unique insight into the properties of material on a scale of 10–30 Å, a scale which is traditionally

insight into the properties of material on a scale of 10–30 Å, a scale which is traditionally difficult to study. Besides the collaborative efforts noted above, we continue to carry out characterizational measurements on films from other laboratories by the special methods we have developed (GE and DSC).

Conclusions

Our very extensive studies of a-Ge:H produced by PECVD have confirmed that this material is much poorer than a-Si:H from the photoelectronic standpoint. They have established that relatively small excursions from the optimum parameters for the production of a-Si:H are not sufficient to give good quality films. We have had considerable difficulty in assessing progress in the improvement of a-Ge:H and of low energy-gap $a\text{-Si}_{1-x}\text{Ge}_x\text{:H}$ alloys from the literature because of the incompleteness of the characterizations reported. Nevertheless, we have concluded, taking these difficulties into account, that the photosensitivity of our best PECVD films is comparable to those reported elsewhere, but that it is not as high as is desirable for practical use of the material. It appears that the best preparation conditions approach more those to be found in sputtering than in glow discharge plasmas, so that if PECVD apparatus is to be used, the conditions in it should be adjusted to provide more surface bombardment.

A major focus and contribution of our work has been the study of the microstructure of films of a-Si:H and a-Ge:H through the examination of GE, TEM and DSC spectra on co-deposited films. Taken together with the optical and electrical data, and especially the (structural) studies by DMR of the Norberg group, these establish the correctness of a model for hydrogenated amorphous semiconductor films of a two-phase (island and tissue) material. The two phases have quite likely different chemical composition (different amounts of hydrogen), different structure and density, and different electronic band structure. This model leads naturally to an inhomogeneous material having potential fluctuations which vitally affect the photoelectronic properties. The heterostructure and the potential fluctuations are demonstrably greater in a-Ge:H than in a-Si:H. The question arises, to what extent the heterostructural nature can be reduced, and whether, when it is reduced to a minimum, the electronic band structure of *homogeneous* a-Ge:H is still such that rapid photocarrier recombination prevents good photoelectronic properties. Given that the extent of the conduction and valence band tail densities of states is comparable in a-Ge:H and a-Si:H (they may be different but there is little indication that the extent of tails is smaller in a-Ge:H, rather the inverse) and that the gap state density provided by dangling bonds is larger in a-Ge:H, it is clear that trapping and recombination will always be faster in a-Ge:H. The problem we seek to solve is the reduction of structural heterogeneity to a minimum, and the establishment of the limiting $\eta\mu\tau$'s for *both electrons and holes* in such material. Our work during the past year has brought us much closer to definitive statements on such issues.

References

1. Annual Report on Subcontract No. XX-8-18131-1-1, period 1 September 1988 – 30 June 1989, submitted October 1989.
2. Li, Turner, Lee, and Paul, Substrate temperature dependence of the optical and electronic properties of glow discharge produced a-Ge:H, to be published in the Proceedings of the Spring 1989 meeting of the Materials Research Society, San Diego.
3. Turner, Jones, Lee, Lee, Li, and Paul, The effect of hydrogen dilution on glow discharge a-Ge:H, to be published in the Proceedings of the Spring 1989 meeting of the Materials Research Society, San Diego.
4. Jones, Lee, Turner, and Paul, Substrate temperature dependence of the structural properties of glow discharge produced a-Ge:H, to be published in the Proceedings of the Spring 1989 meeting of the Materials Research Society, San Diego.
5. Jones, Turner, and Paul, The effect of sample substrate on the structural properties of co-deposited films, to be published in the Proceedings of the 13th International Conference on Amorphous and Liquid Semiconductors, (ICALS), Asheville, NC, August 1989.
6. Volz, Fedders, Norberg, Turner, and Paul, Deuteron magnetic resonance in a-Ge, to be published in the Proceedings of the 13th International Conference on Amorphous and Liquid Semiconductors, (ICALS), Asheville, NC, August 1989.
7. Santos-Filho, Volz, Corey, Kim, Fedders, Norberg, Turner, and Paul, Molecular HD and D₂ in amorphous semiconductors, to be published in the Proceedings of the 13th International Conference on Amorphous and Liquid Semiconductors, (ICALS), Asheville, NC, August 1989.
8. Fournier, Roger, Boccara, Theye, Chahed, Turner, and Paul, to be published in the Proceedings of the 6th International Meeting on Photoacoustic and Photothermal Phenomena, Baltimore, Maryland, July–August, 1989.
9. Volz, Santos-Filho, Conradi, Fedders, Norberg, Turner, and Paul, Unique deuteron spin echoes from HD and ortho-D₂ in large crystal fields, *Phys. Rev. Letts.*, to be published.

Title: Photochemical Vapor Deposition of Amorphous Silicon Alloy Materials and Devices

Organization: Institute of Energy Conversion
University of Delaware
Newark, Delaware 19716

Contributors: B. N. Baron, Project Director;
C. M. Fortmann and S. S. Hegedus,
Principal Investigators; W. A. Buchanan and
T. X. Zhou, Research Contributors.

Objectives:

The project is a continuation of research on photochemical vapor deposition of amorphous silicon materials in order to determine and understand the limits of material preparation and to demonstrate proof-of-concept solar cells. The present objectives are to develop low band gap a-SiGe:H cells for use in high efficiency, stable multijunction thin film solar cells and determine and understand the origin of Staebler-Wronski effect degradation in a-Si:H cells.

Technical Approaches:

IEC is focussing on the transport properties of low band gap a-SiGe:H alloys as they relate to solar cell performance. Studies of the relationships between i-layer electronic transport and deposition conditions are integrated with detailed investigations of device behavior. The a-SiGe:H materials are prepared in a photo-CVD deposition system that has demonstrated state-of-the-art a-Si:H materials and devices [1]. Alloy films and devices are being prepared with a range of H and Ge contents. Film analyses include: optical absorption, conductivity, IR analysis, and Raman scattering. The performance of p-i-n solar cells with an i-layer bandgap of approximately 1.3 eV are studied as a function of H and Ge content and i-layer thickness. The effects of i-layer compositional grading on alloy cell performance are studied by fabricating and characterizing the I-V behavior and spectral response of p-i-n devices with graded alloy i-layers. A mathematical model for transport in graded i-layer devices is being developed.

The origins of the defects involved in Staebler-Wronski (S-W) effect are being investigated using a-Si:H p-i-n cells as the test device. Cells are degraded at high temperatures (150-175°C) by current injection and the steady state density of defects is measured using the short wavelength quantum efficiency (SWQE) method [2]. The effect of H content on S-W defect formation is studied by using photo-CVD to fabricate cells with i-layers having a range of H contents.

Significant Results

Materials Growth and Characterization

The relationship between H₂ dilution and film properties was explored. Unlike He dilution, in which there is a constant ratio between GeH₄ partial pressure (relative to SiH₄) and film composition over a wide range of conditions, with

H₂ dilution the ratio depends on deposition temperature and pressure. In a recent publication [3] we described how the selective etching by H radicals of Si atoms relative to Ge atoms on the growth surfaces can account for the observed relationship between reactor parameters and film composition. Alloy films were grown under conditions ranging from low H radical flux (H₂ or He dilution above 1 torr or He dilution at low pressure) to high H radical flux conditions obtained at low pressure (0.5 torr with 9:1 hydrogen dilution). Under high H radical fluxes, Raman spectroscopy of films showed high microcrystalline content (μ X-Si, μ X-Ge, and a-SiGe:H were all present in the same film) while films grown under low H radical fluxes were amorphous and randomly mixed (to the extent of the accuracy of the measurement) alloys.

Table 1 lists properties of a-SiGe:H films for various deposition conditions. Figure 1 shows the photoconductivity as a function of band gap for a-SiGe:H films grown by photo-CVD. The photoconductivity improved as the substrate temperatures increased for either dilution case. As observed by others [4] the electronic transport decreased with decreasing band gap. It appears that the film composition (Si, Ge and H content) determines the material properties of the alloy films, with the best alloy films having the lowest H content. In an associated study [5], microcrystalline p-layers were developed with high conductivities ($\sigma \sim 1$ S/cm).

Low Band Gap a-SiGe:H Devices

In order to investigate the electron transport limitations, p-i-n devices shown in Figure 2 were fabricated and analyzed. Figure 3 shows the quantum efficiency of these devices. The highest overall QE was obtained with the "front-loaded" device in which the i-layer contained a 400 Å thick region of 1.3 eV a-SiGe:H. The corresponding short circuit current for this device under global AM 1.5 illumination at 100 mW/cm² was $J_{sc} = 18.5$ mA/cm². These results are consistent with electron mobility limiting the performance of a-SiGe:H alloy devices. A model which predicts improved performance for compositionally graded i-layer devices on the basis of gradients in electron mobility due to spatial variation of i-layer composition is being developed.

Staebler-Wronski-Effect in a-Si:H Cells

p-i-n solar cells were degraded by current injection at 175°C and quenched to room temperature. Steady state S-W defect densities were determined using the SWQE technique [2].

The effect of current injection at 300 mA/cm² was studied for i-layers containing both high (~8%) and low (~5%) H content. Two series of p-i-n solar cells with i-layers ranging from 0.6 to 1.0 μ m were degraded for one hour at 175°C. For i-layer thickness greater than 0.6 μ m, the steady state S-W defect density in the samples with high H content was larger than that of samples with lower H content.

Conclusions

Low band gap a-SiGe:H alloy films with band gap of 1.3 eV and photoconductivity greater than 3E-6 S/cm have been deposited using Hg sensitized photo-CVD from

mixtures of silane and germane. Analysis of p-i-n devices with 1.3 eV a-SiGe:H i-layers indicates that electron mobility is a critical material parameter limiting the performance of a-SiGe:H alloy solar cells. Thin compositionally graded i-layers in the red sensitive component of multi-junction devices are expected to lead to the development of stable high efficiency thin film solar cells. The H content of the i-layer in a-Si:H p-i-n cells governs the extent of degradation under current injection. Increasing the H content leads to an increase in density of weak bonds that are associated with generation of S-W defects in a-Si:H.

References

1. 0 S. S. Hegedus, et al., Conference Record of the 20th IEEE Photovoltaic Specialists Conference, Las Vegas, NV, September 26-30, 1988, IEEE, New York (1989) p.129.
2. Z C. M. Fortmann, et al., J. Appl. Phys. 64 (8), (1988) p.4219.
3. Z D. E. Albright, et al., Materials Research Society Symposium, Vol. 149 (1989) p.521.
4. Z K. Mackenzie, et al., Phys. Rev. B31 (1985) p.2198.
5. 0 N. Saxena, et al., Materials Research Society Symposium, Vol. 149 (1989) p.97.

Table 1: FILM PROPERTIES VERSUS DEPOSITION CONDITIONS

FILM	E _{gap}	PHOTO	DARK	E _a	DEPOSITION CONDITION
a-Si:H	1.75eV	6.7E-5	4.2E-11	0.84	230 C, 1 torr, He
a-Ge:H	1.07eV	2.4E-5	1.1E-5	0.50	200 C, 3 torr, He
a-SiGe:H	1.44eV	1.9E-5	5.0E-9	0.69	230 C, 2 torr, H ₂
a-SiGe:H	1.33eV	3.6E-6	2.3E-8	0.64	230 C, 5 torr, H ₂
a-SiGe:H	1.26eV	3.0E-6	1.0E-7	0.60	230 C, 5 torr, H ₂

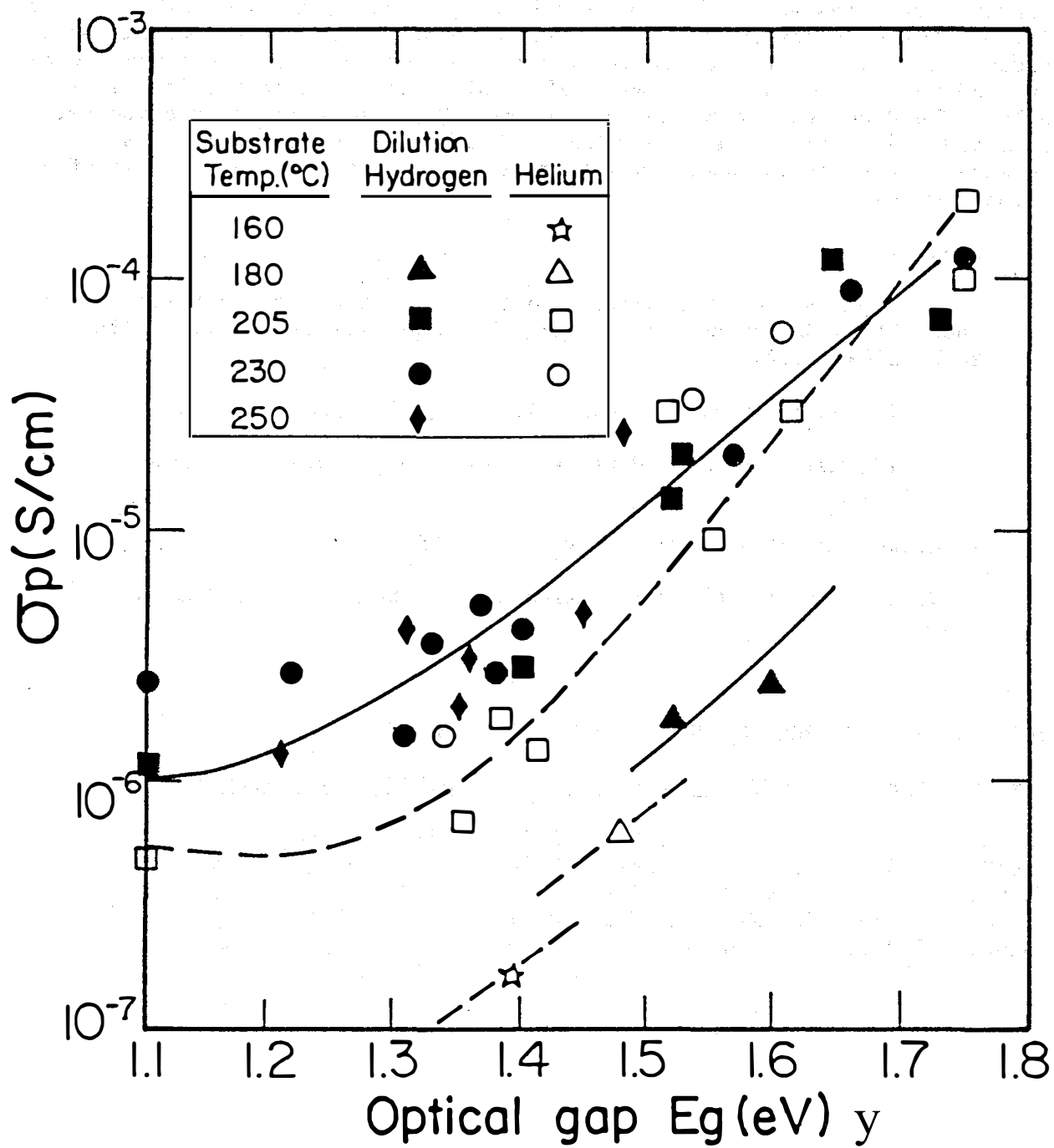


FIGURE 1: Photoconductivity of a-SiGe:H Intrinsic Films Deposited by Photo-CVD.

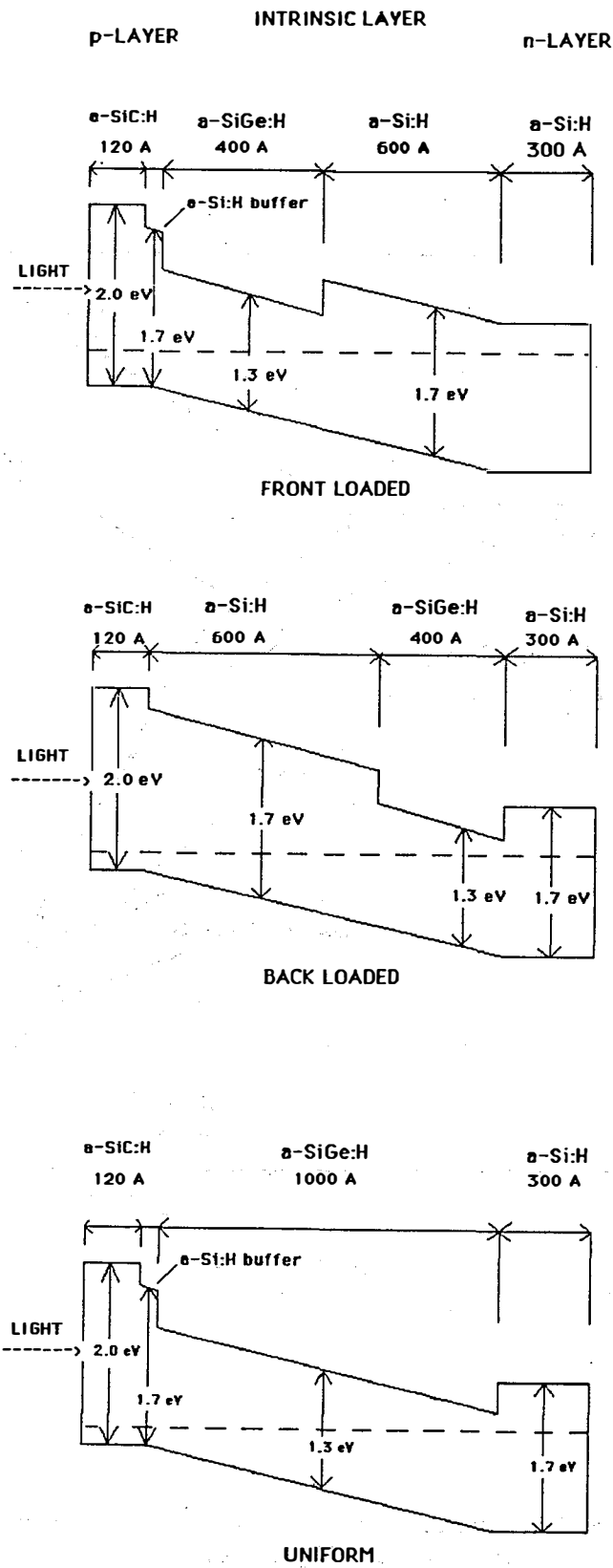


FIGURE 2: Band Diagrams of a-SiGe:H Alloy i-layer Devices.

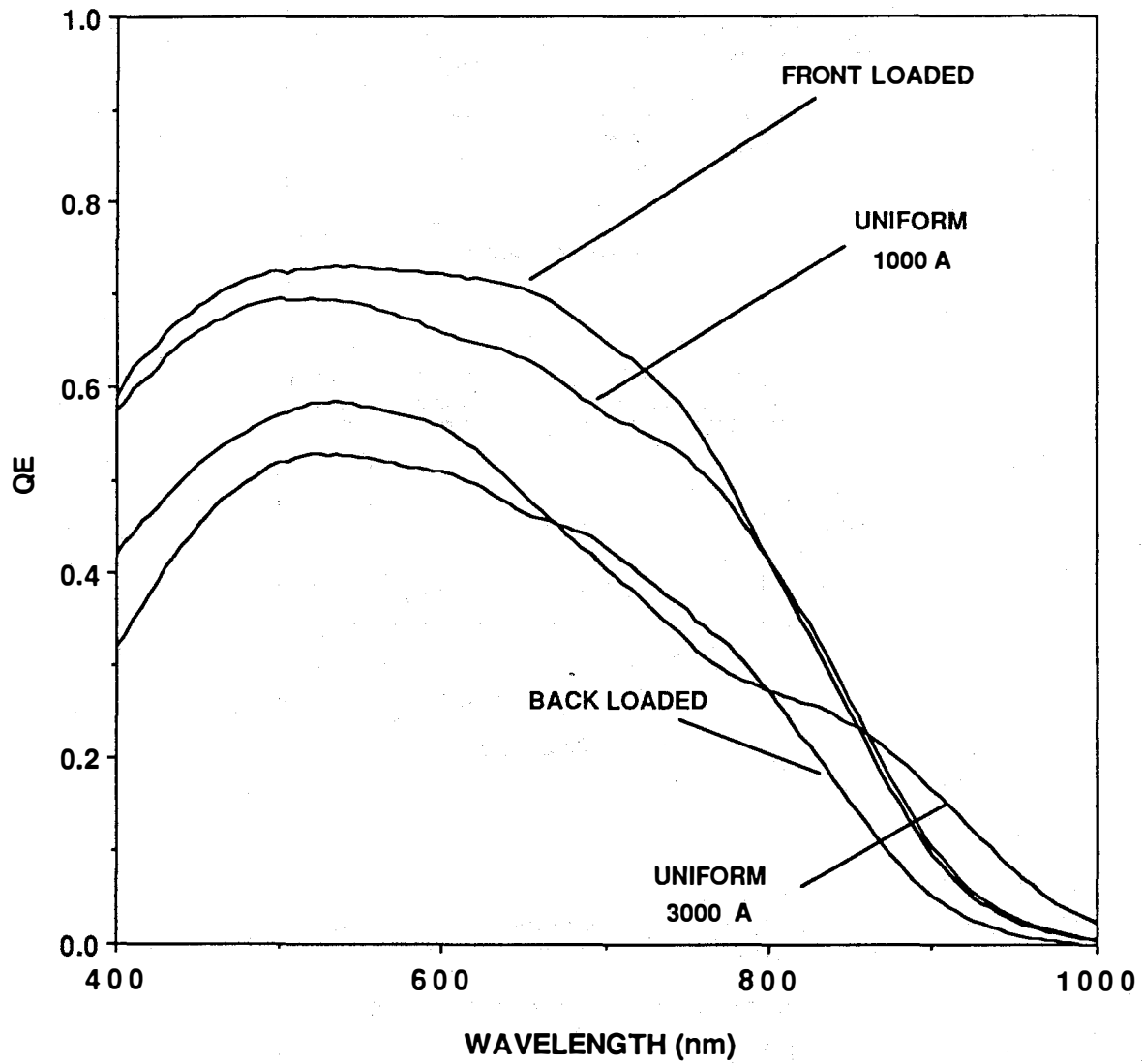


FIGURE 3: Quantum Efficiency Behavior of a-SiGe:H Devices of Figure 2.

Title: Amorphous Silicon Deposition Research with In Situ Diagnostics

Organization: Jet Propulsion Laboratory, California Institute of Technology, Pasadena, California

Contributors: Y.H. Shing, principal investigator; F.S. Pool, C.E. Allevalo, and C.L. Yang

Objective

The objectives of this task are: (1) to develop device-quality hydrogenated amorphous silicon carbon alloy thin films (a-SiC:H) using electron cyclotron resonance deposition technology; and (2) to evaluate electron cyclotron resonance and glow discharge deposition processes through in situ plasma diagnostics and device performance.

Approach

JPL has established state-of-the-art amorphous silicon deposition capabilities using radio frequency (13.56 MHz) glow discharge and microwave (2.45 GHz) electron cyclotron resonance (ECR) techniques. The JPL glow discharge and ECR deposition systems [1] are capable of performing in situ plasma diagnostic experiments. An RF induction heated sample stage has been designed and installed in the ECR deposition system. The high temperature (up to 1000°C) heating capability is employed to investigate ECR deposition processes in a wide temperature range for developing an understanding on the film stability and growth mechanisms. ECR microwave plasma CVD has been developed at low pressures (10^{-4} - 10^{-2} Torr), at ambient and high substrate temperatures (up to 750°C), to achieve large-area (>4" diameter) depositions of amorphous silicon (a-Si:H), amorphous carbon (a-C:H) and a-SiC:H alloy films [2,3]. The ion energy effect in modifying the electronic and structural properties of ECR-deposited films is studied by applying an RF bias to the substrate stage [4]. In situ optical emission spectroscopy (OES) plasma diagnostics are employed to determine the characteristic difference between ECR and RF glow discharge deposition processes. The optical, electrical and morphological properties of thin film samples are characterized by infrared, visible transmission, Raman spectroscopy, light and dark conductivity measurements.

Plasma Diagnostics Using Optical Emission Spectroscopy

The extracted ECR plasmas in the deposition chamber have been examined by OES using an optical multichannel analyzer detection system. The OES intensity ratio of atomic to molecular hydrogen in ECR plasmas is about a factor of 3 to 5 higher than the ratio of RF plasmas. The high concentration of atomic hydrogen species in ECR plasmas results from the high ionization ratio due to the ECR condition. The CH* emission intensity of CH₄ and H₂ mixed gas ECR plasmas is shown in Figure 1 as a function of microwave power. The CH* emission intensity is linearly dependent on microwave power. The increase in the CH* emission intensity does not lead to an increase in the deposition rate of a-C:H films. In comparison with ECR depositions of a-Si:H films, a linear correlation between the SiH* emission intensity and the a-Si:H film

deposition rate has been found [2]. This indicates that the film growth mechanism of ECR-deposited a-C:H films may be substantially different from that of a-Si:H films. The abundance of atomic hydrogen species in the ECR plasma can play a significant role in etching a-C:H films. Consequently the deposition rate of a-C:H films is dependent on both the hydrogen etching and the depositing species, which may be related to the CH* emission intensity.

ECR-Deposited a-C:H Films

ECR depositions of a-C:H films were investigated in the parameter space of flow rate, microwave power, substrate bias and substrate temperature. ECR-deposited a-C:H films, at ambient temperature, without external substrate bias, show a typical optical bandgap of 2.8 eV and a deposition rate of 2-3 Å/s. These films can be scratched and have a broad fluorescence in the spectral range of 450-650 nm as shown in Figure 2. Hard a-C:H films have been deposited by ECR using RF bias. Experiments with DC bias in ECR depositions have shown no significant effect on the optical and mechanical properties of a-C:H films. However, it is found that RF bias is critically needed in ECR depositions to produce diamond-like a-C:H films. Two types of hard a-C:H films have been produced by ECR plasmas using low (-4 V) and high (-100 V), RF induced self-biased voltages, respectively. Raman spectrum of one type of hard a-C:H films, deposited by ECR plasmas with low self-bias voltages, consists of two broad, overlapping lines centered at 1360 and 1590 cm^{-1} , as shown in Figure 3. These Raman lines are used as the diagnostic features of various graphitic (sp^2 bonding) carbon structures and are designated as the D (1360 cm^{-1}) and the G (1590 cm^{-1}) lines. Another type of hard a-C:H films is deposited by ECR plasmas using high RF induced self-bias voltage of -100 V, shows a broad Raman peak at $\sim 1500 \text{ cm}^{-1}$ superimposed on a luminescent background as shown in Figure 4. The optical bandgap of this type of hard a-C:H films is determined to be 1.7 eV by the Tauc plot. The broad Raman peak at $\sim 1500 \text{ cm}^{-1}$ is distinctly different from the D and G lines of graphitic structures and is probably related to the carbon-carbon vibrational band. Both types of hard a-C:H films are characterized as diamond-like a-C:H films.

RF and ECR Depositions of a-SiC:H Films

RF glow discharge and ECR depositions of a-SiC:H films have been performed using SiH_4 , CH_4 , and H_2 gas mixtures. The ECR deposition rate of a-SiC:H films is found to be strongly dependent on the magnetic field settings for achieving the ECR condition. The deposition rate under the ECR condition is a factor of 2 - 4 higher than that of the off-resonance condition. The optical bandgap of RF-deposited a-SiC:H films as a function of the CH_4 gas composition is shown in Figure 4. The optical bandgap of these films can be varied over the range of 1.8 - 2.3 eV by increasing the CH_4 gas composition from 30% to 85%. The nominal 2.0 eV optical bandgap a-SiC:H films can be deposited with a CH_4 gas composition of 60%.

ECR microwave plasma and RF glow discharge deposition rates of a-SiC:H films are shown in Figure 5. A similar dependence of the deposition rate as a function of the hydrogen flow rate has been observed in both ECR and RF depositions of a-SiC:H films, where a large decrease in the deposition rate is caused by a small fraction of hydrogen dilution. The hydrogen dilution effect in SiH_4 and CH_4 mixed gas plasmas suggests that the hydrogen etching

also plays an important role in depositing a-SiC:H films. The optical bandgap of ECR- and RF-deposited a-SiC:H films as a function of hydrogen dilution is shown in Figure 6. The ECR-deposited a-SiC:H films have shown a slightly wider optical bandgap than that of RF-deposited a-SiC:H films. The hydrogen dilution in the plasma is found to have no significant effect on the optical bandgap of a-SiC:H films. With a CH₄/SiH₄ flow rate ratio of about 3, we have achieved an optical bandgap of 2.5 eV for ECR-deposited a-SiC:H films.

Conclusions and Future Plans

In situ OES plasma diagnostics show that ECR plasmas have a high concentration of atomic hydrogen species indicating a higher chemical reactivity than RF glow discharge plasmas. The CH* emission intensity and the deposition rate of a-C:H films do not correlate, indicating that the hydrogen etching and the depositing species relating to the CH* emission may play a balancing role in a-C:H film growth. ECR-deposited a-C:H films, without external substrate bias and at ambient temperature, show a typical optical bandgap of 2.8 eV, a deposition rate of 2-3 Å/sec and a broad fluorescence in the spectral range of 450-650 nm. Two types of diamond-like, hard a-C:H films have been produced by ECR plasmas using low (~-4 V) and high (~-100 V), RF induced self-bias voltages, respectively. The application of an RF bias to the substrate is found to play a critical role in determining the film structure and the carbon bonding configuration of ECR-deposited a-C:H films.

Wide bandgap (up to 2.5 eV) a-SiC:H films have been deposited by using ECR microwave plasmas. The ECR-deposited a-SiC:H films have shown a slightly higher optical bandgap than that of RF-deposited a-SiC:H films. The hydrogen dilution has no significant effect on the optical bandgap of a-SiC:H films. The deposition rate as a function of hydrogen dilution demonstrates that the hydrogen etching also plays an important role in a-SiC:H film depositions.

In our future research, the substrate bias effect will be investigated in the ECR deposition of a-Si:H and a-SiC:H films. Low energy ion bombardment will be employed to improve the density and optoelectronic properties of ECR deposited a-Si:H and a-SiC:H films. The role of ion bombardment in the ECR deposition will be systematically evaluated by correlating film characterizations and plasma diagnostic experiments. The hydrogen dilution effect in the deposition of microcrystalline silicon carbon alloy films (μ c-SiC:H) will be determined. The hydrogen plasma etching will be investigated to determine the compositional inhomogeneity of μ c-SiC:H films. Solar cells incorporating ECR- and RF-deposited a-Si:H and μ c-SiC:H films will be fabricated to provide a comparative, device-oriented evaluation of ECR deposition processes.

References

1. Y.H. Shing, J.W. Perry, and C.E. Allevato, Proc. 20th IEEE Photovoltaic Specialists Conference, IEEE, New York, 1988, p.224.
2. D Y.H. Shing, C.L. Yang, C.E. Allevato, and F.S. Pool, Materials Research Society Symposium Proc., San Diego, California, 1989, (in press).
3. Y.H. Shing, Solar Cells, 1989, (in press).
4. Y.H. Shing, and F.S. Pool, Vacuum, 1989, (in press).

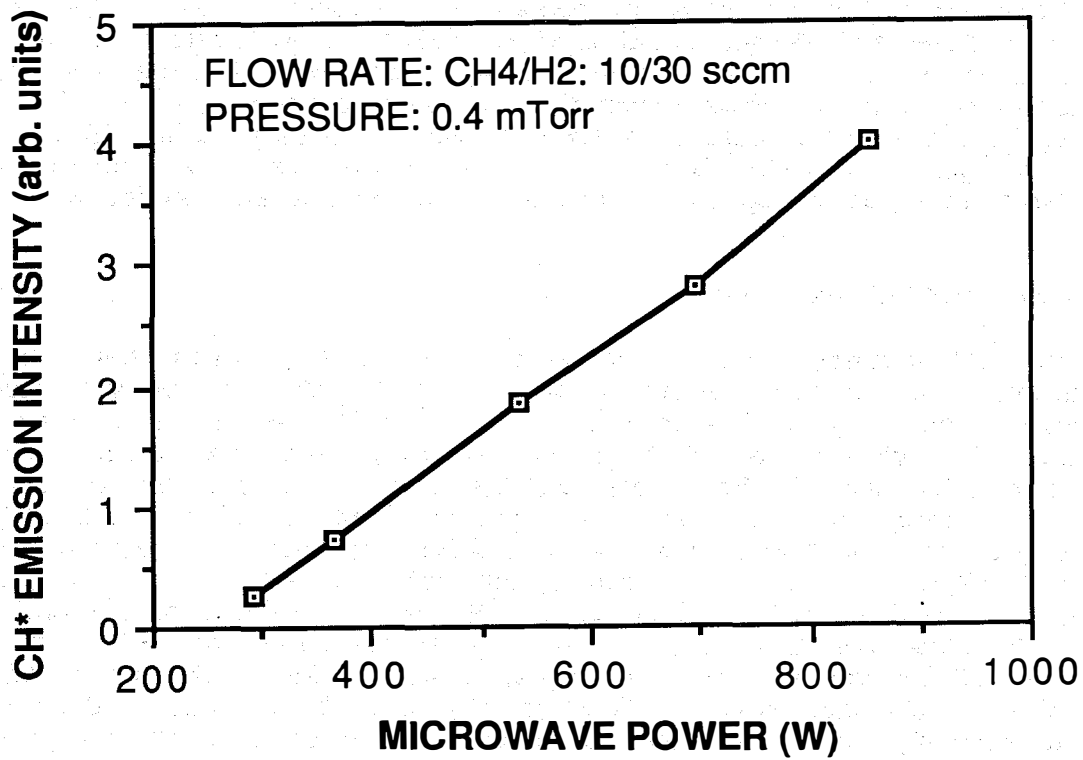


Figure 1. The CH* emission intensity of CH₄ and H₂ mixed gas ECR plasmas as a function of microwavepower.

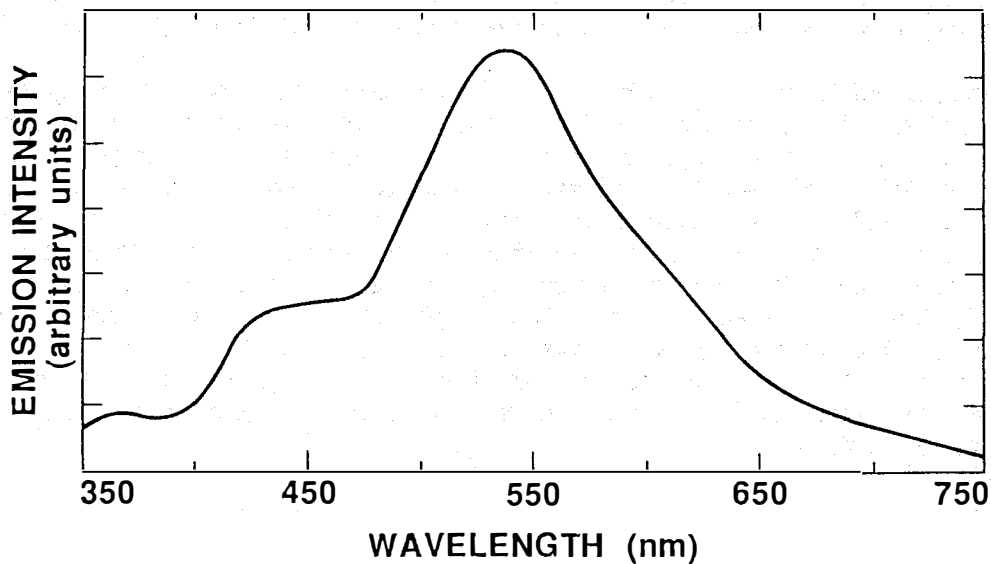


Figure 2. Fluorescent spectrum of ECR-deposited, soft a-C:H films.

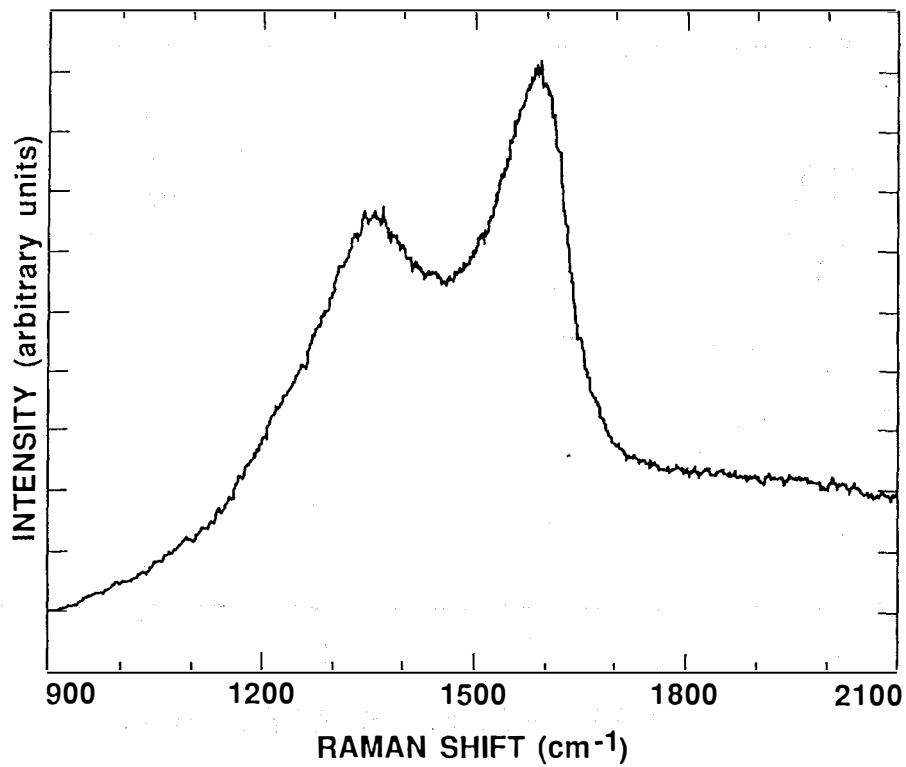


Figure 3. Raman spectrum of ECR-deposited, hard a-C:H films; deposition conditions: flow rates, CH₄ = 20 sccm, H₂ = 20 sccm; microwave power = 360 W; deposition pressure = 4 mTorr; RF bias power = 50 W, self-bias voltage = 5.7 V; substrate temperature = amb.

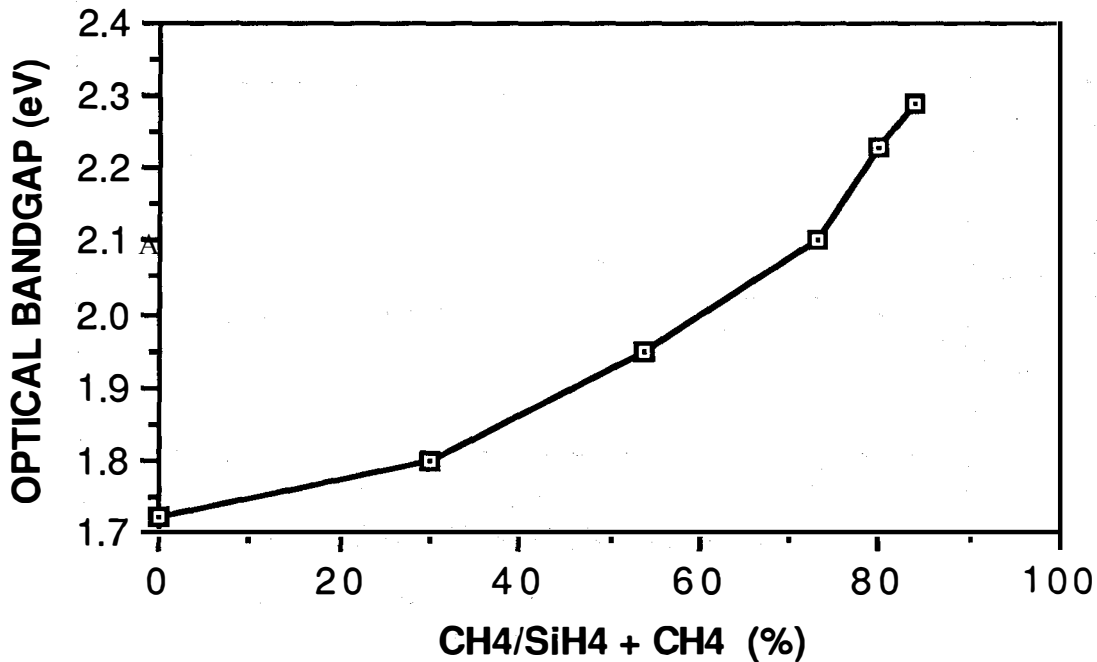


Figure 4. Optical bandgap of RF-deposited a-SiC:H films as a function of the CH₄ gas composition.

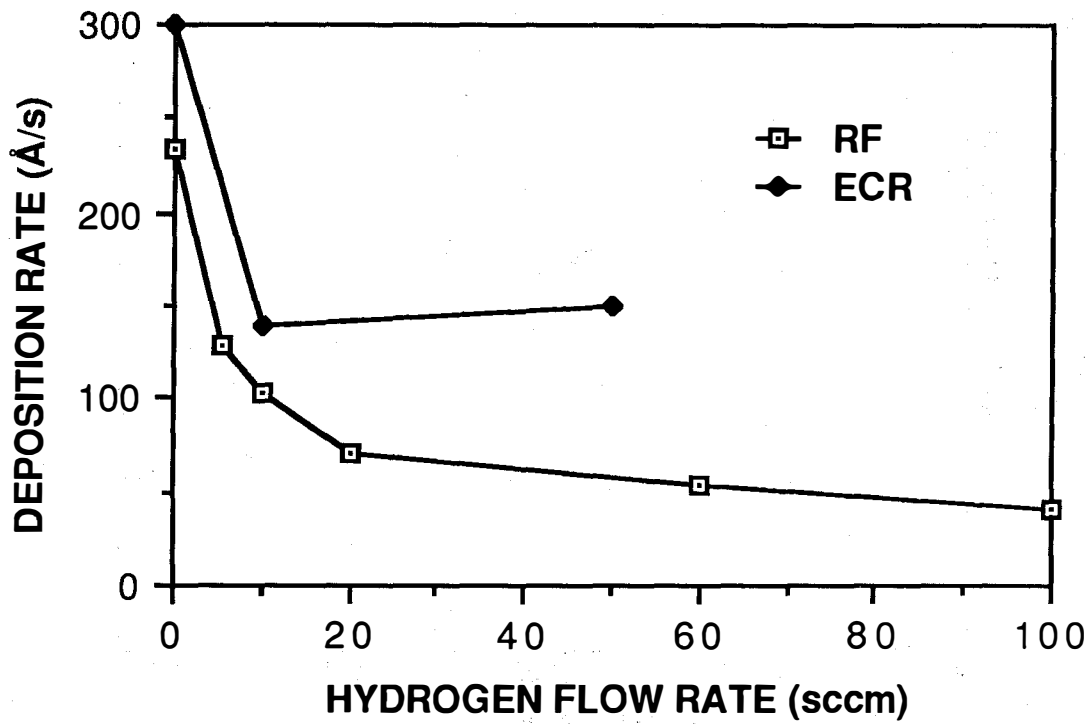


Figure 5. RF glow discharge and ECR deposition rates of a-SiC:H films as a function of the hydrogen flow rate.

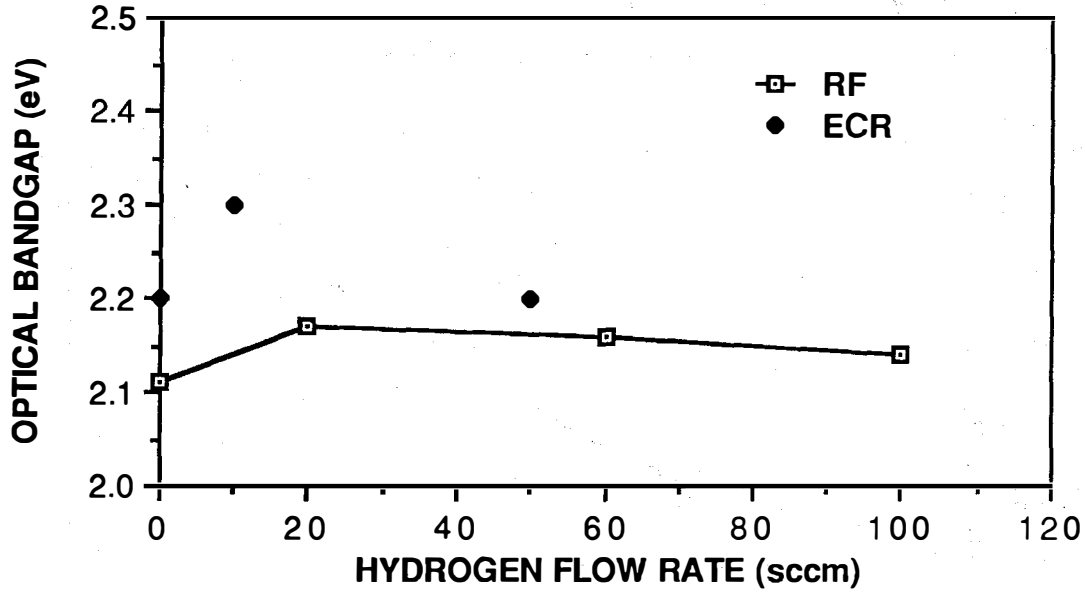


Figure 6. Optical bandgap of ECR- and RF-deposited a-SiC:H films as a function of hydrogen dilution in the plasma.

Title: **Diagnostics of Glow Discharges Used To Produce Hydrogenated Amorphous Silicon Films.**

Organization: National Institute of Standards and Technology, Boulder, Colorado

Contributors: A. Gallagher, D.A. Doughty, J. Doyle.

The overall objective of this work is to explain causes of glow-discharge produced a-Si:H and a-Si:Ge:H film quality, and its dependence on deposition discharge conditions. During this contract period this involved: (1) measuring substrate reaction probabilities, β , of depositing species in silane and silane-germane discharges as a function of conditions, (2) measuring the spatial distribution of deposition $D(x)$ throughout silane, germane and silane-germane discharges under a variety of conditions relevant to a-Si:Ge:H film production, (3) interpreting these measurements to test and improve current deposition models, and explain causes of film-quality variations.

SURFACE REACTION PROBABILITY MEASUREMENT AND INTERPRETATION

The method developed and employed here to measure β is based on analogy to an optical "black-body," in which almost all photons entering a small hole (area A_H) in the side of a large box (surface area A_B) are absorbed before reescape, independent of the exact internal-surface absorption-coefficient k as long as $k A_B/A_H \gg 1$. In the present context this translates into all reactive molecules that pass in through a small hole in the substrate being absorbed inside the "box". In contrast, only a fraction β react on the substrate, so that $\beta = A_H t/T$, where t is the substrate film thickness A_H is the hole area and T is the total film deposited inside the "box".

We have thus measured β , at $T_s = 300$ and 510 K from low-power rf and dc silane, disilane and germane discharges, using stainless-steel electrodes with a 3.8 cm gap and typically 0.15 Torr gas pressure, at discharge powers that yield deposition rates of 0.5-2 Å/s. In essence, these are appropriate conditions for optimum quality intrinsic a-Si:H production. H_2 or F mixtures are preferable for a-Si:Ge:H films, but we did not add these additional complications to the present diagnostics.

We have found that $\beta = 0.3$ to 0.4 for $T = 300$ - 550 K in silane, disilane, and silane/germane discharge deposition of a-Si:H and a-Si:Ge:H, in rf discharges as well in at the substrate of a dc-triode discharge. In a pure-germane rf discharge we obtained $\beta = 0.55$, and at the cathode of a dc silane discharge $\beta = 0.6$.

All of these are surprisingly large β values from the standpoint of prior ideas regarding the cause of film morphology. In particular, Tsai et. al.¹ had observed that discharge conditions (low-power-rf, silane) used to produce high-quality a-Si:H films also produced "CVD-like" trench-filling, apparently corresponding to small β . In contrast, discharge conditions (high-power, SiH_4/Ar) that produce low-quality, columnar films also cause "PVD-like" trench filling, corresponding to $\beta \sim 1$. Previous explanations of this relationship suggested that in the "CVD", small- β case depositing radicals (primarily SiH_3)

sample many surface sites and thereby had an opportunity to fill atomic-scale film-surface valleys. In contrast in the "PVD", $\beta \sim 1$ case depositing radicals (primarily SiH_2) adhere at the point of contact, producing film voids and columns. The present β data has led us to recognize that the key film-quality growth characteristic is actually radical surface diffusion before incorporation, combined with preferential incorporation in atomic-scale valleys. This can be further illustrated as follows.

Due to the stochastic nature of the deposition process, the surface of a growing film contains high points and valleys on an atomic scale. Because the valleys are partially shadowed, they will receive a smaller flux of depositing radicals than the high points for an isotropic incident radical flux. If radicals only stick or bounce from the initial point of contact, the high points will then propagate faster and cover the valleys, forming voids. This will occur regardless of the size of β , because the relative probability of striking a high point rather than a valley is independent of how many times each radical strikes the surface before reacting. Thus, it appears that no value of β can produce compact films if the film-producing radical reacts at the initial point of contact. This conclusion is supported by calculations of the effect of surface diffusion on surface roughness.² (Of course, energetic ion bombardment can compact films that would otherwise be porous,³ but overall quality is still relatively poor.)

How, then, are relatively void-free, high-quality films produced by neutral radical deposition when $\beta \approx 0.4$? The crucial point is that β is the probability that an incident radical reacts with the surface, but it is not necessarily the probability of reacting at the initial point of contact. Similarly, $1-\beta$ is the probability that the radical is reemitted from the surface, but not necessarily the probability of direct reflection from the initial point of contact. When a radical encounters the surface it may be reflected or adsorbed. If this is a free radical such as SiH_3 and the surface site does not contain a dangling bond, then no chemical bond will form and the radical will be physisorbed to the surface (it cannot exothermically react with the H-passivated film surface). Once adsorbed, the free radical can more easily diffuse about the surface than desorb, and it will preferentially dwell in the valleys where it is more strongly bonded. The position of initial surface contact then becomes irrelevant, as many diffusion steps can occur before a deposition reaction occurs. Dangling bonds as well as adsorbed free radicals can surface diffuse, and they will also dwell preferentially in valleys. Chemical (Si-Si) bonding occurs when a dangling bond and adsorbed SiH_3 meet, and this will occur preferentially in valleys. Thus, the radical characteristic that determines film quality is surface diffusion before incorporation. In the "CVD-like" case physisorbed free radicals (primarily SiH_3) diffuse about the surface filling in the shadowed valleys. In the PVD-like case the SiH_2 radicals primarily responsible for film growth can insert directly into an H-passivated surface site, so that film growth tends to occur at the initial point of contact with little radical surface diffusion. In all cases a fraction of the radicals will reflect without adsorption or reaction, but this will not effect film morphology.

Our studies of laser-scattering from a-Ge:H films produced in pure GeH_4 discharges indicate that, in contrast to a-Si:H from SiH_4 discharges, a microscopically rough surface is produced. This and the larger β value for the germane case suggest that poor a-Ge:H film quality occurs because the

depositing GeH_n radical is not diffusing sufficiently before incorporation. The improvement generally obtained in H_2/GeH_4 discharges is then probably due to H and H^+ etching of this poorly structured Ge surface.

DISCHARGE STOICHIOMETRY

We have measured and analyzed the stable gases production in discharges of silane, germane, disilane and mixtures thereof. By measuring the ratios of film and product-gas production/primary gas depletion in static chambers we have inferred many dissociation and reaction pathways. As an example, in SiH_4 discharges the saturated higher silanes (Si_2H_6 , Si_3H_8 , etc.) are produced by SiH_2 reactions with SiH_4 , hence they trace the proportion of SiH_2 produced in the initial SiH_4 dissociation. Film, on the other hand, is produced by SiH_3 deposition so it traces the H and SiH_3 products of the initial SiH_4 dissociation. (H converts to SiH_3 by the $\text{H} + \text{SiH}_4 \rightarrow \text{SiH}_3 + \text{H}_2$ reaction). From the $t \rightarrow 0$ limit of the measured ratios, corresponding to a pure SiH_4 discharge, we find that the primary initial dissociation channel is $\text{SiH}_4 \rightarrow \text{SiH}_2 + 2\text{H}$. Although this rf-discharge dissociation is caused primarily by electron collisions, this result is very similar to that found in UV photodissociation.⁴ This similarity is quite reasonable, since both dissociations occur by predissociation from the manifold of electronically-excited SiH_4 states between 8 and 11 eV.

Another result is that a major fraction of film growth in silane discharges normally results from disilane dissociation by H-atom reactions, where the disilane was initially produced by the $\text{SiH}_2 + \text{SiH}_4$ reaction. Nonetheless, free radicals (SiH_3 and Si_2H_5) dominate deposition for normal conditions. In GeH_4 discharges, much less Ge_2H_6 and more film occurs compared to the silane case. This suggests that most GeH_2 from the initial dissociation may reach the surface and incorporate as film, in contrast to the silane case where almost all SiH_2 reacts to form Si_2H_6 before reaching a surface. This further suggests that the higher β and poorer film morphology of the a-Ge:H films may be due to GeH_2 induced growth that occurs without surface diffusion. The spatial distribution of depositing radicals in GeH_4 rf discharges is somewhat different than in SiH_4 , but in both cases a diffusing, relatively non-reactive radical is indicated by our data.⁵ But, whereas this is known to be SiH_3 in silane, the above analysis suggests that it may be primarily GeH_2 in the germane case, due to a much slower GeH_2 gas reaction rate.

1. Z C.C. Tsai, J.C. Knights, G. Chang, and B. Wacker, J. Appl. Phys. 59, 2998 (1986).
2. + M.J. McCaughey and M.J. Kushner, J. Appl. Phys. 65, 186 (1989).
3. Z B. Drevillon, J. Perrin, J.M. Siefert, J. Huc, A. Lloret, G. deRosny, and J.P.M. Schmitt; Appl. Phys. Lett. 42, 801 (1983).
4. 0 G.G.A. Perkins, E.R. Austin, and F.W. Lampe, J. Am. Chem. Soc. 101, 1109 (1979).
5. Z D.A. Doughty and A. Gallagher, J. Appl. Phys., to be published.

Title: **Research on Stable, High-Efficiency, Large Area, Amorphous Silicon Based Submodules**

Organization: Solarex Thin Film Division
826 Newtown-Yardley Road
Newtown, PA 18940

Contributors: A. Catalano, Principal Investigator; R.R. Arya, M.S. Bennett, B. Fieselmann, B. Goldstein, J. Morris, J. Newton, R.S. Oswald, R. Podlesny, S. Wiedeman, A. Wilczynski and L. Yang

Objective

The major objective of the present program is to demonstrate a conversion efficiency of at least 14% for a large area ($\geq 900 \text{ cm}^2$) multijunction submodule.

Subtask B1: Semiconductor Materials Research

Doping

Trimethylboron (TMB) has proved to be a superior dopant for a-SiC:H p-layers. A 0.1 eV increase in optical bandgap has been found for these films compared to control films doped with diborane. Small area ($< 1 \text{ cm}^2$) devices have exhibited open circuit voltages as high as 0.943 Volts and unoptimized devices have yielded AM1.5 conversion efficiencies as high as 11.4%. Table I compares device performance to a diborane doped control, and compares the properties of the doped films.

a-SiGe:H Alloys

Deposition of a-SiGe:H alloy films from the hydrogen diluted feedstock yields diffusion lengths approximately 200Å larger over a wide range of bandgap (1.7 eV - 1.38 eV). In general, the hydrogen diluted silicon-germanium alloys appear to be more stable than their undiluted counterparts as shown in Figure 1. The Urbach Energy determined from Photothermal Deflection Spectroscopy is low and increases little with decreasing bandgap. The midgap density of states does not appear to increase with Ge content but a large thickness dependence in Urbach Energy midgap state density and diffusion length has been found which suggests that these measurements are strongly affected by surface recombination.

Boron doping has a marked effect on the photoconductivity and diffusion length, L of a-Si:H and the a-SiGe:H alloys. An increase in L occurs for low levels of B-doping up to about 0.4 and 0.2 ppm for a-Si:H and 1.6 eV a-SiGe:H. A concurrent minima in photoconductivity is also found. Taken together this indicates a transition from hole to electron minority carrier transport. Comparing the results of a-Si:H to 1.6 eV a-SiGe:H shows that the $\mu\tau$ product of electrons decreases much more than that for holes as Ge is added. No discernable effect is seen for 1.45 eV alloys.

The intensity dependence of the photoconductivity is consistent with the existence of "safe hole traps". At higher dopant concentrations ($> 1 \text{ ppm}$) the diffusion length (of electrons) increases

with light intensity. This suggests that at higher light intensity, the quasi Fermi level uncovers a trap near the valence band edge which more effectively traps holes and acts as a sensitizing center for electrons, leading to an effective higher electron diffusion length. Since this is only seen in B-doped films, it suggests the defect is related to the dopant. In contrast, the photoconductivity which represents the majority carrier (holes) decreases with increasing light intensity consistent with this model.

Microcrystalline alloys for tunnel junctions continue to be of interest although device results have so far been disappointing. Extensive optical measurements indicate only a factor of 2 decrease in the optical absorption coefficient. However, initial results indicated that this advantage is lost because of the necessity of having to grow a much thicker n+ layer to achieve microcrystallinity. By varying deposition conditions it was possible to achieve the necessary high conductivity films in only 100Å. Increases in the open circuit voltage of close to 0.1 V were obtained in tandem a-Si/a-Si devices.

Subtask B2: Non-Semiconductor Materials Research

ITO/Ag Rear Contacts

A major part of the Subtask B2 activity has been directed at the scale up of reactively sputtered ITO for submodules over 900 cm². Initial problems with non-uniformity lead to premature erosion of the indium-tin targets at the edges. This was corrected by adjusting gas flow geometry and target magnet arrangement, leading eventually to satisfactory, uniform ($\pm 5\%$) films with contact resistances low enough to sustain the necessary 70% + fill factors required for high performance submodules. The index of refraction of films was also found to be high (~ 2.0) reducing reflectivity at the a-Si:H/ITO interface; this was corrected by adjusting the gas composition and thermal post deposition annealing schedule.

A spray-on rear encapsulant, which is easily automated, is low cost and has passed all environmental tests for durability, has been developed. This encapsulant replaces the EVA/Tedlar and tape encapsulants presently in use.

Subtask B3: Submodule Research

Computer-assisted modeling has taken place on two levels - cell design to itemize losses in multi-junction cells and module design to determine the origin and magnitude of resistive losses. Figure 2 illustrates the light losses in a triple junction solar cell. The model accurately accounts for the effects of scattering, including that occurring at interfaces within the device. As noted in the illustration, major losses are associated with the front surface, e.g. glass/air, tin oxide and p-layer. The first tunnel junction also accounts for significant losses.

The module design program accounts for interconnect resistance, sheet resistance losses, geometric losses and other effective series resistance sources. Figure 3 plots the fraction of power loss in triple junction submodules with $V_{mp} = 2.000$ V, $J_{mp} = 0.006$ A/cm² as a function of segment width for several front surface sheet resistance values.

Table II summarizes the single tandem and triple junction cell results. Single junction cells with a conversion efficiency of 12% have been obtained using high reflectivity rear contacts and graded interface layers. Tandem junction cells comprised of a-SiC:H top junction and a-SiGe:H bottom junction have achieved efficiencies as high as 10.5%. Triple junction cells with a-SiC:H top junctions, a-Si:H middle and a-SiGe:H have attained an efficiency of 10.7%.

In order to prepare high efficiency cells and submodules ITO/Ag rear reflecting contacts have been utilized. In order to fabricate submodules, it has been further necessary to develop an effective method of reliably laser scribing the ITO/Ag film. This has proven to be a difficult but tractable problem. Problems have included metal bridging of the scribe (shunts) and delamination of the silver (high series resistance). Nonetheless, by careful control of film thicknesses and preparation conditions, as well as laser power and feed rate, satisfactory interconnects are routinely made.

Table III summarizes the performance values obtained for interconnected submodules. A conversion efficiency of 9.36% aperture area and 10.2% active area were under global AM1.5 illumination for single junction submodules (area > 900 cm²). Triple junction submodules with an aperture area efficiency of 8.2% and 8.5% active area were measured outdoors (area > 900 cm²). This submodule utilized a cell design of 1.85 eV a-SiC/1.78 eV a-Si:H/1.38 eV a-SiGe:H. Smaller area submodules (~37 cm²) yielded a conversion efficiency of 9.16% active area, 8.5% aperture area.

A dual source simulator has been developed to overcome the inherent inaccuracies in using a filtered Xenon source which contains insufficient output at long wavelengths. We have modified a conventional Oriel simulator by including via a dichroic mirror, an incandescent source to compliment the Xenon source in the red. By regulating the power to each source, a good match is obtained between the simulator and the global AM1.5 spectrum as shown in Figure 4.

Table I

Comparison of Diborane and TMB Doped P-Layers and Devices

	<u>Solar Cell Properties</u>				<u>p-layer Bulk Properties</u>	
	<u>Voc</u>	<u>Jsc</u>	<u>FF</u>	<u>Eff</u>	<u>B conc., cc atoms</u>	<u>Bandgap, eV</u>
TMB	0.917	16.9	0.736	11.4	5X10 ¹⁹	2.14
diborane	0.850	16.8	0.731	10.4	5X10 ¹⁹	2.06

Table II
Photovoltaic Parameters of
Amorphous Silicon Based Solar Cells

Material	Junction(s)	E _g (eV)	V _{oc} (V)	J _{sc} (mA/cm ²)	FF	η (%)
a-Si	Single	1.7	0.891	19.13	0.70	12.0
a-Si(TMB)	Single	1.70	0.917	16.90	0.736	11.4
a-SiC	Single	1.8	0.880	9.59	0.704	5.9
a-SiC	Single	1.85	0.932	9.44	0.670	5.9
a-SiC	Single	1.90	0.952	9.52	0.605	5.5
a-SiGe	Single	1.61	0.851	19.34	0.654	10.8
a-SiGe	Single	1.55	0.823	20.08	0.611	10.2
a-SiGe	Single	1.50	0.752	19.50	0.547	8.0
a-Si/a-Si	Tandem	1.7/1.7	1.69	8.3	0.710	10.0
a-SiC/a-Si	Tandem	1.85/1.7	1.75	8.16	0.712	10.2
a-SiC/a-SiGe	Tandem	1.85/1.55	1.72	9.11	0.670	10.5
a-SiC/a-SiGe	Tandem	1.85/1.50	1.52	10.2	0.677	10.5
a-SiC/Si/SiGe	Triple	1.85/1.7/1.55	2.481	4.99	0.669	8.3
a-SiC/Si/SiGe	Triple	1.85/1.7/1.45	2.172	7.30	0.642	10.2
a-SiC/Si/SiGe	Triple	1.85/1.7/1.40	2.38	7.01	0.64	10.7*

* measured outdoors

Table III
Photovoltaic Parameters of a-Si:H Based Submodules

Material(s)	# of Segments	V _{oc} (V)	I _{sc} (mA)	FF	η _{active} (%)	η _{aperture} (%)	Power (W)	Active Area (cm ²)	Aperture Area (cm ²)	Measured At
a-Si:H	12	10.428	53.07	0.6660	10.10	9.29	-	36.60	39.78	Solarex
Single Junction Submodule	12	10.590	53.37	0.6595	10.18*	9.40	-	36.60	39.78	SERI
	50	44.201	302.00	0.6560	10.20	9.36	8.80	859.50	936.36	Solarex
	50	42.316	300.00	0.6700	9.86*	9.06	8.48	859.50	936.36	SERI
a-SiC/a-Si/a-SiGe	6	13.619	40.30	0.6100	9.00	8.38	-	37.20	39.96	Solarex
Triple Stack Submodule	6	13.630	41.23	0.6050	9.16*	8.50	-	37.20	39.96	SERI
	15	30.920	380.00	0.6600	8.50**	8.20	7.85	908.00	938.00	Solarex

* Calculated

** Outdoor Measurements

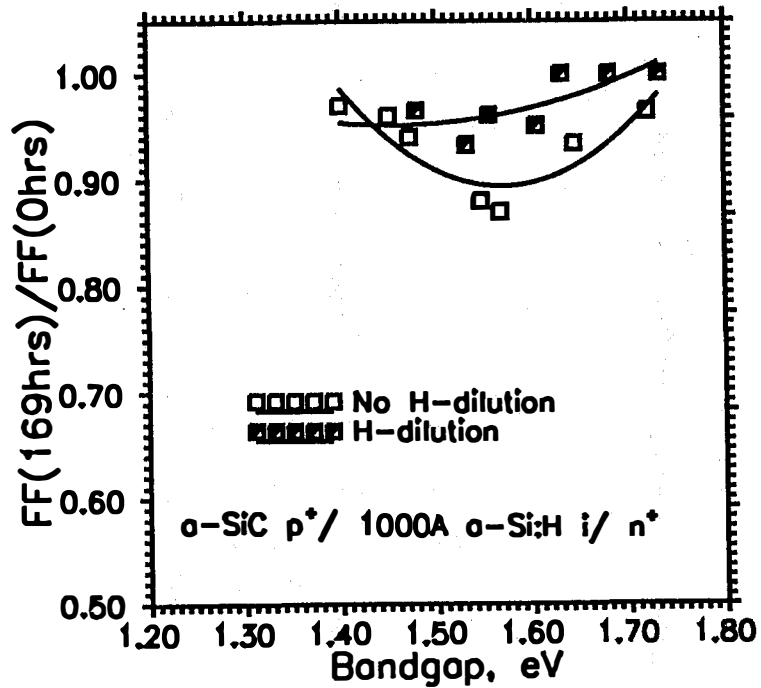


Figure 1. Comparison of the rates of degradation of fill factor of silicon-germanium alloy devices prepared with and without hydrogen dilution

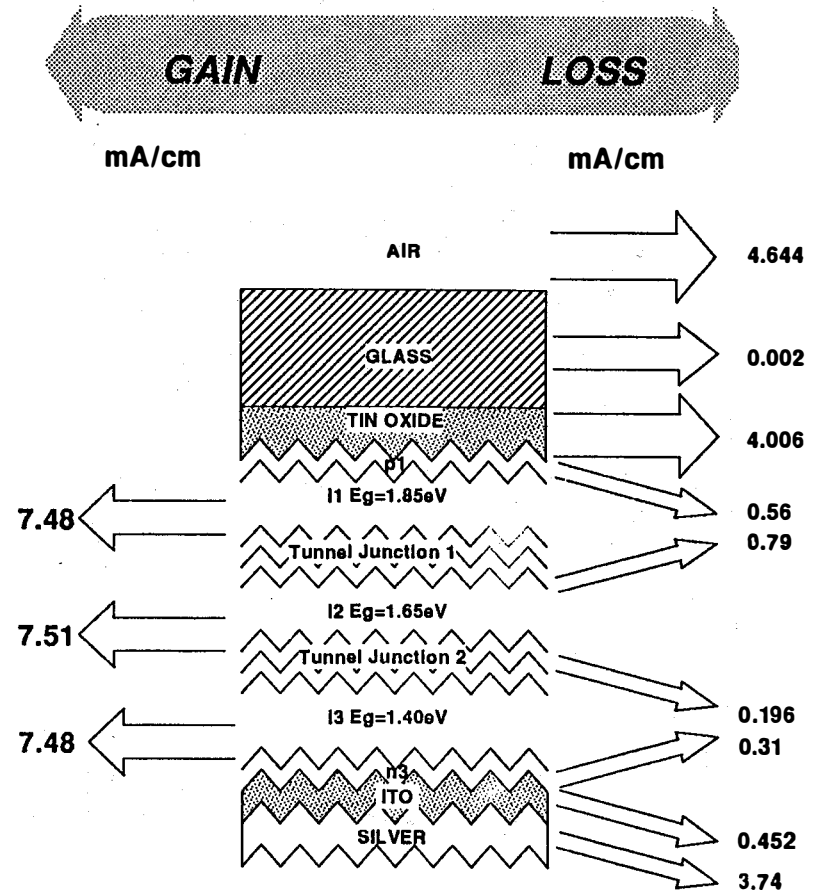


Figure 2. Calculated light losses for a triple junction a-SiC:H/a-Si:H/a-SiGe:H device

Power Losses in Stacked Submodules Fraction Lost vs Stripe Width

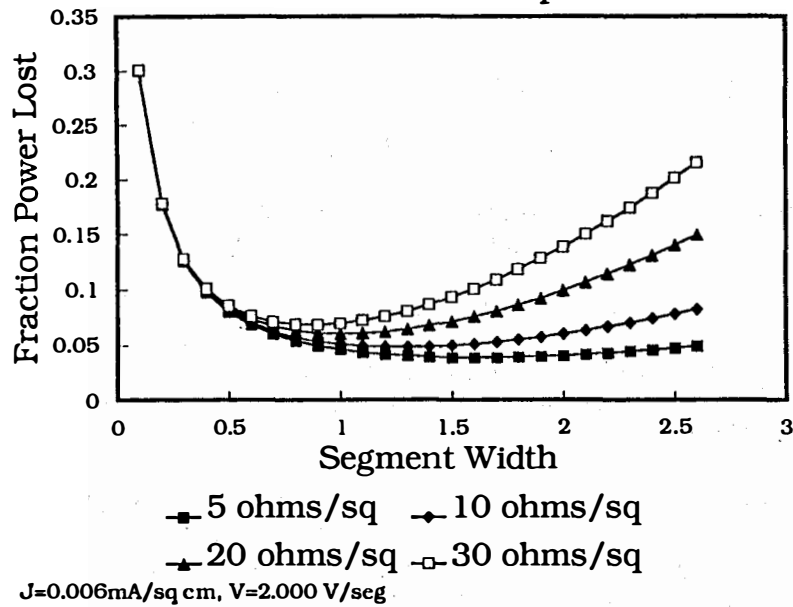


Figure 3. Fraction power lost vs. segment width for triple junction submodule

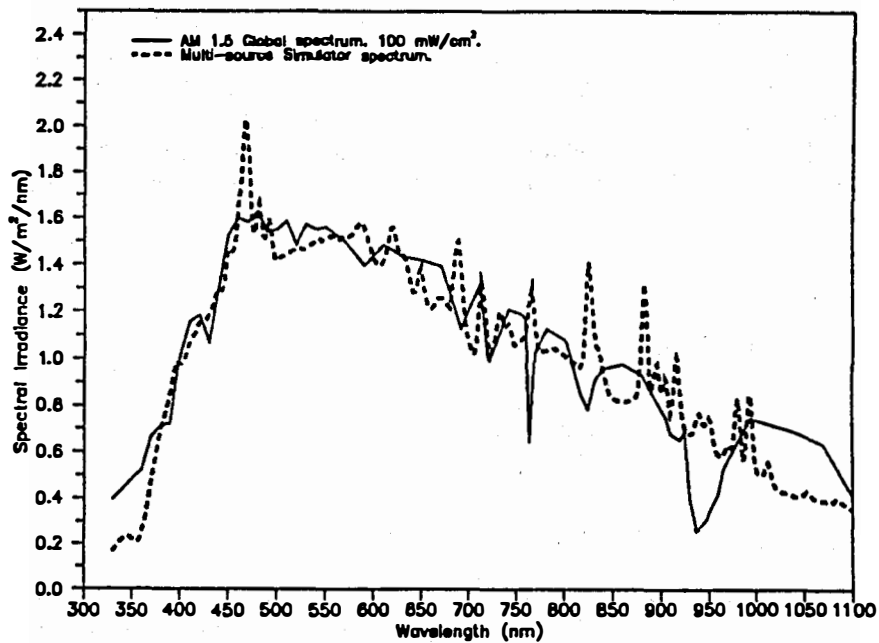


Figure 4. A comparison between the AM1.5 Global spectrum and the measured spectrum of the Solarex dual source simulator

Title:

Organization: Department of Physics and Astronomy
University of North Carolina
Chapel Hill, North Carolina 27599-3255

Contributors: Professor M. Silver; Drs. Daching Han, Keda Wang, M. E. Zvanut and Mr. M. Kemp

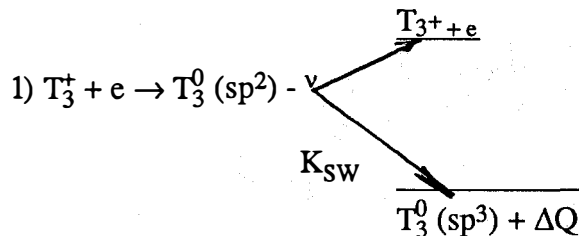
The objectives of our research program were to evaluate the relative effects of neutral and charged defects by theoretical and experimental means. In this endeavor, we collaborated with many other groups. Our most extensive work was with Howard Branz of S.E.R.I. We also worked closely with Professor Bassler of the University of Marburg FRG and were kindly supplied with samples from Alan Delahoy of Chronar.

Perhaps the most important theoretical results were the prediction that copious amounts of charged defects (T_3^+ can co-exist with neutral dangling bonds and that these charged defects can be responsible for the exponential band tails. We further found a reasonable mechanism for metastability based on the photo-neutralization of the charged defects by excess carriers.

Experimentally, from a study of forward bias currents on p/i/n devices we believe that we have measured the temperature for a transition from band motion to hopping.

Theoretical Research

The basic idea for the high density of charged defects comes from the inclusion of short range ($\sim 20 \text{ \AA}$) potential fluctuations due to inhomogeneities in the energy of formation of defects. If the r.m.s. value $\langle \Delta V \rangle$ of the fluctuation is greater than the correlation energy, U_{eff} then the film can lose energy by transferring an electron from a defect in a region of low electrostatic energy to a region of high electrostatic energy. This is illustrated in the cartoon in figure 1. Further we show a possible mechanism for the Staebler-Wronski effect by noting that when an electron (for example) is captured by a T_3^+ , in an sp^2 state, then there may be a rehybridization with a change in energy to a T_3^0 in an sp^3 state. Kinetically this may be seen by the following rate equation



and where the efficiency for the defect formation is approximately K_{SW}/ν .

Figure 2 shows the results of computer simulations on the width of the band tails due the random charged defects as a function of the dielectric constant ϵ and the mean distance, a , between Anderson localized states due to the very short range ($\approx 2 \text{ \AA}$) disorder. The more compact are the Anderson localized states, the wider is the band tail.

Experimental Results

We studied the transient behavior of the forward bias current in p/i/n structures. The final current is proportional to:

$$2) i_f \propto CV (b_c \mu / b_n^2)$$

There is an earlier minimum current which is proportional to:

$$3) i_{\min} \propto CV$$

Thus, the ration of the currents i_f/i_m yield information on μ , the mobility at the transport level, b_c , the capture rate constant to an occupied recombination state and b_n , the capture rate constant to an unoccupied recombination center. One predicts that with band motion $\mu b_c/b_n^2$ can be large while in the hopping regime, $\mu b_c/b_n^2$ is of order 1. Figure 3 shows the ratio i_f/i_{\min} vs T as can be seen there is a sharp drop at around 140°K. We suggest that this is due to a change in the transport mechanism.

Publications

"Drift Mobilities Far from Thermal Equilibrium in Hydrogenated Amorphous Silicon (with E. Schiff) Amorphous Silicon and Related Materials, World Scientific Singapore, Ed. Hellmut Fritzsche, 825-852 (1989).

"Comments on Electron Drift Mobility in Doped Amorphous Silicon" (with H. Overhof), Phys. Rev. B 39, 10426 (1989).

"Experiment and Discussion on Electron Mobility in Amorphous Silicon" (with G. Winborne, L. Xu), Phil. Mag. Lett. 59, 197 (1989).

Papers Submitted for Publication

"Current-Voltage Characteristics - What do Experiments Really Tell Us?" (with Finley Shapiro), to be published MRS 1989.

"Electronic Transport at Low Temperatures in Amorphous Silicon" (with W. E. Spear) to be published MRS 1989.

"Comment on Electronic Transport at Low T," to be published.

"On the Origin of Exp. Band Tails, " Sol. Stat. Comm.

"Simulation of the Effects of Capture Rates on Transient Currents," ICALS 13.

"Charged Dangling Bonds," ICALS 13.

"A Unified Model Based on Charged Dangling Bonds," ICALS 13.

"Low T Transport in a Si:H," 3rd Hopping Conference.

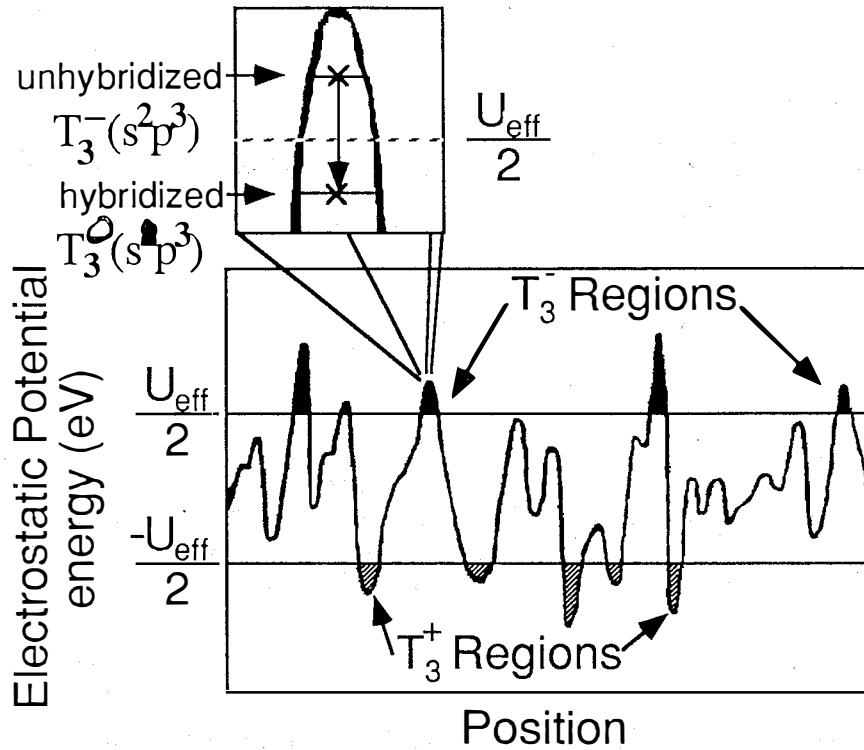


Figure 1. Schematic diagram showing inhomogeneous potential fluctuations in comparison with the magnitude of the energy (U_{eff}) needed to doubly occupy a defect. The insert shows the difference in energy between the lowest energy state for an occupied (T_3^-) and a rehybridized unoccupied neutral (T_3^0) state.

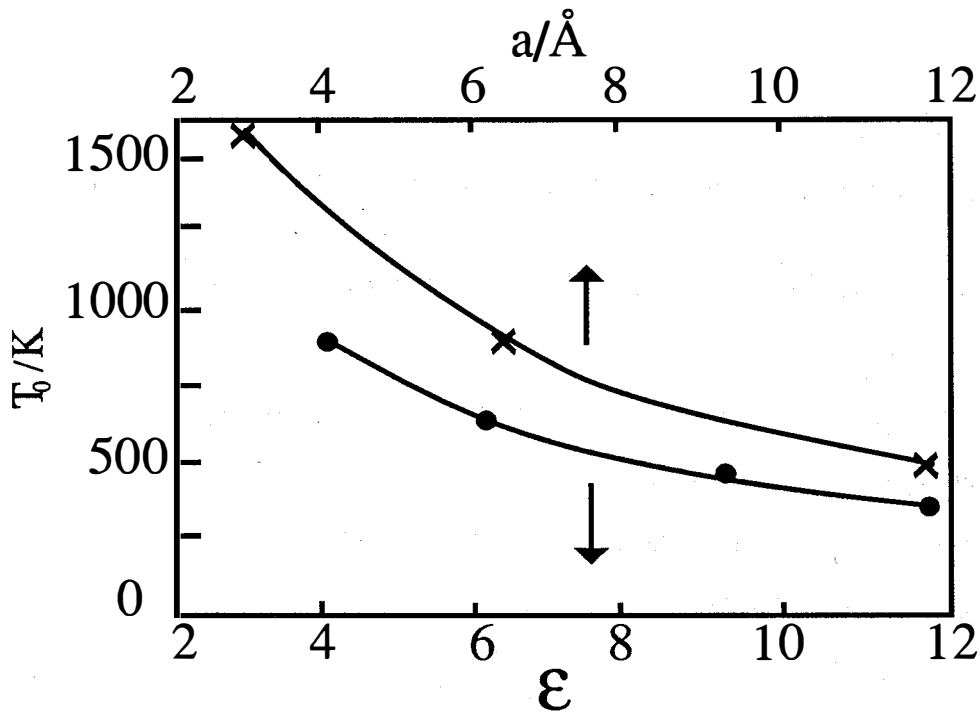


Figure 2. The computed width (kT_0) of a band tail vs the dielectric constant, ϵ , and the mean distance, a , between localized states.

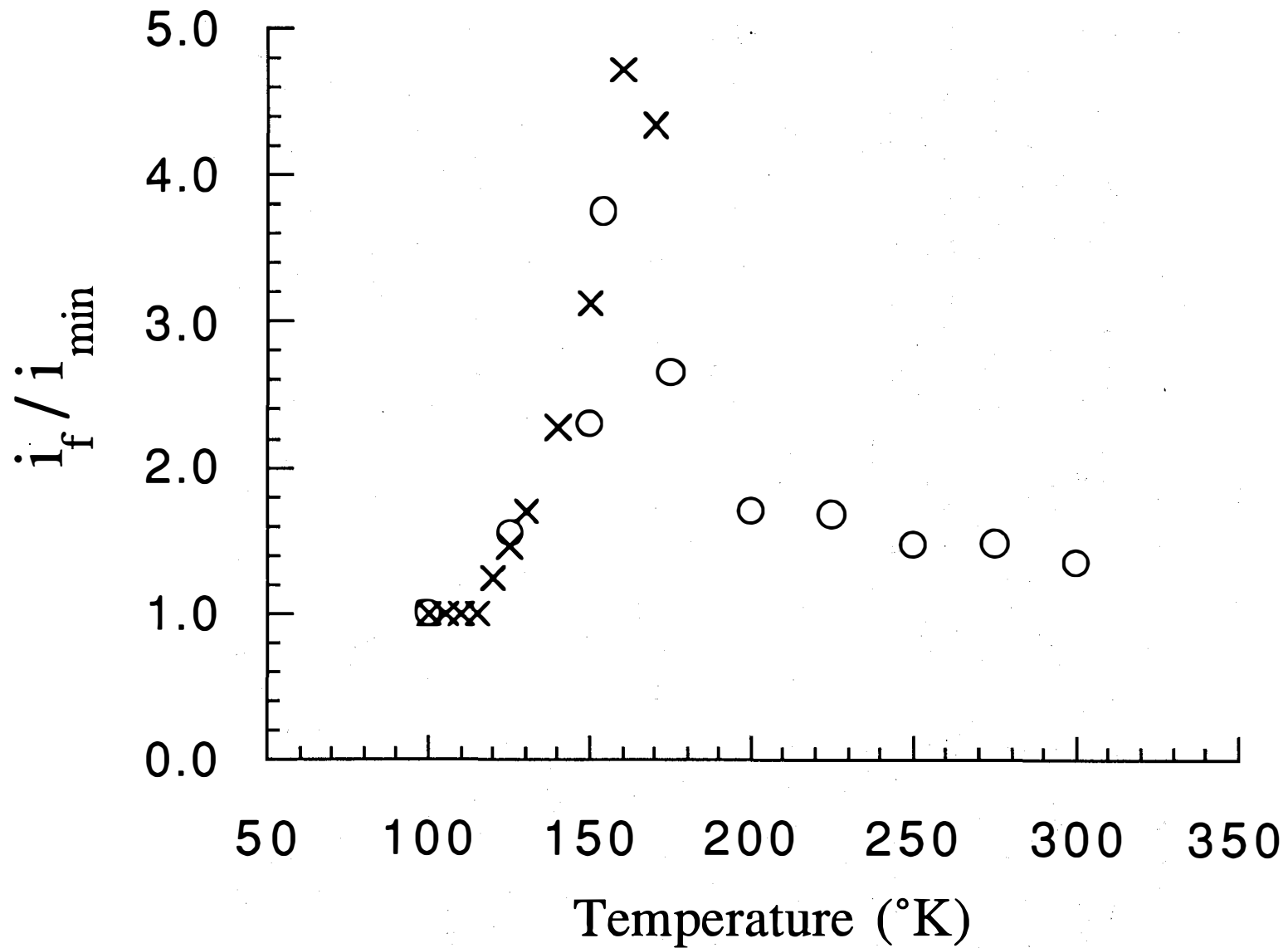


Figure 3. Measured ratio of forward bias transient currents vs T. The sharp drop at approximately 140 $^{\circ}\text{K}$ indicate a transition from band motion to hopping.

Title: Investigations of the Origins of Light-Induced Changes in Hydrogenated Amorphous Silicon

Organization: University of Oregon, Eugene, Oregon

Contributors: J. David Cohen (Principal Investigator), John M. Essick, Tom Leen, Thomas Unold

Distinguishing Among Proposed Defect Reactions for Metastable Effects in n-type a-Si:H

The photoinduced increase in the midgap region of the density of states in undoped a-Si:H is generally attributed to a creation of dangling bond defects induced when the recombination of photoinduced carriers breaks weak Si-Si bonds. In the case of *doped* films, however, the situation may be more complicated since we can also have activation or deactivation of dopant atoms. During the previous year (FY1988) we had investigated metastable states produced by prolonged light exposure and partial annealing. During the past year we have expanded our studies to look at metastable changes due to quench cooling and bias annealing in such samples. In all such studies we document the changes that occur both in the occupied bandtail (N_{BT}) states and also dangling bond defects (N_D). Correlations in the changes in N_D and N_{BT} can be used to distinguish among various defect reactions that have been proposed to explain the metastable changes in n-type doped films.

To determine the conduction bandtail occupation of states we used drive-level profiling measurements as described previously.^{1,2} Specifically, for a 10 kHz measurement frequency and a 250K temperature this method gives explicitly the value of the integral of the occupied states from the bulk Fermi level down to an energy of roughly 0.4 eV below E_C . The change in the number of deep gap states, N_D , was studied by the voltage pulse transient photocapacitance technique.^{3,4} Such spectra appear qualitatively similar to and are interpreted in our study like sub-band-gap optical absorption spectra.

In Fig. 1 we compare photocapacitance spectra for a set of different metastable states of a 300 ppm PH_3 doped sample: a light soaked state, a dark annealed but slow cooled state (state A), as well as a fast quenched annealed state. Note that while we observe a substantial increase in the number of deep defects for the light soaked states (by about 10^{17} cm^{-3}), for the fast quenched state we see essentially *zero* change in the deep defect density or shape. At the same time, our drive-level profiling measurements indicate a *decrease* by about $2.5 \times 10^{16} \text{ cm}^{-3}$ in N_{BT} after light soaking but an *increase* of this same amount after fast quenching as compared to state A.

While the changes observed for light soaking in this sample may be adequately explained by a previously proposed defect reaction in which both P_4^+ levels and Si_3^- increase⁵ (this would indeed lead to a small decrease in N_{BT} with a larger increase in N_D as observed), no such reaction can explain the changes observed after fast quenching. We therefore must infer the existence of a defect reaction which can change the doping configuration of phosphorous independent of the changes in the D^- density. We had indeed already proposed such a reaction to explain the details of light-induced metastable changes in lightly doped a-Si:H films.⁶ Thus, in our thermal quenching studies discussed above we find that such a reaction also appears to dominate in metastable changes caused by thermal quenching.

The Carbon Impurity Dependence of Light-Induced Metastable Effects in Undoped a-Si:H

This past year we also began a series of studies employing a-Si:H samples with spatially varying impurity levels to investigate the effects of extrinsic impurities on the light induced defect creation in high quality undoped a-Si:H material. In particular, evidence for a significant role

for carbon impurities at levels below 1at% had been suggested in our own studies⁷ and some earlier studies⁸. However, other recent studies had indicated that only for [C] levels exceeding 5at% would there be a noticeable effect on light-induced degradation.⁹

We grew six a-Si:H samples in which the carbon impurity level was modulated by switching on and off an admixture of CH₄ in our silane glow discharge at roughly 10 minute intervals. Subsequent SIMS analysis disclosed that the actual carbon content in the carbon rich regions of these samples varied from 0.2at% to 2.0at% for CH₄/SiH₄ gas ratios ranging between 4 and 20%. Total modulation periods were 3000 to 4000Å. The results of one such SIMS measurement showing typical impurity profiles is displayed in Fig. 2. Palladium Schottky barriers were then evaporated onto the samples to allow investigation by junction capacitance measurements.

Samples were characterized by drive-level capacitance profiling¹, both in a dark annealed "state A" and a light soaked "state B". For every sample, even at the 0.2at% [C] level, we found a significant increase in the density of light induced metastable defects for the carbon rich region compared to the carbon poor region. For example, we observed roughly 1 to 2 x 10¹⁵ cm⁻³ *extra* light induced defects for the film with 0.2at% [C] modulation, and 1.5 x 10¹⁶ cm⁻³ *extra* defects for the 0.9at% [C] modulated film. Indeed, for the 0.9at% [C] modulated film (see Fig. 3), the defect density after light soaking was nearly *twice* as large in the high [C] regions compared to the low [C] regions compared to only a 25% variation in state A. Note that although the drive-level profiles displayed in Fig. 3 appear to exhibit a "sawtooth" rather than "square-wave" spatial dependence, detailed computer modeling of these data indicate that the variation in deep defect density is indeed nearly constant in each region and thus match the [C] SIMS profiles.

Such studies therefore unambiguously confirm that there is a significant deleterious role of carbon impurities in a-Si:H. We are presently investigating whether there may be other correlations between such increased degradation in these same samples with variations of hydrogen concentration and/or variation in bandtail widths. Further studies are also being planned to similarly investigate the role of other atmospheric impurities on light induced degradation.

References

1. C.E. Michelson, A.V. Gelatos, and J.D. Cohen, Appl. Phys. Lett. 47, 412 (1985).
2. K.K. Mahavadi, K. Zellama, J.D. Cohen, and J.P. Harbison, Phys. Rev. B35, 7776 (1987).
3. A.V. Gelatos, J.D. Cohen, and J.P. Harbison, Appl. Phys. Lett. 49, 722 (1986).
4. A.V. Gelatos, K.K. Mahavadi, and J.D. Cohen, Appl. Phys. Lett. 53, 403 (1988).
5. M. Stutzmann, W.B. Jackson, and C.C. Tsai, Phys Rev. B32, 23 (1985).
6. A.V. Gelatos and J.D. Cohen, Mat. Res. Soc. Symp. Proc. 118, 141 (1988).
7. J.D. Cohen, A.V. Gelatos, K.K. Mahavadi, and K. Zellama, Solar Cells 24, 299 (1988).
8. See, for example, R.S. Crandall, D.E. Carlson, A. Catalano, and H.A. Weakliem, Appl. Phys. Lett. 44, 200 (1984).
9. A. Skumanich and N.M. Amer, Phys. Rev. B37, 8465 (1988).

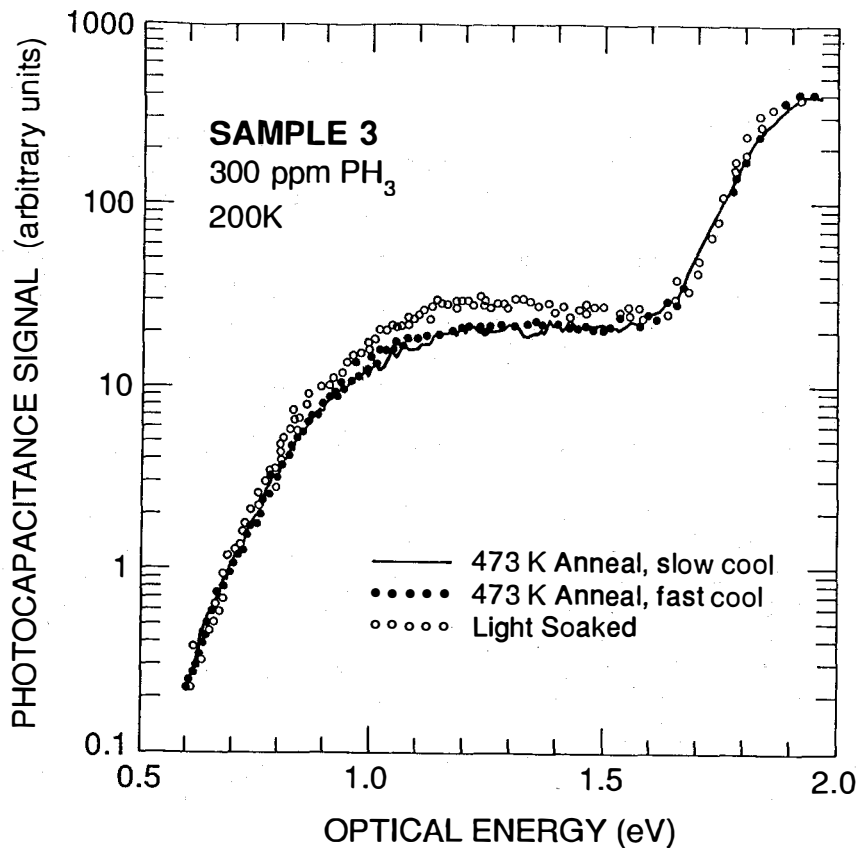
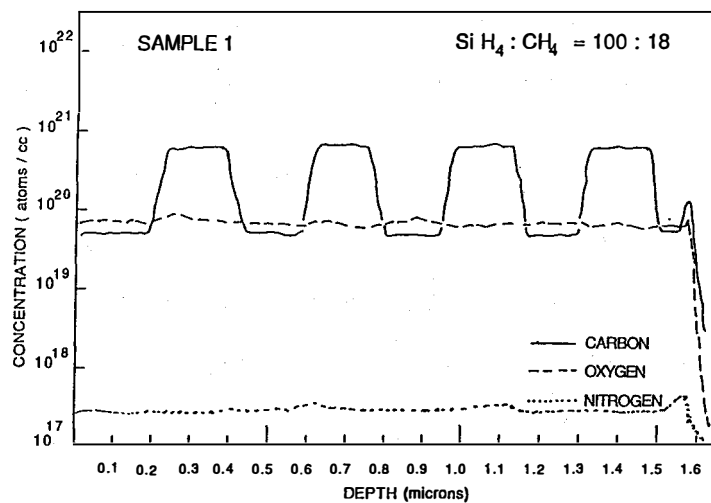


FIG. 1. Voltage pulse transient photocapacitance spectra for a 300 Vppm PH₃ sample in a slow cooled annealed state (solid line), a fast cooled annealed state (solid circles), and a light-soaked state (open circles). "Fast" and "slow" cooling rates from 200°C were 0.1°C/s and 7°C/s, respectively. Note the significant change in the deep defect signal after light soaking and the almost insignificant change between the fast and slow cooled anneal states. Nonetheless, the concentration of occupied conduction bandtail states, N_{BT} , determined by drive-level capacitance profiling, differs significantly between all 3 metastable states.

FIG. 2. A typical SIMS analysis profile for a film grown with a modulated admixture of CH₄ into a SiH₄ discharge at the 18% level. This has resulted in an *actual* carbon modulation within the film at the 0.9at% level.



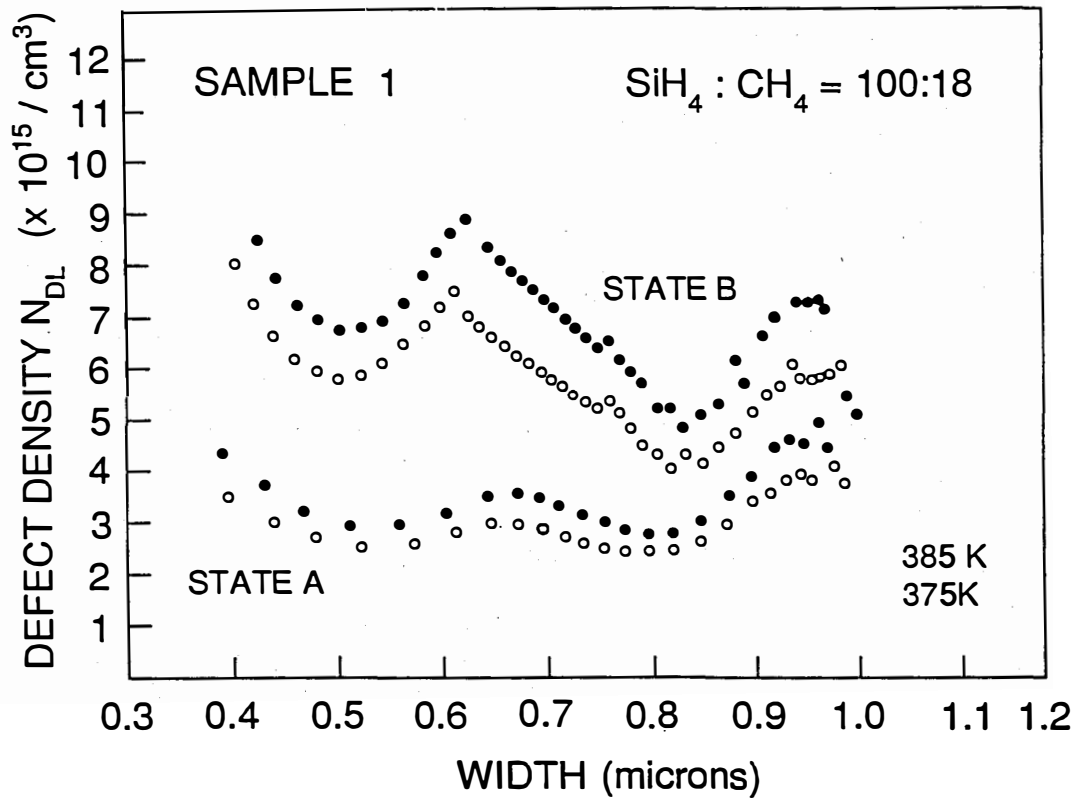


FIG. 3. Variation of the drive-level capacitance density with profiling distance in the 0.9at% [C] modulated sample for the dark annealed (state A) and light-soaked (state B) metastable states. For each state profiles are displayed for two different measurement temperatures.

Title: Structure of Amorphous Silicon Alloy Films

Organization: Department of Physics, Washington University, St. Louis, Missouri

Contributors: R. E. Norberg and P. A. Fedders, principal investigators

The principal objective of this work has been to improve our understanding, at the microscopic level, of the structure of amorphous silicon-germanium alloy films by means of joint theoretical and experimental approaches to the correlation of results of nuclear magnetic resonance, electron spin resonance, transmission electron microscopy, and other measurements. A major focus of the work is the examination of significant rearrangements of hydrogen that take place under various deposition and postdeposition conditions.

Approach

Deuteron magnetic resonance (DMR) has been used to examine the structure of plasma-deposited film samples of a-Si:D,H; a-Si:D; a-Ge:D,H; and a-SiGe:D,F prepared [1] at Harvard by W. Paul and W. Turner. The results have been compared with DMR data obtained in samples provided by other laboratories including Xerox PARC (J. B. Boyce, et al.) and Xerox Webster (S. Kaplan, F. Jansen, and M. Machonkin). DMR resolves and quantifies spectral components for tightly bound deuterium (TBD), weakly bound deuterium (WBD), rotating silyl groups, molecular D₂ and HD in microvoids, and molecular D₂ and HD trapped in ≤ 4 Å nanovoids. Calculations concerning strain effects on defect states are compared with electron spin resonance results.

The measurements are being extended to the examination of the effects of post-deposition annealing and gas evolution on microstructure and on such microdynamics as the intervaid hopping of molecular HD. Proton and deuteron spin-decoupling methods are employed to enhance the spectral resolution. Composite-pulse methods and multiple-pulse echo sequences are used to improve the spectral coverage and to examine the time decay of quadrupolar order. The purpose of the measurements is to correlate DMR-deduced microstructural morphology and microstructural dynamics with electrical properties. The dynamics of molecular D₂ and HD are correlated with preparation methods and with the photoelectronic properties of the alloy material.

Amorphous Silicon and Germanium

We have discovered the first deuteron multiple echoes [2] ever observed in amorphous Germanium. H643 a-Ge:D,H (made at 0.094 W/cm² onto a 301°C substrate) shows weak HD multiple echoes. There were no such signals detected in a lower quality sample H511 a-Ge:D,H, made at the same power level on a 260°C substrate. We anticipate larger multiple echoes in the higher quality a-Ge sample now being made (at higher power levels) at Harvard. In the meantime, we have measured the temperature variations of T₁ and T₂ in H643 and H642, deposited on a 151°C substrate (and presumably having interconnected microvoids). No molecular D₂ or HD signals are observed in H642, so the DMR measurements confirm that the microvoids are completely open in hydrogenated a-Ge deposited on a 151°C substrate.

In a-Si:D (XW895) deuteron spin-lattice relaxation times have been measured (Fig. 1) for the deuterons tightly-bonded to Si, for the molecular D₂ in large microvoids, and for the para-D₂ adsorbed on Si surfaces. The latter two species do not efficiently cross-relax and the observed para-D₂ probably reside in very small voids (≤ 4 Å) remote from the larger voids containing D₂ mobile above 20 K.

In a high quality a-Si:D,H sample (H541) the temperature variation of T₁ (D) has been measured for the multiple echo [2] component of HD trapped on internal surfaces. Figure 2 shows these data (open circles), together with the temperature variation of the J = 1 molecular HD ΔJ rate (solid dots) inferred from the T₁ results. Application of a Boltzmann factor appropriate for the population of the J = 1 states removes the T₁ minimum and yields a J = 1 molecular ΔJ rate which is found to be proportional to T⁴. This may imply that a higher order silicon phonon process is involved in the relaxation of the adsorbed

HD. Among a-Si samples the HD multiple echo intensity increases with film quality, as inferred from conductivity measurements.

Figure 3 shows the observed correlation between the deuteron spin-lattice relaxation rate $1/T_1$ for lattice-bonded D in a-Si:D,H (and a-Ge:D,H) with the ESR-determined density of neutral dangling bonds. The solid dots indicate recent results for six sample films whose deposition parameters are given in Table I. Sample 895 contained O_2 , as indicated by an electron g-factor 9% larger than those for the other samples and hence does not fit the otherwise orderly correlation of $1/T_1$ and N_β . The open circles indicate our previous results for a similar correlation in the case of a single sample (XP II) progressively annealed between 250 and 600°C. Overall the two sets of data indicate a correlating relation:

$$T_1(D)^{-1} = 8 \times 10^{-9} N_\beta^3 \text{ sec}^{-1}$$

Dangling Bonds and Floating Bonds

We have theoretically investigated the determination of structural properties from ESR experiments [3,4]. In particular we have investigated the strain or environmental dependence of the three-fold coordinated defect or dangling bond and the five-fold coordinated defect or the floating bond. Our calculations show conclusively that it is the dangling bond and not the floating bond that form a state in the middle of the gap of a-Si and is responsible for the ESR signal.

For the dangling bond our results are as follows:

1. The energy eigenvalue lies in the middle of the gap for an ideal or unstrained configuration. This state readily moves as the atoms are disturbed, changing by about 0.5 eV for a 10° distortion.
2. The wavefunction or charge distribution of the dangling bond is very insensitive to changes in its environment. This is cell consistent with DLTS and ESR-hyperfine experiments. Figure 4 illustrates the point.

For the floating bond we find that:

1. The energy eigenvalue lies within 0.2 eV of the conduction band and is very insensitive to strain. These are far too close to the conduction band to agree with experiments.
2. The charge distribution of the state is very dependent on configuration. This directly contradicts the ESR-hyperfine data.

The techniques developed in this project will enable us to study other defects and dopants on a-Si, a-Ge, and Si-Ge alloys.

Conclusions

DMR provides quantitative measures of many different D components in amorphous semiconducting films, including tightly bonded D, weakly bonded D, silyl rotors, microvoid-contained D_2 and HD, frozen out p- D_2 , vacancy-isolated HD and o- D_2 . These components are examined as a function of sample preparation conditions, post-deposition anneals, and illumination sequences. We seek to correlate structural changes with photo conversion efficiency and with light-induced metastabilities.

We have determined that:

- the presence of deuteron multiple echoes from HD trapped in ≤ 4 Å nanovoids is a reliable indicator of high quality deuterated a-Si and a-Ge films.
- the relaxation rate of Si-bonded deuterons increases with increasing ESR-determined density of neutral dangling bonds.
- the dangling bond forms a state in the middle of the gap in a-Si and is responsible for the ESR signal. The floating bond forms no such state.

References

1. K. D. Mackenzie, J. R. Eggert, D. J. Leopold, Y. M. Li, S. Lin, and W. Paul, Phys. Rev. B **31**, p. 2198 (1985).
2. Ó M. P. Volz, P. Santos-Filho, M. S. Conradi, P. A. Fedders, W. Turner, and W. Paul, Phys. Rev. Lett. **63**, 2582 (1989).
3. M. Stutzmann, Z. Phys. Chem. Neue Folge **151**, 211 (1987).
4. M. Stutzmann and D. Biegelsen, Phys. Rev. Lett. **60**, 1082 (1988).
5. Ó P. A. Fedders and A. E. Carlsson, Phys. Rev. Lett. **58**, 1156 (1987), and Bull. Am. Phys. Soc. **33**, 228 (1988).
6. P. A. Fedders and A. E. Carlsson, Phys. Rev. **B37**, 8506 (1988).

Table I. Sample Film Parameters

Sample	Power Density (w/cm ²)	T ₂ (°C)	Flow (sccm)	N(D) (at.%)	N _β (cm ⁻³)
Si H541	0.12	230	SiH ₄ 4 D ₂ 76	4	1.2 x 10 ¹⁶
Si XPVI	0.10	230	9% SiH ₄ 1% B ₂ H ₆ 90% D ₂	3	8.7 x 10 ¹⁶
Si XPV	0.75	230	5% SiD ₄ /Ar	10.3	1.0 x 10 ¹⁸
Si XPI	0.90	25	5% SiH ₄ /D ₂	24	2.0 x 10 ¹⁸
Ge H511	0.094	260	GeH ₄ 1 D ₂ 40	1.3	6.0 x 10 ¹⁸
Si XW895	0.12	230	SiD ₄ 200	23	(2.3 x 10 ²⁰)
Si XP11	0.10	25	5% SiH ₄ /D ₂	10.5	1.5 x 10 ¹⁶ to 1.7 x 10 ¹⁸ after anneals
Ge H642	0.094	151	GeH ₄ 1 D ₂ 40	< 1	
Ge H643	0.094	301	GeH ₄ 1 D ₂ 40	2	

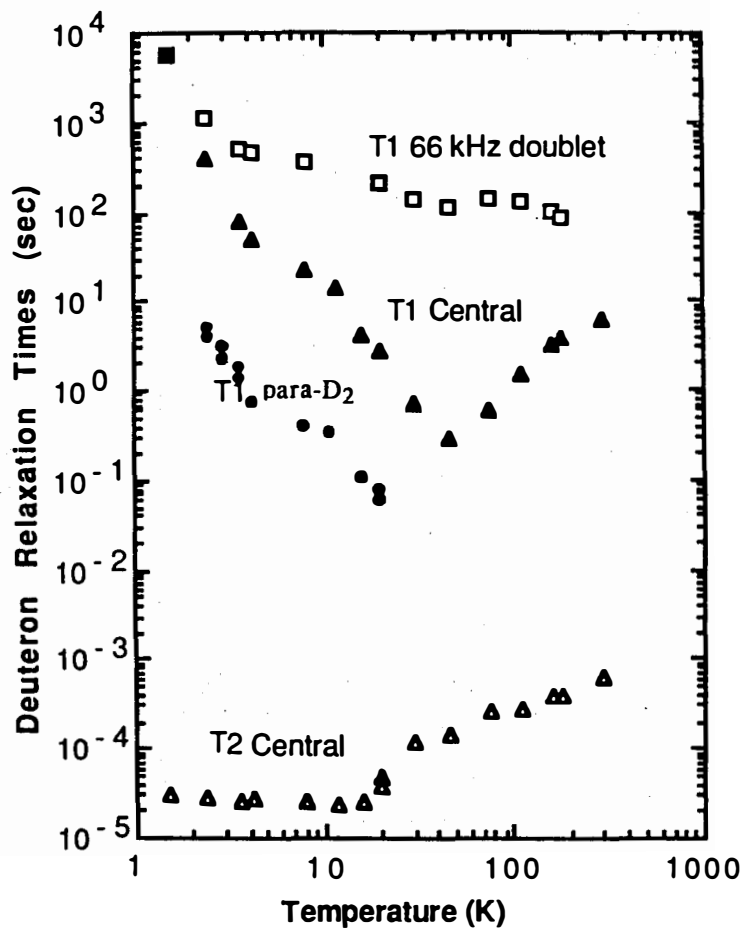


Fig. 1. Deuteron spin relaxation times at 30 MHz in an a-Si:D film (XW895) for Si-bonded D (squares), molecular D₂ in microvoids > 4 Å (triangles), and surface-adsorbed para-D₂ (solid dots).

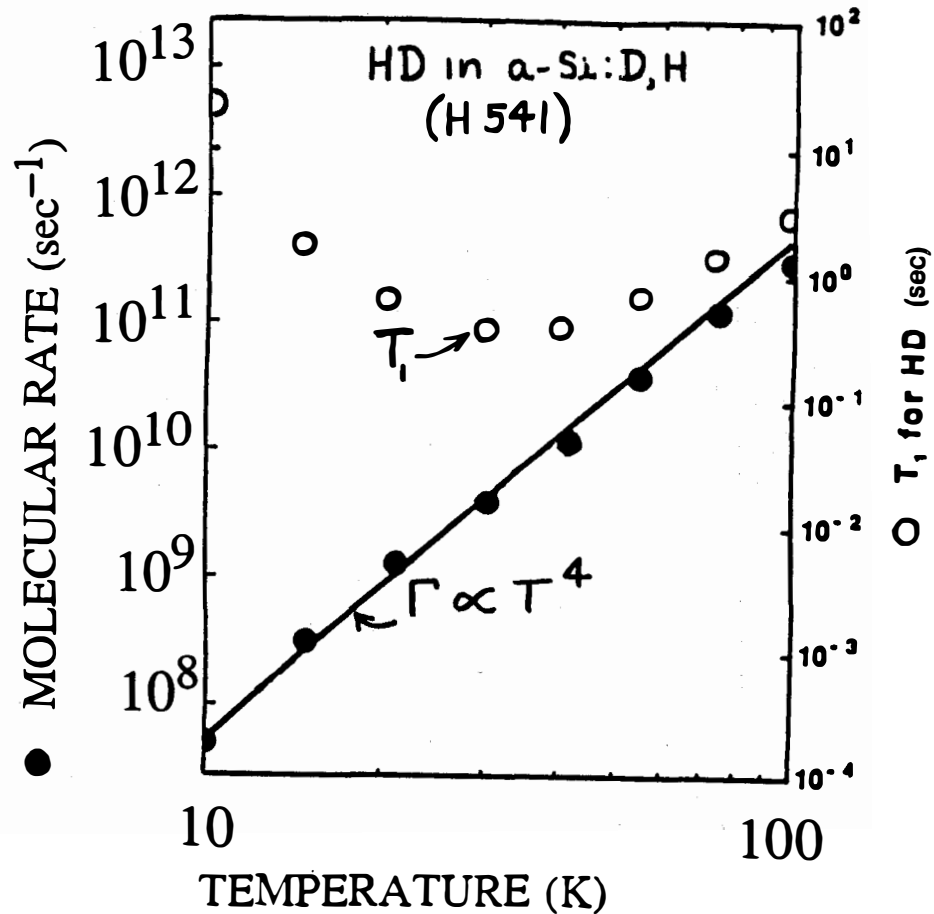


Fig. 2. Multiple echo spin-lattice relaxation times (open circles) for HD in nanovoids ≤ 4 Å in a high quality a-Si:D,H film (H541). The solid dots show the inferred $l = 1$ electric dipolar molecular ΔJ rates for $J = 1$ molecules.

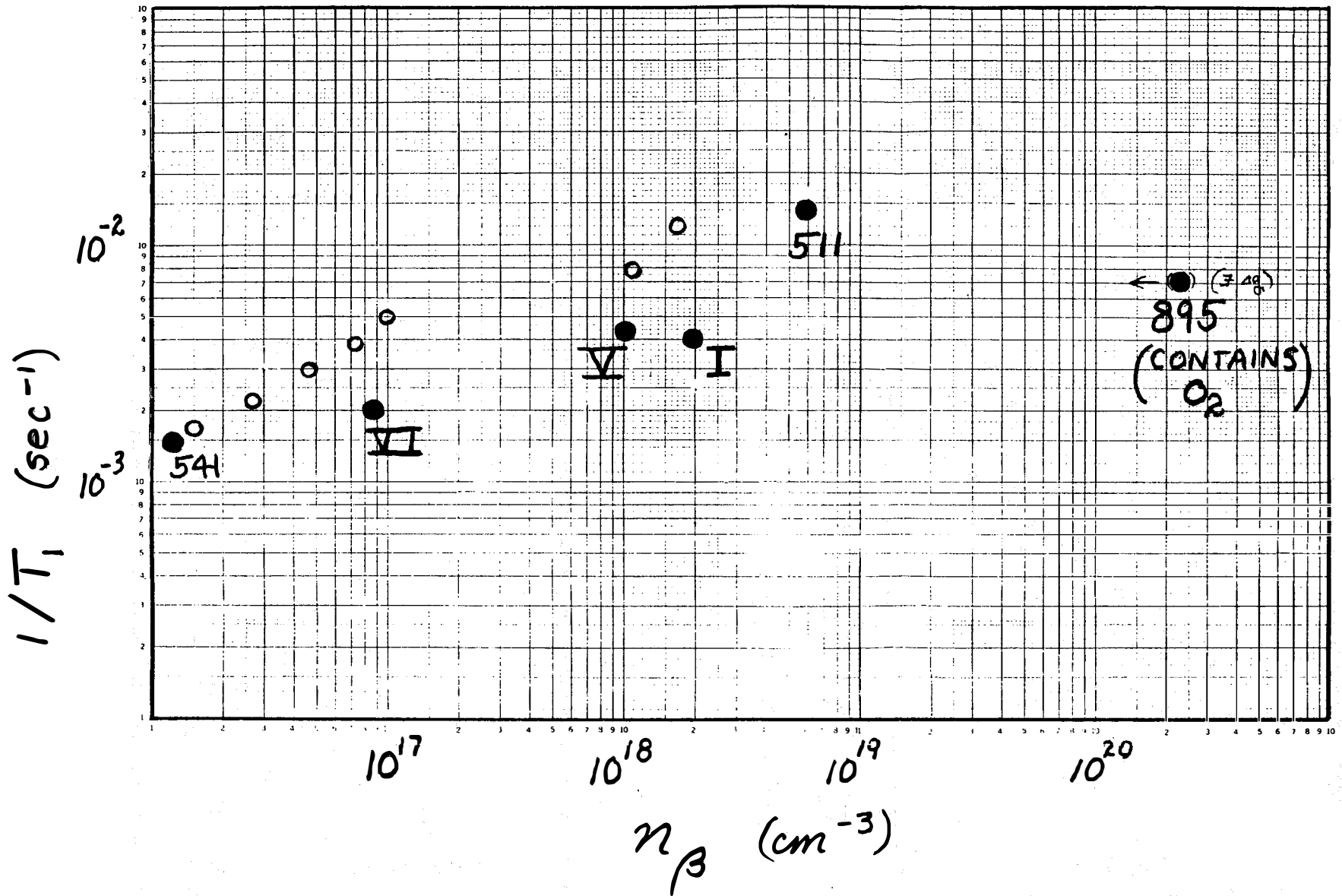


Fig. 3. Correlation between deuteron spin-lattice relaxation rates T_1^{-1} for lattice-bonded D in deuterated a-Si and a-Ge films and the ESR-determined densities of neutral dangling bonds.

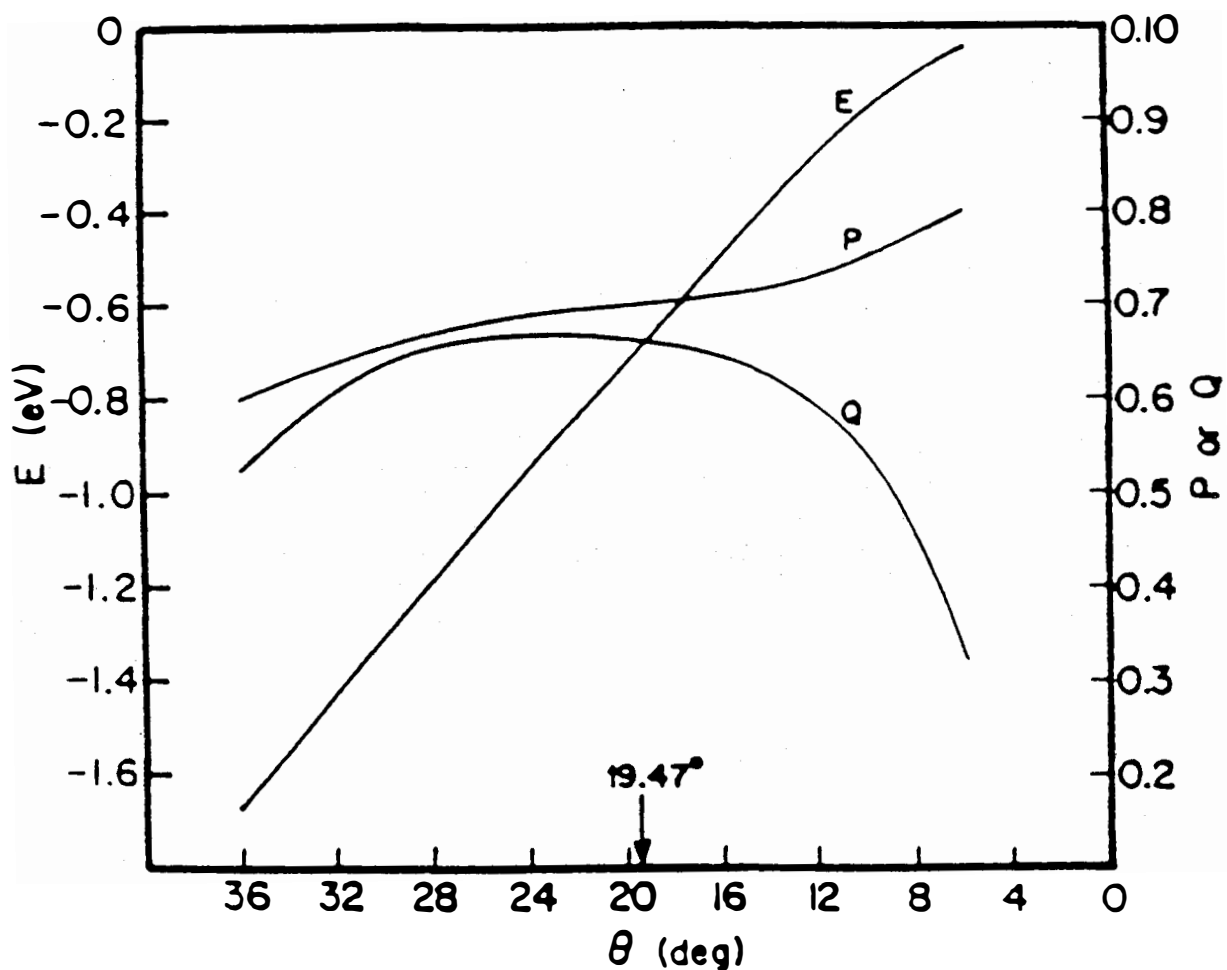


Fig. 4. The energy eigenvalue (E), the fraction (Q) of charge on atom 1, and the fraction (P) of charge on atom 1 that is from p states, for the dangling bond. The angles $\phi_3 = \phi_4 = 0$.

Title: **Research on the Structural and Electronic Properties of Amorphous Silicon Alloys**

Organization: Xerox Palo Alto Research Center, Palo Alto, CA 94304

Contributors: J. B. Boyce, W. B. Jackson, N. M. Johnson, R. A. Street (Principal Investigator), R. Thompson, C. C. Tsai, K. Winer

The primary research goals of this project are to improve the performance of a-Si:H-based solar cells through the understanding of metastability, doping and growth.

Thermodynamics of Defects

One of the main materials problems of amorphous silicon technology is the phenomenon of metastability, in which the electronic properties depend on the thermal and electrical history of the sample. A key observation is that the defects are in thermal equilibrium with the disordered structure. We have made experimental and theoretical studies of the thermal equilibrium defect density in undoped a-Si:H. The defect density measured by electron spin resonance, increases with temperature with an activation energy of 0.15-0.2 eV as is shown in Fig. 1. The equilibration time

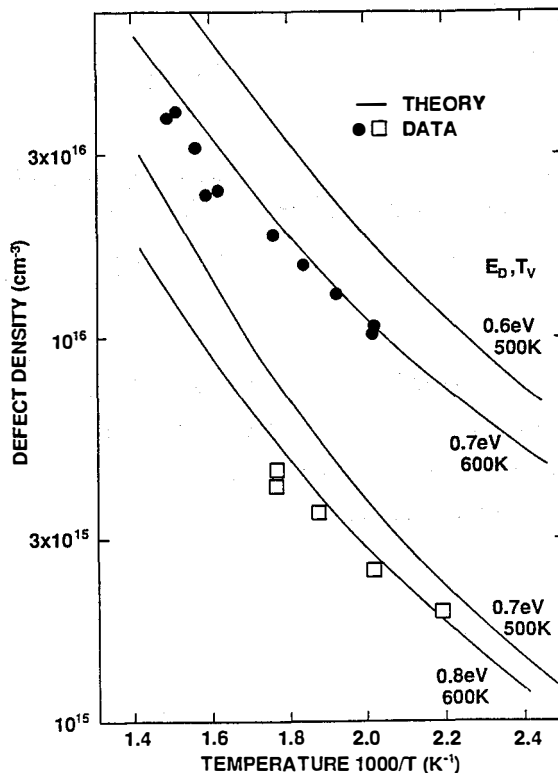


FIG. 1. Dependence of the equilibrium spin density on quench temperature for two samples of undoped a-Si:H. Also shown is the fit to the equilibrium model discussed in the text.

is activated with an energy of about 1.5 eV and the shape of the decay follows a stretched exponential, as in doped a-Si:H. The experiments confirm that defect equilibration occurs over a range of temperatures and sample deposition conditions. The relaxation time depends on the growth conditions, and the thermal defects are shown to anneal more slowly than optically induced defects.

The temperature dependence of the thermodynamic equilibrium defect density is calculated, based on a hydrogen mediated weak-bond/dangling-bond conversion model,



The model is illustrated in Fig. 2. The distribution of defect formation energies is

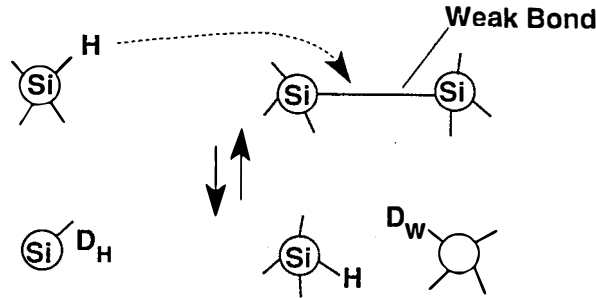


FIG. 2. Schematic illustration of the defect reaction corresponding to the model described in the text.

introduced by associating a different density of valence band tail states with each formation energy. The valence band tail is assumed to be exponential with slope T_v . We obtain the result for the defect density

$$N_D = N_H N_{vo} \exp(-E_D/kT_v) \int \frac{h \exp(U/kT_v) dU}{N_H + N_D \exp(2U/kT)} \quad 2$$

A numerical integration of this equation is shown in Fig. 1 and is compared to the ESR data. A good fit is obtained when T_v is 500-600K and $E_D = 0.6-0.7$ eV, which agrees well with the experimental information. Thus the defect properties of a-Si:H may be calculated from first principles.

Chemical Equilibrium Model of Growth

Understanding the process of impurity incorporation and dopant activation during plasma-enhanced chemical vapor deposition of a-Si:H is of fundamental importance for current efforts to develop a-Si:H-based solar cells. We have completed a detailed study of phosphorus and arsenic incorporation in a-Si:H over a wide range of deposition conditions. Fig. 3 shows that the distribution coefficient varies strongly with rf power and dopant concentration, particularly for arsenic doping.

A chemical equilibrium model for plasma-enhanced chemical vapor deposition of a-Si:H has been developed to interpret the irregular incorporation of As and P. The model shows that the irregularity occurs only for non-doping impurities; their distribution coefficient is inversely proportional to the rf plasma power, which leads to the large As concentration enhancement observed under low power growth

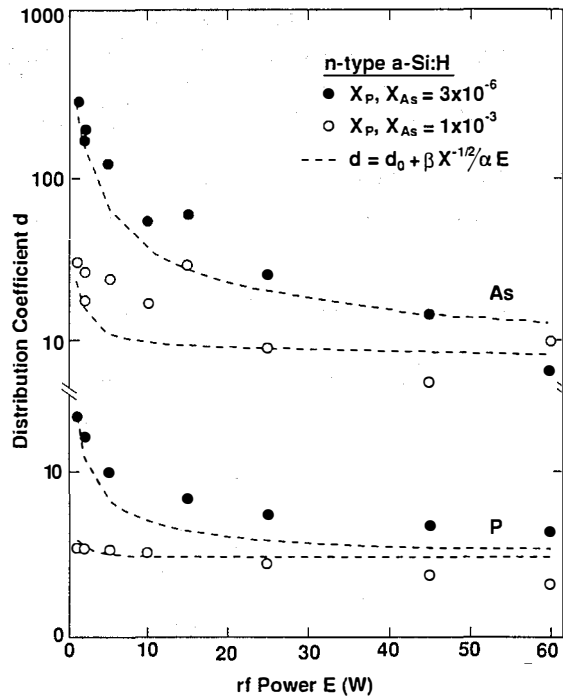


FIG. 3. Distribution coefficients as a function of rf power for As- and P-doped a-Si:H for gas-phase impurity mole fractions of 3×10^{-6} (filled circles) and 1×10^{-3} (empty circles), respectively. Dashed lines are the fits to the data.

conditions. The conclusion is that chemical reactions at the growth surface rather than kinetic reactions in the plasma determine impurity incorporation in a-Si:H.

Light Induced Defects

In a-Si:H material deposited at low temperature, the defect creation rate of light induced defects is greatly enhanced, and it is suggested that the presence of excess Si-H₂ bonding structures are responsible. We have studied structural changes and light induced defects in low substrate temperature material, in order to investigate how the deposition conditions affect the defect creation and annealing. The light soaking experiment was performed on partially annealed samples in which some, but not all, of the initial excess defects are annealed away before the light soaking. Fig. 4 compares the light induced defect density ΔN_S (for the same illumination conditions as before) with the initial defect density before the light soaking, N_{Sinit} . The induced defect density is largest when the initial defect density is large and is given by,

$$\Delta N_S \approx \beta N_{Sinit} \quad 3$$

Thus, the susceptibility to light induced defect creation decreases as the irreversible defects are annealed away within the same sample. It is known from earlier infra-red studies that the hydrogen bonding of these samples does not substantially change during annealing to 200-250°C. It is therefore clear that the rate of defect creation cannot be directly the result of the specific hydrogen bonding structures in the material.

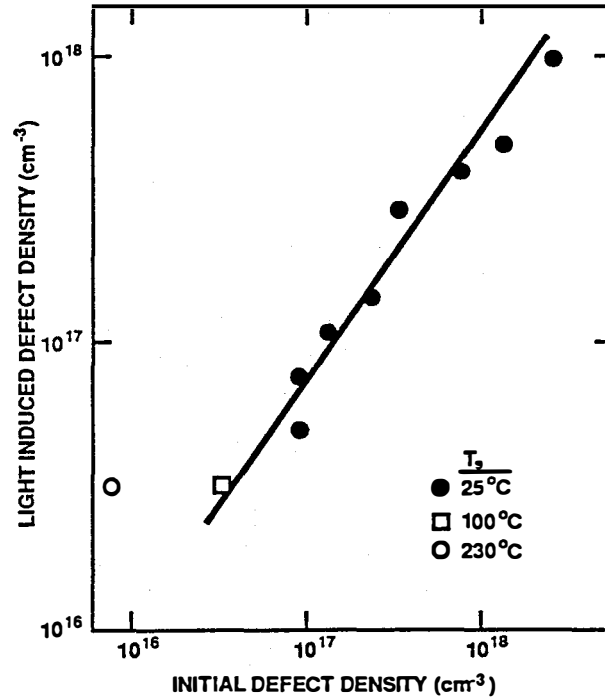


FIG. 4. Dependence of the light induced defect density on the initial defect density for different stages of annealing of a sample deposited at 25°C. Similar data for other deposition temperatures is shown.

Solid Source Doping

A new method of doping a-Si:H, using solid arsenic as the dopant source in a remote plasma reactor has been demonstrated. High doping levels are achieved and the electrical properties of doped films are indistinguishable from those produced by standard rf glow discharge, as is shown by the dc conductivity data in in Fig. 5. The reactor generates atomic hydrogen and allows it to react with the arsenic, forming volatile hydrides which are etched from the surface, transported to the substrate, and deposited in the growing a-Si:H film. The atomic hydrogen serves the dual purpose of both transporting the arsenic and dissociating the gases to cause deposition. The technique is applicable to other dopants and alloying elements and has been demonstrated recently with antimony.

Defect Kinetics

A detailed analysis of the connection between hydrogen diffusion and the relaxation kinetics finds excellent agreement with the data. In further studies of the effect of Fermi energy position on the metastable defects, the time-dependence of the defect creation process was examined in MIS structures. The rate of defect formation was measured as a function of gate bias and varies inversely as the square root of the band tail carrier density, so that higher carrier densities result in somewhat faster defect generation. The results are consistent with the measured carrier dependence of the hydrogen diffusion rate. The rate equation model is used to predict the relation between the time dependence of the defect generation, τ , and a carrier dependent H diffusion rate, D . The theoretical model make three main assumptions. (1) The kinetics are limited by hopping over an exponential distribution of energy barriers.

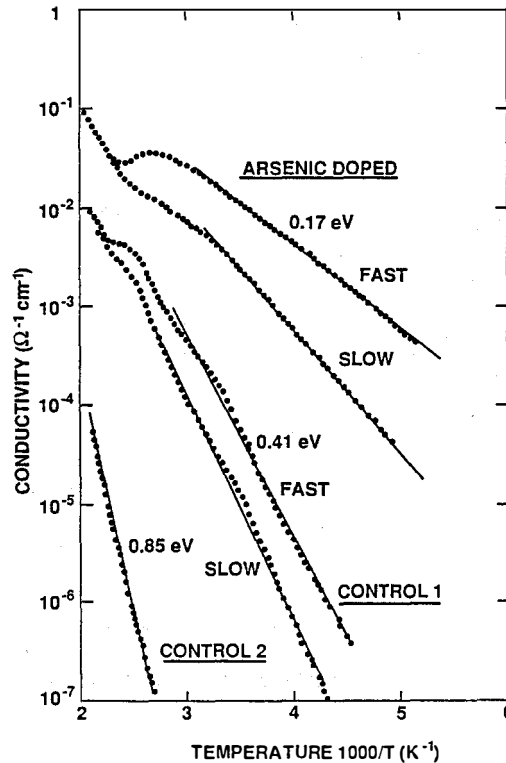


FIG. 5. The temperature dependence of the dc conductivity of a solid-source arsenic doped sample and the two controls. The results of annealing at 220°C and subsequent slow or fast quenching are shown.

(2) The barrier heights (or hopping rates) depend on the carrier density. (3) The total energy for defect creation depends on the Fermi level. The relation between τ and D is,

$$\tau = \left(\frac{\beta 4^{\alpha}}{AL^{2\alpha}} \right)^{1/\beta} \frac{1}{D}$$

and is confirmed by experiment.

Bibliography

Jackson, W. B. The connection between dispersive hydrogen motion and the kinetics of light-induced defects in hydrogenated amorphous silicon. *Philos. Mag. Lett.*, 1989, 59, 103.

Jackson, W. B.; Marshall, J. M.; Moyer, M. D. Role of hydrogen in the formation of metastable defects in hydrogenated amorphous silicon. *Phys. Rev.* 1989, B39, 1164.

N. M. Johnson, J. Walker, C. M. Doland, K. Winer, and R. A. Street, Hydrogen Incorporation in Silicon Thin Films Deposited with a Remote Hydrogen Plasma, *Appl. Phys. Lett.*, 54, 1872, 1989.

N. M. Johnson, J. Walker, C. M. Doland, K. Winer, and R. A. Street, "Deposition of a-Si:H Thin Films with a Remote Hydrogen Plasma," Mat. Res. Soc. Symp. Proc. 1989, 149, 39.

N. M. Johnson, R. A. Street, J. Walker, and K. Winer, "Solid-Source Doping of a-Si:H Thin Films Deposited with a Remote Hydrogen Plasma," Proc. Int. Conf. on Amorphous and Liquid Semiconductors, "in press.

R. A. Street, N. M. Johnson, J. Walker, and K. Winer, Solid-Source Doping of Hydrogenated Amorphous Silicon, Philos. Mag. Lett., 1989, 60, 177.

R. A. Street and K. Winer, Defect equilibria in undoped a-Si:H, Phys. Rev. 40, 6236.

K. Winer and R.A. Street, Equilibration Kinetics in Interstitially-Doped a-Si:H, Mat. Res. Soc. Symp. Proc. 1989, 149, 137.

R.A. Street and K. Winer, Thermal Equilibrium, Metastable and Irreversible Defects in a-Si:H, Mat. Res. Soc. Symp. Proc. 1989, 149, 137.

K. Winer and R.A. Street, Chemical Equilibrium Model of Dopant Incorporation in n-type a-Si:H, Phys. Rev. Lett. 1989, 63, 880.

K. Winer, "Chemical Equilibrium Description of the Gap State Distribution in a-Si:H," Phys. Rev. Lett., to be published.

K. Winer, "Dependence of Equilibrium Growth Temperature on Carbon Content in a-SiC:H Alloys," Appl. Phys. Lett., to be published.

3.0 POLYCRYSTALLINE THIN FILMS

Kenneth Zweibel (Manager), Harin Ullal, and Richard Mitchell

The objective of the Polycrystalline Thin Film Program is to develop thin-film, flat-plate modules that meet DOE's long-term goals of reasonable efficiencies (15%-20%), very low cost (near \$50/m²), and long-term reliability (30 years). The approach relies on developing PV devices based on highly light-absorbing compound semiconductors such as CuInSe₂, CdTe, and their alloys. These semiconductors are fabricated as thin films (1-3 μm thick) with minimal material and processing costs.

Very high efficiencies have been achieved by these promising materials. CuInSe₂ cells made by ARCO Solar and by Boeing were measured at SERI at 13.1% and 12.9% efficiency (active area), respectively. ARCO Solar reports achievement of a 14.1% efficiency which has not been confirmed. Others surpassing 10% efficiency in CuInSe₂ are SERI, International Solar Electric Technology, and Institute of Energy Conversion. Larger area CuInSe₂ devices have also been fabricated with very high efficiencies. ARCO Solar has made a 938-cm² (aperture area) CuInSe₂ module with 11.1% efficiency (10.4 W), and an 8.5% (4-ft²) module, both measured at SERI.

CuInSe₂ shows good proven stability under controlled conditions (9000 of illumination), and initial outdoor tests (ARCO) are also promising. We have conducted a full year outdoor testing on two ARCO Solar CuInSe₂ panels with very little change in their efficiencies (under 4%). These are the first such tests on CuInSe₂ by an independent agency and show the great potential stability of CuInSe₂ panels.

Three U.S. laboratories (University of South Florida, Ametek, and Photon Energy) report CdTe cell efficiencies between 10.5% and 12.5%. Photon Energy has fabricated near-square-foot CdTe submodules measured outdoors at SERI at 7.3% efficiency (aperture area). They also have the world record in CdTe cell efficiency (12.3%), measured at SERI. Innovative designs are now addressing past difficulties in contacting CdTe. We have recently begun testing encapsulated CdTe submodules provided by Photon Energy. After four months, they show no degradation. As with the CuInSe₂, these are the first independent tests of encapsulated devices made from this material. Since stability has been an identified issue with CdTe, these initial results are considered very favorable.

The improved efficiencies and larger areas of CuInSe₂ and CdTe devices, and their apparent stability, are the major recent advances in these technologies, but polycrystalline cells require continued development to achieve 15%-20% conversion efficiencies. Two strategies are being used: development of single-junction cells and an innovative effort on two-junction cascade cells. Improvement of the single-junction technologies has been steady and reliable. This strategy remains the major focus of the task. Potentially achievable cell efficiencies approach 20%, and projections indicate the likelihood of fabricating modules of more than 15% efficiency. Developing two-junction, CuInSe₂-based cascade cells permits even more ambitious long-term efficiency goals. Combining two well-matched, single-junction modules into a cascade cell design could lead to module efficiencies of better than 20% at costs under \$60/m². The materials being investigated for the top cells include CdTe and ZnTe alloyed with Mn, Mg, Zn, and Hg.

Developing scalable, low-cost fabrication methods is important in providing industry with a foundation for future large-area, high-throughput commercial processes. Research methods for fabricating polycrystalline cells include, for CuInSe_2 , an e-beam evaporation/selenization method (International Solar Electric Technology), a reactive-sputtering and hybrid sputtering/evaporation method (University of Illinois), and evaporation (Boeing); for CdTe , close-spaced sublimation (USF), evaporation (Institute of Energy Conversion), electrodeposition (Ametek), metal-organic chemical vapor deposition (MOCVD) (Georgia Tech and University of South Florida), and spraying (Photon Energy).

An initiative in the Polycrystalline Thin Film Program was begun with the release of an RFP in FY 1989. The objective of the solicitation was to stimulate progress in CuInSe_2 and CdTe submodule development and to deepen the U.S. participation in these promising technologies. The research community responded favorably, as reflected in the many excellent technical proposals received in response to the solicitation. The contracts resulting from that RFP will begin in spring 1990.

Title: Polycrystalline Thin-Film Cadmium Telluride Solar Cells

Organization: Ametek Applied Materials Laboratory, Harleysville, Pennsylvania

Contributors: P. Meyers, R. Liu, Principal Investigators

The overall objective of this subcontract is to develop thin-film solar cells that are improvements on the present state of the art. The work is centered around the polycrystalline n-i-p configuration utilizing CdS/CdTe/ZnTe. Already devices of this structure have been produced with confirmed efficiency of 11.2%. See Figure 1. Stability testing of mini-modules indicates that these devices are stable under load and illumination for at least 4200 hours.

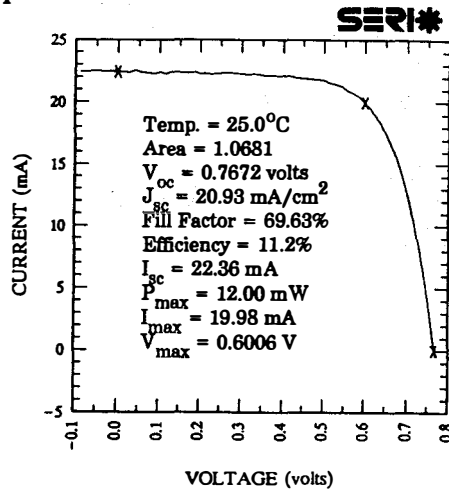


Figure 1. I-V curve of CdS/CdTe/ZnTe cell

Polycrystalline n-i-p Solar Cells

The structure CdS/CdTe/ZnTe, shown in Figures 2 and 3, is well suited to the n-i-p design for the following reasons [1,2]:

1. Each semiconductor material is utilized in its preferred type. CdS is always n-type, ZnTe is generally p-type, and AML's process produces good-quality, high-resistivity (intrinsic) CdTe.
2. Reviews of the published literature corroborate the prediction that there is no spike either in the conduction-band edge at the n-i interface or in the valence band at the i-p interface. Such spikes would inhibit the collection of photogenerated carriers.
3. At each interface there is a step that prevents collection of unwanted charge carriers, i.e., holes are reflected from the n-i interface and electrons are reflected from the i-p interface.

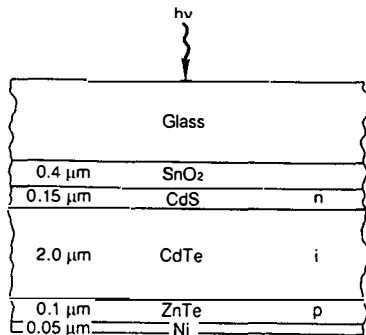


Figure 2. Structure of the CdS/CdTe/ZnTe cell

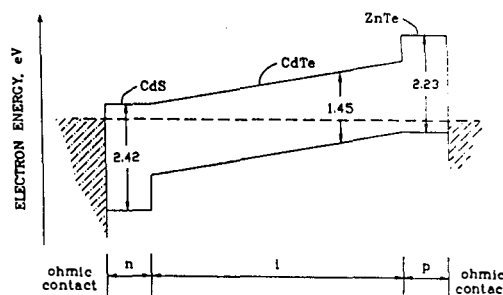


Figure 3. Idealized n-i-p energy band diagram

During the course of this subcontract AML has produced, by intentional variations of the fabrication procedure, devices with the CdS/CdTe/ZnTe configuration in which the location of the maximum field strength within the CdTe layer varied from device to device. This effect was observed with spectral response, and with EBIC measurements performed at SERI [2]. In the most efficient devices, most of the CdTe layer is active in carrier collection, but the maximum field strength occurs at a depth of approximately 0.5 μm from the CdS/CdTe interface. These experiments demonstrate that material engineering is possible with this design.

Loss Analysis

At present we have produced a device with an efficiency of 11.2% (22.4 mA/cm^2 J_{sc} , .70 FF, and .767 V_{oc}) We believe, however, that significant improvement is possible with continued improvements in the design of the solar cell. More specifically, loss analysis indicates that substantial increases in current can be obtained through proper optical design of the cell. It is estimated [3] that absorptive and reflective losses account for current reduction by over 7 mA/cm^2 . In addition, proper passivation of recombination centers in the bulk and at the interfaces could increase V_{oc} by 100 mV, and a similar increase could be realized by increasing V_{bi} .

Modules

At the same time, we are studying the commercial viability of this process. Preliminary experiments using a laser scriber have produced a 13.23 cm^2 four cell submodule [4]. This device had an area ratio of 0.91, an aperture area efficiency of 8.0%. (Active area efficiency was 8.8%.) The I-V curve is displayed in Figure 4. In other devices, using mechanical scribing, we have demonstrated the same active area efficiency over virtually the entire 3" X 6" substrate. The mechanically scribed device had an area ratio of 0.78 and an aperture area efficiency of 6.8% over 100.25 cm^2 .

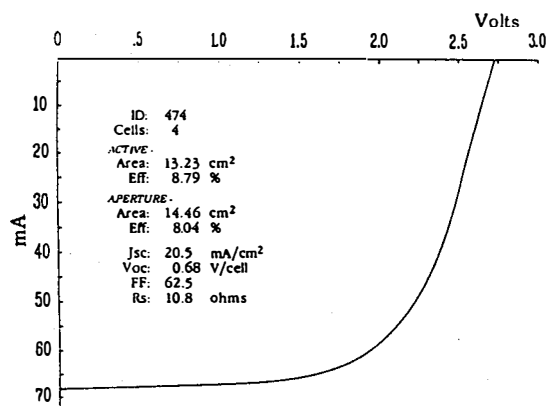


Figure 4. I-V data from a laser scribed mini-module

Stability

Stability testing of 3" X 6" modules is in progress. Figure 5 presents the average and standard deviation of the equivalent, i.e. cell, efficiency of six 13 cell, 100 cm² modules currently under test. These modules are being tested indoors using the illumination cycle six hours on, two hours off. Results to date indicate that the modules are stable for at least 4200 hours. Additional short term - 1 week - testing of fully encapsulated modules both outdoors and under water, indicate that with proper encapsulation, stable operation is possible.

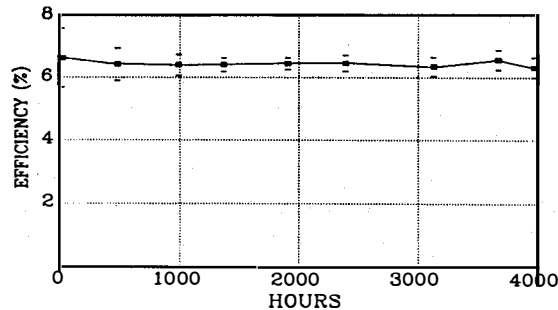


Figure 5. Module stability data

Conclusions

Results to date indicate that the polycrystalline n-i-p structure has the potential to make significant advances to the state of the art of thin-film solar cells. In order to realize that potential, additional work needs to be done: control over deposition parameters must be improved so that film quality can be reliably optimized; the effects of interface states and interdiffusion at the heterojunction interfaces must be understood and controlled; and we must utilize new materials whose properties are better suited to high-efficiency devices. All of these avenues are addressed by the current subcontract plan.

References

1. Meyers, P.V., 7th E.C. PV Solar Energy Conf., 1986, pp. 1211-1213.
2. Meyers, P.V., "Design of a Thin Film CdTe Solar Cell," Solar Cells, 23 (1987) pp. 59-67.
3. ½ Meyers, P.V. and R.C.H. Liu, "Status and Potential of CdTe based n-i-p Solar Cells", Proceedings PVSEC-4, IREE, Sydney, Australia, pp 881-888, 1989.
4. ½ Meyers, P.V., "Advances in CdTe n-i-p Photovoltaics" presented at SERI 8th PV Advanced R&D Proj. Rev. Mtg., Denver, Co., Aug. 1989.

Title: High Efficiency CuInSe₂ and CuInGaSe₂ Based Cells
and Materials Research

Organization: Boeing Aerospace & Electronics
Seattle, Washington

Contributors: Walter E. Devaney, Wen S. Chen,
John M. Stewart, Reid A. Mickelsen.

The overall objective of this research program was the demonstration of improved performance for photovoltaic devices based on the ternary compound CuInSe₂ and its quaternary analog CuInGaSe₂. The program was for two years and has just been completed. The detailed objectives and a more complete description of the first year results are contained in the 1988 Photovoltaic Program Branch Annual Report.

During the first year of the contract a ZnO/CdZnS/CuInGaSe₂ cell of area 1 cm² was fabricated with a total area efficiency of 12.5% and an active area efficiency of 12.9% (AM1.5 global spectrum, 100 mW/cm² equivalent intensity) as measured at SERI. The CuInGaSe₂ layer was vapor deposited on a molybdenum coated alumina substrate by vacuum deposition from elemental sources. The CdZnS was grown on the CuInGaSe₂ by chemical deposition from solution and the ZnO was deposited by reactive sputtering.

During the past year an extensive optical analysis of this device was done. The structure which resulted from this analysis is summarized in Figure 1. A more extensive description of the device fabrication process and structure is given in Reference 1. The major result of this first year effort was the demonstration of higher efficiencies with the ZnO/CdZnS/CuInGaSe₂ structure than with the ZnO/CdZnS/CuInSe₂ or CdZnS/CuInSe₂ devices.

During the past year we have concentrated on extending the CuInGaSe₂ deposition and the thin CdZnS solution growth to devices of 4 cm² area as a first step toward demonstrating CuInGaSe₂ based cells of larger areas. This essentially involved improving the reliability, reproducibility and uniformity of the CuInGaSe₂ deposition process and of the CdZnS growth process. The ZnO/CdZnS/CuInGaSe₂ devices with areas of 4 cm² were fabricated with the same basic structure described in Reference 1.

The best device performance obtained for such a 4 cm² cell is shown in Figure 2. A total area efficiency of 10.65% was obtained as measured at Boeing. The composition of the selenide layer in this device as measured using EDX was

Cu:Ga:In:Se::23.3:7.0:19.6:50.2 (atomic %). The CdZnS contained 13% atomic fraction Zn ($([Zn]/([Zn]+[Cd]))$).

The Quantum Efficiency (QE) as a function of wavelength for a similar 4 cm² cell is shown in Figure 3. This cell also had an efficiency greater than 10%. The structure due to coherent optical interference effects in the ZnO and CdZnS layers is clearly visible in the curve. Unlike the results for the best of the 1 cm² cells we have fabricated, this QE curve shows a clear shoulder at the sulfide absorption edge. From this shoulder we estimate the thickness of the CdZnS layer in these cells to be 40-50 nm, considerably thicker than the 16 nm previously reported for the best of the 1 cm² devices. This results in lower QE at 400 nm than the value of over 0.7 seen in the previous cell results and a slightly lower current density for the device. Also from the QE results we believe that the ZnO layers in this cell are somewhat thicker than the values given in Figure 1.

The uniformity which has been achieved in the selenide deposition process is illustrated by the results of Table 1 below. In the present process 4 4-cm² cells are fabricated on a 5 cm square substrate. Table 1 gives I-V parameters and particularly the efficiency of the 4 cells made on a single substrate. The average efficiency of the 4 4-cm² cells is 10.2%. These results demonstrate the excellent uniformity achieved over at least 16 cm² of this substrate.

In summary, we have demonstrated that the added complexity of the CuInGaSe₂ fabrication process is manageable and that use of the quaternary results in higher efficiency devices in the ZnO/CdZnS/selenide structure. In addition we have extended CuInGaSe₂ based device fabrication to 4 cm² areas while maintaining efficiencies of over 10%.

Table 1: I-V Parameters for the 4 4-cm² cells fabricated on a single 5 cm square substrate. Test conditions are as in Figure 2. All tests are after 5 minutes light soak at open circuit conditions. Average Efficiency for the four cells is 10.2%

Cell #	Eff.	Voc [V]	Isc [mA]	ff
1356E	10.38	0.530	123.4	0.635
1356F	10.48	0.530	123.4	0.641
1356G	9.71	0.524	123.6	0.600
1356H	10.18	0.528	123.3	0.626

References

1. Devaney, W. E. and Chen, W. S., "Structure and Properties of High Efficiency ZnO/CdZnS/CuInGaSe₂ Solar Cells", Trans. El. Dev. Special Issue on Photovoltaics, to be published (1990).

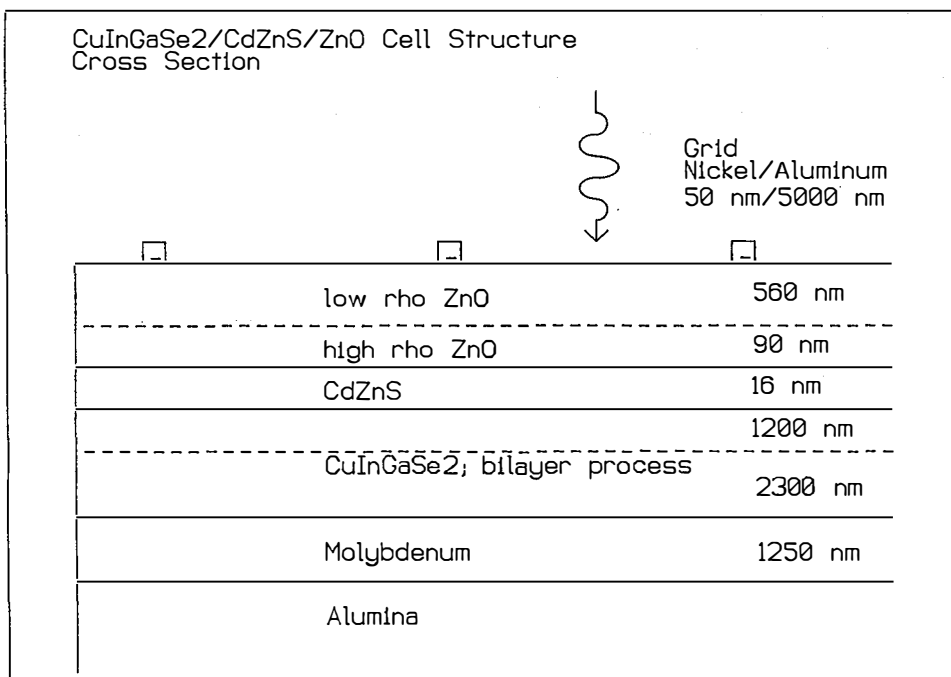


Figure 1. Structure and layer thicknesses inferred from optical and quantum efficiency measurements for 12.5% efficient 1-cm² ZnO/CdZnS/CuInGaSe₂ solar cell.

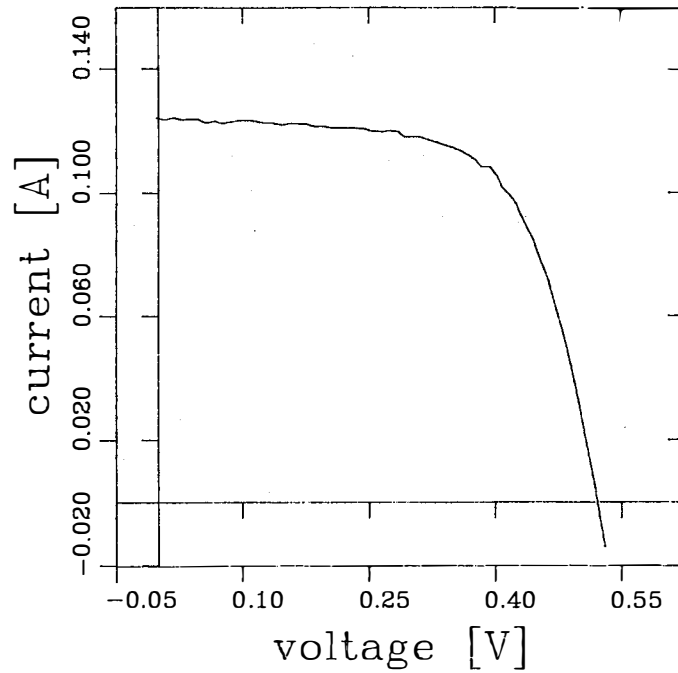


Figure 2: I-V characteristics of 4-cm² ZnO/CdZnS/CuInGaSe₂ solar cell #1354F measured at 25°C sample temperature under simulated AM1.5 global spectrum at 100 mW/cm² equivalent intensity as measured at Boeing. Curve parameters are Voc = 0.522 V., Isc = 123.9 mA., ff = 0.659, Eff. = 10.65%.

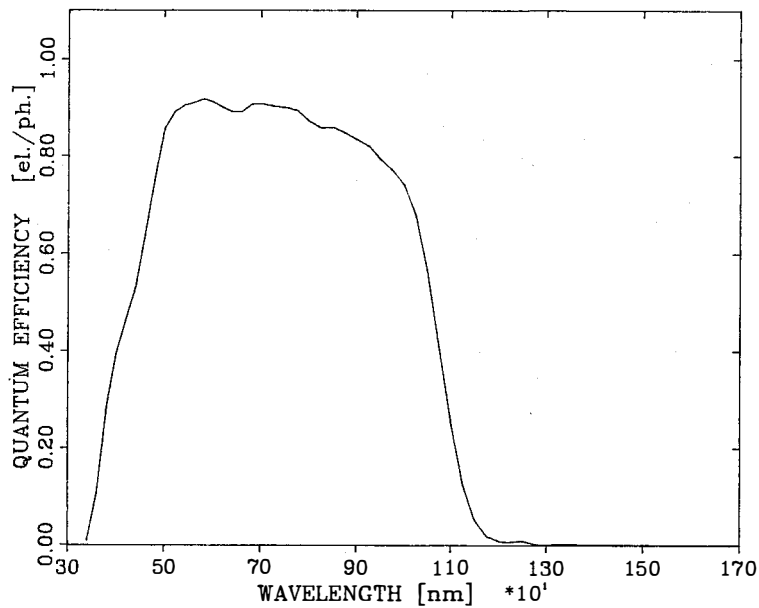


Figure 3: Quantum Efficiency plot for 4-cm² ZnO/CdZnS/CuInGaSe₂ solar cell #1356F. Data taken at short circuit loading without bias illumination.

Title: Investigations of CuInSe₂ Thin Films and Contacts
Organization: California Institute of Technology
Pasadena, California
Contributors: S. Raud (Principal Investigator), M.A. Nicolet

1. Objectives

Solar cells made of CIS (CuInSe₂) polycrystalline thin films with close to 14% efficiency have been fabricated. The objective of this work is to investigate the microstructure, the contact stability between Mo and CIS in an effort to clarify limitation on these solar cells.

2. Approach

The whole study was carried out with two kinds of samples provided by ARCO Solar Inc.: 1) CIS #1 films deposited on a glass substrate, and 2) CIS #2 films deposited on a Mo layer on a glass substrate.

To investigate the stability of the metal/CIS interface by RBS, we have deposited thin Mo or W layers on the top of these samples using two techniques: rf magnetron sputtering and e-beam evaporation. Tungsten films were deposited in addition to Mo films because W has chemical, crystallographic, and electrical properties that are close to those Mo. But W has a heavier mass than Mo and this bypasses the overlapping problem of the Mo and In signals in the RBS spectra of a sample.

We have carried out XTEM, SEM, EDX, and X-ray diffraction studies to obtain insights in the microstructure and defect chemistry of CIS. The interface stability after annealing at 600°C for 10 min. to 1 hour in argon atmosphere was investigated by RBS and X-ray diffraction.

3. Results

3-1. CIS film analysis

3-1-1. XTEM

We have embedded the CIS film into epoxy and prepared cross-sectional TEM samples using a diamond knife. This technique is suspected to produce important mechanical damage that may alter the film in an unspecified way. The study of the CIS #2 samples is less complete than that of the CIS #1 samples. The TEM observations of these cross-sectional samples provided the following information:

- For both types of films, electron diffraction patterns of as-deposited samples (fig. 1) are consistent with the tetragonal CuInSe₂ chalcopyrite structure (lattice parameters: $a = 0, 5782 \text{ nm}$, $c = 1, 1621 \text{ nm}$).
- The films are inhomogeneous. Figure 1 shows microvoids (see arrows) filled with epoxy during cross-section preparation for the CIS #1 film. Further TEM experiments are needed to confirm this observation for the CIS #2 film.

-EDX analyses performed on as-deposited CIS #1 film with a small electron beam on individual grains give an atomic ratio of Se/In=2 ±10% which is consistent with the CuInSe_2 phase stoichiometry.

The two types of films present some differences:

-The average thickness of the films is near 1.5 μm . The thickness is regular for the CIS #2 film while irregular for the CIS #1 film, varying between 1 to 1.5 μm (figure 1).

-Bright and dark field images performed on CIS #1 films show that grains are sometimes elongated in the direction normal to the surface. The grain size varies from less than 0.1 μm in diameter to 0.3 μm in width and 1 μm in length for the biggest. The CIS #2 grain size seems to be inferior to 0.5 μm in diameter. These grains show no obvious elongation.

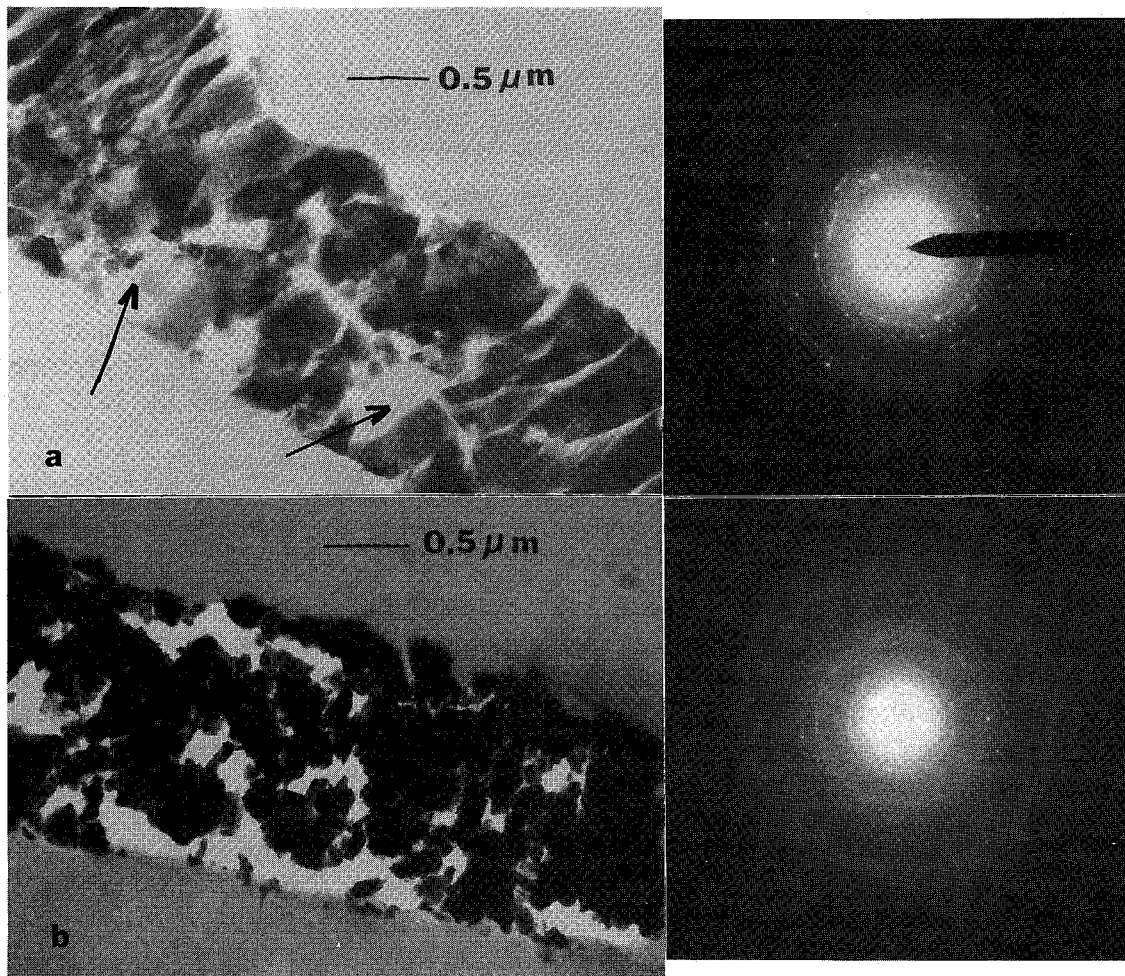


Fig. 1a Bright field XTEM view of a CIS #1 film, as-deposited, with a selected-area diffraction pattern. Arrows point to microvoids.
1b Bright field XTEM view of a CIS #2 film, as-deposited, with a selected-area diffraction pattern.

3-1-2. X-RAY

We have used both a Read camera and a θ - 2θ diffractometer for the X-ray analyses of the films. Both techniques confirm the chalcopyrite structure of the CIS films.

With the Read camera, we observe extra rings whose d spacings for both #1 and #2 do not fit with any of those listed in the ASTM files for any compound of a Cu-In-Se-O combination. All the diffraction rings sharpen and become punctuated for the films analyzed after annealing at 600°C. These observations suggest that the diffracting grains grow in size during annealing. The unexplained diffraction rings must therefore be part of the CIS film.

The diffractometer data allows the study of relative peak intensities of diffraction lines. The as-deposited films show a slight preferred grain orientation in (112) plane which appears during film growth. The preferred orientation factor of the (112) plane, $f(112)$, determined by using the method described in refs. 1 and 2 are calculated from diffraction spectra (fig. 2) (The f factor varies between zero for a non-oriented polycrystal to 1 for a perfect orientation). The f value difference between the two type of films is not very pronounced ($f=0.11$ for CIS #1 and $f=0.06$ for CIS #2). The f factors do not change significantly after annealing the films at 600°C for 10 min to 1 hour.

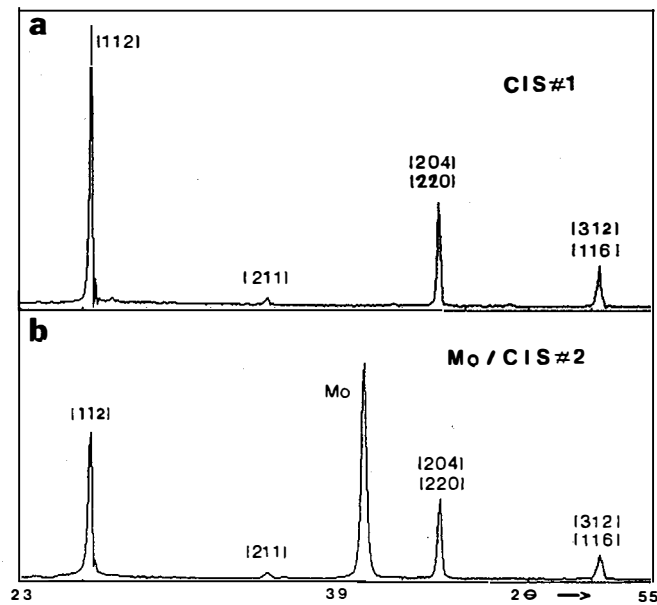


Fig. 2 X-ray diffractometer diffraction pattern of (a) CIS #1 film, as-deposited, and (b) CIS #2 film, as-deposited.

3-1-3. SEM AND EDX

Figure 3 shows the surface morphology differences between the two types of CIS films, as-deposited. The CIS #1 film surface looks very irregular with cracks. The CIS #2 film surface is smoother than that of type 1 films, with some dispersed protusions. We do not observe any surface morphology evolution of the films after annealing. The EDX analysis performed with a small e-beam do not reveal real compositional differences between protrusions and sample bulk.

The EDX technique which analyzes only the near-surface regions of samples (1 μm for 25 keV e-beam energy) reveals a decrease of about 17% in the Se initial concentration for species annealed at 600 $^{\circ}\text{C}$ for 1 hour.

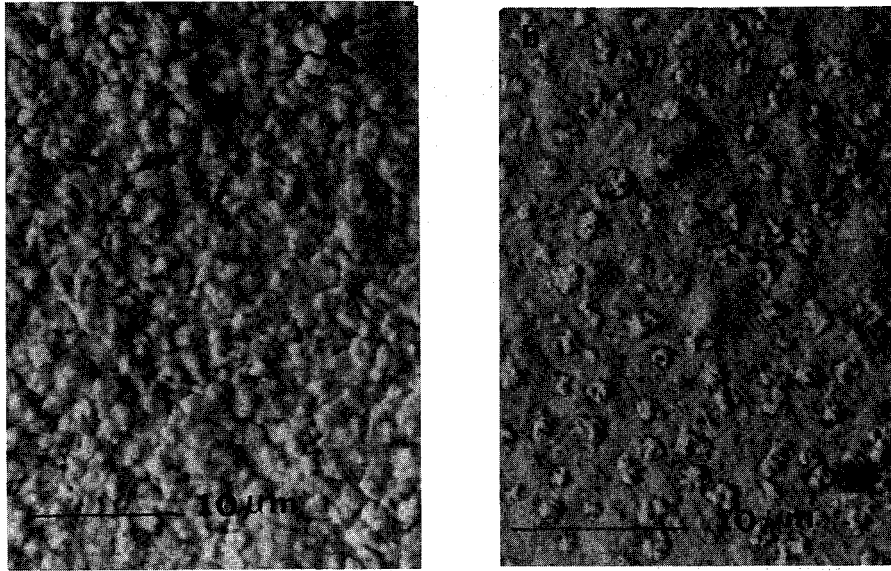


Fig. 3 Surface morphology of the as-deposited films of type (a) CIS #1, and (b) CIS #2.

3-1-4. RBS

Backscattering analyses were performed with ^4He ions with normal incidence of the beam on the sample and 170 $^{\circ}$ scattering angle.

Figure 4a shows an RBS spectrum that is characteristic of both types of CIS films. The composition calculated from the height of the surface signal of each element reveals that the films have the same composition. Within 5% of error the composition is determined as $\text{Cu}_{1.2}\text{In}_1\text{Se}_2$, i.e. the films are Cu-rich.

Figure 4b presents RBS spectra of a CIS #2 film before and after 10 min and 1 hour annealing at 600 $^{\circ}\text{C}$ in an argon atmosphere. After annealing, the spectra show a pronounced increase of the In signal at the surface associated with an atomique rearrangement in the near surface region of the sample. The thickness of this In rich transformed layer increases with annealing duration (about 100 nm after 1 hour).

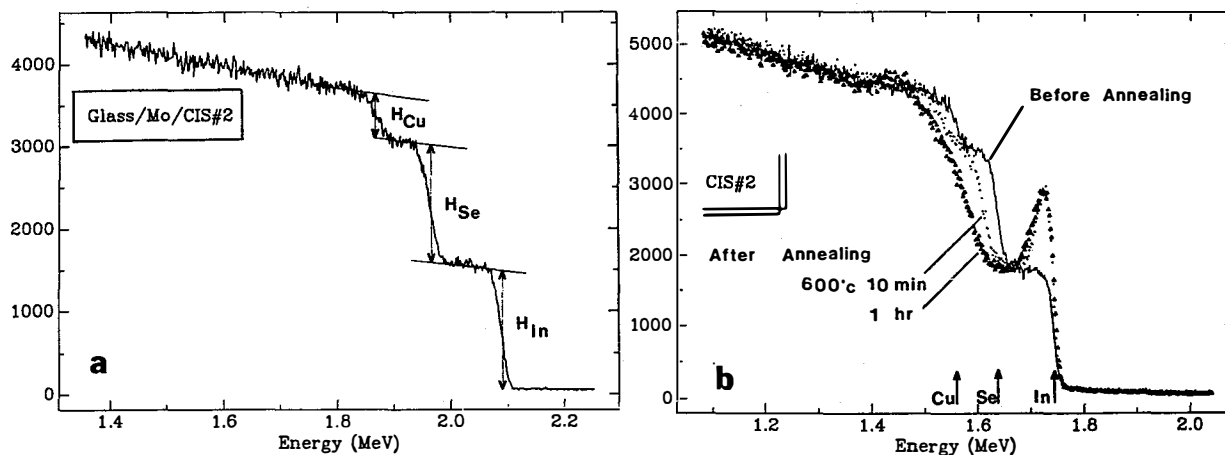


Fig. 4a 2.4 MeV $^4\text{He}^+$ backscattering spectrum of a CIS #2 film.

4b 2 MeV $^4\text{He}^+$ backscattering spectra of a CIS #2 film before and after 10 min, and 1 hour annealing at 600°C.

3-2. Contact study

For the purpose of these investigations, we have covered CIS films with a Mo or W top layer.

A CIS #1 film was covered by a rf magnetron-sputtered Mo film 45 nm thick (base chamber pressure: 7×10^{-7} Torr). An RBS analysis performed on a Mo film deposited on a carbon substrate reveals a 25% oxygen concentration in the deposited film. Planar TEM micrographs show that the Mo grain size of the as-deposited film is around 24 nm with a bcc structure. No Mo oxide compound could be detected in selected area diffraction patterns (SADP). Figure 5a presents RBS results for this specimen before and after 10 min annealing at 600°C. It is evident that some interaction between Mo and CIS takes place but details are difficult to extract from these spectra. X-ray diffraction performed on these samples before and after annealing shows no difference in regards to new compound formation, or Mo grain size evolution.

A CIS #1 film was covered by an rf magnetron-sputtered film of W (rather than Mo) 45 nm thick (base chamber pressure: 7×10^{-7} Torr). The oxygen concentration in the W was not measured in this case. The RBS spectra are shown in figure 5b for a sample before and after 10 min annealing in vacuum at 600°C. An interaction between the two layers is again evident. If the sample is laterally uniform, the spectra indicate a penetration of W into the CIS film (extended W signal towards lower energies near 1.75 MeV), and some possible diffusion of In, Se and/or Cu into W (reduced signal height of W).

A CIS #2 film was covered by an e-beam evaporated Mo film, 200 nm thick (base chamber pressure: 3.10^{-7} Torr). The RBS analyses of a film on carbon

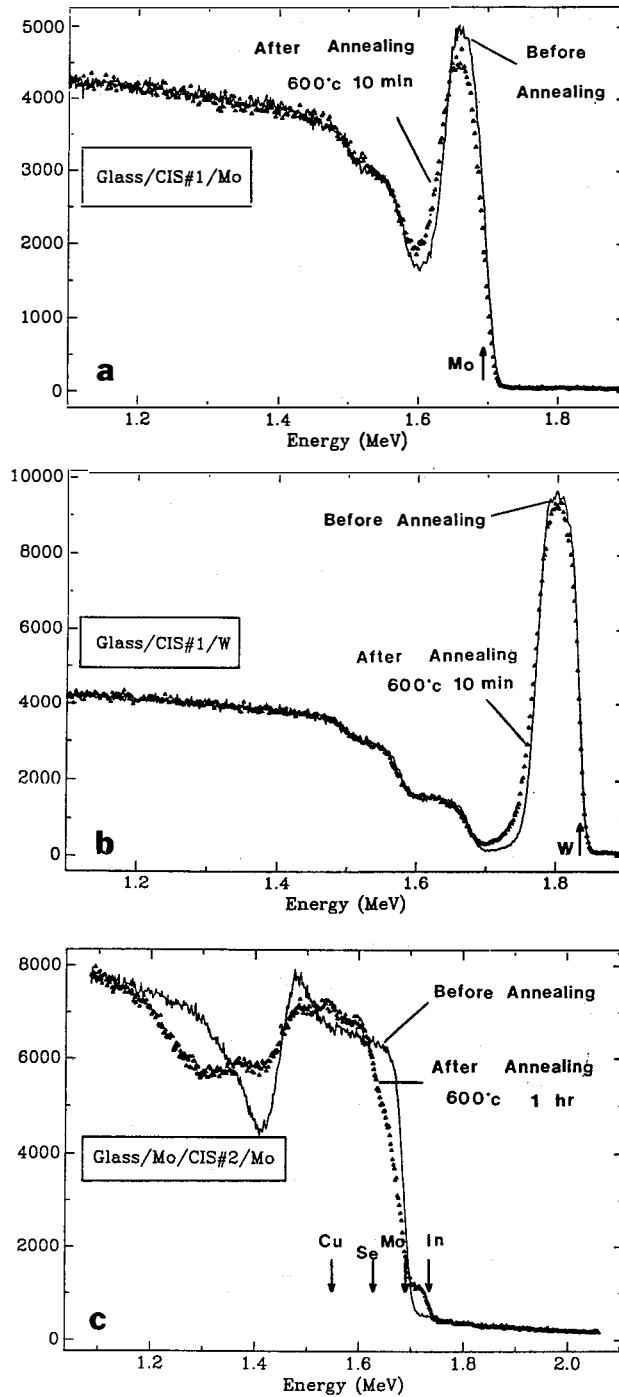


Fig. 5 2 MeV $^4\text{He}^+$ backscattering spectra of: (a) CIS #1 film covered with a magnetron-sputtered 45 nm thick Mo layer before and after 10 min. annealing in vacuum at 600°C, (b) CIS #1 film covered with a magnetron-sputtered 45 nm thick W layer before and after 10 min annealing in vacuum at 600°C, (c) CIS #2/film covered with an e-beam evaporated Mo film 200 nm thick before and after 1 hour annealing at 600°C. }

substrate reveals a 18% concentration of oxygen in the Mo film. The grain size measured from X-ray diffraction peak width is around 20 nm. The structure is bcc type without Mo oxide compound. Figure 5c presents RBS spectra for this CIS/Mo sample before and after 10 min and 1 hr. annealing at 600°C. The main observation is a general interdiffusion between CIS and Mo which increases with annealing duration. The In peak which appears after annealing at the top surface reveals a diffusion of In through the whole Mo layer. X-ray diffraction again shows no difference between these samples before and after annealing, and no evolution of the Mo grain size.

4. Discussion

We have analyzed two kinds of CIS films, one deposited on glass, the other deposited on a Mo layer. Both films are Cu rich [$\text{Cu}_{1.2}\text{In}_1\text{Se}_2$], contain microvoids and have a chalcopyrite microstructure. The main differences, apparently due to the original surface of growth, are the surface morphology, an enhanced grain size and columnar structure which is observed for films growing on Mo (CIS #1). The [112] preferential grain orientation, perpendicular to the film surface seems to be slightly more important for films on Mo than on glass. X-ray diffraction reveals the existence of rings which are presently not interpretable. They could either originate from a second phase or from ordered vacancies in the CIS chalcopyrite structure. The RBS analyses of films on glass (CIS #2) before and after annealing reveals atomique rearrangements which are difficult to specify. The RBS spectra can be interpreted in correlation with EDX surface analyses, as being generated by an In rich (Cu, In) surface layer that is depleted of Se which evaporates from the samples during annealing.

We have investigated the metal/CIS interface stability using different samples. In all cases, the Mo seems to diffuse into the CIS films. We assume that the phenomenon is made easier by defects like microvoids that exist in CIS films. This is confirmed by the W/CIS interface study. The diffusion of Cu, In or Se into Mo are not clear and seems to depend partially on the Mo layer quality and therefore on the elaboration process. Indeed, we observe an important In diffusion to the top surface of the e-beam evaporated Mo film. This diffusion process occurs probably at the grain boundaries. The process is not observed in the case of the rf magnetron-deposited Mo film of which the grain size is a little larger and the impurity content clearly bigger (25% of oxygen) than in evaporated Mo films. The resulting enhanced decoration of grain boundaries may be responsible. X-ray diffraction technique that we have used are not sensitive enough to detect the interaction between Mo/CIS.

5. Conclusion

We will pursue CIS films characterization by RBS, TEM, and X-ray diffraction to clarify the issue of a possible second phase and to investigate the lateral, chemical and structural uniformity. Optical uniformity by IR transmission measurements will be performed and correlated with the previous study. A systematic investigation of thermally induced bilayer reactions of Mo with Cu, In and Se individually using RBS and XTEM analysis will be undertaken to seek a correlation with results obtained similarly on Mo/CIS samples.

The CIS films prepared on substrates of glass or Mo-coated glass show the same polycrystalline structure, a Cu rich composition, and a preferential grain orientation, but different surface morphologies, grain sizes and shapes. RBS measurements have been performed on different samples before and after 600°C annealing. This treatment induces Se evaporation from the CIS films and interdiffusion between Mo/CIS.

REFERENCES:

- 1) F.J. Pern, A. Mason, J. Dolan, R. Nouf, SERI Proceedings of the Polycrystalline Thin Film Program Meeting of August 16-17, 1987.
- 2) F.K. Lotgering, J. Inorganic. Nucl. Chem., 9 (1959) 113.

Title: **Analysis of Loss Mechanisms in Polycrystalline Thin-Film Solar Cells**

Organization: Physics Department, Colorado State University
Fort Collins, Colorado

Contributors: J. R. Sites, principal investigator; P. H. Mauk, H. Tavakolian, R. A. Sasala

The objective of this program is to design and demonstrate a system for routine, unambiguous, and quantitative analysis of loss mechanisms in individual polycrystalline solar cells. To be effective these procedures must be practical with equipment commonly available in solar cell laboratories and must be compatible with straightforward mathematical analysis.

Analysis Techniques

Three areas of analytical technique have undergone detailed examination and refinement [1-4].

The first area is an accurate determination of the diode quality factor for non-ideal photodiodes [2]. The procedure is to measure the slope of dV/dJ vs. $(J + J_L)$, with correction for shunting effects when necessary. This technique allows one (1) to deal with large deviations from superposition, (2) to unambiguously separate the illuminated diode quality factor and the series resistance, and (3) to easily recognize the onset of current shunting or limiting effects. For reasonably well behaved polycrystalline cells the diode quality factor uncertainty is ± 0.04 . Fig. 1 shows the increase in diode quality factor for a SERI fabricated CuInSe_2 cell from near 1.6 in the dark to just over 2.0 at AM1 intensity. It also shows the corresponding decrease in series resistance.

The second area is the use of the frequency and voltage dependence of capacitance to determine (1) carrier density, and hence Fermi level position, in the more lightly doped semiconductor, (2) width of the intrinsic layer often found adjacent to a polycrystalline heterojunction, and (3) density of extraneous states at the Fermi level in the depletion region [3]. For CuInSe_2 cells from three laboratories, the values extracted show a relatively modest dependence on temperature and light intensity. Reliable interpretation of the capacitance measurements requires continual monitoring of actual junction voltage, the real to imaginary impedance ratio, and the degree of voltage sweep hysteresis.

The third area is the apparent quantum efficiency of a solar cell as a function of voltage [4]. Quantum efficiency measurements are generally reliable input for photocurrent loss analysis when the forward current of the diode is small compared to the photogenerated current. All cells, however, exhibit major reductions in apparent quantum efficiency under forward bias. For the crystalline cells, this reduction is fully explained by the series resistances of the circuit and the cell. For polycrystalline cells, the voltage dependence is often additionally affected by an increase in diode quality factor or a reduction in series resistance with radiation intensity.

In no case does the voltage dependence of collection efficiency play a significant role.

Current Losses

Fig. 2 indicates how such data can be utilized to separate current loss mechanisms in a polycrystalline thin-film solar cell. It assumes that the measured quantum efficiency QE can be used without correction. The lost photon fraction, $1-QE$, can be assigned to at least four loss mechanisms. The grid fraction loss is simply the geometric grid coverage. Reflection can be measured independently, or alternatively, approximated by extending the broad valley of the photon loss data. Such an approximation is reasonable when a cell has a rough front surface and thus washed out interference effects. The remaining loss at short wavelengths is attributed to window layer absorption, and that of long wavelengths to photons that penetrate to depths comparable or greater than the diffusion length. This separation of long and short wavelength losses is generally clear for good quality cells. Furthermore, the feature of Fig. 2, where essentially all loss at intermediate wavelengths is accounted for by reflection and grids, is not unusual. The photocurrent reduction for each loss mechanism is easily calculated by integration of the photon loss weighted by the solar spectrum from the top half of the figure.

Voltage Losses

Voltage losses compare the actual maximum power voltage V_{MP} with that available for a single crystal cell of the same band gap. Fig. 3 illustrates the procedure for CdTe. The solid lines are data and the dash-dot lines the series resistance correction. The voltage loss is divided between that due to the polycrystallinity (PX), the difference between light and dark curves (L), and the series resistance (R). For today's best CdTe cells, all three are significant, and the total voltage loss at maximum power is 0.3-0.4 volt. For good $CuInSe_2$ the PX loss is generally dominant, and it has a magnitude near 0.2 volt.

References

1. Sites, J.R., "Analysis of Loss Mechanisms in Polycrystalline Thin-Film Solar Cells," SERI/STR-211-3545 (July 1989).
2. Sites, J.R. and P.H. Mauk, "Diode Quality Factor Determination for Thin-Film Solar Cells," Solar Cells, in press.
3. Mauk, P.H., H. Tavakolian, and J.R. Sites, "Interpretation of Thin-Film Polycrystalline Solar Cell Capacitance," IEEE Trans. Electron Devices, in press.
4. Sites, J.R., H. Tavakolian, and R.A. Sasala, "Analysis of Apparent Quantum Efficiency," submitted to Solar Cells.

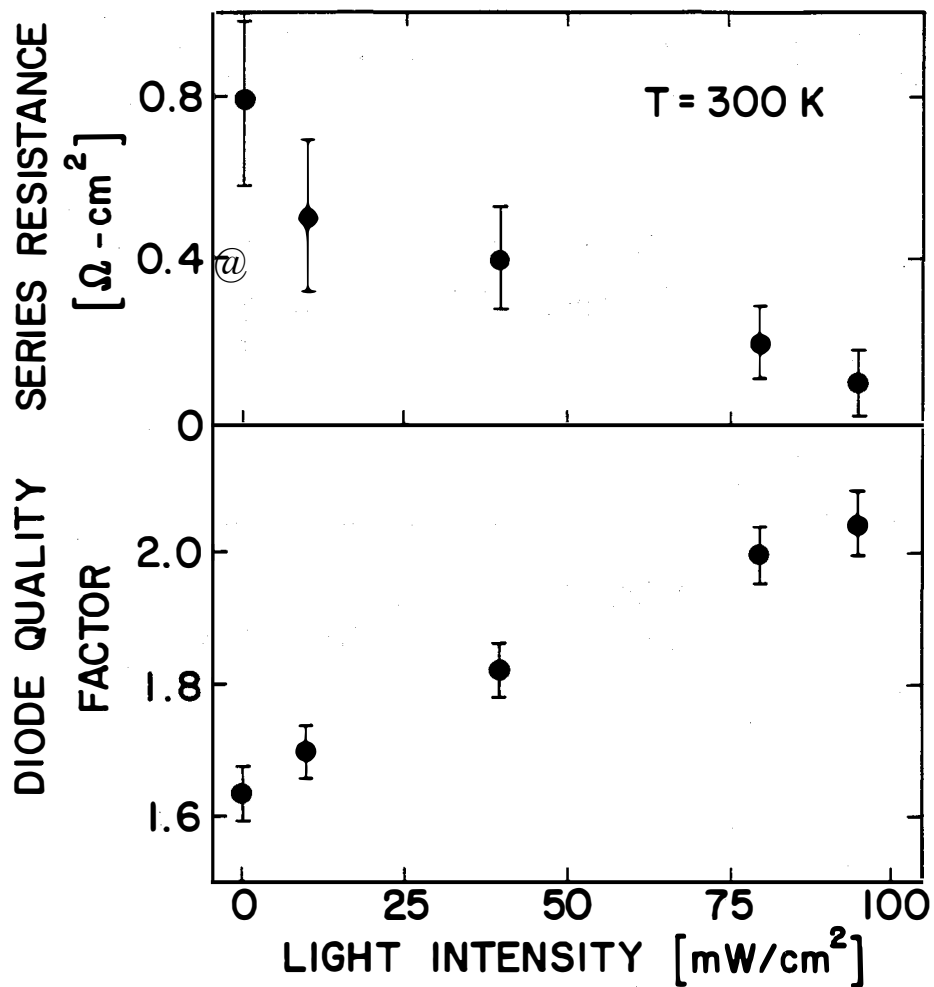


Figure 1. Variation of series resistance and diode quality factor with illumination intensity. Evaporated SERI CuInSe_2 cell.

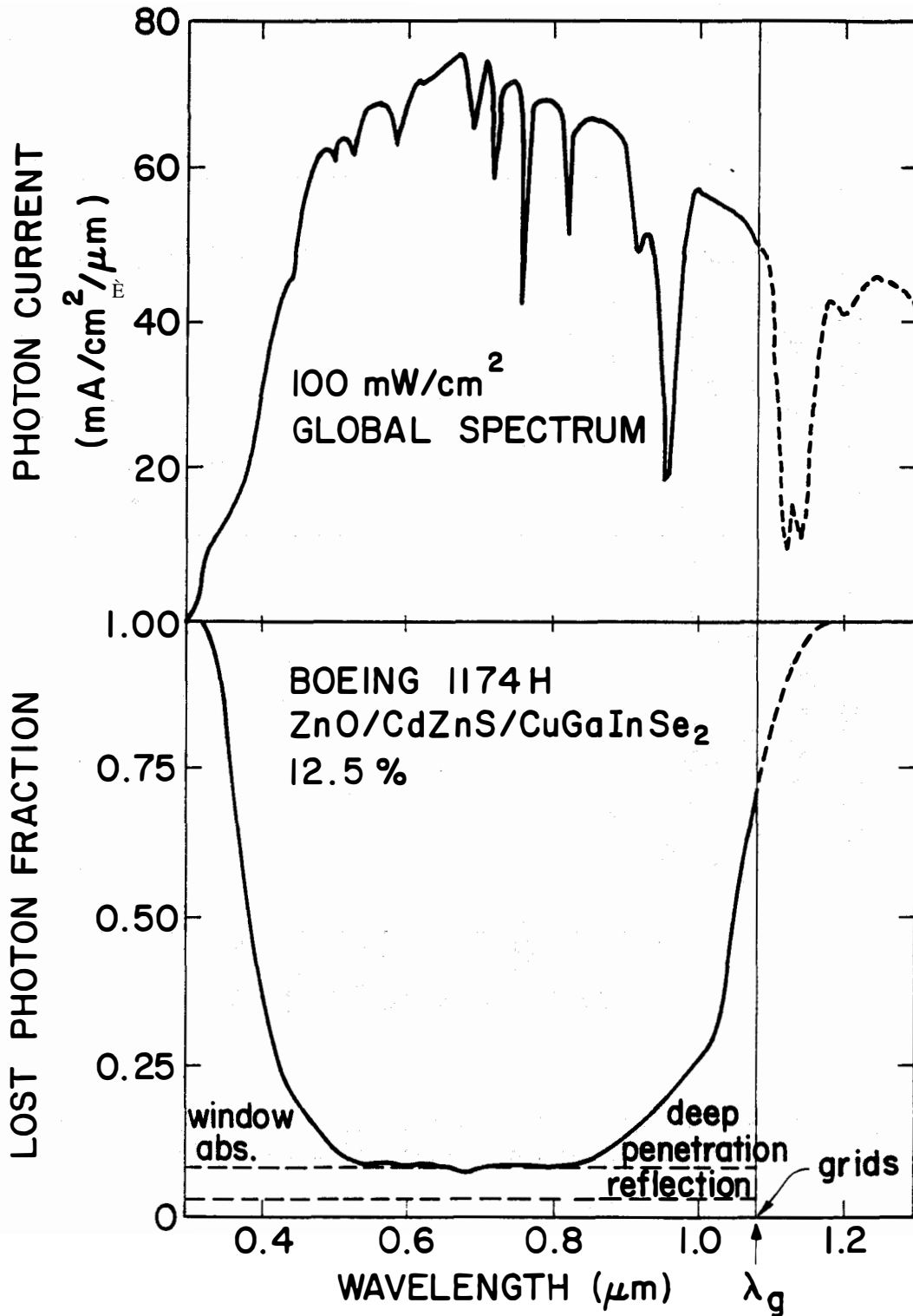


Figure 2. Standard solar spectrum and separation of photon losses.

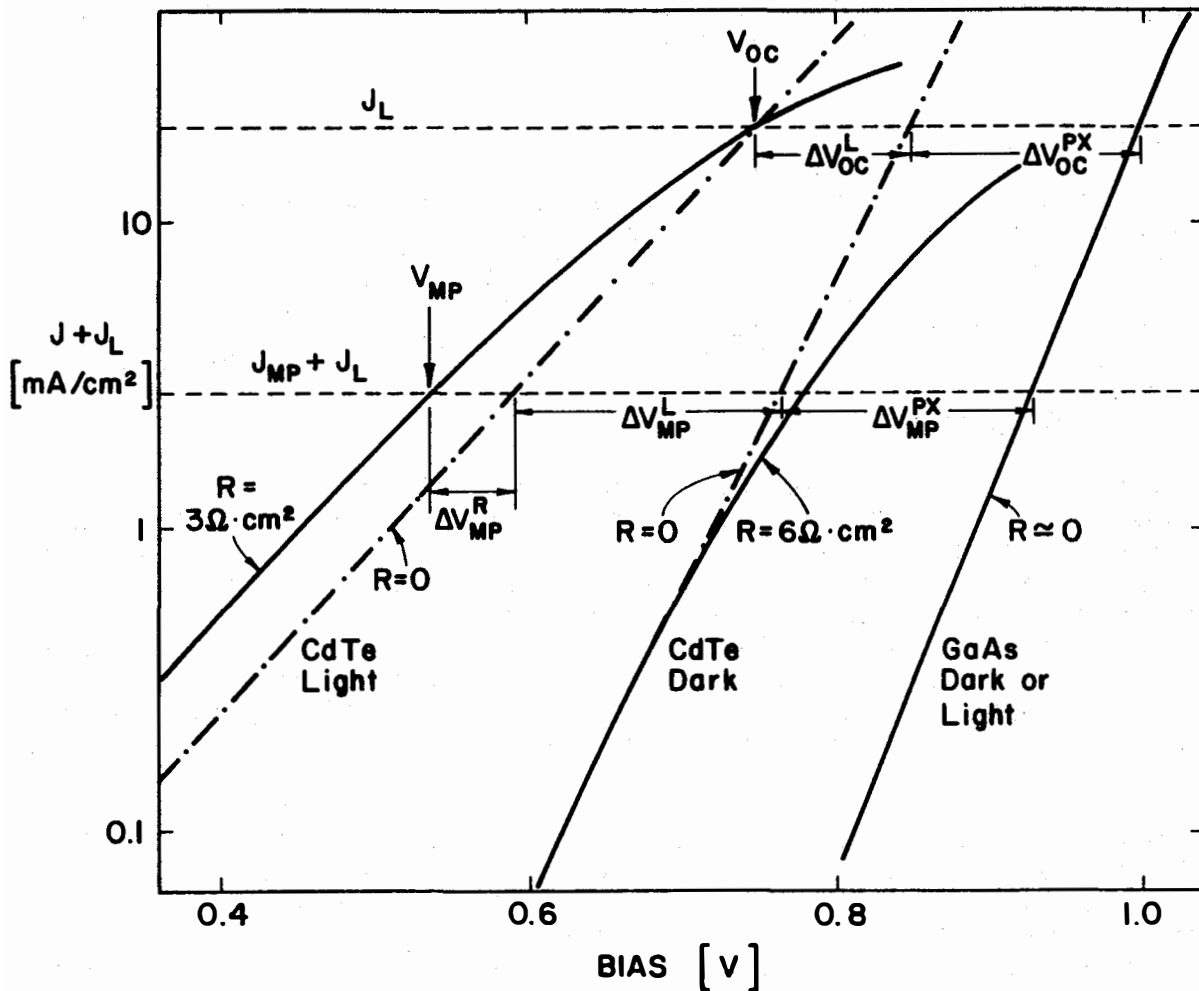


Figure 3. Analysis of voltage losses in CdTe solar cells.

Title: High Efficiency Cadmium and Zinc Telluride Based Thin Film Solar Cells

Organization: Georgia Institute of Technology
Atlanta, Georgia 30332

Contributors: A. Rohatgi, C. J. Summers, A. Erbil, R. Sudharsanan, and S. A. Ringel

Objective:

The objective of this program is to develop wide bandgap (1.6 -1.8 eV) polycrystalline thin films to be used as absorber material in the top-cell of the cascade cell structure. Target-cell efficiency for the wide bandgap cell is 10% with 80% subgap transmission. CdMnTe films are being grown by MOCVD while CdZnTe films are being deposited by MBE along with CdTe as a baseline material.

Thin-Film Growth:

CdTe and CdMnTe films were grown by metalorganic chemical vapor deposition (MOCVD) on glass/SnO₂/CdS substrates. CdMnTe films were grown using dimethylcadmium, diethyltellurium, as source materials for Cd and Te respectively and tricarbonyl methylcyclopentadienyl manganese and Bis-isopropylcyclopentadienyl manganese as source materials Mn. The CdMnTe films were grown at substrate temperature of 420 C, while CdTe films were grown at substrate temperature in the range of 300 to 400 C with diallyltellurium and diisoproyltellurium as sources for Te.

CdZnTe and CdTe films were grown by MBE. Elemental sources were used instead of CdTe and ZnTe binary sources, with a purity of at least 5N. The substrate temperature was kept at 275 C for 30 minutes to commence film growth and increased to 300 C for the remainder of the run. Growth rates were typically ~1 um/hr for both CdTe and CdZnTe. In selected instances Sb was used as a dopant and few attempts were made to grow ~100 Å thick CdTe interlayer between CdS and CdZnTe films to modify the interface quality.

Film Characterization:

As-grown films were characterized by several techniques like X-ray diffraction (XRD), surface photovoltage (SPV), Auger electron spectroscopy (AES), Infrared spectroscopy (IR), and photoluminescence (PL) measurements to determine composition, bandgap, thickness, compositional uniformity, and quality. All the above measurements confirmed successful growth of CdMnTe and CdZnTe films with the bandgap of 1.7 eV with uniform composition.

Cell Fabrication and Analysis:

Front-wall solar cells were fabricated with glass/SnO₂/CdS/CdZnTe or CdMnTe/ZnTe/Ni structure. This was done in collaboration with

AMETEK corporation. The films were annealed at 400 C for 30 minutes in air followed by a mild etch of Br:MeOH. Both n-i-p and n-p solar cells were fabricated. n-i-p structure was fabricated by depositing Cu doped ZnTe layer. Ni contacts were deposited through a shadow mask.

CdTe cells were also fabricated using both growth techniques to provide a baseline for ternary cell development.

Figure 1 shows the lighted I-V data for our best CdTe cell, grown by MOCVD. The 9.7% efficiency achieved is the highest reported efficiency for MOCVD-grown CdTe. The V_{oc} (.730V) and fill factor (.6) values of MOCVD-grown CdTe/CdS cells are lower than the best (11-12%) CdTe/CdS cells grown by other techniques like electrodeposition. Bias dependent spectral response measurements (figure 2) show a uniform decrease in spectral response with increasing forward bias voltages. These results suggest a voltage dependent recombination of carriers at CdTe/CdS interface. Model calculations were performed on the highest efficiency MOCVD-CdTe cell to shed more light on the loss mechanisms. The calculations suggest efficiency as high as 13.5% can be achieved on MOCVD-grown CdTe cells just by improving the CdTe/CdS interface. Further improvements can be realized by reducing the absorption in CdS layer.

CdZnTe cells were fabricated using the CdTe cell process sequence. It was found that the standard CdTe processing reduces the ternary bandgaps from 1.7 to 1.55 eV, resulting in significantly reduced subgap transmission with cell efficiencies of 3-4%. More detailed research revealed that the CdCl₂ treatment used in CdTe processing is the cause for bandgap reduction in ternary films. A new chemical treatment (CdCl₂ + ZnCl₂) was developed to retain the bandgap during annealing (figure 3), however the cell performance was still limited by high series resistance.

Effects of Processing:

Process development was necessary to reduce the high series resistance of the ternary cells. The effects of annealing and surface preparation on the properties of CdZnTe films were studied by X-ray photoelectron spectroscopy, AES, SPV, and C-V measurements. Though the air annealing is necessary to enhance the uniformity of the p-type conductivity of CdZnTe films, but it results in a thick oxide layer of zinc at the surface. It was found by AES measurements that Br:MeOH used for CdTe cells etch does not remove zinc oxides formed due to air annealing. The presence of zinc oxide and the absence of Te rich layer on the surface of the film may be responsible for the high series resistance observed in CdZnTe devices. In contrast to Br:MeOH etch, etching of the annealed CdZnTe surfaces with a concentrated K₂Cr₂O₇:H₂SO₄ solution removed all oxides and left a surface completely depleted in Cd and Zn. Figure 4 shows the AES depth profiles on as-grown and air annealed CdZnTe films etched with Br:MeOH and potassium dichromate solutions. Subsequently fabricated In/CdZnTe Schottky barrier diodes on etched surfaces confirmed a significant reduction in

barrier height, from ~1.2 eV for the Br:MeOH surface to ~0.65 eV for the $K_2Cr_2O_7:H_2SO_4$ etched surface due to a Te-rich surface layer with a p-type doping concentration of $\sim 3 \times 10^{17} \text{ cm}^{-3}$. Figure 5 shows the dark I-V characteristics of various annealed and chemically etched CdZnTe surfaces.

Future Work:

We plan to apply the basic understanding developed through materials characterization, process development, and device analysis to improve the CdTe and CdZnTe cell performance. We intend to a).investigate preheat treatments of CdS, prior to CdTe deposition, to improve interface quality, b). optimize $CdCl_2+ZnCl_2$ chemical treatment to improve CdZnTe cell efficiency and the understand the exact role of chloride treatment, c). optimize $K_2Cr_2O_7:H_2SO_4$ treatment to reduce the series resistance of ternary cells, and d). perform DLTS measurements and investigate carrier transport mechanisms to develop a better qualitative and quantitative understanding of interface recombination mechanisms in CdTe and CdZnTe devices.

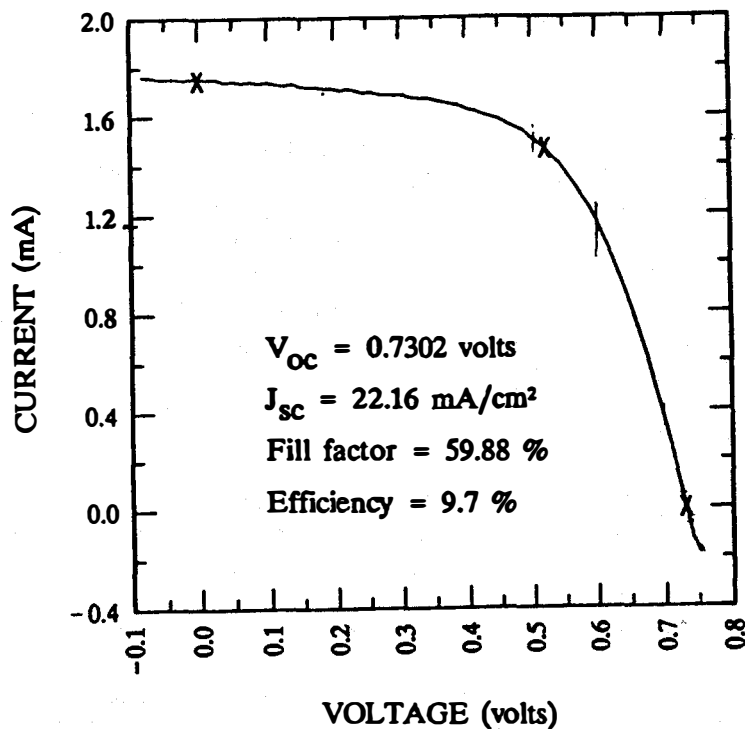


Figure 1. Light I-V data of 9.7% MOCVD-grown CdTe/CdS solar cell.

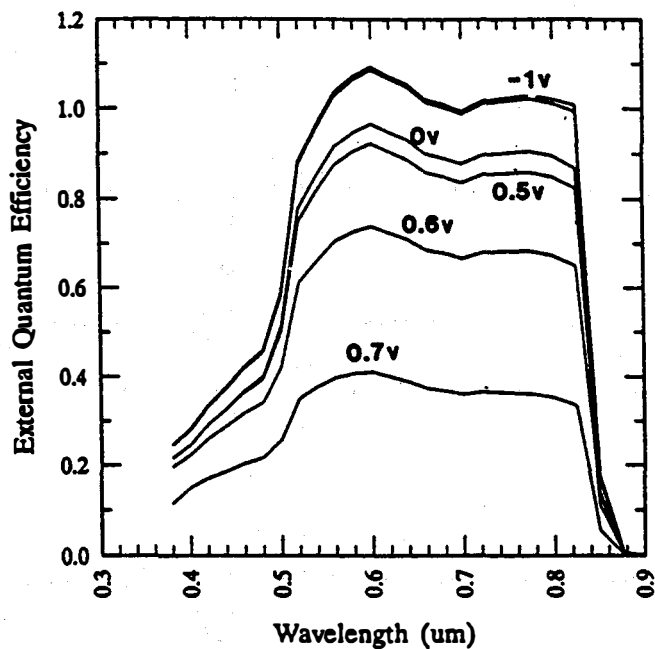


Figure 2. Bias-dependent spectral response data of 9.7% MOCVD-grown CdTe/CdS solar cell.

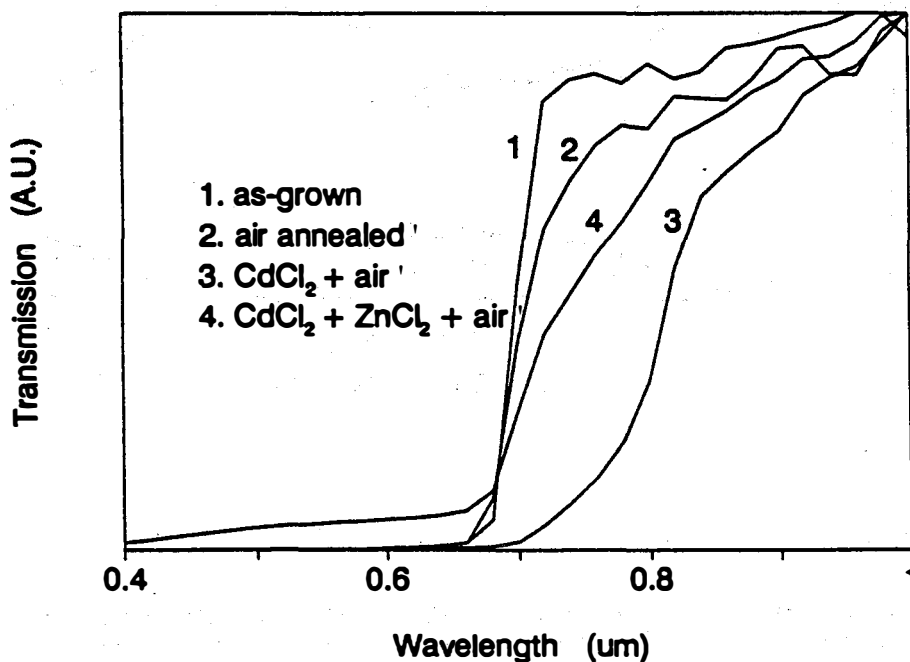


Figure 3. Transmission spectra of polycrystalline CdZnTe films on CdS/SnO₂/glass substrates for various processing conditions.

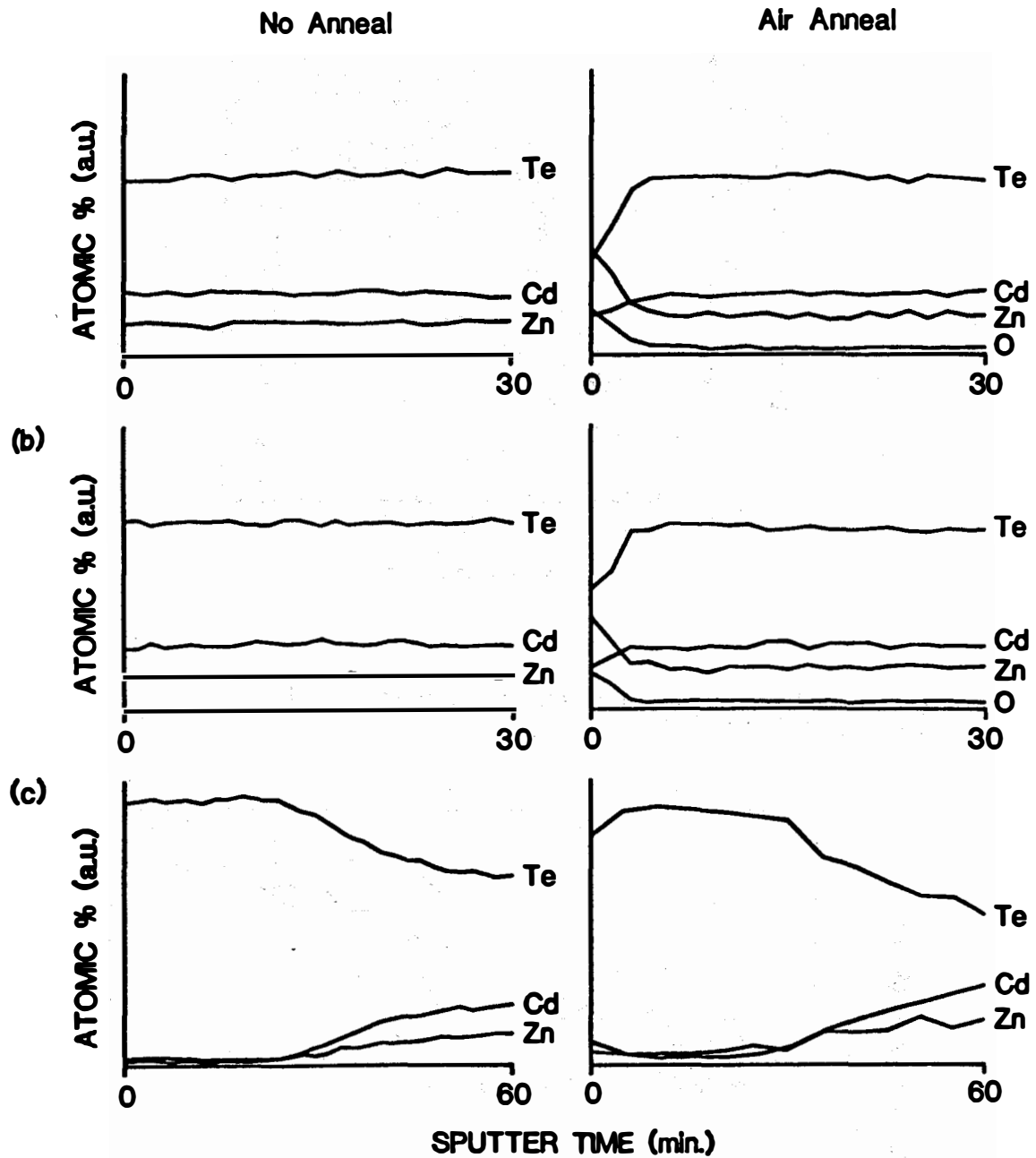


Figure 4. Auger depth profiles of as-grown and air annealed CdZnTe after (a) no etch, (b) Bromine-methanol etch, and (c) saturated dichromate etch.

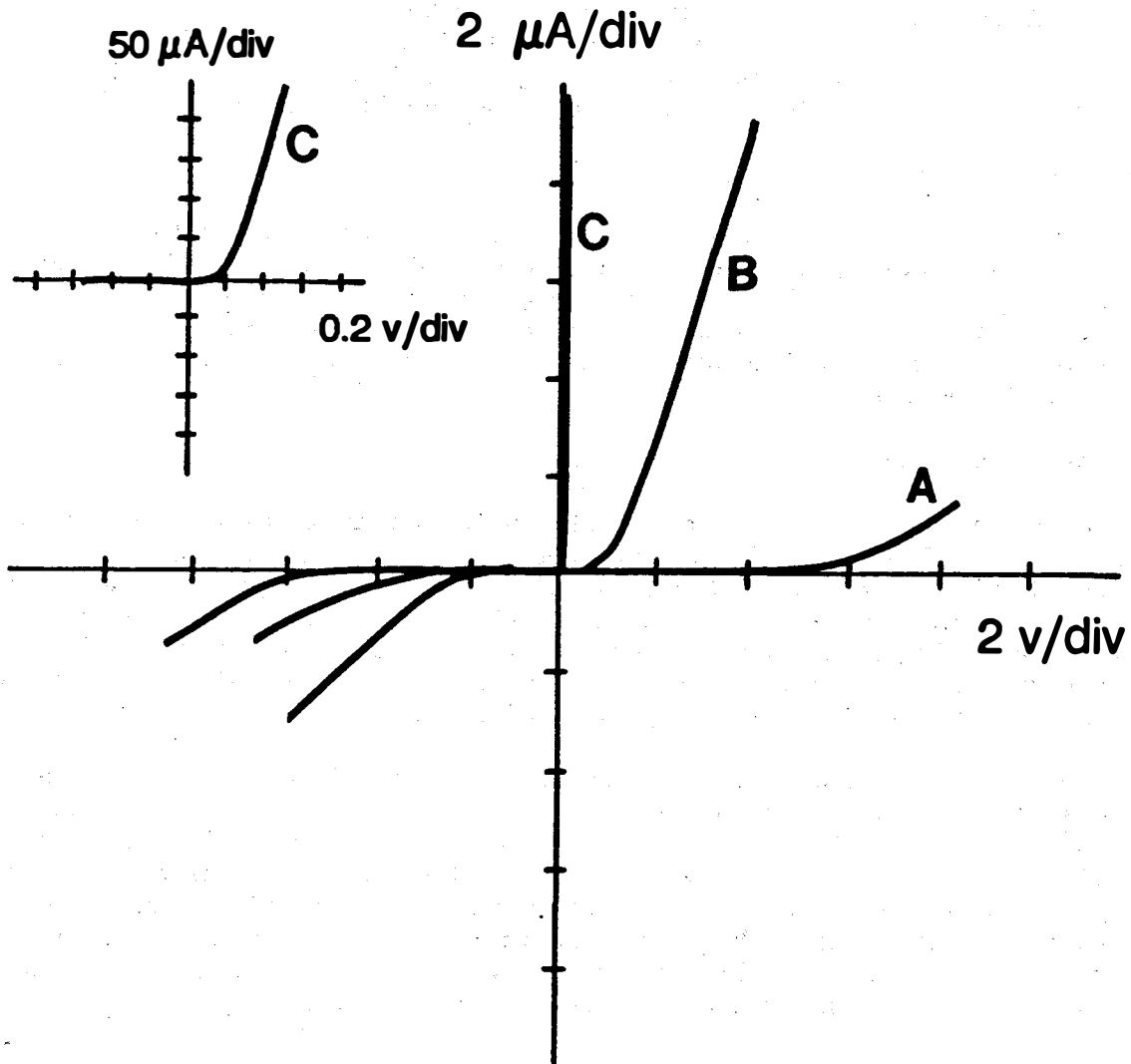


Figure 5. Dark I-V characteristics of In/CdZnTe junctions made on (a) air annealed, (b) air annealed + bromine-methanol etched, and (c) air annealed + saturated dichromate etched CdZnTe surfaces. Curve (c) is shown at a larger scale in the inset for clarity.

Title: Fundamentals of Polycrystalline Thin-Film Materials and Devices

Organization: Institute of Energy Conversion
University of Delaware
Newark, Delaware 19716

Contributors: B. N. Baron, Project Director;
R. W. Birkmire and J. E. Phillips,
Principal Investigators; B. E. McCandless, M. Roy and
W. N. Shafarman, Research Contributors.

Objectives:

The objective of this research is to gain a deeper understanding of the materials, processing, and device issues needed to improve the performance, reliability, and cost of polycrystalline thin film solar cells. A further objective of this research is to support the efforts of the SERI polycrystalline thin film task through collaboration with other research groups, especially the thin film PV industry.

Technical Approaches:

Procedures for fabricating device-quality CuInSe_2 thin films by selenization of Cu and In metal layers are being developed. The metal layers are deposited by electron beam evaporation. Selenization reactions of hydrogen selenide and elemental selenium are being studied. CuInSe_2 thin films are evaluated for chemical composition, structure, and morphology. Characterization of relevant opto-electronic properties of CuInSe_2 thin films is accomplished by fabrication and analysis of diagnostic CuInSe_2 photovoltaic devices.

Modifying the band gap of CuInSe_2 is being investigated in order to reduce space charge recombination and increase open circuit voltage of CuInSe_2 solar cells. Approaches include alloying with Ga to form $\text{CuIn}_{1-x}\text{Ga}_x\text{Se}_2$ and graded band gap structures. CuInSe_2 devices with thin window layer and high transparency conductive oxide top contact layers are being investigated in order to assess approaches to achieving high short circuit current. Emphasis is on thin CdS window layers deposited at low temperatures from aqueous solution and ZnO and ITO transparent top contact layers deposited by sputtering.

CuInSe_2 thin film solar cells in a superstrate configuration - glass/transparent conductor/window layer/ CuInSe_2 /back contact - are being investigated.

CdTe solar cells deposited by physical vapor deposition are being studied in order to understand the effects of post-deposition processing steps (e.g. heat treatments, chemical treatments and contacting) on material properties and device performance.

Measurements and analysis of bi-facial quantum efficiency of CuInSe_2 devices fabricated on semi-transparent substrates are used to determine diffusion length and optical absorption coefficients of CuInSe_2 in operational devices. Measurements and analysis to quantify recombination losses in CuInSe_2 and CdTe

devices are performed with emphasis on accurate determination of mechanisms that limit open circuit voltage. The analyses are used to develop predictive models of thin film CuInSe_2 and CdTe device behavior which will be used to guide further improvements in the efficiency and reliability of polycrystalline thin-film solar cells.

Significant Results:

A system to grow CuInSe_2 films by selenizing Cu/In layers in H_2Se gas was designed and constructed. Single phase CuInSe_2 films were obtained by reacting Cu and In layers (250 and 400nm thick, respectively) with H_2Se at 400°C by flowing a mixture of 2.1 mole% H_2Se in Ar at 50 sccm for 2 hours.

Increasing the band gap within the space charge region by growing a thin $\text{Cu}(\text{GaIn})\text{Se}_2$ layer on the surface of CuInSe_2 was selected as an approach for improving V_{oc} without loss in J_{sc} . An open circuit voltage, $V_{oc}=0.48$ V was achieved for a $(\text{CdZn})\text{S}:\text{In}/\text{Cu}(\text{GaIn})\text{Se}_2/\text{CuInSe}_2/\text{Mo}$ device in which the $\text{Cu}(\text{GaIn})\text{Se}_2$ layer was $\sim 500\text{nm}$ thick.

In the investigation of window layers for achieving high J_{sc} , CuInSe_2 cells with thin CdS ($<500\text{\AA}$) grown from aqueous solution and a ZnO transparent contact were fabricated. Figure 1 shows the quantum efficiency of a cell with a thin solution grown CdS window layer along with data from cells with $(\text{CdZn})\text{S}:\text{In}/\text{ITO}$ and just ZnO . The $(\text{CdZn})\text{S}:\text{In}$ was deposited by co-evaporation of CdS , ZnS and In and was $1.5 \mu\text{m}$ thick with 15% Zn and $E_g=2.6\text{eV}$. The cells with thin CdS and ZnO alone had enhanced quantum efficiency below 500nm compared to the cell with $(\text{CdZn})\text{S}:\text{In}$. $\text{CuInSe}_2/\text{ZnO}$ cell had the highest quantum efficiency at 400nm but lower J_{sc} than the cell with thin CdS due to greater reflection losses and low V_{oc} . Although cells with both thin solution grown CdS and thicker evaporated $(\text{CdZn})\text{S}:\text{In}$ had comparable efficiencies, the most promising approach to higher efficiency is with solution grown CdS since both high J_{sc} and V_{oc} should be achievable.

CuInSe_2 cells were made in a superstrate configuration with the CuInSe_2 film deposited onto a glass/ ITO/CdS substrate. The CuInSe_2 was deposited by vacuum evaporation at a substrate temperature of 300°C with only a single layer of CuInSe_2 . Devices were completed with a 3mm Pt dot as the back contact to the CuInSe_2 . The best device had an efficiency of 5.9% with $V_{oc}=0.325\text{V}$ and $J_{sc}=34.6 \text{ mA}/\text{cm}^2$. The reason for the low voltage on these devices is not understood, but the voltage is similar to those measured on cells with single layer CuInSe_2 using a substrate design. The low FF may be due to series resistance and, possibly, a non-ohmic Pt contact.

By analyzing the current-voltage behavior and spectral response of thin film $\text{CuInSe}_2/(\text{CdZn})\text{S}$ and CdS/CdTe polycrystalline solar cells with transparent contacts, it has been possible to determine and quantify the mechanisms controlling device behavior under illumination. Current-voltage analysis done on $\text{CuInSe}_2/(\text{CdZn})\text{S}$ devices as a function of temperature have identified space-charge-recombination as the dominant mechanism limiting V_{oc} [1].

Spectral response measurements as a function of applied voltage have been found to include significant series resistance effects which cause the magnitude and shape of the spectral response curve to change with applied voltage. These

changes in the spectral response curves of $\text{CuInSe}_2/(\text{CdZn})\text{S}$ devices as a function of applied voltage have been quantitatively explained by series-resistance effects while interface recombination was found to play a negligible role [2].

The spectral response through both the CdS and the back Mo contact have been measured on CuInSe_2 devices with transparent contacts. Figure 2 shows the internal quantum efficiency measured through a 400Å semi-transparent Mo back contact and through the ITO/CdS. Using the bi-facial response and standard photocurrent formulas [3], the diffusion length (0.9 μm) and the absorption coefficient as a function of wavelength were determined (Figure 3).

High efficiency CdTe/CdS cells were fabricated by physical vapor deposition using a series of post-deposition process steps to optimize the cell. The optimization process was also successfully applied to cells using CdTe and CdS deposited by different methods. Bi-facial current-voltage and quantum efficiency analysis of the CdTe devices at various stages of the optimization process showed the evolution of the device from a p-i-n structure to a p-n heterojunction and pointed strongly to the role of grain boundaries in determining effective lifetime in the CdTe. The best CdTe device fabricated by PVD had 9.6% efficiency with a $V_{oc}=0.73\text{V}$, $J_{sc}=19 \text{ mA/cm}^2$ and $\text{FF}=69\%$, measured at the Solar Energy Research Institute under AM1.5 Global conditions at 25°C.

Conclusions:

CuInSe_2 solar cells with $J_{sc} > 40 \text{ mA/cm}^2$ have been achieved using thin CdS and ZnO as window layers. Modifying the band gap of the space charge region in a CuInSe_2 cell by growing a thin layer of $\text{Cu}(\text{GaIn})\text{Se}_2$ has been shown to be a promising approach for improving V_{oc} . Superstrate CuInSe_2 solar cell with efficiencies approaching 6%, were fabricated. Higher efficiency superstrate CuInSe_2 cells are expected from optimization of CuInSe_2 deposition conditions. Analysis of bi-facial spectral response of transparent CuInSe_2 devices resulted in determination of optical absorption coefficients and a minority carrier diffusion length of 0.9 micron for CuInSe_2 in an operational CuInSe_2 solar cell.

CdTe/CdS solar cells with an efficiency over 9.5% were fabricated by a physical vapor deposition process.

References:

1. M. Roy, et al., 20th IEEE Photovoltaic Specialists Conf., Las Vegas, 1618 (1988).
2. J. E. Phillips and M. Roy, 20th IEEE Photovoltaic Specialists Conf., Las Vegas, 1614 (1988).
3. H. J. Hovel "Solar Cells" (R. K. Willardson and A. C. Beers, eds.), Semiconductors and Semimetals, Vol. 11, 16-19, Academic Press, New York.

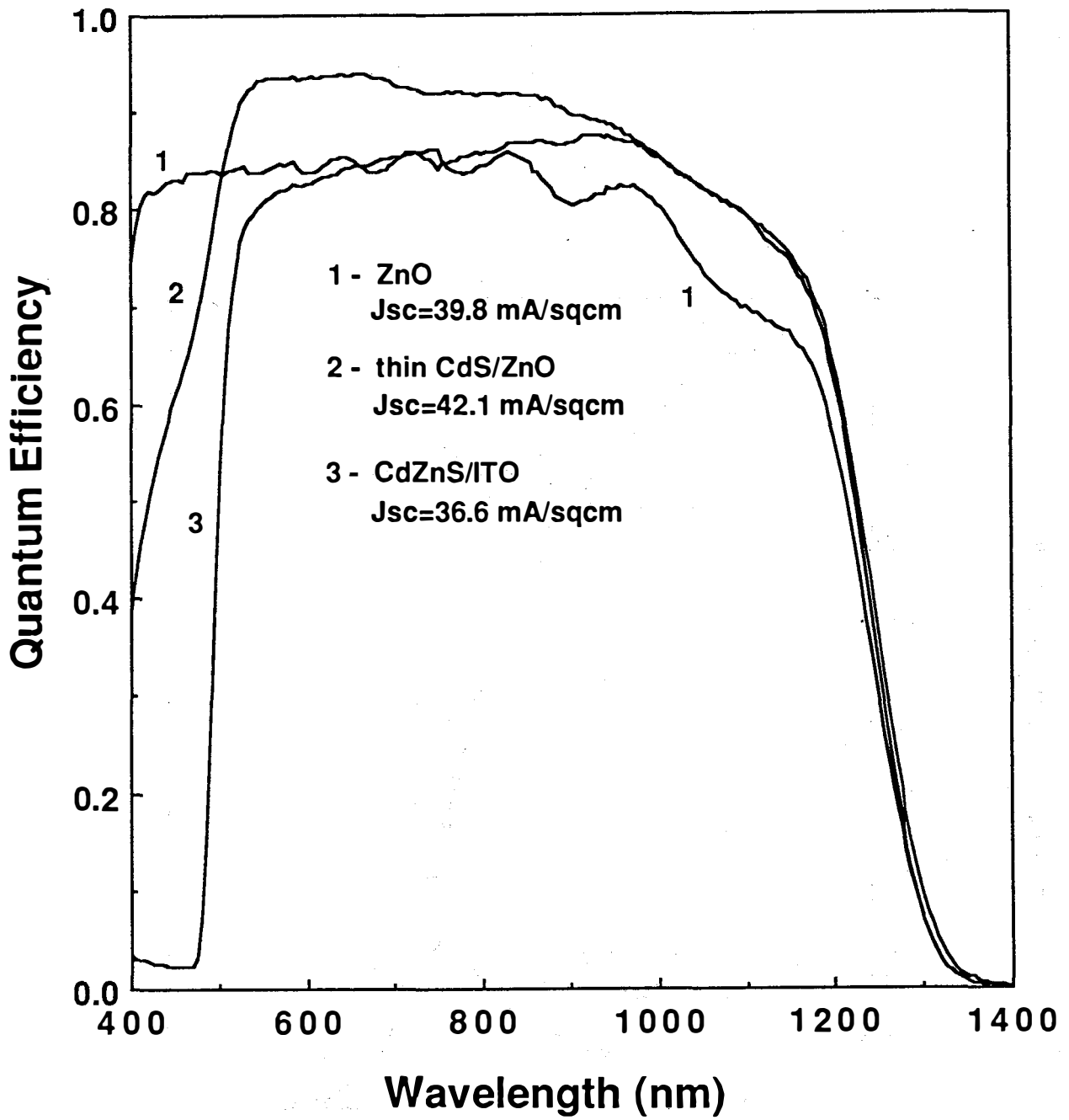


Figure 1: Quantum Efficiency of CuInSe_2 Cells with Different Window Layers.

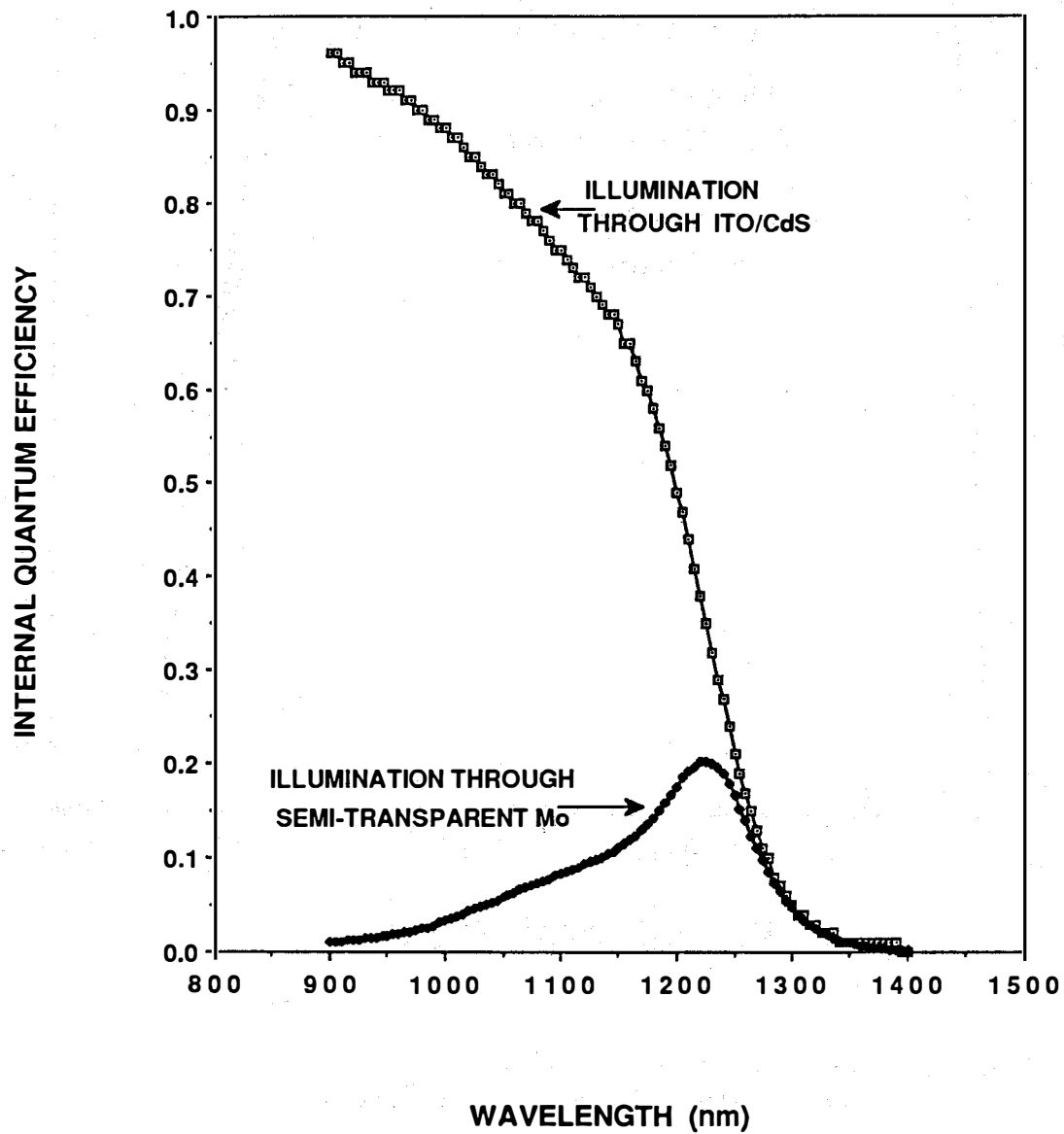


Figure 2: Internal Quantum Efficiencies of ITO/CdS/CuInSe₂/Mo/glass Solar Cells with Illumination through ITO/CdS and through Semi-transparent Mo Back Contact.

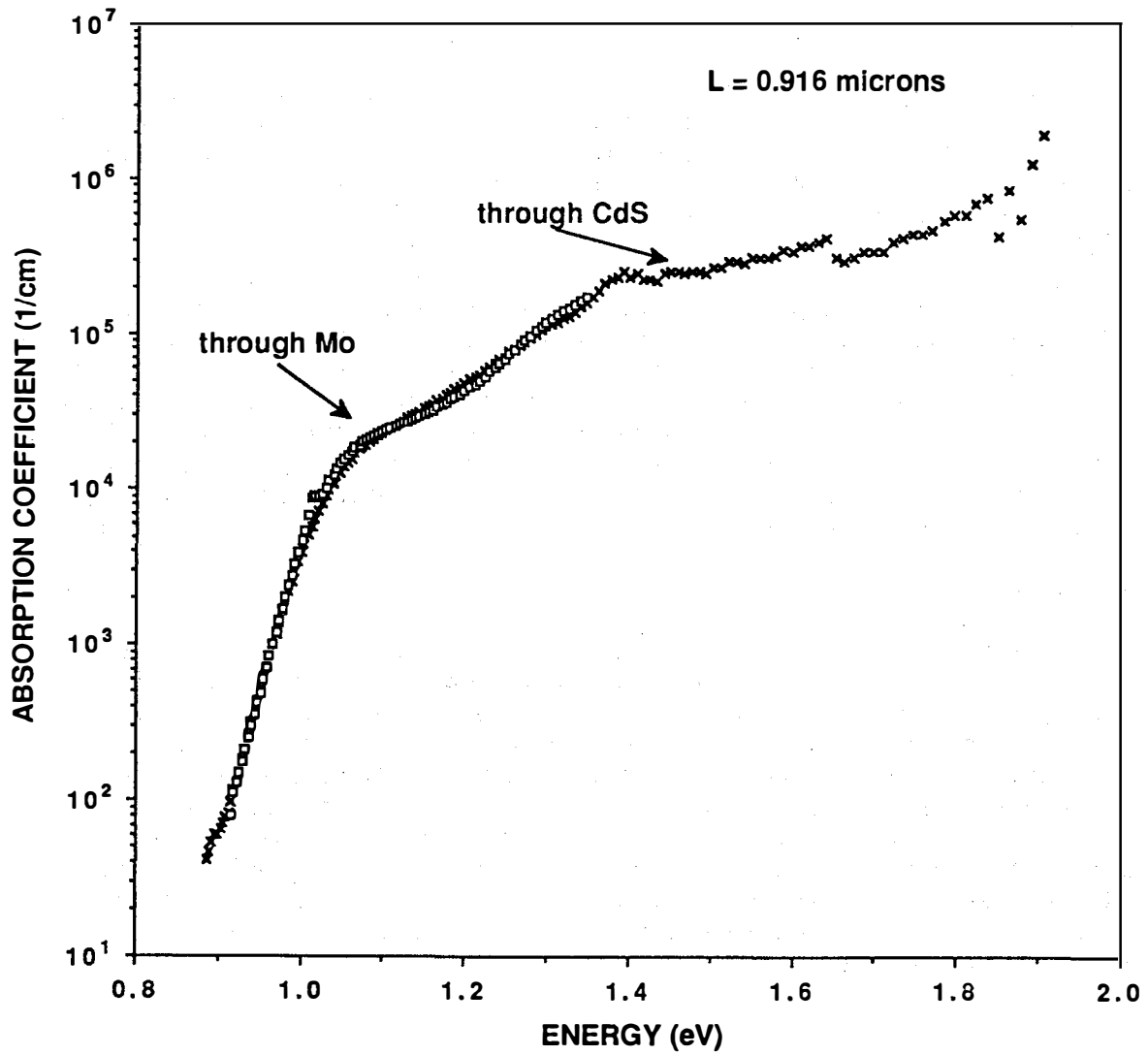


Figure 3: 0 Absorption Coefficient of CuInSe_2
 Determined From Bi-facial Spectral Response
 of ITO/CdS/ CuInSe_2 /Mo/glass Solar Cell.

Title: High Efficiency CuInSe₂ and CuInSe₂-Alloy Cells

Organization: International Solar Electric Technology (ISET), Inglewood, California

Contributors: V. K. Kapur and B. M. Basol, principal investigators; and R. C. Kullberg

The objective of this program is to develop thin film CuInSe₂ (CIS) and CIS-alloy solar cells with conversion efficiencies approaching 12%. The technique used in preparing the CIS films is the two-stage process which consists of the selenization of Cu-In layers deposited on metalized substrates. E-beam evaporated Mo has been used as the back contact metal to the CIS films in this work.

Our efforts during the present contract period were concentrated on evaporated/selenized CIS films. We had presented our results on high efficiency devices made on electrodeposited/selenized layers in our previous reports [1]. That work had resulted in the demonstration of small area cells with over 10% efficiency. However, adhesion of these CIS films to their Mo-coated substrates was poor and this presented a problem for large area processing. During the present period of work we have totally eliminated the problem of poor adhesion by optimizing the evaporation/selenization approach [2,3,4].

Film Deposition

An electron-beam evaporator with a four-pocket hearth was used in this work. Cu and In films were sequentially deposited onto Mo coated glass (Corning 7059) substrates at a pressure of around 2×10^{-5} Torr using 5-9's pure source materials. The Mo layers were also electron-beam evaporated. The typical thickness and sheet resistivity of a Mo layer were 2 μ m and 0.1 ohms/square respectively. After the evaporation step the substrates were placed in a tube furnace and the metallic layers were selenized in an atmosphere of H₂Se at 400 C for about 1 hour. The resulting films were analyzed using SEM, electron microprobe, and X-ray diffraction techniques. In-plane resistivity measurements were carried out on films deposited on plain glass substrates.

Solar Cell Fabrication

Solar cells were fabricated by depositing CdS/Transparent Conductive Oxide (TCO) window layers over the CIS films. CdS films were chemically formed on the CIS surfaces using an aqueous alkaline bath that consisted of 150 cc of 1M cadmium acetate, 75 cc of triethanolamine, 150 cc of ammonium hydroxide and 150 cc of 1M thiourea in 1 liter solution. Deposition was carried out for 5 minutes at 60 C and the resulting thickness of the CdS film was approximately 1000 A. The TCO windows had a bi-layer structure. First a 8000 A thick Al-doped ZnO layer was sputter deposited over the CdS surface. This was then followed by a 2000 A thick ITO layer which was also sputter deposited [5]. The sheet resistance of the composite TCO structure was about 20 ohms/square. Nickel bus-bars were used to make contact to the TCO films.

Results

A. CIS films

Fig. 1 is the X-ray diffraction pattern for a CIS film obtained by the two-stage process utilizing electron-beam evaporation. The diffraction peaks at 40.5 and 73.7 degrees are due to the underlying Mo layer. All the other major peaks belong to CIS. It should be noted that all of the characteristic peaks associated with the chalcopyrite phase of this material (i.e., the $\langle 211 \rangle$, $\langle 103 \rangle$, $\langle 101 \rangle$ and $\langle 105, 213 \rangle$ peaks) have been resolved in this data. The intensity ratio of the $\langle 112 \rangle$ peak to the $\langle 220 \rangle$ peak is around 1.9 indicating that there is only a small degree of $\langle 112 \rangle$ preferred orientation in this film.

The grain size of a CIS film prepared by the commonly used co-evaporation technique is known to be a strong function of its stoichiometry. Cu-rich compositions in these films have been shown to promote grain growth. Although the two-stage method is quite different from the co-evaporation technique, we have observed the same phenomenon in our CIS films. Near-stoichiometric or Cu-rich layers displayed grain sizes that were typically larger than 1 μm [2], whereas, the grain size decreased to around 0.1 μm for films with In-rich compositions. Fig. 2 is a cross-sectional SEM of a glass/Mo/CIS structure where the Cu-to-In ratio for the CIS film is around 0.9. The morphology of the film of Fig. 2 is smoother than the morphology of the near-stoichiometric films we had previously reported [2]. The average grain size of the film of Fig. 2 is about 0.1 μm , as is expected from its In-rich composition.

Film resistivities were measured using samples prepared on plain glass samples which were placed near the Mo coated glass substrates during the evaporation. Dark resistivity values were found to be in the range of 50 to 500 ohm-cm for films that yielded high-efficiency devices. In-plane resistivity data obtained from the glass/CIS structures, however, may not reflect the real values for films deposited on the Mo coated substrates. The growth characteristics of the evaporated metallic layers and the properties of the CIS films obtained after the selenization step may be highly substrate sensitive.

B. Solar cells

Fig. 3 is the illuminated I-V characteristics of a solar cell measured at SERI at 25 C (AM1.5 global spectra, 100 mW/cm²). Some gallium was included in the absorber layer of this device. The total area of this device is 0.1 cm² which includes the two Ni contact pads deposited along its two edges. The active area of the cell is 0.075 cm². The active-area solar cell parameters are: $V_{oc}=0.4627$ V, $J_{sc}= 35.36$ mA/cm², FF= 66.59% and $E_f=10.89\%$. Another group of cells fabricated on a 1cm x 1cm area of a similarly prepared CIS film yielded active-area efficiency values of 10.47%, 10.74%, 10.74% and 10.74%, thereby demonstrating that the uniformity of the film was quite good. The spectral response of the cell of Fig. 3 was measured under light bias and the data is shown in Fig. 4. Good carrier collection in the blue region of the spectra is due to the use of a highly transparent CdS/ZnO/ITO window layer. Response in the long wavelength region extends to 1.3 microns as expected from a CIS absorber layer.

Conclusions

The two-stage process is a very promising technique for depositing polycrystalline thin films of I-III-VI₂ compounds for solar cell applications. In this work we have used the two-stage process and the electron-beam evaporation technique to prepare high quality CIS films. Solar cells with active-area efficiencies approaching 11% have been fabricated on these layers. Further improvements, especially in the short circuit current density values of these devices, are expected to increase the conversion efficiencies to over 12% range in the near future.

References

1. Kapur, V.K., B.M. Basol, and R.C. Kullberg, "High Efficiency Copper Ternary Thin Film Solar Cells", Annual Report (March 1, 1987-April 30, 1989), SERI Contract No:XL-7-06031-6.
2. Basol, B.M., and V.K. Kapur, Appl. Phys. Lett., vol.54, p.1918, 1989.
3. Basol, B.M., V.K. Kapur and R.C. Kullberg, Solar Cells (in press), 1989.
4. Basol, B.M., and V.K. Kapur, IEEE Trans. Electron. Devices (in press), 1990.
5. TCO layer depositions were provided by Dr. Robert Birkmire of IEC, University of Delaware.

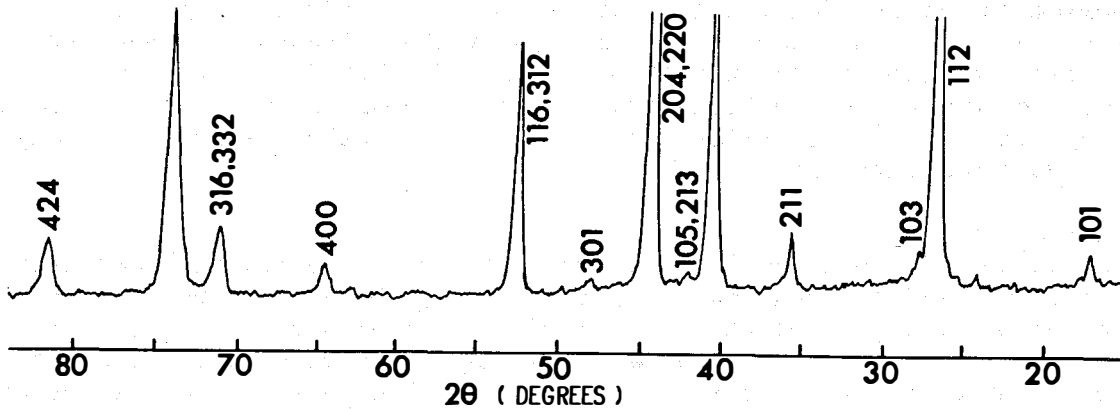


Fig. 1 X-Ray diffraction data for a CuInSe₂ film prepared by the two-stage process.

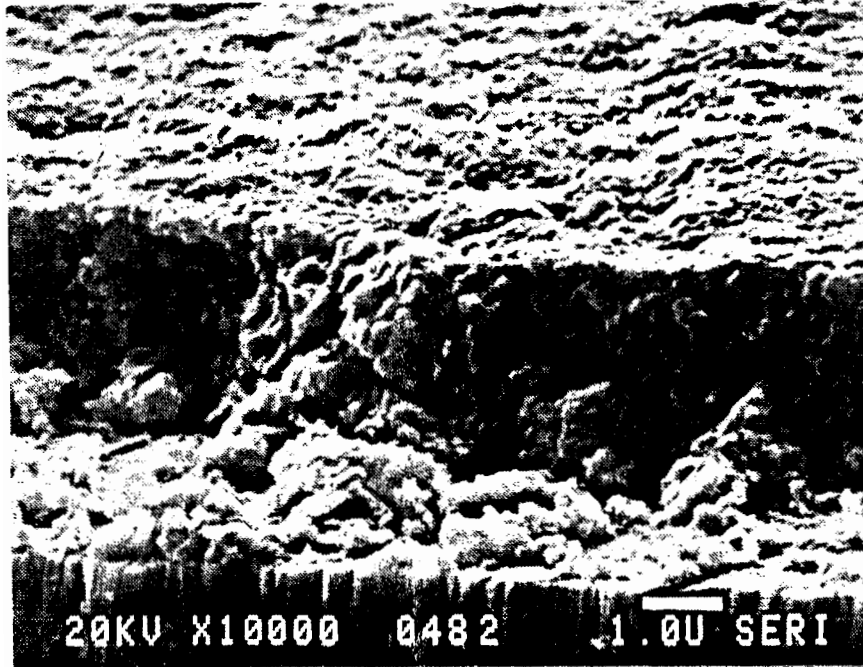


Fig. 2 SEM of a CuInSe₂ film prepared by the two-stage process. The Cu/In ratio is around 0.9.

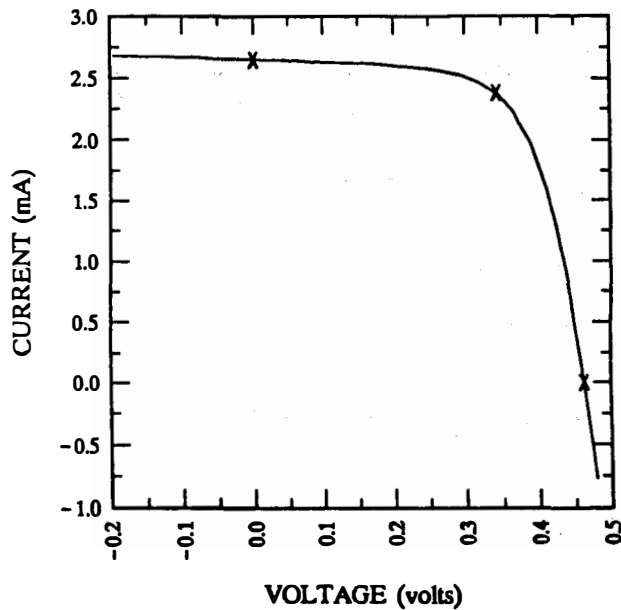


Fig. 3 Illuminated I-V characteristics of a CuInSe₂ cell. Active-area (0.075 cm²) parameters are: Voc= .4627V, Jsc=35.36mA/cm², FF=66.59%, eff.=10.89%. SERI global spectra, 100 mW/cm². Total device area is 0.1 cm².

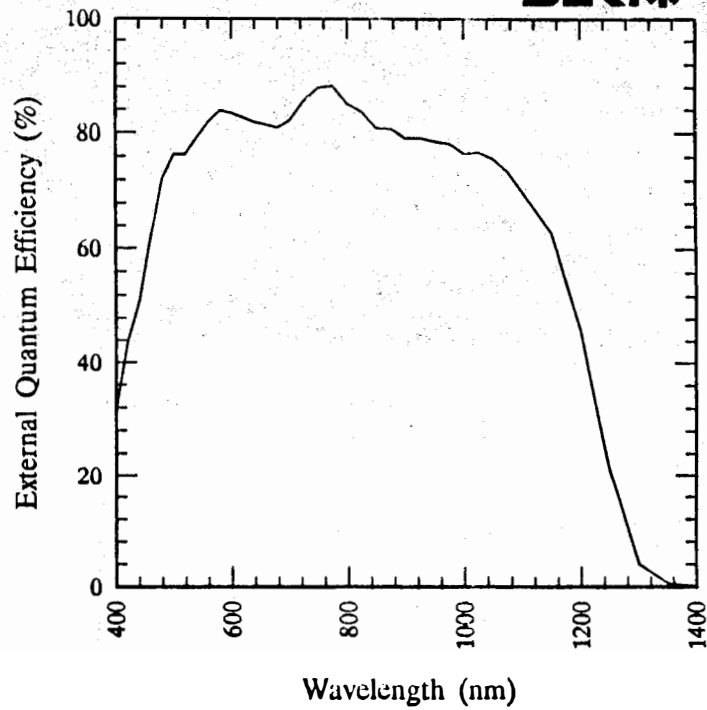
ISET/IEC, CuInSe₂ / thin CdS

Temperature = 25.0°C

Mar. 27, 1989 12:08 pm

Area used = 0.075 cm²

SERI



Light bias = 2.50 mA

Zero voltage bias

Fig. 4 Quantum efficiency of the device of figure 3.

Title: High-Efficiency, Large-Area CdTe Panels

Organization: Photon Energy, Inc., El Paso, Texas

Contributors: S.P. Albright, principal investigator; B. Ackerman, R. R. Chamberlin, J. F. Jordan, and V. P. Singh

Objectives and Approaches

Under subcontract ZL-7-06031 through SERI, the research effort at Photon Energy Inc. has been directed toward development of an improved materials technology and fabrication processes for limited volume production of 1 ft² and 4 ft² CdS/CdTe photovoltaic modules, with improved stability and improved efficiency being the most significant milestones.

The research program has been separated into research tasks which include:

- * Efficiency Improvement
- * Large Area Panel Uniformity Improvement
- * Contact Passivation and Electrode Improvement
- * Encapsulation Improvement and Long-Term Reliability Testing

Utilizing the results of these tasks progress has included device efficiency, module output improvement, and module reliability improvement.

Device Characterization and Efficiency Improvement

Electrical and optical measurements have been performed in order to assess the greatest potential areas for improvement in the process. It has earlier been concluded [1-3] that the effects due to interface states or midgap recombination centers significantly affect performance. However, the 6 μ m thick CdS window layer used in the PEI devices holds the greatest potential area for immediate efficiency improvement.

Preliminary work on improved window materials has resulted in improved device efficiencies. A "thick CdS" device made at PEI has attained 10.8% efficiency and a $V_{oc} = 785$ mV, $I_{sc} = 19.1$ mA/cm², and Fill Factor = 72%. A "thin CdS" device having 0.313 cm² area was delivered to SERI in May 1989. efficiency at SERI was 12.3% [4]. Figure 1 shows the current-voltage characteristics for the 12.3% efficient device with $V_{oc} = 783$ mV, $I_{sc} = 25.0$ mA/cm², and Fill Factor = 62.7%. The improvement in I_{sc} is due to an improved quantum efficiency as exemplified by the comparison of a "thin" and a "thick" CdS device shown in Figure 2. Combining the best parameters on a single device should result in an efficiency of 14%. [4]

Analysis done on the limited fill factor of this 12.3% cell by J. Sites of Colorado State has indicated that the series resistance contribution is only 1.0 ohm-cm², and that the present potential to reach 14% efficiency lies mostly in the improvement of the high ideality factor (3.5 for the 12.3% cell). [5]

Module Output Improvement

A module measuring 30.5 cm x 30.5 cm (1 ft²) produced at PEI has been measured at SERI with an output of 6.11 watts. The $V_{oc} = 20.5$ volts, the $I_{sc} = 0.519$ amps, the fill factor = 57%, the active area efficiency = 8.1%, and the

aperture area efficiency = 7.3%.

In addition, the world's largest single-substrate CdTe-based module (4 ft²) has been delivered to SERI.

Module Reliability

Details of encapsulation and life testing results have been previously reported.[6]

Submodules measuring 4" x 6" have indicated that no inherent degradation mode exists for properly encapsulated CdTe-based devices or modules after 9 months of outdoor life testing in El Paso. Figure 3 indicates the results of ongoing SERI life testing.[7] No significant degradation is observed after 5 months of outdoor exposure on 5 out of 5 submodules. Further life testing on larger-area modules must be done to fully evaluate the technology.

Preliminary thermal cycling tests (-40 to 90 Celsius) indicate no degradation of modules and no structural integrity problems.

Conclusions and Future Projections

Efficiencies up to 12.3% on small devices made at PEI have been substantiated by SERI. Cells with fill factors as high as 72% have also been achieved. Combining these already-observed parameters on a single device would result in greater than 14% efficiency.

Greater than 15% efficiency should be achievable with a nearly fully-optimized junction and device structure. Additionally, over 17% efficiency should be achievable in the long term after further optimization of the alloying, doping, and surface passivation of the CdTe and through improvement of the morphology of the crystals near the junction.

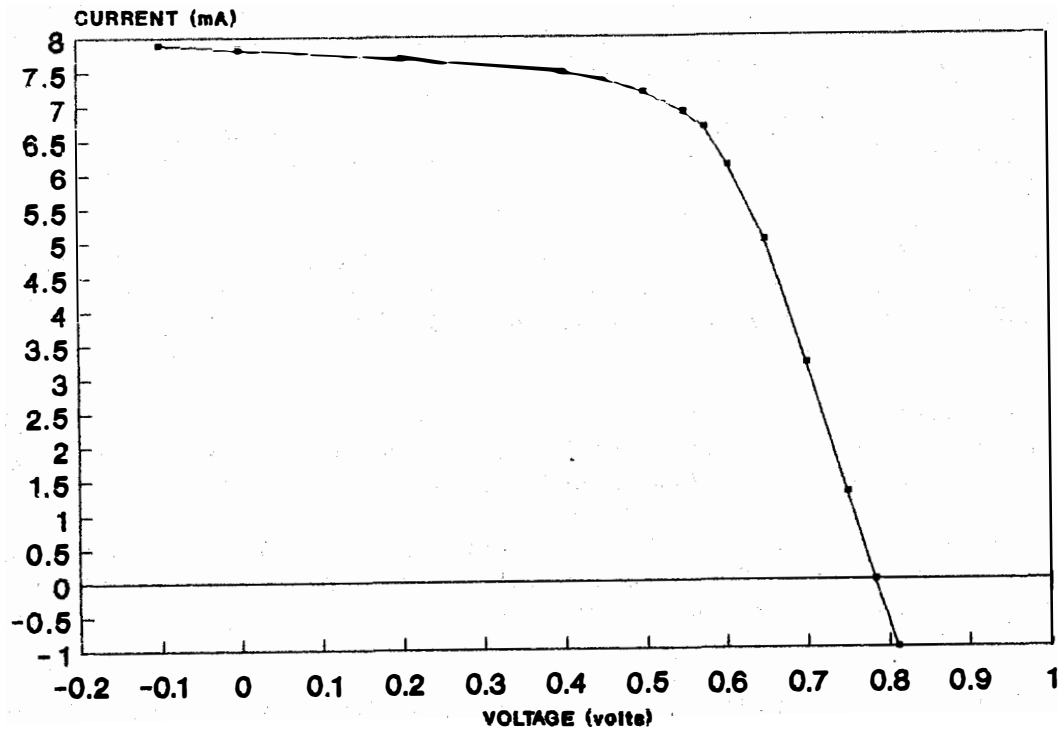
Life testing indicates no inherent degradation problems with the device itself. Life testing will continue to provide statistical data on the performance of larger-area CdS/CdTe modules.

References

- 1 V.P.Singh, R.H.Kenny, J.C.McClure, S.P.Albright, B.Ackerman and J.F.Jordan, *Proc. 19th IEEE Photovoltaic Specialists Conf.*, May 4-8, 1987, New Orleans, 216-221.
- 2 S.P.Albright, V.P.Singh, B.Ackerman, "High-Efficiency Large-Area CdTe Panels", Annual Report from Photon Energy, Inc. under SERI subcontract ZL-7-06031-3 during period from 6/87 to 6/88.
- 3 S.P.Albright, V.P.Singh and J.F.Jordan, "Junction Characteristics of CdS/CdTe Solar Cells", *Solar Cells*, Elsevier Sequoia, The Netherlands, 24 (1988) 43-56.
- 4 S.P.Albright, J.F.Jordan, B.Ackerman, R.R.Chamberlin, "Development on CdS/CdTe Photovoltaic Panels at Photon Energy, Inc.", Presented at SERI PVAR&D 9th Review Meeting, Lakewood, CO, May 24, 1989, submitted to *Solar Cells*.
- 5 S.P.Albright, B. Ackerman, R.R.Chamberlin, J.F.Jordan, "Progress on Polycrystalline Thin Film CdTe Modules," Presented at *Polycrystalline Thin Film Program Meeting, Lakewood, Colorado, August 16-17, 1989*.
- 6 B.Ackerman, S.P.Albright, "Encapsulation and Life Testing Issues for 1 ft² CdS/CdTe Modules", From Photovoltaic Thin Film Module Reliability Testing and Evaluation Workshop, Sponsored by SERI under DOE, June 1989, Lakewood, CO.
- 7 Laxmi Mrig, SERI Outdoor Testing and Reliability Laboratory, Golden, CO. Personal Communication, November 1989.

PHOTON ENERGY - SAMPLE 789A2#4

Area=0.313 cm², Temperature 25C, 6/19/89



Voc = 0.7832 volts	Isc = 7.826 mA
Jsc = 24.98 mA/cm ²	Pmax = 3.840 mW
Fill Factor = 62.66%	I _{max} = 6.668 mA
Efficiency = 12.3%	V _{max} = 0.5759 V

Figure 1 -- Performance Characteristics of 12.3% Efficient Device Measured at SERI

QUANTUM EFFICIENCY vs WAVELENGTH

for Photon Energy vs IEC Devices

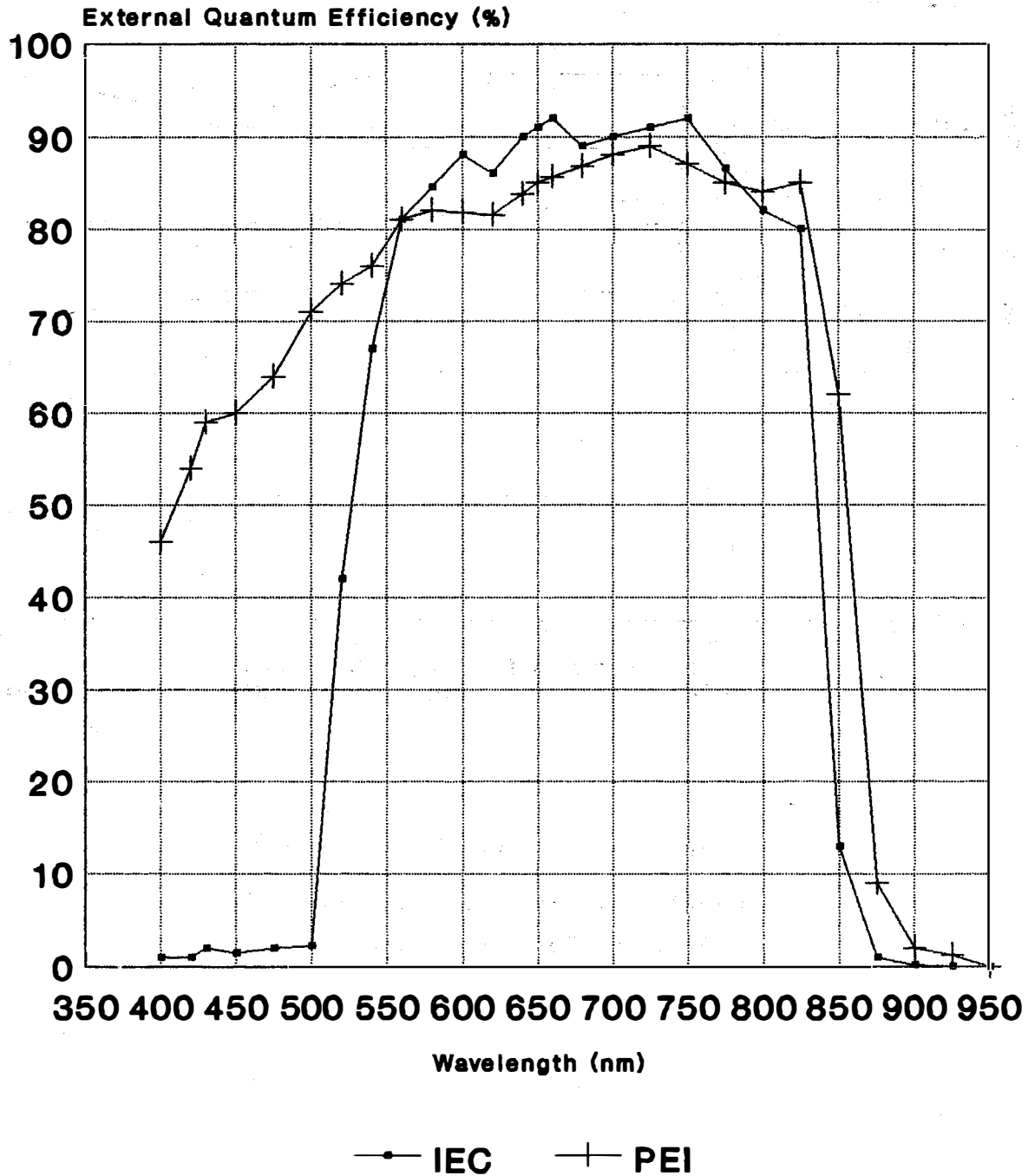


Figure 2 -- Comparison of the Quantum Efficiencies of 'thin' PEI vs 'thick' IEC CdTe/CdS Devices

OUTDOOR LIFE TEST DATA
TAKEN AT SERI

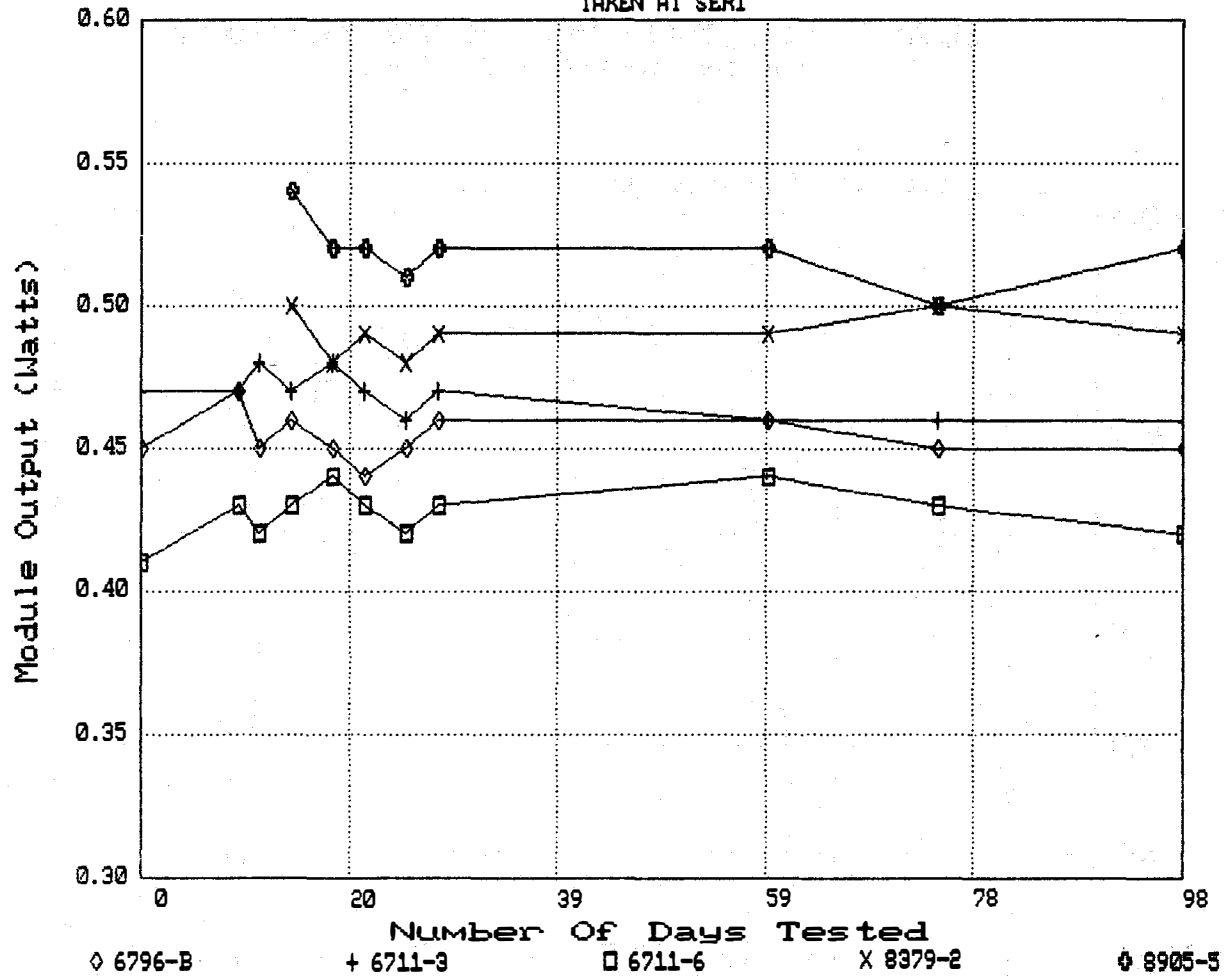


Figure 3: Outdoor Life Testing
Results on Submodules From SERI
Outdoor Testing Laboratory

Title: Novel Thin Film CuInSe₂ Fabrication

Organization: Department of Physics, University of Arkansas, Fayetteville, Arkansas

Contributors: A. M. Hermann and G. D. Mooney, Principle Investigators

1. Summary

The objective of this work is to study the feasibility of fabricating CuInSe₂ (CIS) for use in photovoltaic cells by rapid annealing processes including laser processing and rapid thermal processing (RTP). Presently, the chalcopyrite phase of CIS is obtained by thermally annealing elemental Cu and In layers in H₂Se gas. This type of selenization process is hazardous, however, because of the high toxicity of the hydrogen selenide gas. This feature makes the process unattractive for large-scale production because of the danger and expense incurred in handling the hydrogen selenide. The ability to form the desired chalcopyrite structure with favorable optical and electrical properties by rapid annealing processes would be safer and more conducive to large-scale production.

Initial studies of the feasibility of laser annealing the elemental layered structures have been performed using a CW argon and Nd:Yag lasers on films that were fabricated by means of thermal resistance evaporation in a vacuum of 10⁻⁶ Torr. Characterization of the post-annealed films by x-ray diffraction analysis has shown encouraging results. The laser annealed films have all contained the chalcopyrite phase of CIS. The percentage of the chalcopyrite phase has been small however. The formation of undesirable binary compounds has also occurred. To produce higher quality films, future work will concentrate on increasing the percentage of the desirable phase and the elimination of all binary compounds.

Initial studies of the feasibility of RTP have yielded the most encouraging rapid processing results to date. Characterization of post annealed films by X-ray diffraction analysis (XRD), thermoelectric power measurements (TEP), and microprobe analysis has shown that the desirable chalcopyrite structure has been formed in the RTP films over a wide range of temperatures and anneal times. The films have a somewhat low percentage of chalcopyrite phase with a significant amount of amorphous material present. Some Cu-Se compounds could be present but this has not been resolved. To produce higher quality films, future work will concentrate on deposition parameters in an attempt to bring the percentage of the desired phase up close to 100 percent.

2.1 Deposition of Elemental Cu, In, and Se Layers

To prepare films for the rapid annealing processes, elemental layers of Cu, In, and Se were deposited by means of thermal resistance evaporation in a vacuum in the 10^{-6} Torr range. This system allows sequential deposition of the elemental layers without exposing the individual layers to atmosphere. In order to obtain the proper stoichiometry in the post annealed films, the original elemental layers were deposited so that the desired atomic ratio of 1:1:2 (Cu:In:Se) was maintained. This was achieved by determining the layer thicknesses that correspond to this ratio and monitoring the layer thicknesses with a quartz crystal rate monitor. Deposition parameters were easily and accurately controlled with the deposition rates being held to between 1 and 5 angstroms per second. The final thicknesses, as determined by the rate monitor were verified with a Dektak thin film profilometer to be within about 1 percent of the target thickness. The ordering of the elemental layers is shown in Figure 1. This ordering was chosen so that the less stable Se was sandwiched between the In and Cu with the more stable Cu being the "sealing" outer layer.

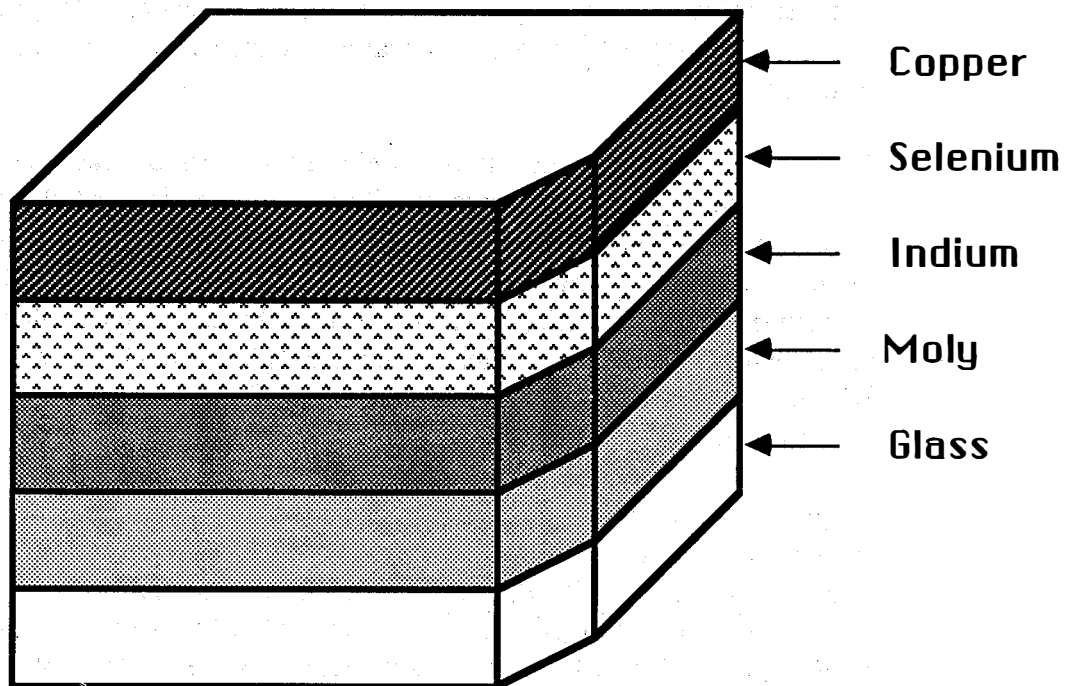


Figure 2-1 Pre-Annealed Sandwich Structure on Corning 7059 Glass

2.2 Laser Annealing of Elemental Sandwiched Structures

The films used in the laser anneal phase of the experiment typically had a Cu thickness of 200 Å, an In layer thickness of 445 Å, and a Se layer thickness of 930 Å yielding a total film

thickness of about 1500 Å. The details of the scanning procedure are given in reference 1. In addition to what is outlined there, we have designed an air-tight annealing box with an optical quality quartz window that can be filled with an inert gas. This enabled us to laser anneal our samples in an argon atmosphere. In addition to annealing with a CW Ar⁺ laser, we have annealed some of the films with a pulsed, Nd:YAG laser. The set-up for this experiment was identical to that of the CW laser experiment.

2.3 Characterization of Laser Annealed Films

Figure 2 shows the XRD pattern of a typical sample that was annealed by a CW argon laser with

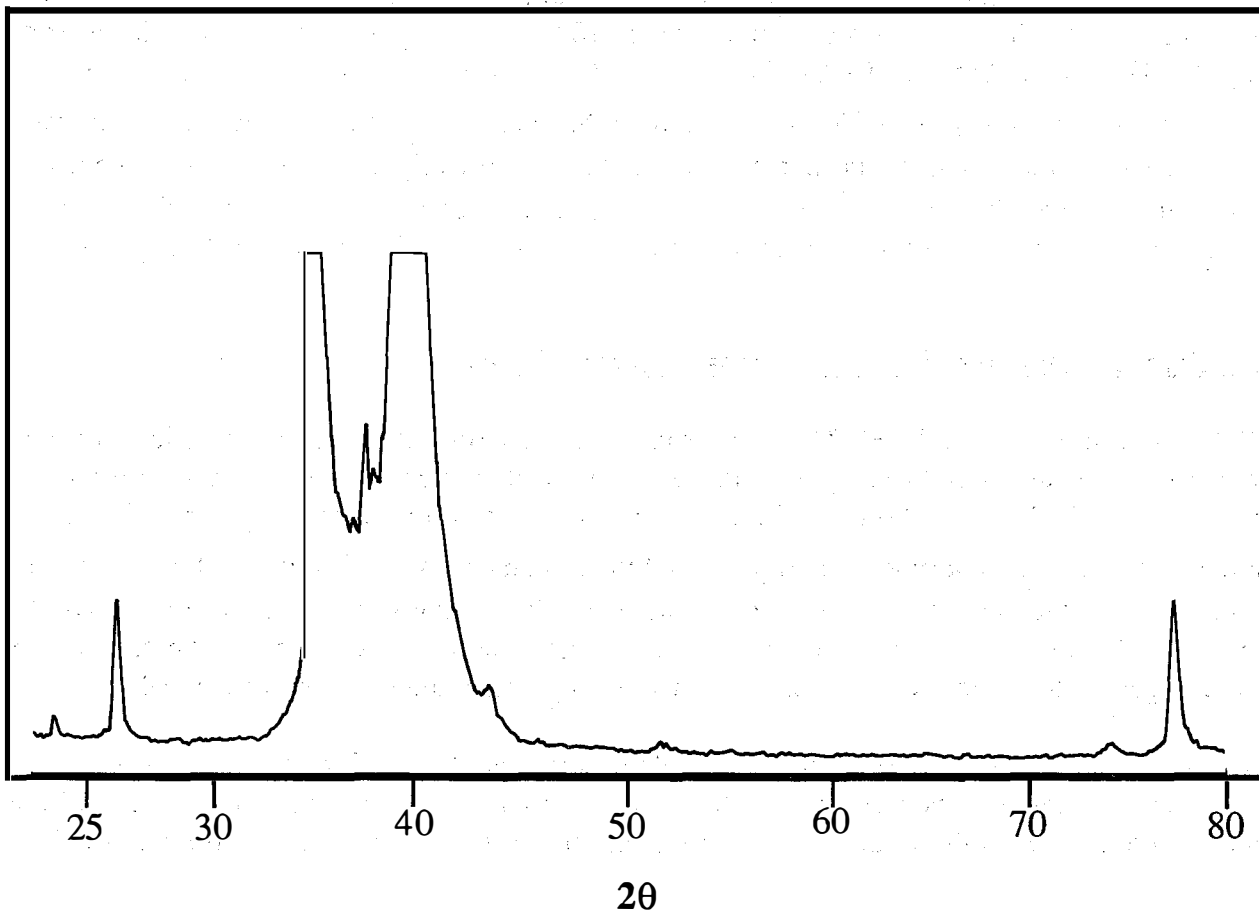


Figure 2-2 XRD Pattern of CW Argon Laser Annealed Sandwich Structure

the power held at 4 watts, a beam diameter of about 1mm, and a scan speed of 2mm/s. As can be seen in Figure 2, the three largest CIS peaks are evident but undesirable binary compounds are still present. The largest peak at $2\theta = 40.5$ is the primary peak of Mo.

We also annealed several samples with a frequency doubled Nd:YAG laser using a variety of pulse energies (ranging from 35 to 55 joules per pulse) and pulse frequencies (ranging from 10

to 20 pulses per second). It was verified with XRD that small percentages of CIS were formed in these films using XRD with mostly binary compounds prevalent. This effort shows promise but more detailed work is needed before any definite conclusions can be drawn.

2.4 Rapid Thermal Processing of Elemental Sandwiched Structures

The RTP used was an AG Associates Heatpulse 210T-03. This system consists of 15 quartz heating lamps, a sealed quartz chamber to allow annealing in flowing argon. The thermocouple that monitors sample temperature was placed in direct thermal contact with the sample.

The films used in the RTP phase of the experiment to date have been of two different thicknesses. The first group had a Cu thickness of 200 Å, an In layer of 445 Å and a Se layer of 930 Å. The second batch had a Cu thickness of 666 Å, an In layer of 1450 Å, and a Se layer thickness of 3103 Å to yield a film with total layer thickness of about .5 μm. A matrix approach was used to systematically anneal the sandwiched structures from 400°C for 10 seconds to 600°C for 35 seconds. In these initial experiments, the temperature was not ramped so that the sample was brought from room temperature to the set temperature in the shortest time possible.

2.5 Characterization of Rapidly Thermal Processed Films

XRD Characterization of the RTP films has shown the chalcopyrite phase of CIS to have formed in every sample annealed at every time and temperature attempted to date. A typical diffraction pattern of an RTP film is shown in Figure 4. As can be seen, the sample appears to be nearly single phase with an amorphous "hump" around the primary peak at $2\theta = 26.6$. Our preliminary results show that the largest peaks were obtained for the samples annealed at 600 °C for 10 seconds. Within the realm of our experiments, the general trend seems to be that larger percentages of the chalcopyrite structure form at higher temperatures and shorter times.

We have also taken limited data on the RTP samples that includes optical absorption measurements, microprobe analysis, and thermoelectric power. All of these measurements have been done on the 1500 Å samples. The results of these experiments support the XRD in showing that the samples contain some CIS but are not 100 percent CIS by mass. The microprobe analysis shows that the samples are copper poor resulting in films that are only about 50 percent CIS by mass.

The optical absorption measurements also indicate that the samples are not pure CIS. As can be seen in Figure 5, these preliminary results do not show a definitive band gap. In the lower

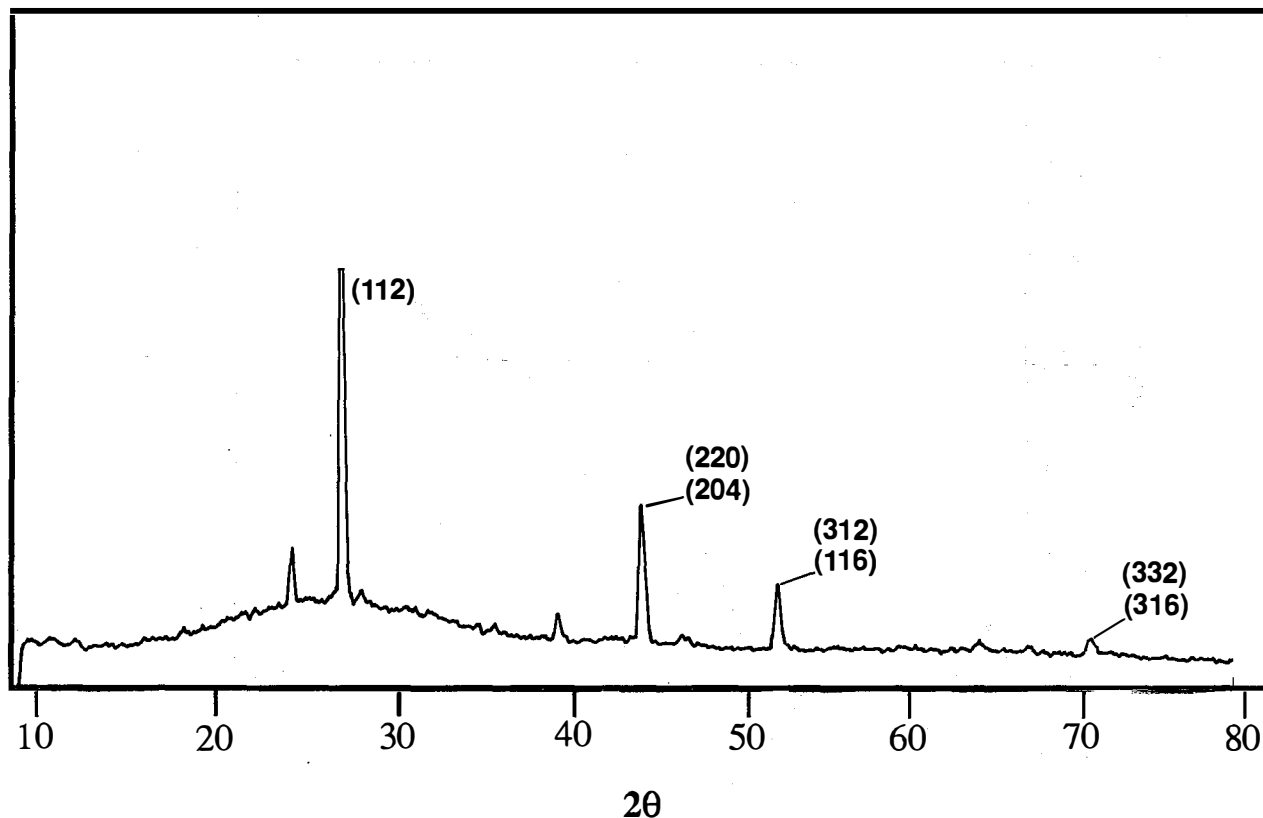


Figure 2-3 XRD of Rapid Thermally Annealed Sandwiched Structure

photon energy region ($< .975$ eV), the absorption is erratic. We believe one explanation for this might be the amorphous material is contributing to states in the band gap of CIS. The 1500 Å films have also been confirmed to be p-type with a room temperature TEP measurement.

3.0 Conclusions

Our preliminary work in RTP leads us to believe that this technique shows more promise than laser annealing in its ability to produce higher quality CIS. Also, RTP can be more easily scaled up for uniform annealing of large surface areas. To improve the laser annealing experimental results, a more accurate, more controllable method must be used to scan the films than that outlined in reference 1.

There are several approaches we can take to improve the RTP samples. In the immediate future, we will perform Auger analysis to determine the uniformity of the volume of the films, and to determine the composition of the pinholes that have appeared in some of the post annealed

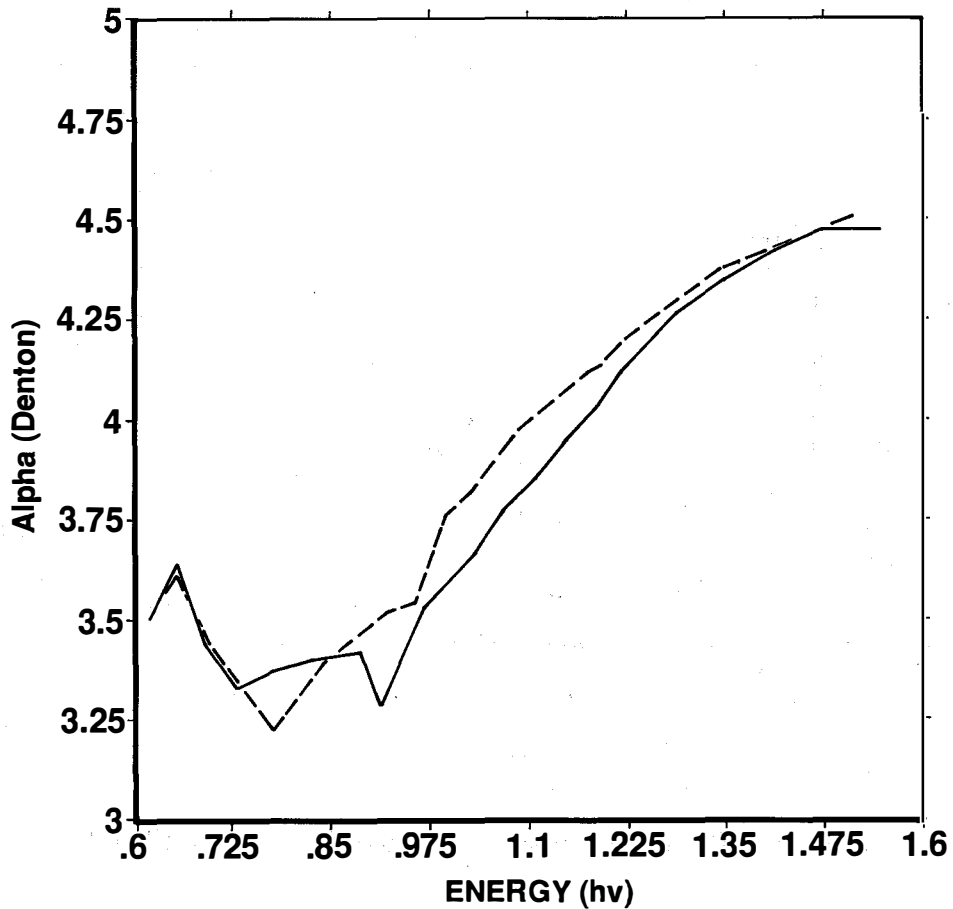


Figure 2-4 Optical Absorption of an RTP Sample

samples compared to the composition of the peaks.

Also we will adjust the deposition parameters to fine tune the stoichiometry in order to compensate for any material that may be evaporating during the anneal. The goal of any adjustments is to obtain 100 percent reaction of the deposited layers thus eliminating the large percentage of amorphous material. This, in turn will sharpen the band edge and yield more favorable optical absorption results. Other annealing experiments to be done include ramping the temperature over a given time. It is believed a somewhat slower heating rate will allow all the elements to react before they can evaporate. In the ramping experiments we will use a three dimensional matrix approach in order to determine which annealing parameters yield films with the largest percentage CIS with the most favorable optical and electrical properties. When the parameters are optimized, experiments will be initiated to form active solar cells with the structure 7059 glass/Mo/CIS/CdS/ITO. We will also experiment with depositing the elemental layers on glass/ITO/CdS substrates so that CIS can be form directly on this structure to make the heterojunction.

4.0 References

1. G. D. Mooney and A. M. Hermann, 1988 SERI Final Report for Contract XL-8-18017-1.

Title: Alternative Fabrication Techniques for High-efficiency CuInSe₂ and CuInSe₂-alloy Films and Cells

Organization: University of Illinois

Contributors: A. Rockett, principal investigator; E. Banda, G. Kenshole, H. Talieh, and P. Campos.

Objectives

The objective of this project is to investigate CuInSe₂ thin film deposition techniques which are clearly scalable to large areas and which are capable of producing material suitable for solar cell applications. In addition, fundamental studies of CuInSe₂ are underway with the objective of learning how the CuInSe₂ materials properties contribute to the success or failure of solar cells. This understanding will serve to improve the processes under development, optimize deposition conditions, and ultimately to accelerate the return to service of large deposition facilities after periods of maintenance.

Technical Approach

Only magnetron sputtering is in common use for coating very large area substrates with thin films. This coating technology is well established for architectural glass applications, although evaporation has also been used to coat smaller-area surfaces. Both of the CuInSe₂ deposition methods considered by this project are based on sputtering techniques. Reactive sputtering of Cu and In in a mixed H₂Se + Ar atmosphere to produce CuInSe₂ has been examined in previous phases of the program. The current efforts center on a hybrid sputtering and evaporation technique. In this process Cu and In are sputtered with Ar gas while Se is supplied to the growing film by a conventional effusion cell.^{1,2} The substrate temperature is controlled between room temperature and 450°C. The process has been shown to be straightforward to control with a linear relationship between the ion current ratio at the targets and the film composition established by previous results. Film compositions become slightly more Cu-rich as the substrate temperature is increased which appears to result from desorption of In₂Se from the film surface at elevated temperatures.

The experiments underway focus development of a reasonably high efficiency CuInSe₂/CdS heterojunction solar cell, and on understanding the fundamental properties of CuInSe₂. The current research involves characterization of bulk CuInSe₂ single crystals and thin films (deposited by the hybrid process and by other methods) in the transmission electron microscope (TEM) and by chemical analysis techniques. Solar cells based on the hybrid material have been fabricated at the University of Illinois (UIUC), the Institute for Energy Conversion at the University of Delaware (IEC), and at International Solar Electric Technology (ISET). The devices produced at UIUC and ISET are point contact cells. The devices produced at IEC consisted of the CuInSe₂ (deposited on Mo at the University of Illinois), coated and patterned with 1.8 μm (Cd_{0.93}Zn_{0.07})S:In, 0.19 μm of indium-tin oxide (ITO), and contacted with Ni fingers.

Results for FY 89

Solar cells with conversion efficiencies exceeding 7% have been fabricated based on CuInSe₂ produced by the hybrid process. As a first step, Cu-In alloy layers deposited in the hybrid system were selenized and fabricated into devices at ISET. These exhibited V_{oc} values as high as 0.34 V, demonstrating that acceptable control of the Cu and In fluxes could be achieved. Following

calibration of the deposition rates and film compositions as a function of substrate temperature and constituent fluxes, single-layer films were produced exhibiting the chalcopyrite structure and with resistivities in agreement with previous observations ($0.797 \Omega\text{-cm}$ for Cu-rich films and $2.094 \times 10^4 \Omega\text{-cm}$ for In-rich layers). Bilayers were produced consisting of Cu-rich regions, $3 \mu\text{m}$ thick, capped with In-rich layers of varying thickness. For the initial series of films these layers had nominal atomic percent compositions of 26 % Cu, 22 % In, and 52 % Se for the Cu-rich layers and 19 % Cu, 29 % In, and 52 % Se for the In-rich layers.

Optical absorption, transmission, and reflection spectra for In-rich, Cu-rich, and bilayer films were recorded as a function of incident light wavelength. These data were analyzed and values of the absorption coefficient α were determined as a function of photon energy. Figure 1 shows a plot of $(\alpha E)^2$ as a function of E , where E is the photon energy. Assuming a simple band structure for the semiconductor this plot should increase linearly above the bandgap with a value of $\alpha=0$ at the gap energy. Extrapolated gaps for the hybrid materials measured are 1.07, 0.95, and 0.95 eV for the In-rich, Cu-rich, and bilayer films, respectively. Furthermore, the Cu-rich and bilayer films exhibit a significant sub-gap absorption, probably associated with band tails near the edge of one or both band edges. This would be expected for off-stoichiometry material in which a large number of electrically-active vacancy and antisite defects occur. Such states in the band tail may give rise to excessive recombination in the heterojunction depletion region and reduce the depletion width. This, in turn, will decrease the efficiency of the resulting device. A large number of defects which could give rise to such states have been observed by our group in both Cu-rich and In-rich material by TEM.³ However, no significant Cu-rich second phases have been observed in moderately Cu-rich or In-rich films on any size scale by TEM or X-ray diffraction.

Point-contact $\text{CuInSe}_2/\text{CdS}:\text{In}$ devices based on this material exhibited diode-like behavior which improved significantly with air annealing. Under illumination these devices produced V_{oc} values as high as 0.34V. Glass/ $\text{Mo}/\text{CuInSe}_2/(\text{Cd}_{0.93}\text{Zn}_{0.07})\text{S}:\text{In}/\text{ITO}/\text{Ni}$ devices with an active area of 0.08 cm^2 produced and tested at IEC using similar films had an as deposited best conversion efficiency of 2.35 %. The best performance after air annealing for 12 hours at 200°C improved to 7.2 % efficiency, $V_{\text{oc}}=0.348 \text{ V}$, $J_{\text{sc}}=0.32.9 \text{ mA}$, and 55 % fill factor under simulated 87.5 mW cm^{-2} solar illumination.⁴ Subsequent analysis at SERI demonstrated a further improvement in the device performance after several months of exposure to the room environment. The best performance measured at SERI was for the same best device tested at IEC. The device parameters had changed to 7.7 % efficiency (active area), $V_{\text{oc}}=0.385 \text{ V}$, $J_{\text{sc}}=24.18 \text{ mA/cm}^2$, and 61 % fill factor under the SERI solar simulator conditions. The current/voltage characteristic for the best device measured at SERI is shown in Figure 2.

As a baseline for evaluation of thin films, single crystals grown by Tomlinson⁵ using the vertical Bridgeman technique were analyzed by transmission electron microscopy (TEM) for comparison with polycrystalline thin films. The crystals were slightly In-rich with a composition, determined by wavelength-dispersive X-ray analysis (WDX), of 25.1 atom % (at. %) Cu, 25.6 at. % In, and 49.4 at. % Se. The selected-area electron diffraction patterns in various zone axes show reflections which are normally forbidden for the chalcopyrite structure. We hypothesize that these are due to defects on specific positions within the unit cell of the lattice. These may consist of vacancies on one or more of the sublattices and may permit the crystal to deviate from stoichiometry while retaining a single-phase structure. Similar features were observed in diffraction patterns obtained from within individual grains of single-phase polycrystalline films. The compositions of several individual grains for these films were determined by energy-dispersive X-ray analysis (EDX) to vary by as much as 4 at. % in one or more constituents from the stoichiometric value. Average film compositions determined in a scanning electron microscope (SEM) for the entire sample were found to be in excellent agreement with the average of the

composition values obtained from individual grains. Furthermore, no evidence of second phases was found either within the individual grains or at grain boundaries of the polycrystalline films. The conclusion we draw from this is that a much larger range of equilibrium or very-long lived metastable solid solubilities exists, far in excess of that corresponding to the equilibrium $\text{Cu}_2\text{Se}/\text{In}_2\text{Se}_3$ phase diagram single-phase chalcopyrite structure reported previously.⁶

The TEM results on single and polycrystalline samples have also permitted characterization of the various predominant defects present in CuInSe_2 as a function of crystal composition. The polycrystalline thin film samples deposited by the hybrid process and by three-source evaporation both show evidence of dislocations, voids, stacking faults, and (112)-type microtwins. The microtwins were the most common extended defect and exhibited a higher density in the In-rich material. These defects do not carry an electrical charge at their boundaries and are common in rapidly grown materials. The increased density of microtwins in In-rich material as compared with Cu-rich material is not surprising as the nominal grain size of In-rich CuInSe_2 is smaller than for Cu-rich material, suggesting a lower average atomic diffusion rate during growth. Stacking faults are also occasionally observed with the greatest density in Cu-rich polycrystalline films. Stacking faults in CuInSe_2 will carry a charged defect at every site along their boundary which could lead to significant changes in film conductivity. No stacking faults or microtwins were observed in the single crystals.

Conclusions and Future Research

The performance of small solar cells based on hybrid-sputtered CuInSe_2 , while not state-of-the-art, are very encouraging and represent the best performance obtained to date for a sputtered material without post-deposition selenization. All of the parameters of the best device can be improved by further optimization of the CuInSe_2 layer and the post-deposition processing suggesting that further improvements in cell performance should be obtainable. The results to-date clearly demonstrate the potential of the hybrid process.

To extend the current work we will attempt to optimize the deposition parameters to obtain better performance in the conventional devices, as well as modifying the deposition process to improve its potential for scalability. Depositions at lower temperatures, below 200°C will be carried out with a post-deposition anneal to increase grain size to determine if a lower temperature process is viable. $\text{CuIn}_x\text{Ga}_{1-x}\text{Se}_2$ alloy devices will also be produced in an attempt to improve performance. Finally, fundamental studies will be continued to examine the electronic and lattice structure of CuInSe_2 deposited by various techniques to understand how these limit device performance.

Relationship to Other Contracts

The research program described above is funded by SERI for development of high-performance photovoltaic devices based on CuInSe_2 deposited by sputtering-based techniques. The development of the hybrid sputtering and evaporation process itself is funded by the Electric Power Research Institute.

FY '89 Publications

- [1] A. Rockett, T.C. Lommasson, L.C. Yang, H. Talieh, P. Campos, and John A. Thornton, "Deposition of CuInSe_2 by the Hybrid Sputtering and Evaporation Method", Proceedings of the 20th IEEE Photovoltaic Specialists Conference (Institute of Electrical and Electronics Engineers, New York, 1988).

- [2] A. Rockett, T.C. Lommasson, P. Campos, L.C. Yang, and H. Talieh, "Growth of CuInSe₂ by Two Magnetron Sputtering Techniques", *Thin Solid Films* **171**, 109 (1989).
- [3] B.-H. Tseng, A. Rockett, T.C. Lommasson, L.C. Yang, C.A. Wert, and John A. Thornton, "Chemical and Structural Characterization of Physical-Vapor Deposited CuInSe₂ for Solar Cell Applications", *J. Appl. Phys.*, in press.
- [4] H. Talieh and A. Rockett, "Device-Quality CuInSe₂ Produced by the Hybrid Process", *Solar Cells*, in press.
- [5] R.D. Tomlinson, *Solar Cells* **16**, 17 (1986).
- [6] See, for example, C. Rincón, C. Bellabarba, J. González, and G. Sánchez Pérez, *Solar Cells* **16**, 335 (1986).

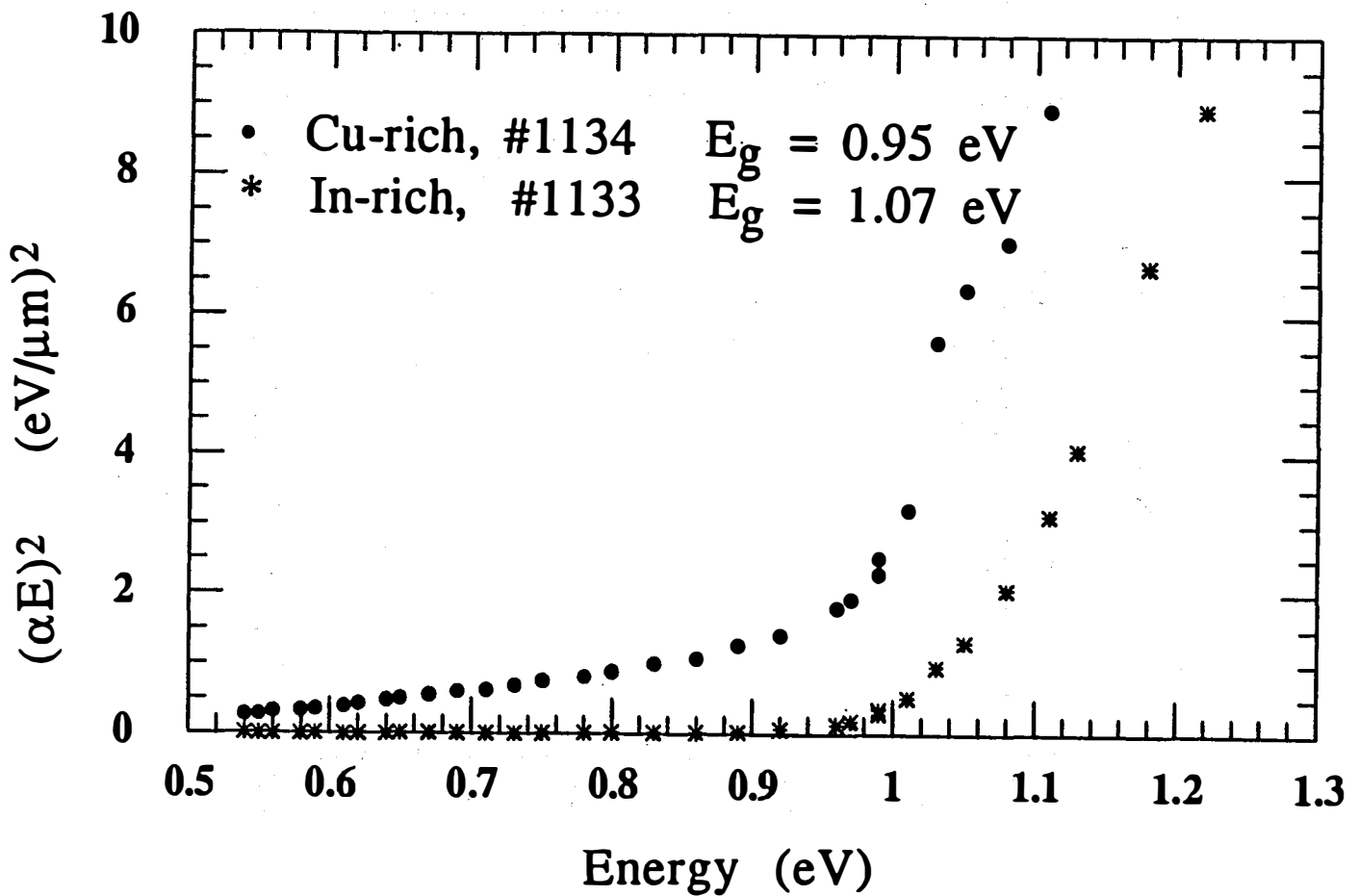


Figure 1. The absorption coefficient α for Cu- and In-rich films calculated from absorption, transmission, and reflection data for a range of photon energies E . The data are plotted as $(\alpha E)^2$ as a function of E which should give an approximately linear increase above the band gap.

Sample: 1120A#7

Temperature = 25.0°C

Jun. 29, 1989 9:58 am

Area = 0.108 cm²

SERI 

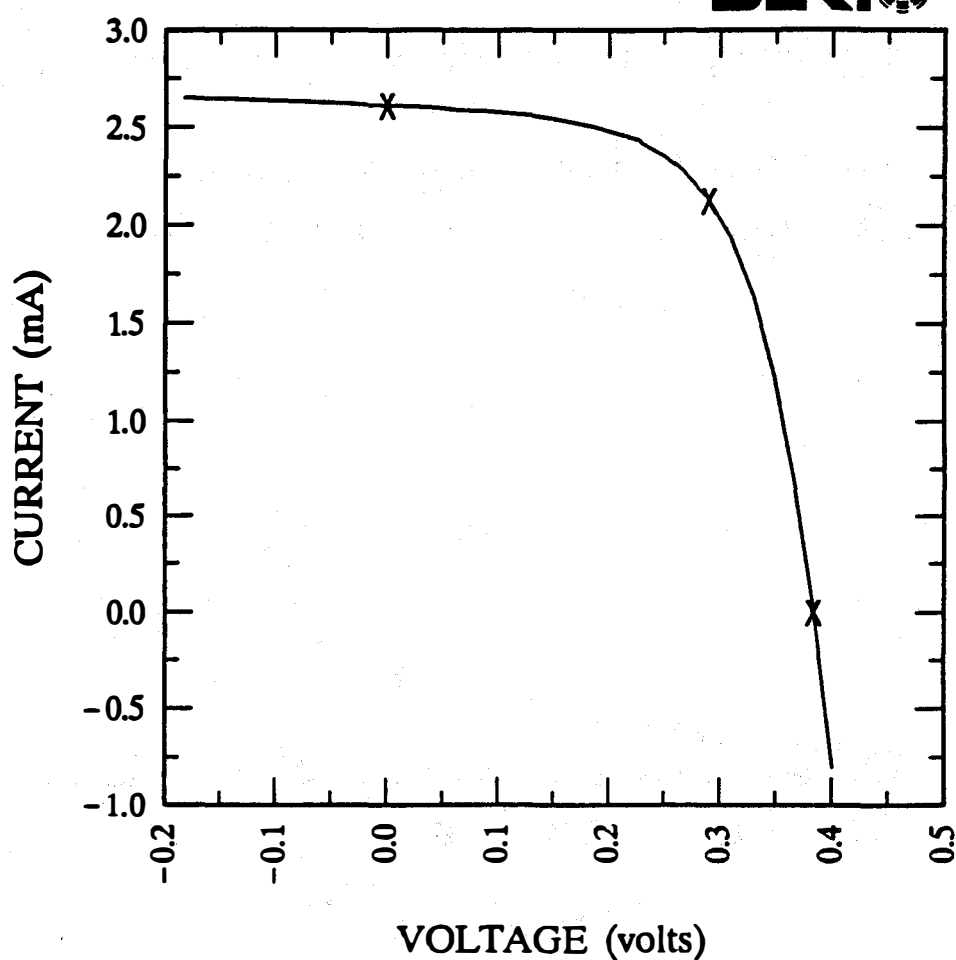


Figure 2. The current-voltage characteristics for the best device produced from hybrid material to-date as measured at SERI. The device exhibited the following active area (0.08 cm²) parameters: Efficiency=7.7 %, V_{oc} =0.3846 V, J_{sc} =32.64 mA cm⁻², Fill Factor 61.31%, I_{sc} =2.611 mA, P_{max} =0.616 mW, I_{max} =2.124 mA, V_{max} =0.2900 V.

Title: Thin Film Cadmium Telluride , Zinc Telluride, and Mercury Zinc Telluride Solar Cells

Organization: University of South Florida, Tampa, Florida

Contributors: T.L. Chu and S. S. Chu, Principal Investigators; J. Britt, C. Ferekides, S. Kadamani, M. Song, B.Tseng, and C. Wu

The major objective of this program is to investigate the preparation, characterization, and optimization of thin-film cadmium telluride solar cells in order to demonstrate a quantum efficiency of 75% at 0.44 μm and a photovoltaic conversion efficiency of 11.5% or greater. In addition, thin film zinc telluride and mercury zinc telluride solar cells with photovoltaic conversion efficiencies of 5% and 8%, respectively, will be developed; thin film mercury zinc telluride solar cell is suitable as the top member in two-cell cascade structures. The cadmium telluride solar cell has the configuration: ohmic contact/p-CdTe/TCS (or n-CdTe/SnO₂)/glass substrate. The technical approach consists of (1) the deposition of a transparent conducting semiconductor (TCS) on a glass substrate, (2) the deposition of CdTe films by close-spaced sublimation (CSS) and metalorganic chemical vapor deposition (MOCVD), (3) the formation of ohmic contacts to p-CdTe films, and (4) the characterization and optimization of solar cells. Zinc telluride and mercury zinc telluride solar cells have a similar configuration as CdTe heterojunction cells, and zinc telluride and mercury zinc telluride films are deposited by metalorganic chemical vapor deposition (MOCVD).

Transparent Conducting Semiconductor (TCS)

The photovoltaic characteristics of thin-film heterojunction solar cells depend strongly on the properties of TCS or heterojunction partner. Cadmium sulfide is the most commonly used TCS for CdTe solar cells; however, CdS has a bandgap of 2.42 eV, and thin films of 300 - 500 Å in thickness should be used in order to minimize the above bandgap absorption. The growth of CdS films from aqueous solutions using the reaction of thiourea with cadmium acetate and ammonium hydroxide on the substrate surface is best suited for this purpose. The process parameters have been investigated, and the optical, crystallographic, chemical, and electrical properties of CdS films evaluated. The solution grown CdS films is essentially stoichiometric and shows significantly higher above-bandgap transmission than vacuum-deposited CdS films (Fig. 1). The dissolution rate of CdS in 0.4 M HCl is used as a criterion of the quality of films. A post-deposition heat treatment is used to densify the films and to reduce the electrical resistivity. CdTe solar cells prepared by the deposition of p-CdTe films on CdS/SnO₂/glass substrates by CSS have conversion efficiencies of about 9.5%.

ZnO films and ZnS films have also been grown from aqueous solutions; however, MOCVD has produced films of superior quality. ZnO films, deposited by the oxidation of dimethylzinc (DMZn), have resistivities of 0.01 - 200 ohm-cm, depending on the O₂/DMZn ratio. ZnS films, deposited by the reaction of DMZn and H₂S, show high resistivity (>10⁶ ohm-cm), and doping has reduced the resistivity to about 5 X 10⁴ ohm-cm.

CdTe Films and Junctions

In addition to the deposition of CdTe films by CSS, the MOCVD of CdTe films has also been investigated with the objective of producing homojunction solar cells. The preparation of thin film CdTe homojunction solar cells by other deposition techniques has not been successful. The reaction of dimethylcadmium (DMCd) and diisopropyltellurium (DITe) on glass or SnO₂/glass substrates at 350° - 400°C in a hydrogen or helium flow has been investigated. Deposited films have

been identified as essentially stoichiometric CdTe from crystallographic, electron microprobe, and optical bandgap measurements. The films deposited by using DMCD/DITe molar ratios of 0.8 - 15 all showed positive photovoltages indicating p-type conductivity. Further, the deposited films show high lateral resistivity (Fig.2). These results are different from inorganic CVD, where n-type CdTe can be deposited by using a tellurium-deficient reaction mixture, and the resistivity of p-CdTe films can be controlled by varying the Cd/Te molar ratio in the reaction mixture. The reduction of resistivity of p-CdTe films by As-doping and the deposition of n-CdTe films by Al-doping are under investigation.

The annealing behavior of MOCVD CdTe films has been investigated using photovoltage as a criterion of evaluation. The photovoltage of CdTe/glass is increased from 250 - 300 mV to 400 - 450 mV after heating in He at 250°C, indicating improvements of structural properties. The photovoltage of CdTe/SnO₂/glass is degraded from 300 - 350 mV to 50 - 80 mV after heating in He at 300°C due presumably to the reaction between SnO₂ and CdTe at the interface. However, the heating of CdTe/SnO₂/glass at 500°C in He increased the photovoltage to 450 - 500 mV. The photovoltage of CdTe/CdS/SnO₂/glass, 350 - 400 mV, showed essentially no change after heating at 300°C and increased to 600 - 650 mV after heating at 500°C. Thus, the heating of CdTe/SnO₂/glass and CdTe/CdS/SnO₂/glass at 500°C results in the movement of the rectifying junction away from the interface.

ZnTe Films and Junctions

ZnTe films have been deposited on glass and coated glass substrates at 270° - 350°C by the reaction of diethylzinc (DEZn) and diisopropyltellurium (DITe) in a hydrogen atmosphere using UV irradiation (about 10¹⁸ photons/sec at 4.5 - 6 eV). The use of low temperature permits the in-situ formation of TCS/ZnTe heterojunction with minimal interface reaction. Crystallographic, electron-microprobe, and optical bandgap measurements all confirm the deposited films as ZnTe. ZnTe films deposited without intentional doping had high lateral resistivity (>10⁷ ohm-cm), and low resistivity films were readily obtained by using arsine as a dopant (Fig.3).

ZnTe/ZnS/SnO₂/glass structures have been prepared by the successive in-situ deposition of ZnS and ZnTe films on SnO₂/glass substrates. Photovoltages of up to 700 mV have been measured; however, the photocurrent was low due to the high resistivity of ZnS films. The use of Zn_{0.7}Cd_{0.3}S as the TCS improved the photocurrent (about 2 mA/cm²) but yields lower photovoltage.

Conclusions and Future Research

During this reporting period, the growth and characterization of CdS films from aqueous solutions and the deposition of ZnO, ZnS, and SnO₂ films by MOCVD have been carried out, and the usefulness of these films for heterojunction solar cells demonstrated. The MOCVD of CdTe films has been investigated in detail, and the properties of MOCVD CdTe films (conductivity type and resistivity) have been found to be significantly different from those of inorganic CVD CdTe films. The resistivity of MOCVD ZnTe films has been controlled reproducibly by doping, and Zn_{0.7}Cd_{0.3}S/ZnTe heterojunctions prepared by in-situ MOCVD appear to be promising.

The current efforts are directed to (1) the control of resistivity of n- and p-type MOCVD CdTe films, (2) the preparation and characterization of thin film CdTe homojunction solar cells, (3) the use of other TCS as heterojunction partners for CdTe solar cells, (4) the optimization of TCS/ZnTe junctions, and (5) the deposition and characterization of Hg_{0.3}Zn_{0.7}Te films and solar cells.

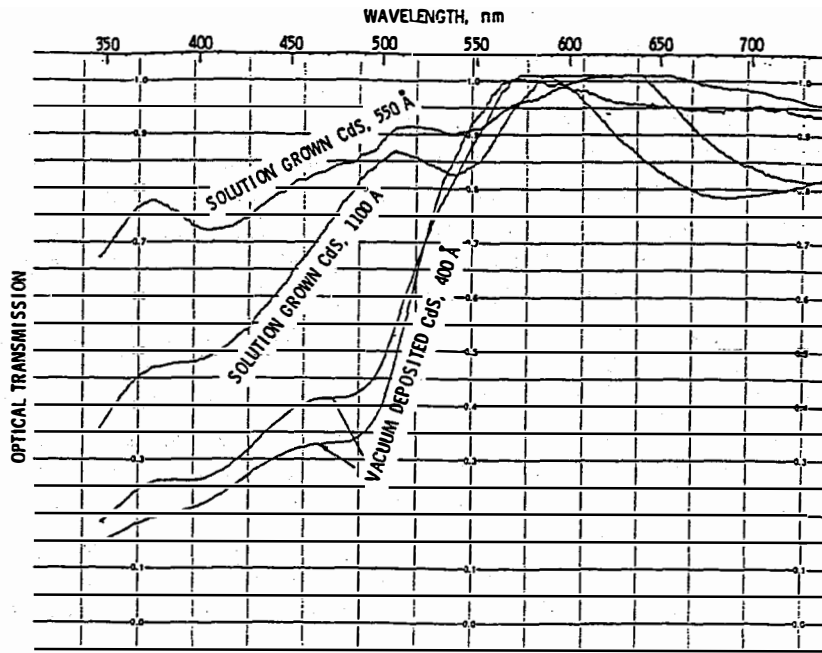


Fig. 1 Optical transmission of CdS films deposited by solution growth and by vacuum evaporation.

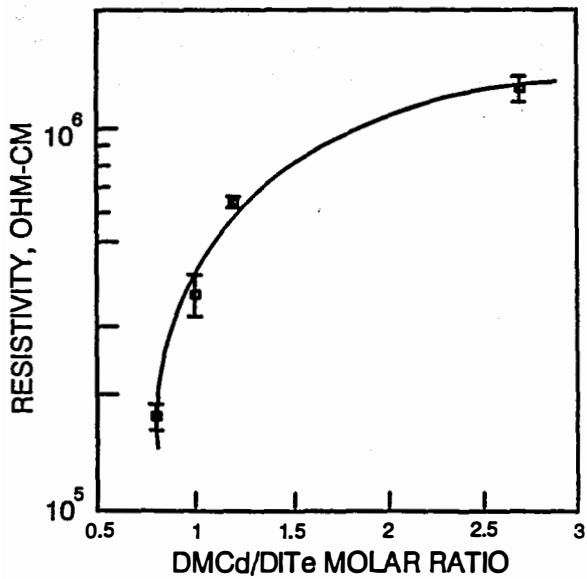


Fig. 2 Lateral resistivity of MOCVD CdTe films as a function of reactant composition.

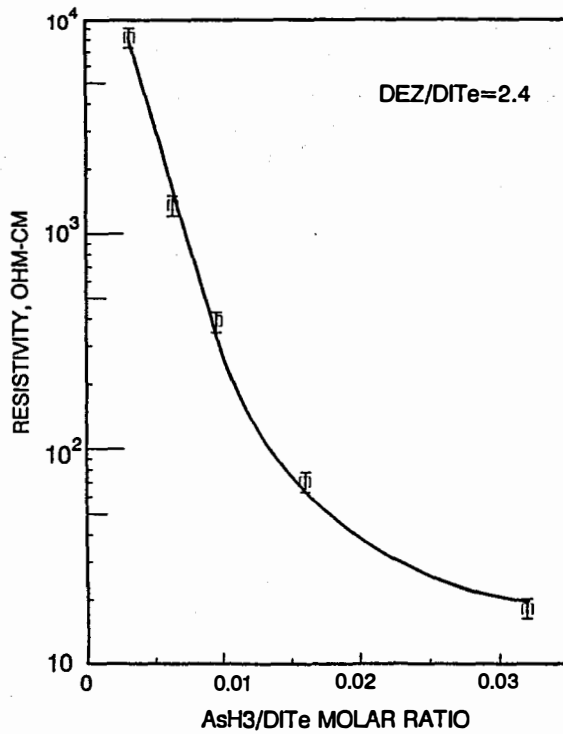


Fig. 3 Lateral resistivity of As-doped ZnTe films by MOCVD

4.0 CRYSTALLINE SILICON MATERIALS RESEARCH

John Benner (Manager), Bhushan Sopori

Although crystalline silicon technologies for material growth and device processing are considered to be mature for a variety of applications, there remain a host of issues about which the current understanding is only marginal. These issues pertain to the role of defects and impurities in altering the properties of silicon and silicon solar cells. It is generally recognized that the presence of impurities/defects in the substrate can degrade the cell performance; however, recent data show that in the presence of crystal defects, the influence of impurities on the cell performance is somewhat mitigated. It is also known that some defects can be passivated by presence of hydrogen or oxygen, although a detailed knowledge of these effects is certainly lacking. Clearly, these issues are critical to photovoltaic technology based on use of low-cost substrates which contain high concentrations of impurities and/or defects. The current research program was developed in collaboration with industry representatives to ensure that the industry research needs, pertaining to basic material issues, are adequately addressed. In this coordinated research effort between industry, universities and SERI, the SERI role is primarily to support the area of test device fabrication/analysis in order to relate material characteristics directly to solar cell performance.

This research program is aimed at developing understanding of basic mechanisms related to influence of impurities and defects on the important photovoltaic parameters in silicon. In processes that can be applied to low-cost substrates, preferably as a part of solar cell fabrication process, in order to improve subcontracts that are supported by SERI in-house research participation. Major areas of research are: (1) mechanisms of hydrogen, oxygen interaction in low-cost silicon; (2) mechanisms of hydrogen passivation and kinetics of hydrogen diffusion; (3) effects of hydrogen on solar cells containing different types of crystal defects; (4) development of techniques for impurity characterization in silicon containing crystal defects; and (5) nondestructive testing of the photovoltaic parameters of commercial material. In the coming year an effort will be made to develop some low-cost cell processing techniques that incorporate the knowledge obtained from this research, to fabricate high-efficiency cells on commercial solar cell silicon.

Title: **Basic Studies of Point Defects and Their Influence on Solar Cell Related Electronic Properties of Crystalline Silicon**

Organization: School of Engineering, Duke University, Durham, North Carolina

Contributors: U.M. Goesele, principal investigator; B. Marioton, W.S. Yang, and W.J. Taylor

I. INTRODUCTION

Agglomerates of oxygen, carbon, and intrinsic point defects together with dislocations are suspected to limit the minority carrier diffusion length in solar-grade crystalline silicon. The agglomeration of oxygen and carbon is associated with volume changes which may partly be accommodated by intrinsic point defects. In order to formulate a quantitative model of precipitation and agglomeration during crystal growth the thermal equilibrium concentration and the diffusivity of self-interstitials, as well as the source/sink efficiency of dislocations for point defects have to be measured. Progress has been made this year in all areas.

II. INFLUENCE OF DISLOCATIONS ON POINT DEFECT SUPERSATURATIONS

In the presence of a non-equilibrium concentration of intrinsic point defects dislocations absorb or emit point defects by climb processes and thus reduce the deviation from the point defect equilibrium concentration. The rate at which equilibrium throughout the crystal is reached depends upon the magnitude of the point defect deviation from equilibrium ($C_I - C_I^{eq}$), the diffusivity of the defect (D_I), the density of dislocations (ρ), and the efficiency of the dislocation as a sink or source (α_{eff}).

$$(dC_I/dt)_{climb} = -\alpha_{eff} \rho D_I (C_I - C_I^{eq})$$

Since the point defect deviation and diffusivity are investigated in other phases of this project (see Section IV) and the dislocation density is measurable, we are left with the problem of determining the dislocation efficiency.

III. INVESTIGATIONS OF DISLOCATION EFFICIENCY

The dislocation efficiency α_{eff} depends upon two factors: 1) the ease with which the dislocation can climb, thus eliminating/generating the point defects, and 2) the mobility of the point defects, allowing gradual changes in the point defect concentration away from the dislocation. In solar grade crystalline silicon, neither factor seems to dominate, so approximating the efficiency by one of the limiting values (1 or 0) is inappropriate. Therefore, this efficiency is being investigated through experiments involving gold diffusion in silicon.

Gold in silicon is mainly dissolved on substitutional sites (Au_s), but diffuses primarily along interstitial sites (Au_i). The change-over from interstitial to substitutional involves the silicon self-interstitial I, through the kick-out mechanism [1]



The incorporation of gold into silicon requires the generation of self-interstitials and their subsequent annihilation at sinks such as surfaces or dislocations. Two limiting cases exist. When dislocations are present in high concentrations and can quickly absorb the generated self-interstitials, a constant Au diffusivity results, providing an erfc-type profile.[2] When dislocations are absent, the self-interstitials supersaturate, resulting in a strongly concentration-dependent diffusivity [3], the well-known U-shaped Au profile. Since in polycrystalline solar grade silicon the dislocation density is fairly high ($>10^7$ cm⁻²) we expect, in a gold in-diffusion experiment from one side, an erfc-type profile. However, experiments have shown behavior somewhat in between the erfc-type and the U-shaped profiles, indicating that the dislocations are not perfectly efficient sinks. Since computer simulations using the versatile program ZOMBIE [4] showed that a concentration of 10^6 cm⁻² perfect dislocations should produce the erfc-type profile (see Figure 1), we are able to estimate an average sink efficiency of about 1/20 or less. This result is corroborated by experiments involving dislocation densities of 10^6 - 10^8 cm⁻², which were found to have almost negligible influence upon gold diffusion.[5] efficiency corresponds only to dislocations induced by the plastic deformation incurred during the high cooling rates of crystal growth. are 'grown in' as part of the crystal prior to cooling are known to be perfect sinks [6] and are assumed here to be present in much smaller concentrations. experiment we have shown that plastically deformed single crystalline silicon samples with an extremely high dislocation density lead actually to erfc-type profiles after gold diffusion at 1200° C.

The quantitative analysis of the gold diffusion profiles is performed by two complementary methods. Spreading Resistance Profiles (SRP) are readily available in the Duke laboratories. A considerable amount of time was spent this year in finding the capabilities and limitations of this machine as it applies to our problem. SRP results appear to be very sensitive to the twinning boundaries prevalent in the polycrystalline material. Even the direction in which the measurements are taken (parallel vs perpendicular to the twin boundaries) has noticeable effects. See Figure 2. The resistance information can be roughly translated into concentration by comparison to several known samples. A more exact process is currently being incorporated, including automation of the data analysis. In addition to its availability, this procedure also provides the benefit of good lateral resolution. Unfortunately, spreading resistance provides data only on electrically active species, so any inactive agglomerations caused by rapid cooling conditions are undetected. Our concern about the magnitude of this undetected species prompted us to employ an additional method. Neutron Activation Analysis (NAA), is capable of detecting all gold species, whether or not it is electrically active, but has less lateral resolution than SRP. These tests are being performed with the collaboration of Professor H. Mehrer, Institute of Metal Physics, in Münster, West Germany. The latest NAA result, taken from the front side of a gold in-diffusion experiment is shown in Figure 3. NAA analysis on the back side of this same sample, due in the near future, should provide a complete profile.

IV. DETERMINATION OF THE DIFFUSIVITY OF SILICON SELF-INTERSTITIALS

While the self-interstitial component of self-diffusion $D_I C_I^{eq}$ of silicon is well known, the individual components D_I and C_I^{eq} are only estimated to within many orders of magnitude. These values are not only important in the study of the dislocation/point defect phenomena as described above, but are also major

components in the final objective of this project- a quantitative model of agglomeration and precipitation in the polycrystalline solar-cell material. Presently we are working on measuring the value of D_I at 900° C.

It is known that carbon atoms predominantly use self-interstitials as diffusion vehicles.[7] It is also known that phosphorus in high concentrations generates self-interstitials as it in-diffuses. Therefore, we in-diffuse high concentration phosphorus (from a doped spin-on glass) from one side of a highly carbon-doped wafer ($3 \times 10^{17} \text{ cm}^{-3}$) and observe the diffusion of the carbon into an undoped low temperature (850° C, 5µm) epitaxial silicon layer grown on the back side of the wafer. The arrival of the self-interstitials at the back side, prevented from escaping the wafer by an undoped spin-on glass, is marked by an increase in the carbon diffusion, the profiles of which are measured by Secondary Ion Mass Spectrometry (SIMS) at an outside laboratory. Arrival time and wafer thickness provide information on the diffusivity, D_I .

Work this year involved computer simulations, again using the diffusion simulation program ZOMBIE, which allowed us to determine the effect of various boundary conditions and diffusion times. Additionally, these studies showed that the original concept of using the 5µm epi-layer as the separation between the phosphorus doping and the carbon would have been insufficient. The diffusivities involved demanded larger separation distances if meaningful values are to be obtained, prompting our use of the full wafer thickness as described above.

In the first round of experiments, the back-side epi-layer was not used, and we simply measured the carbon out-diffusion profile. Results were severely hampered by the unusually high background level in the SIMS carbon measurements. In the one case where a reasonable profile was obtained, the analysis indicated no enhanced diffusivity of the carbon, indicating either a) the spin-on phosphorus did not generate a self-interstitial supersaturation, b) the undoped spin-on glass on the back side allowed self-interstitials to escape, thus preventing any self-interstitial supersaturation there, c) the self interstitials were absorbed by sinks in the bulk, or the self-interstitials never reached the back side, indicating a maximum diffusivity of $8.7 \times 10^{-8} \text{ cm}^2/\text{second}$. Extensive SRP studies have eliminated a) as a possibility, and c) is unlikely since the material is essentially defect-free float-zone material. A second round of samples is currently being tested in an effort to find whether b) or d) are valid.

In the course of our simulations of gold diffusion profiles we came across a specific feature of gold diffusion which might allow us to determine C_I^{eq} independent of the carbon diffusion experiments. This method is based on the observation that the concentration dependent diffusivity of gold into dislocation free silicon holds only over a limited region close to the surface. For thick silicon specimens the concave profile close to the surface is followed by a more erfc-type tail region (see Figure 4) in which the diffusivity [8]

$$D_{\text{eff}}^{(\text{tail})} = \frac{D_I C_I^{\text{eq}} C_I}{C_s^{\text{eq}} C_I^{\text{eq}}}$$

is dependent upon the self-interstitial supersaturation. Estimating the self interstitial ratio through the mass action law as [8]

$$C_I/C_I^{eq} \approx (C_S^{eq}/C_I^{eq})^{1/2}$$

and obtaining the $D_I C_I^{eq} / C_S^{eq}$ ratio from gold diffusion profiles in highly dislocated samples [9] one only has to measure the experimental $D_{eff}^{(tail)}$ in order to obtain the value C_I^{eq} (and therefore via the known $D_I C_I^{eq}$, find D_I). Such enhanced tail diffusivities have already been observed in bulk samples. [10],[11],[12] Alternatively, $D_{eff}^{(tail)}$ may be determined from lateral gold diffusion profiles as first measured by Hill, Lietz and Sittig. [13] We are presently pursuing this method to determine C_I^{eq} parallel to the originally suggested method via enhanced carbon diffusion.

V. THE AGGLOMERATION MODEL

It is clear from published data concerning carbon and oxygen precipitation that point defects resulting from the crystal growth process have a significant effect upon precipitation and agglomeration of the impurities. [14],[15],[16],[17] S. Hahn of Siltec Silicon, Menlo Park, CA, has supplied samples with known carbon and oxygen concentrations and known thermal histories. Hahn et.al. have shown [18] that appropriate concentrations of carbon and oxygen can lead to very low bulk stress, measured by synchrotron radiation, in spite of the fact that an appreciable part of the carbon and oxygen had precipitated. We will soon perform Surface Photo-Voltage (SPV) experiments on these samples to determine if the minority carrier lifetime is related to the bulk stress. Such data should provide us with a crucial link in our project, relating the thermal history and impurity concentrations to actual carrier lifetimes. Additionally, we are in the process of constructing a device capable of rapidly obtaining carrier lifetime measurements across an entire four inch area. [19] Such a device should prove valuable in investigating polycrystalline material, since lifetimes tends to vary from grain to grain. [20]

REFERENCES

- [1] W.Frank, U.Goesele, A. Mehrer, and A. Seeger, in: Diffusion in Crystalline Solids, G.E. Murch and A.S. Nowick, eds. (Academic Press, New York, 1984) p. 64.
- [2] N.A. Stolwijk, M. Perret, and H. Mehrer, in: Diffusion in High Technology Materials 1988, D. Gupta, A.D. Romig, and M.A. Dayananda, eds. (Trans. Tech. Publ. Brookfield, VT, 1988) p. 79.
- [3] U. Goesele, F. Morehead, Appl. Phys. Lett., **38**,1981 p. 157,
- [4] W. Jüngling, P. Pichler, S. Selberherr, E. Guerrero, and H. Pötzl, IEEE-Trans. ED-32, 1985, p. 156
- [5] S. Kästner and J. Hesse, Phys. Stat. Sol., **A25**,1974, p. 261
- [6] N.A. Stolwijk, J. Hölzl, w. Frank, J. Hauber, and H. Mehrer, Phys. Stat. Sol., **A104**, 1987, p. 225
- [7] J.P. Kalejs, L.A. Ladd, and U. Gösele, Appl. Phys. Lett., **45**,1984, p. 268
- [8] W. Taylor, B.P.R. Marioton, T.Y. Tan, and U. Goesele, Rad. Effects in Defects and Solids, 1989, in press.
- [9] N.A. Stolwijk, J. Hölzl, E.R. Weber, H. Mehrer, and W. Frank, Appl. Phys., **A39**, 1986, p. 37
- [10] G.B. Bronner and J.D. Plummer, Appl. Phys. Lett., **46**,1985, p. 511
- [11] F.A. Huntley and A.F. Willoughby, Phil. Mag., **28**,1973, p. 1319
- [12] C. Boit and R. Sittig, to be published.
- [13] M. Hill, M. Lietz and R. Sittig, J. Electrochem. Soc., **129**,1982, p. 1579

- [14] S. Kishino, Y. Matsushita, M. Kanamori, and T. Iiauka, *Jpn.J. Appl. Phys.*, **21**, 1982, p. 1
- [15] H. Nakanishi, H. Kohda, and K. Hoshikawa, *J. Crystal Growth*, **61**, 1983, p. 80
- [16] H. Furuya, I. Suzuki, and Y. Shimanuki, *J. Electrochem. Soc.*, **135**, 1988, p. 677
- [17] Y. Shimanuki, H. Furuya, and I. Suzuki, *J. Electrochem. Soc.*, **136**, 1989, p. 2058
- [18] S. Hahn, M. Arst, K.N. Ritz, S. Shatas, H.J. Stein, Z.U. Rek, and W.A. Tiller, *J. Appl. Phys.*, **64**, 1988, p. 849
- [19] V. Lehmann and H. Föll, *J. Electrochem. Soc.*, **135**, 1988, p. 2831
- [20] S. Pizzini, A. Sandrinelli, M. Beghi, D. Narducci, F. Allegretti, S. Torchio, G. Fabbri, G.P. Ottaviani, F. Demartin, A. Fusi, *J. Electrochem. Soc.*, **135**, 1988, p. 155

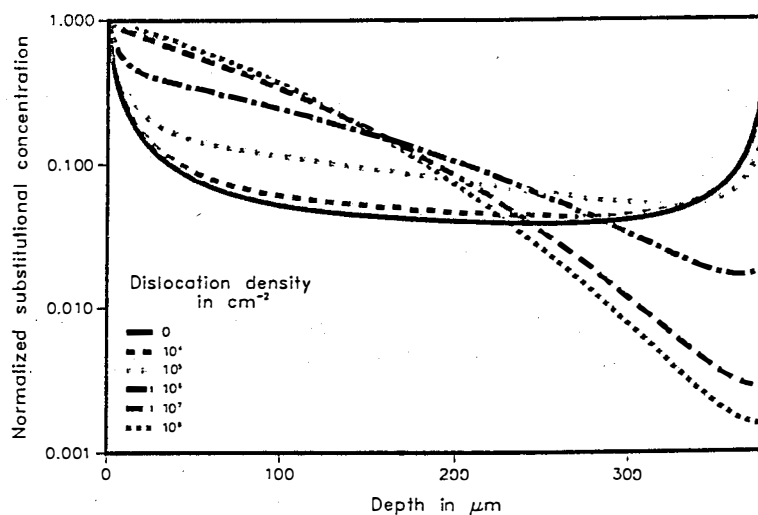


Figure 1: Gold diffusion from the left side into silicon after 30 minutes at 950° C, showing the dependence upon dislocation density

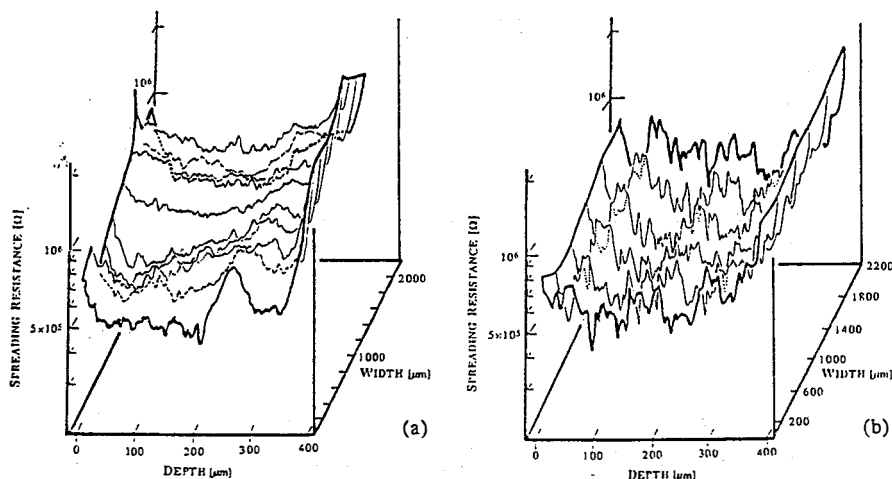


Figure 2: Spreading resistance profiles of gold in polycrystalline silicon after diffusion from left side for 30 minutes at 950° C taken a) parallel and b) perpendicular to twin boundaries.

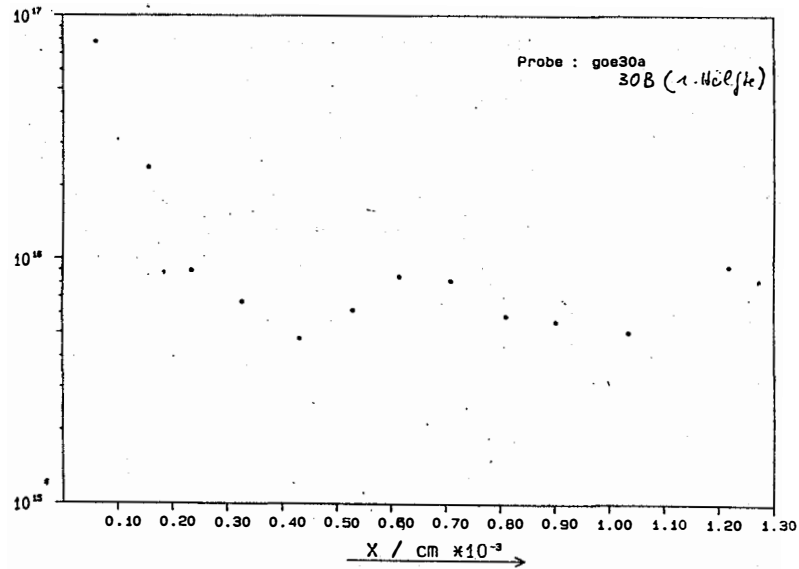


Figure 3: Neutron Activation Analysis of gold concentration profiles in silicon after diffusion from left side for 30 minutes at 950° C.

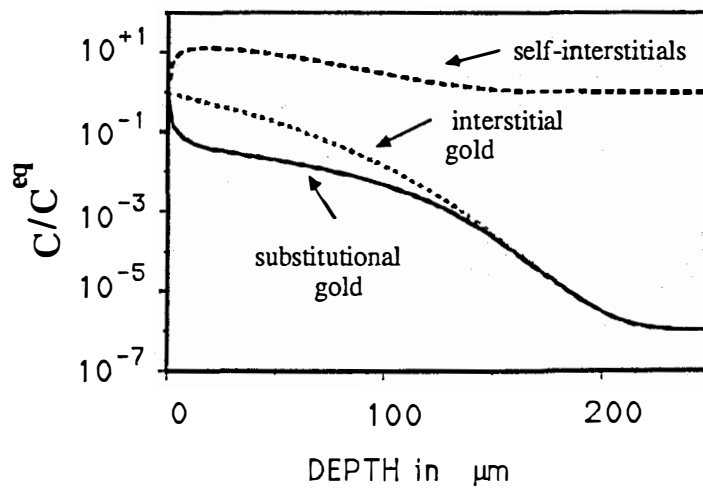


Figure 4: Simulated normalized concentration profiles for gold diffusion into dislocation free silicon after 15 seconds at 1000° C.

Title: Impurity and Defect Characterization in Silicon

Organization: Georgia Institute of Technology
Atlanta, Georgia 30332

Contributors: A. Rohatgi and W.A. Doolittle

Objective:

The objective of this program is to characterize promising photovoltaic materials, develop a fundamental understanding of impurity effects, and provide guidelines for improving materials that are being developed under the SERI subcontracts. The materials/samples will be selected and supplied by the technical monitor at SERI. The work performed under this program will be two-fold: (i) establish appropriate procedures to apply various sophisticated measurement techniques to the samples provided by SERI and (ii) perform various measurements including DLTS, FTIR, PAS, and PL on defective materials and improve data interpretation.

Introduction:

Understanding of defects is necessary to improve the quality of as-grown low-cost silicon substrates as well as post-growth processing procedures which can, concomitantly, lead to better cell performance. In spite of a lot of research done in this area, there is a considerable lack of understanding of various important impurity-defect issues including: (i) kinetics of defects associated with high speed growth, (ii) influence of thermal treatments on the defect dynamics, (iii) interactions between impurities and defects, and (iv) passivation of impurity/defect "activities". Since impurities play an important role in all these processes, it is essential to carry out detailed analysis of the state of impurities in such substrates before and after various process steps. This detailed information on changes in the defect and impurity concentrations and states will be applied in conjunction with other data from electrical analyses to develop suitable models which can predict changes in the photovoltaic parameters caused by post-growth processes parameters. Therefore, the research in this program will be directed toward the understanding of kinetics of defects and impurities, along with some basic measurements of minority carrier lifetime.

Modelling the Grain Boundary Recombination

A model was developed to show the possible increase in performance of a solar cell when a small amount of oxygen precipitates at the grain boundary. This is due to a decrease in current loss due to recombination at the grain boundary. It is known that grain boundaries have distributed states but there are no techniques today that can reveal the distribution of states. This makes it difficult to quantify the recombination losses at the boundaries. In this program, we have made an attempt to develop a model which allows us to calculate recombination current from the distribution

of states at the grain boundaries. For example, we were able to show that a parabolic distribution of states, which could result from oxygen precipitates, is less harmful than a Gaussian type distribution. (Figure 1)

Doping Dependence of EFG Solar Cells

A combination of material characterization, cell fabrication and device modelling was used to show for the first time a possible reason for why most investigators find that (a) optimum resistivity for polycrystalline silicon is somewhat greater than 0.2 ohm-cm. This was explained on the basis of a doping dependent shallow trap in as-grown EFG samples; (b) there is a broad maxima or plateau in cell efficiency in the resistivity range of 0.7-4.0 ohm-cm; (c) single crystal cell efficiency rises more rapidly with doping in the resistivity range of 0.7-10 ohm-cm compared to poly even when the starting lifetime prior to introducing dopants is same. Figure 2 shows a comparison of model calculations and measured cell data for EFG solar cells. More work is in progress and tools like FTIR, PAS, PL, and PCD measurements are being used to obtain even better understanding of this phenomenon.

Defects in FZ, MCZ, and CZ:

Lifetime and defects were measured in three promising single crystal materials. Before oxidation FZ gives the highest lifetime (4ms) and CZ has the lowest lifetime (0.5ms). As-grown MCZ had 2.5ms lifetime. After processing, FZ and MCZ have similar lifetimes (0.6ms) but CZ lifetime went down to 0.1ms. These lifetime differences were explained on the basis of defects, process-induced impurities, and residual impurities incorporated in the three crystal growth techniques.

Future Work:

We plan to improve the basic understanding of defects in promising photovoltaic silicon materials by applying material characterization tools such as DLTS, FTIR, EBIC, TEM, and PCD. Work is in progress to distinguish oxygen precipitates in polycrystalline silicon by low temperature FTIR measurements. Wacker material with different grain size is being analyzed along with EFG and semicrystalline silicon to understand the role of carbon and oxygen in polycrystalline materials.

Defect States in Polysilicon

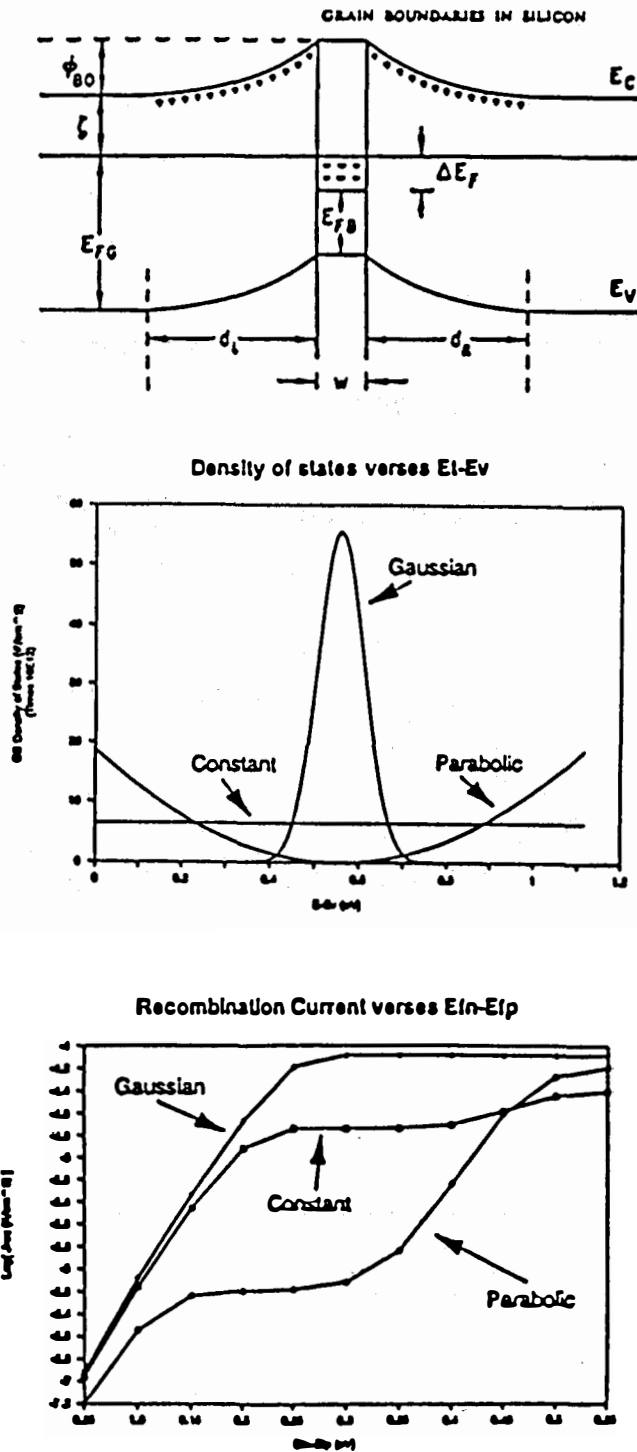


Figure 1: a) schematic representation of grain boundary states in polycrystalline silicon, b) distribution of states, c) calculated recombination current for three different distribution of states.

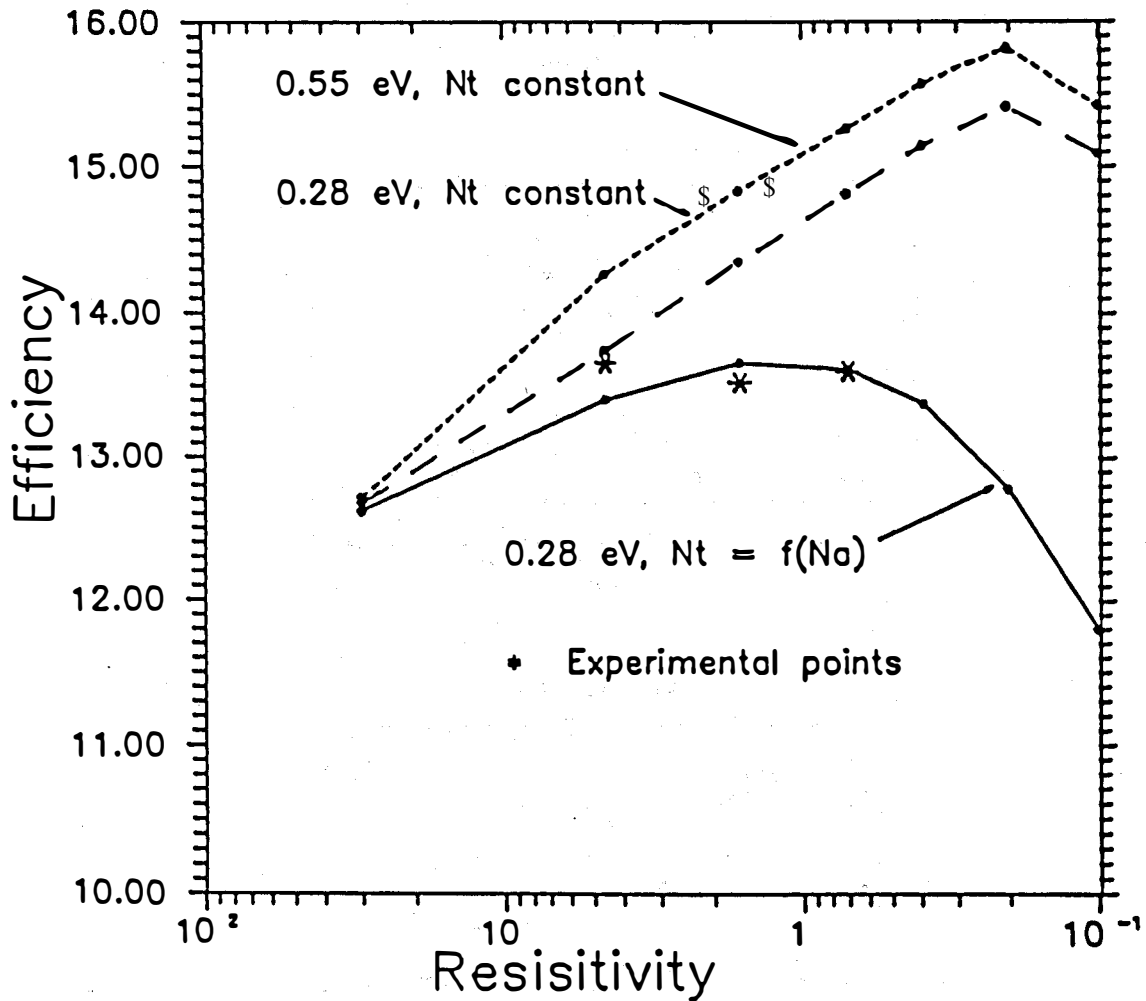


Figure 2: Model calculations for EFG silicon cell efficiency as a function of resistivity. Curves A and B show N_t as constant for two trap levels. Curve C shows N_t as a function of N_a for the shallow level.

Title: Passivation and Gettering Studies in Solar Cell Silicon

Organization: Institute for the Study of Defects in Solids,
Physics Department, The University at Albany,
Albany, N. Y. 12222

Contributors: J. W. Corbett, principal investigator; D. Angell, O. O. Awadelkarim, H. Bakhru, B. Baufeld, T. D. Bestwick, J. T. Borenstein, P. Deák, N. N. Gerasimenko, W. M. Gibson, N. L. Grigorenko, M. Heinrich, P. Jones, J. L. Lindström, J. Liu, F. Lu, G. S. Oehrlein, C. Ortiz, S. J. Pearton, A. Sályom, G. J. Scilla, R. K. Singh, L. C. Snyder, S. A. Suliman, A. J. Tavendale, D. A. Tulchinsky, I. V. Verner, R.-Zh. Wu, A. Yapsir, J.- Zh. Yuan, Q. Xiao, and Y. Zhang. (Not all receive support from the contract.)

This research program has two major aspects: 1) The study of hydrogen in crystalline silicon; and 2) the study of gettering in crystalline silicon. In the hydrogen studies are concerned with all aspects of hydrogen in silicon: how hydrogen is introduced into silicon (by wet-etching, boiling, plasma treatment, injection from a Kaufman source, etc.); its configurations and diffusion mechanisms; and the nature of its interactions with defects; the main emphasis has been the modeling of the diffusion profiles. The gettering studies are concerned with mechanism by which deleterious impurities are introduced into silicon and the mechanism by which these impurities can be removed from the device region, e. g., removal at an external surface or at a precipitate. Using studies on radio-active copper we have established that copper can permeate into and diffuse in silicon at room temperature; we have begun studies of gettering of this element as well.

Hydrogen-Related Studies.

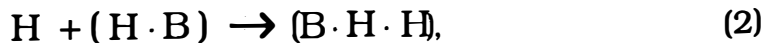
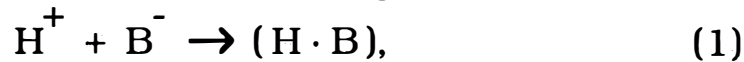
The mechanisms by which hydrogen is introduced into silicon are not fully established¹⁻⁵. Implantation of hydrogen into silicon is well understood, although the resultant damage is not⁶. The other means of introducing hydrogen into silicon are even less understood; some of our work is directed at improving this understanding. We have carried out, and are continuing, studies of the interactions of hydrogen with a silicon surface⁷, of etching of silicon by hydrogen⁸ (such as may occur in a gas or in a liquid), and plasma- and reactive-ion-etching^{9,10}; we will extend these studies to other introduction means as we make progress. We are continuing our studies of the mechanisms by which hydrogen interacts with defects and impurities¹¹⁻¹³.

We have studied the configuration of the hydrogen once it is introduced into silicon, and its diffusion mechanisms, the latter

studies necessarily including the study of the interactions of hydrogen with defects¹⁴⁻²⁰. Our theoretical work¹⁴⁻¹⁸ and that of others²¹⁻²⁵ have argued that the bond-centered (BC) site is the lowest energy configuration for isolated hydrogen in silicon, and that the anti-bonding (AB) site is a higher energy local minimum. The BC-site is clearly indicated in the EPR results of Gorelkinskii *et al.*²⁶ for the AA-9 center, and by the correlative results for the anomalous muon²⁷; channeling studies^{28,29} also support this ordering of sites.

Infra-red³⁰⁻³², channeling^{13, 33, 34} and theoretical^{35, 36} studies supported by perturbed angular correlation studies³⁷⁻³⁹ have established that the hydrogen de-activating a shallow acceptor is essentially at the BC-site as proposed by Pankove *et al.*⁴⁰ as that for the shallow donor is at an AB-site as proposed by Johnson *et al.*³⁵. We have found that there remain some complexities^{13, 41} in the As-H vs Sb-H sequence which we are studying using Rutherford Back-Scattering, channeling, and standing-wave x-ray measurements. In the normal boron-deactivation experiment the hydrogen is introduced at ca. 125°C and the boron activity is restored by annealing at ca. 200°C; we have found⁹ that introducing hydrogen at ca. 50°C results in hydrogen that remains relatively free so that it can move deeper into the material upon annealing at ca. 125°C; this is distinct from the field-induced migration found by Tavendale *et al.*⁴² and the deactivation observed following mechanical-polishing⁴³ in which the boron recovers upon annealing to ca. 100°C. The process which anneals at ca. 170°C we attribute to the hydrogen at the BC-site; that at ca. 70°C to the AB-site, with a small energy barrier between the two sites; and we argue that *both* sites deactivate the hydrogen. Even so this does not explain the relative mobile hydrogen which can migrate deeper into the crystal without an applied field; since the boron is *not reactivated* as Tavendale found, we must assume that this hydrogen is an extra hydrogen, such as might occur if a boron could trap two (or more) hydrogens at AB-sites, the first one being most strongly bound.

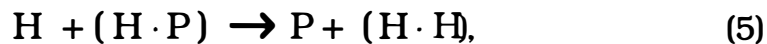
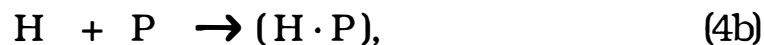
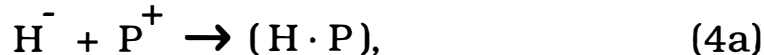
The model which appears to describe the diffusion processes in p-type silicon includes the following reactions:



Equation 1 reflects the Coulombic interaction between the charged boron and a charged hydrogen; the diffusion profiles suggest that the (0/+) level for hydrogen is at ca. ($E_V + 0.3 \pm 0.1$ eV). Equations 2 & 3 describe the capture of additional hydrogens by a boron; the diffusion profiles suggest this additional capture with $n \sim 8-16$, and as we mentioned we have found direct evidence for an additional, slightly

bound hydrogen in C-V experiments⁹. Theoretical studies^{17, 44- 46}, have suggested that hydrogen may agglomerate without forming hydrogen molecules.; we are carrying out theoretical studies⁴⁷ on the agglomeration process (for $n < 8$) at a boron in silicon. It is not clear if the {111} platelet formation observed by Johnson *et al.*⁴⁸ and by Jeng *et al.*⁴⁹ occurs heterogeneously or homogeneously. Although the {111} planar defects observed could be due to the partially dissociated multivacancy defects that we have discussed earlier⁵⁰, we are inclined to the view proposed by Johnson *et al.*⁴⁸ that a number of hydrogens in BC-sites interact through their associated distortions to form an extended planar defect. We have performed calculations^{45, 46} on such a defect, and find that the strain interaction will stabilize a planar defect; we further find that subsequent hydrogens will bond in the same bond axis, i.e., one on each silicon, without forming a molecule, and thereby form an incipient crack, a prototype of a defect causing the brittleness^{45, 46} of silicon grown in hydrogen gas.

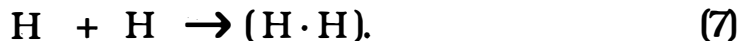
The model which appears to describe the diffusion processes in n-type silicon includes the following reactions:



Equations 4 show the reaction of a single hydrogen with the donor phosphorus; Eq. 4a describes the possibility of a Coulombic interaction. Our diffusion data does not require this reaction, i. e., we see no evidence of a negatively charged hydrogen in the range of resistivities of 100- to 0.1 Ω -cm silicon; more specifically these diffusion profiles do not exhibit the abrupt change in character found in p-type material. Johnson *et al.*⁵¹ and Tavendale *et al.*⁵² have found evidence of H^- in drift experiments, so the Coulombic reaction should occur. Equation 5 indicates that a second hydrogen may reactivate the phosphorus, a process which we use to explain the the "partial deactivation" of the phosphorus and the fact that the diffusion profile does not show the plateau associated with impurity trapping (a plateau observed for boron-doping). The diffusion profile for 100 Ω -cm silicon (both n-type and p-type) shows the shape which is characteristic of diffusion limited by molecule formation. As the phosphorus concentration increases the slope of the profile steepens, which we interpret as reflecting impurity mediated molecule formation. There is also at shallow depths a peak in the profile which tends to increase with the impurity concentration and it is for that reason we invoke the multi-hydrogen agglomeration at a phosphorus shown in Eq. 6. It does

seem from the work of Stavola and co-workers⁵³⁻⁵⁵ that a high percentage (e. g., >80%) of phosphorus can be deactivated with sufficient hydrogen.

We find that we can fit the simple diffusion profiles (e.g., 1 Ω-cm p-type and 100 Ω-cm n-type) with physically reasonable parameters, for example, with a 40 Å capture radius for the process in Eq. 1, and a 4 Å capture radius for those in eqs. 2 and 3, and a similar 4 Å radius for direct molecule formation:



We have also found⁵⁶, however, that these parameters are not unique! For example, we have found that we can fit the molecule-formation data with comparable success for the range of variables described by the following equations:

$$R D H_0^2 = C_1, \quad (8)$$

$$R H_0 = C_2; \quad (9)$$

and for the impurity-trapping regime for the range of variable described by the equation:

$$D H_0 = C_3. \quad (10)$$

In these equations D is the diffusion coefficient, R the corresponding capture radius, and H₀ the (unknown) concentration of hydrogen at the surface of the silicon; C₁, C₂, and C₃ are constants. There are "invariants" associated with conservative systems⁵⁷ described by non-linear equations, but we know of none such as these; we have been unable to derive these "invariants" with any generality. we do not despair of establishing the parameters unambiguously, in particular since some of the parameters may well be the same in different processes.

As we have discussed before¹⁻⁴, there is considerable scatter in the published data for diffusion of hydrogen in silicon. Part of this results from the common presumption that the diffusion profile is described by the conventional erfc profile and that the Einstein relationship holds:

$$D t = \bar{x}^2 \quad (11) G$$

with D the diffusion coefficient, t the time of diffusion and \bar{x} the mean distance in the diffusion profile. But the profiles for the

molecule-forming regime and the impurity-trapping regime is not an erfc profile, nor is Eq. 11 an accurate measure of the diffusion. The breakdown of Eq. 2 is a manifestation of a broader phenomenon, namely, diffusion in a fractal lattice. Equation 11 holds for diffusion in one-, two- and three-dimensional lattices. It does not hold for diffusion in a fractal lattice where the appropriate result⁵⁸ is

$$D t^{\mathbf{R}} = \bar{\mathbf{X}}^2 \quad (11)$$

with

$$\mathbf{R} = 2/(2+\delta) \quad (12)$$

with δ a parameter equal to zero for one-dimension, equal to 0.8 for two, and equal 1.5 for three. The origin of this deviation from Eq. 11 is the hindered motion of the random walk. A hindered motion occurs in hydrogen diffusion in silicon. For example, a random array of impurities at which the hydrogen can be trapped presents a hindrance to penetration into the lattice; similarly a random distribution of diffusing hydrogen with which a hydrogen can form molecules also forms a hindrance. we have not found a derivation of the expression corresponding to Eq. 12 for these cases, and will be exploring that dependence using numerical computations. For impurity trapping with a capture radius of 10 Å, a surface hydrogen concentration of $10^{16}/\text{cm}^3$ we find $\log(D t) \sim 1.3 \log \bar{\mathbf{X}}$ for 0.1 Ω-cm material and $\log(DT) \sim 1.7 \log \bar{\mathbf{X}}$ for 1 Ω-cm material. That is we find $\delta = -0.7$ and -0.3 for 0.1 Ω-cm and 1 Ω-cm, respectively. We presume that the change in sign in our result vs that for diffusion on the fractal lattice relates to the different form of hindrance in the two type of random walk. In the random walk on the fractal lattice the missing sites require the diffusing particle to go further, i. e., there are sites it cannot visit; in the case that we consider if the hydrogen visits a "forbidden" site it is capture and removed from the ensemble and represents a net loss to the advance of profile. We are continuing these studies to establish the broader picture. Ultimately the parameterization of the equations describing the profiles is our goal.

Gettering-Related Studies

It is well known that oxygen precipitates act as gettering sites for the iron-group transition elements, i.e., for the major "fast diffusers." We have completed several studies⁵⁹⁻⁶¹ related to these problems, including identifying⁴¹ the defect created when a vacancy interacts with an iron atom. A major problem in gettering studies is the indirect nature of the measurement studying the transition element, e.g., EPR can identify the transition element if it is in the

proper charge state, DLTS can identify an electrical level which may be associated with a transition element. We have begun studies using radio-active tracers to better follow the introduction and history of the transition elements. Another aspect of gettering at oxygen defects is identifying the oxygen defects of which there are a plethora of varieties⁶². We have carried out a number of studies⁶³⁻⁷¹ helping to clarify the nature of the electrical properties of the 450°C thermal donors, the new shallow donors, the anomalous oxygen diffusion mechanism, and the nature and structure of the core of the thermal donors, and of the thermal donors, and oxygen-related recombination centers. We anticipate exploiting this knowledge in our gettering studies.

It has been found by a number of authors^{1, 42, 72-78} that chemomechanical polishing of silicon results in changes in the resistivity of the material, and Schnegg et al.⁶, using secondary ion mass spectrometry, showed directly the penetration of hydrogen into silicon during polishing. It is well known that hydrogen passivates deleterious defects in semiconductors⁴⁰, and it is now known that in silicon the shallow acceptors can be deactivated by hydrogen¹ as can the shallow donors³⁵. Hydrogen can be introduced into silicon in a variety of ways: crystal growth or annealing at elevated temperatures in an atmosphere of hydrogen molecules; plasma- or reactive-ion treatment; hydrogen implantation; catalysis; boiling in water; and wet etching. It was the perturbed angular correlation studies by Wichert et al.³⁹, however, which suggested that another defect was also entering the silicon during polishing, and suggested that it was copper⁷⁹. Following these leads we investigated the permeation of radio-active copper (⁶⁴Cu) into silicon wafers at room temperature. These results show that copper does indeed enter silicon in routine room temperature processing.

The ⁶⁴Cu isotope⁸⁰ has a 12.70 hour half-life, and decays to ⁶⁴Ni via electron capture (41%) or positron (0.57 MeV) emission (19%) with a 1.35 MeV gamma ray and to ⁶⁴Zn by beta (0.57 MeV) decay (40%). Our detector was a halogen-quenched, end-window Geiger-Mueller counter with a 1-2 mg/cm² mica window, i. e., primarily a beta detector. The silicon samples were polished wafers with either 10¹⁵ or 10¹⁹ boron/cm³. Our initial measurements with low counting sensitivity and 10¹⁵ boron/cm³ samples did not result in our detection of copper penetration into silicon, but our subsequent measurements found penetration at both doping levels, more in the higher doping, presumably because the room-temperature, equilibrium solubility of copper in silicon is miniscule, and the copper which enters the system is trapped at the boron; this trapping is consistent with the electrical measurements made by others above after polishing, although some of the early literature suggested that such trapping was not occurring for copper and boron.

The chemomechanical polishing work indicated that the unknown impurity entered upon polishing in an alkaline slurry, e. g.,

with ammonia or an amine. We therefore carried out polishing with syton polish with ammonia and with HCl. To our surprise we found copper penetration into silicon with both polishing media. We also simply put the radio-active isotope in a solution on top of the silicon to see if it could be introduced in this manner; we used an HNO₃, an HCl, an HF, and an NH₄OH solution, and found, again to our surprise, that copper was introduced from each of these solutions, although apparently with less effectiveness than by polishing.

In our first example, ⁶⁴Cu was introduced into Si(10¹⁹ B/cm³) by polishing (against another Si wafer) for five minutes with syton in an ammonia solution into which the radio-isotope was introduced. The sample was then washed twice with water and ethyl alcohol. The samples counting rate was 2.5 x 10⁵ normalized to ten minutes; defining that as 100 %, 62.6 % remained after 1/2 microns was removed with CP-4, and 54.9 % remained after an additional 2 microns were removed by CP-4. (In each case the counting rate is corrected for the decay of the isotope.) If the ⁶⁴Cu from NH₄OH for 2 hr. *without polishing*, then washed with H₂O, and ethyl alcohol, the initial 100 % counting rate (in this case 1.8 x 10⁷ normalized for ten minutes) falls to 0.23 % after 1/2 microns of silicon was removed with CP-4, and to 0.007 % after an additional 2 microns was removed by CP-4. Since the specific activity of the radio-active solution in contact with the silicon varies, we attach no significance to the difference in the initial counting rate in different solutions; the difference in the profiles we believe to be significant. The comparable data for silicon in contact with a radio-active HNO₃ solution for six hours, then washed again with water and ethyl alcohol, the 100% initial counting rate (4.7 x 10⁶ in ten minutes) falls to 5.2 % after 1/2 micron of the silicon was removed by CP-4, and to 0.4 % with an additional 2 microns similarly removed. As we indicated similar data are obtained for ⁶⁴Cu in HF and in HCl solutions. A sample of silicon with 10¹⁵ B/cm³ was polished in the NH₄OH and Syton polish for 5 min. against the sample described above with 10¹⁹ B/cm³, then washed with H₂O, and ethyl alcohol and resulted in only 3.8 x 10⁴ counts in ten minutes (which we believe to be significantly different from the 2.5 x 10⁵ observed for the 10¹⁹ B/cm³ sample polished at the same time); the 100 % counting rate dropped to 30.9 % after 1/2 micron was removed with CP-4, again indicating a deeper penetration in the polishing case. One problem in such experiments is redeposition of the impurity (copper in this case) during dissolution of the silicon; we have had extensive discussions with chemists specializing in metal chemistry, including copper chemistry, but have been unable to find a suitable chelate to retain the dissolved copper, since chelates require a basic solution. We argue from the different profiles obtained for different introduction processes, but profiled using the same solution, that we are seeing copper introduced into the bulk of the silicon; the

different amount of copper introduced for different doping levels in the silicon also supports that view.

Further experiments with PIXE, SIMS, and RBS measurements establish that copper penetrates silicon; since the measurements do not require etching to establish a profile, they support the other measurements. We are seeking to establish the most effective means of introducing copper, the diffusion profile and its electric field dependence, and the reason for polishing being more effective than simple contact with a solution in introducing copper into silicon.

We also diffused ^{64}Cu from a drop of an NH_4OH solution into silicon by heating the sample at 900°C in a N_2 atmosphere for one hour. After washing in HF , H_2O , and ethyl alcohol, the initial ten minute counting rate was 7.9×10^8 ; this 100% counting rate fell to 9.2 % after removing 1/2 micron of the silicon with CP-4 and to 5.3 % after an additional 2 microns was removed; after annealing for 1 and 1/2 hours at 900°C with an HCl atmosphere, the ten minute counting rate was 5.1×10^4 , or 0.0071 %. Further gettering studies are in progress.

References

- ¹ S. J. Pearton, J. W. Corbett, and T.-S. Shi, *Appl. Phys. A* **43** (1987) 153.
- ² J. W. Corbett, J. L. Lindström, L. C. Snyder, and S. J. Pearton in *Defects in Electronic Materials*, eds. M. Stavola, S. J. Pearton, and G. Davies (MRS, Pittsburgh, 1988) pp. 229-239.
- ³ S. J. Pearton, M. Stavola, and J. W. Corbett in *Defects in Semiconductors 15*, ed. G. Ferenczi (Trans Tech, Switzerland, 1989) 25-37.
- ⁴ J. W. Corbett, S. J. Pearton, and M. Stavola in *Control of Defects in Semiconductors*, ed. K. Sumino, in press.
- ⁵ *Hydrogen in Semiconductors*, S. J. Pearton, J. W. Corbett, and M. Stavola (Springer Verlag, Berlin, 1990).
- ⁶ J. W. Corbett, P. Deák, U. Desnica, and S. J. Pearton in *Hydrogen in Semiconductors*, eds. J. I. Pankove and N. M. Johnson (Academic Press, NY 1990).
- ⁷ J. W. Corbett, D. Peak, S. J. Pearton, and A. Sganga in *Hydrogen in Disordered and Amorphous Solids*, eds. G. Bambakidis and R. C. Bowman (Plenum, N.Y. 1986) p. 61.
- ⁸ F. Lu, J. W. Corbett, and L. C. Snyder, *Phys. Lett.* **133** (1988) 249.
- ⁹ J. L. Lindström, G. S. Oehrlein, G. J. Scilla, A. S. Yapsir, and J. W. Corbett, *J. Appl. Phys.*, **65** (1989) 3297.
- ¹⁰ T. Bestwick, G. S. Oehrlein, D. Angell, P. Jones, and J. W. Corbett, *Appl. Phys. Lett.* **54** (1989) 2321.

-
- 11 A. S. Yapsir, P. Hadizad, T.-M. Lu, J. C. Corelli, J. W. Corbett, W. A. Lanford, and H. Bakhru in *Defects in Electronics Materials*, eds. M. Stavola, S. J. Pearton, and G. Davies (MRS, Pittsburgh, 1988) 297.
 - 12 A. S. Yapsir, P. Deák, R. K. Singh, L. C. Snyder, J. W. Corbett, and T.-M. Lu, *Phys. Rev. B* **38** (1988) 9936.
 - 13 Y. Zhang, J. W. Corbett, Q. Xiao, W. M. Gibson, and S. J. Pearton, to be published.
 - 14 P. Deák, J. L. Lindström, J. W. Corbett, S. J. Pearton, and A. J. Tavendale, *Phys. Lett. A* **126** (1988) 427.
 - 15 P. Deák, L. C. Snyder, and J. W. Corbett, *Phys. Rev. B* **37** (1988) 6887.
 - 16 P. Deák, L. C. Snyder, and J. W. Corbett in *New Developments in Semiconductor Physics*, eds. G. Ferenczi and F. Beleznyay (Springer Verlag, Berlin, 1988) 163.
 - 17 P. Deák, M. Heinrich, L. C. Snyder, and J. W. Corbett in EMRS Proc. 1989, in press.
 - 18 P. Deák, L. C. Snyder, M. Heinrich, and J. W. Corbett, to be published.
 - 19 J.W. Corbett, J.L. Lindström, S.J. Pearton, and A.J. Tavendale, *Solar Cells* **24** (1988) 127-133.
 - 20 J. T. Borenstein, D. Angell, and J. W. Corbett, Fall MRS meeting, 1988, in press.
 - 21 C. G. DeLeo, M. Doragi, and W. B. Fowler, *Phys. Rev. B* (1988), in press.
 - 22 A. A. Bonapasta, A. Lapicciarella, N. Tomassini, and M. Capizzi, *Europhys. Lett.* **7** (1988) 145.
 - 23 C. G. Van der Walle, Y. Bar-Yam, and S. T. Pantelides, *Phys. Rev. Lett.* **60** (1988) 2761.
 - 24 DeLeo and W. B. Fowler, *Phys. Rev. B* **31** (1985) 6861.
 - 25 DeLeo and W. B. Fowler, *Phys. Rev. Lett.* **56** (1986) 402.
 - 26 Yu. V. Gorelkinskii and N. N. Nevinyi, *Pis'ma Zh. Tekh. Fiz.* **13** (1987) 105.
 - 27 R. Kiefl, M. Celio, T. L. Estle, G. M. Luke, S. R. Kreitzman, J. H. Brewer, D. R. Noakes, E. J. Ensaldo, and K. Nishiyama, *Phys. Rev. Lett.* **58** (1987) 1780.
 - 28 S. T. Picraux and F. Vook, *Phys. Rev. B* **18** (1978) 2066.
 - 29 B. Bech Nielsen, *Phys. Rev. B* **37** (1988) 6353.
 - 30 M. Stavola, S.J. Pearton, J. Lopata, and W.C. Dautremont-Smith, *Appl. Phys. Lett.* **50** (1987) 1086-1088.
 - 31 K. Bergman, M. Stavola, S.J. Pearton, and T. Hayes, *Phys. Rev. B* **38** (1988) 9643.
 - 32 B. Pajot, A. Chari, M. Aucouturier, M. Astier, and M. Chantre, *Solid State Comm.* (1988) in press.
 - 33 A.D. Marwick, G.S. Oehrlein, and N.M. Johnson, *Phys. Rev. B* **36** (1987-1) 4539-4542.
 - 34 A.D. Warwick, G.S. Oehrlein, J.H. Barrett, and N.M. Johnson, *Phys. Rev. B* **36** (1987) in press.

-
- 35 N. M. Johnson, C. Herring, and D. J. Chadi, *Phys. Rev. Lett.* **56** (1986) 769.
- 36 K.J. Chang and D.J. Chadi, *Phys. Rev. Lett.* **60** (1988) 1422-1425.
- 37 M. Deicher, G. Grübel, E. Recknagel, and T. Wiechert, in *Defects in Semiconductors*, ed. H.J. von Bardeleben (Trans Tech Publ., Zürich, 1986) 1141-1146.
- 38 T. Wichert, H. Skudlik, M. Deicher, G. Grübel, R. Keller, E. Recknagel, and L. Song, *Phys. Rev. Lett.* **59** (1987) 2087.
- 39 T. Wichert, M. Deicher, G. Grübel, R. Keller, N. Schulz and H. Skudlik, *Appl. Phys. A* (1988) in press.
- 40 J.J. Pankove, P.J. Zanucchi, C.W. Magee, and G. Lukovsky, *Appl. Phys. Lett.* **46** (1985) 421.
- 41 Y. Zhang, J. W. Corbett, Q. Xiao, and W. M. Gibson, to be published.
- 42 A.J. Tavendale, A.A. Williams, D. Alexiev, and S.J. Pearton, in *Oxygen, Carbon, Hydrogen, and Nitrogen in Crystalline Silicon*, eds., J. C. Mikkelsen, S. J. Pearton, J. W. Corbett, and S. J. Pennycook, (Materials Res. Soc. Pittsburgh, 1986) p. 469.
- 43 A. Schnegg, H. Prigge, M. Grundner, P.O. Hahn, and H. Jacob in *Defects in Electronic Materials*, eds. M. Stavola, S. J. Pearton, and G. Davies, (MRS, Pittsburgh, 1988) p. 291.
- 44 K. J. Chang and D. J. Chadi, *Phys. Rev. Lett.* **62** (1989) 937.
- 45 J. W. Corbett, P. Deák, C. Ortiz, and L. C. Snyder, *J. Nucl. Materials*, in press.
- 46 C. Ortiz, D. Deák, L. C. Snyder, and J. W. Corbett, to be published.
- 47 L. Korpás, S. K. Estreicher, J. W. Corbett, and L. C. Snyder, to be published.
- 48 N.M. Johnson, F.A. Ponce, R.A. Street, and R.J. Nemanich, *Phys. Rev. B* **35** (1987-1) 4166.
- 49 S.-J. Jeng, G.S. Oehrlein, and G.J. Scilla, *Appl. Phys. Lett.* **53** (1988) 1755.
- 50 J. W. Corbett, J. P. Karins, and T.-Y. Tan, *Nucl. Instr. & Meth.* **182/183** (1981) 457.
- 51 N. M. Johnson and C. Herring in *Defects in Semiconductors 15*, ed. G. Ferenczi (Trans Tech, Switzerland, 1989) p. 961.
- 52 S. J. Pearton, private communication.
- 53 M. Stavola, S.J. Pearton, J. Lopata, and W.C. Dautremont-Smith, *Appl. Phys. Lett.* **50** (1987) 1086-1088.
- 54 K. Bergman, M. Stavola, S.J. Pearton, and J. Lopata, *Phys. Rev. B* **37** (1988) 2770.
- 55 K. Bergman, M. Stavola, S.J. Pearton, and T. Hayes, *Phys. Rev. B* **38** (1988) 9643.
- 56 J. T. Borenstein, D. A. Tulchinsky, and J. W. Corbett in Proc. Fall-MRS-89, to be published.
- 57 R. Z. Sagdeev, D. A. Usikov, and G. M. Zaslavsky, *Nonlinear Physics: From the Pendulum to Turbulence and Chaos* (Harwood Academic Publishers, New York, 1988).
- 58 Y. Gefen, A. Aharony, and S. Alexander, *Phys. Rev. Lett.* **50** (1983) 77.

-
- 59 P. W. Wang, H. S. Cheng, W. M. Gibson, and J. W. Corbett, *J. Appl. Phys.* **60** (1986) 1336.
- 60 P.W. Wang, Y. P. Feng, W. L. Roth, and J. W. Corbett, *J. Non-Cryst. Solids* **104** (1988) 81.
- 61 Zh.P. You, M. Gong, J.-Y. Chen, and J. W. Corbett, *J. Appl. Phys.* **63** (1988) 324.
- 62 See the several pertinent review articles in *Oxygen, Carbon, Hydrogen and Nitrogen in Crystalline Silicon*, eds. J. C. Mikkelsen, Jr., S. J. Pearton, J. W. Corbett, and S. J. Pennycook (MRS, Pittsburgh, 1986) and in *Defects in Electronic Materials*, eds. M. Stavola, S. J. Pearton, and G. Davies, (MRS, Pittsburgh, 1988).
- 63 J. T. Borenstein, J. W. Corbett, M. Herder, S. N. Sahu, and L. C. Snyder, *J. Phys. C: Solid State Phys.* **19** (1986) 2893.
- 64 J. T. Borenstein, D. Peak, and J. W. Corbett, in *Oxygen, Carbon, Hydrogen and Nitrogen in Crystalline Silicon*, eds. J. C. Mikkelsen, Jr., S. J. Pearton, J. W. Corbett, and S. J. Pennycook (MRS, Pittsburgh, 1986)
- 65 J. A. Griffin, H. Navarro, J. Weber, L. Genzel, J. T. Borenstein, J. W. Corbett, and L. C. Snyder, *J. Phys. C: Solid State Phys.* **19** (1986) L579.
- 66 L. C. Snyder, J. W. Corbett, P. Deák, and R.-Zh. Wu in *Defects in Electronic Materials*, eds. M. Stavola, S. J. Pearton, and G. Davies (MRS, Pittsburgh, 1988) p. 179.
- 67 K. Banerjee, V. A. Singh, and J. W. Corbett, *Semicond. Sci. & Tech.* **3** (1988) 542.
- 68 L. C. Snyder, J. W. Corbett, P. Deák, and R.-Zh. Wu in *New Developments in Semiconductor Physics*, eds. G. Ferenczi and F. Beleznyay (Springer Verlag, Berlin 1988) 147-156.
- 69 P. Deák, L. C. Snyder, J. W. Corbett, R.-Zh. Wu and A. Sályom in *Defects in Semiconductors 15*, ed. G. Ferenczi (Trans Tech, Switzerland 1989) 281.
- 70 L.C. Snyder, P. Deák, R.-Zh. Wu, and J. W. Corbett in *Defects in Semiconductors 15*, ed. G. Ferenczi (Trans Tech, Switzerland 1989) 329.
- 71 L. C. Snyder, P. Deák, R.-Zh. Wu, and J. W. Corbett in *Proc. Shallow Donor Conf., Linköping, Sweden, 1988*, in press.
- 72 J. Reichel and S. Sevcik, *Phys. Stat. Sol.* **103** (1987) 413-420.
- 73 A. Schnegg, M. Grunder, and H. Jacob in *Semiconductor Silicon/1986*, ed. H.R. Huff, T. Abe, and B. Kolbesen (Electrochem. Soc., Pennington, NJ 1986) p. 186.
- 74 S. J. Pearton, A. J. Tavendale, A. A. Williams, and D. Alekiev in *Semiconductor Silicon/1986*, ed. H.R. Huff, T. Abe, and B. Kolbesen (Electrochem. Soc., Pennington, NJ 1986) p. 826.
- 75 A. Chantre, L. Bouchet, and E. Andre, *J. Electrochem. Soc.* **135** (1988) 2867-2869.
- 76 T. Zundel, J. Weber, B. Benson, P. O. Hahn, A. Schnegg, and H. Prigge, *Appl. Phys. Lett.* **53** (1988) 1426-1428.

-
- 77 A. Schnegg, H. Prigge, M. Grunder, P. O. Hahn, and H. Jacob, in *Proc. ICDS-15*, in press.
- 78 M. Deicher, G. Grübel, R. Keller, E. Recknagel, N. Schulz, H. Skudlik, Th. Wichert, H. Prigge, and A. Schnegg, *Proc. 3rd Conf. on Shallow Impurities in Semiconductors*, Linköping, Sweden, 1988, in press.
- 79 Th. Wichert, private communication.
- 80 *Table of Isotopes*, eds. C. M. Lederer, and V. Shirley (John Wiley & Sons, N.Y.) 7th Edition.

Title: **The Effectiveness and Stability of Impurity/Defect Interaction and Their Impact on Minority Carrier Time**

Organization: Material Science and Engineering Department,
North Carolina State University Raleigh,
North Carolina 27695-7916

Contributor: George A. Rozgonyi and Fumio Shimura, principal investigators; Tian Qun Zhou, graduate student; Andrzej Buczkowski, visiting scientist; and Bhushan Sopori, Solar Energy Research Institute.

Objectives

The project is based on the chemical and electrical behavior of defect interfaces in crystalline silicon wafers, dendritic web and EFG ribbons as photovoltaic materials. Of particular interest at these interfaces is the practical issue of how stable a particular gettered element will be during subsequent thermal processing or device operation. We believe the fundamental aspects of gettering processes and the local improvement range of gettered material, or hydrogen deactivation, can be readily determined using a model epi/misfit dislocation system. This information will then be extended to EFG and web materials. The emphasis in this initial study has been on the hydrogen passivation of defects in silicon, particularly at pure or metal decorated dislocations. The primary tasks for the first year have been to investigate the effectiveness of hydrogen passivation of defects using epi/misfit dislocation silicon wafers and to determine if MCZ silicon wafers are equal, or superior to FZ and CZ silicon wafers in performance characteristics such as minority carrier lifetime, resistance to process induced defects and overall gettering capabilities.

Experimental and Major Accomplishments

The p-type epitaxial silicon wafers used in this study contained two buried interfaces which had a controlled number of deliberately introduced misfit dislocations^[1]. The silicon layers were grown with an addition of approximately 2% GeH₄ to a SiCl₂H₂ Chemical Vapor Deposition reactor. The samples were then anisotropically etched, as schematically shown in Fig.1, so that misfit dislocation end points were exposed along the (111) side walls of the etched trench. The top (100) surface was masked by a 700Å oxide to reduce hydrogen exposure to the top surface. An unetched (111) oriented silicon wafer was also plasma treated. Hydrogen passivation was carried out using a Kaufman Ion Beam System at SERI. Diagnostic procedures included secondary ion mass spectroscopy (SIMS), transmission electron microscopy (TEM), and scanning electron microscopy

in the electron beam induced current mode (EBIC/SEM). SIMS was used to determine the hydrogen profile, TEM to reveal the defects and surface radiation damage due to the hydrogen plasma process, while EBIC/SEM provided an image of the electrical activities of individual crystal defects.

A two dimensional SIMS hydrogen-distribution image which has an area of 150- μm diameter was obtained on a beveled and polished surface as shown in Fig.2. Note that the hydrogen intensity on the directly exposed (001) surface and along the trenches is much higher than that in the bulk. A hydrogen-depth profile was also obtained by sputtering the top (001) surface about 1 μm deep. It showed that most of hydrogen was accumulated on the surface within the range of 2500 \AA .

Figure 3 shows EBIC/SEM images before and after the hydrogen plasma process. In Fig.3a, a clear EBIC image was obtained only within space charge created by the Schottky diode; whereas a similar image (Fig.3b) taken on the beveled surface of the hydrogenated sample exhibits contrast all over the top surface area. Note that on the beveled area only the Schottky diode is in contrast. This is interpreted as revealing that an inversion layer was created on the surface associated with the hydrogen. It reflects an initial treatment with hydrogen far in excess of a practical passivation procedure.

Structural degradation of the surface region is generally observed when samples are exposed to a high flux hydrogen plasma. Figures 4(a) and (b) are cross-section TEM bright field images of a sample before and after hydrogenation. The heavily damaged surface region extended to a depth of approximately 2500 \AA . Individual defects such as gas bubbles and extended planar defects lying on {111} habit planes are evident. A plan view TEM bright field image of the near surface region of a $\langle 111 \rangle$ silicon wafer after hydrogenation is shown in Fig.4(c). Planar defects are evident with a density from 10^8 - 10^{10}cm^{-2} which are similar to defects reported by Ponce^[2,3] who identified them as H-stabilized platelets. Similar extended defects were found along the buried misfit dislocation interfaces after hydrogenation, as shown in Fig. 5(b). In Fig.5(a), cross-section TEM image shows a clear two dimensional dislocation network, where lines indicate the dislocations parallel to the image plane and end points indicate the dislocation perpendicular to the plane. Gas bubbles and hydrogen stabilized (111) platelets are present in Fig.5(b) along the dislocations indicating a strong interaction with misfit dislocations after the hydrogen plasma process particularly for the upper interface which is closer to the source of hydrogen.

Comparing SIMS and TEM, we found that hydrogen was concentrated in the near surface 2500 \AA region and its density decreased gradually with

distance into the bulk. In this hydrogen concentrated region, the surface was heavily damaged and many microdefects were formed. Hydrogen diffused into the crystal to form Si-H bonds to stabilize these microdefects, as mentioned by Ponce[2,3]. Therefore, this surface layer containing hydrogen decorated defects or hydrogen stabilized defects has a different energy state than the bulk crystal. The difference of the energy state between surface and bulk can form a junction and results in an unusual EBIC/SEM image. On the other hand, hydrogen can neutralize the dopant[4,5], effectively reducing the concentration of acceptors on the hydrogen-rich surface. The surface compensation or even inversion to n-type silicon, can form a junction between the surface layer and the p-type bulk. Because of both above reasons, hydrogen plasma process can result in an internal electrical field on the surface which gives rise to the EBIC image in the SEM outside the Schottky contact area.

Minority carrier lifetime measurements were performed on MCZ, reference CZ, and FZ silicon wafers. MOS capacitors were fabricated on these samples for subsequent C-t measurements. The generation lifetime τ_g was measured at room temperature, while the recombination lifetime τ_r was measured at 90°C by monitoring the relaxation of a MOS capacitor to a pulsed voltage. The measurement results show that magnetic field-applied Czochralski silicon has a higher minority carrier lifetime than that of CZ silicon because of fewer recombination centers such as oxygen precipitates.

Recommendations

The study will be continue using the model epitaxial silicon wafer system with lower exposure doses in the coming year. We will focus the study on hydrogen diffusion mechanisms and improvement of minority carrier lifetime and extend the work to defect boundaries in web and EFG material. Deuterium plasma source is expected to be used for high sensitivity SIMS measurement to profile the hydrogen from surface to bulk, as well as along the misfit dislocations. Furthermore, the interaction of hydrogen with some metal, which are carrier lifetime killers, will be studied by using the same model system on simultaneously gettered metal and hydrogen.

REFERENCE

1. G. A. Rozgonyi et al. J. Cryst. Growth 85,300 (1987)
2. F. A. Ponce et al.,Inst. Phys. Conf. Ser. 87(1), 49 (1987)
3. S. J. Jeng, G. Oehrleih and G. Scilla, Appl. Phys. Lett. 53,1735 (1988)
4. N. M. Johnson and M. D. Moyer, Appl. Phys. Lett. 46(8), 787 (1985)
5. N. M. Johnson, Appl. Phys. Lett. 48(11), 709 (1986)

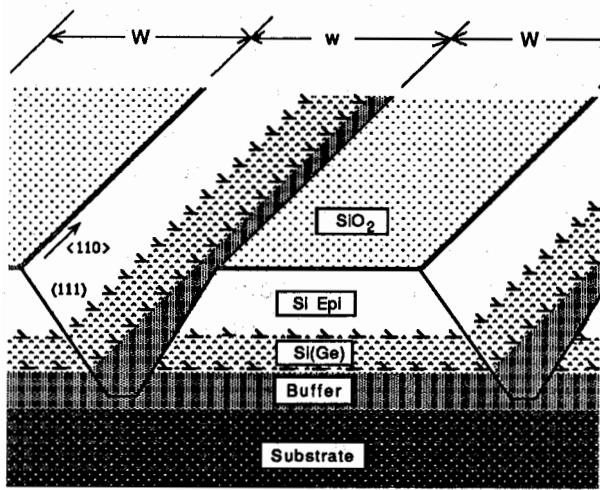


Fig.1 Schematic diagram of anisotropically etched grooves in oxidized epitaxial layer with misfit dislocation

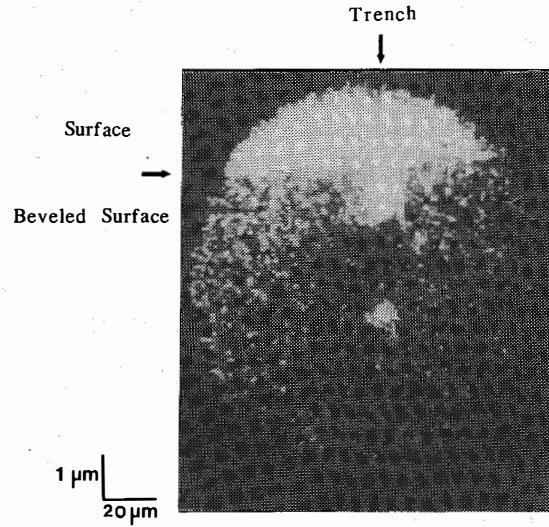


Fig. 2 Two dimension SIMS image of (100) epitaxial silicon wafer on bevel surface

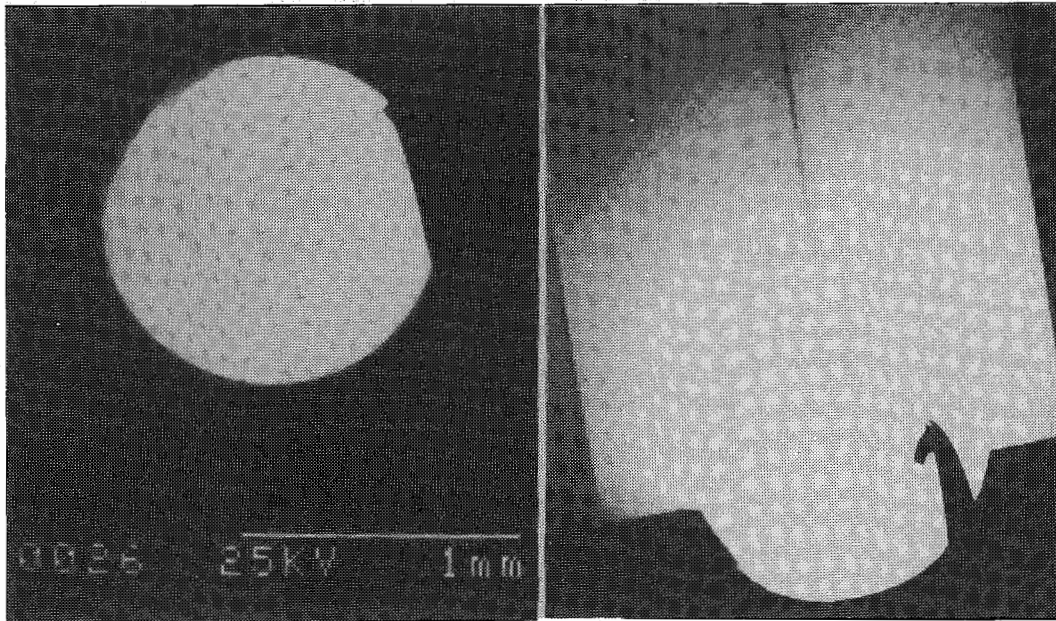


Fig. 3 EBIC/SEM image of epitaxial silicon wafer (a) before and (b) after hydrogenation

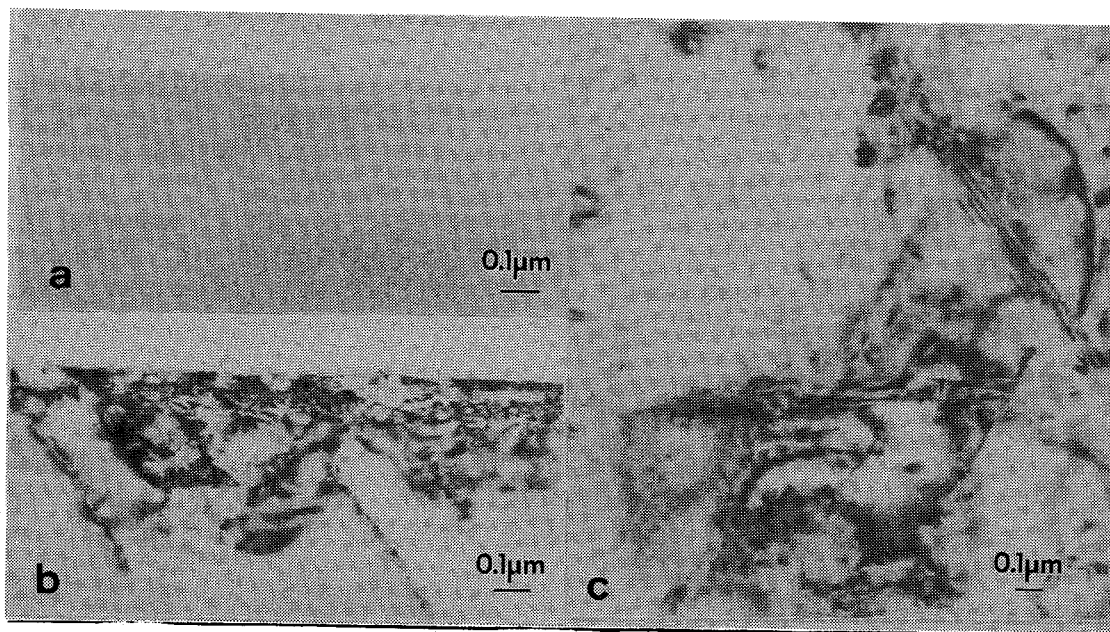


Fig. 4. Bright field image of TEM (a) X-section image of (100) Si before hydrogenation, (b) as (a), after hydrogenation, and (c) Pane-view image of (111) Si after hydrogenation

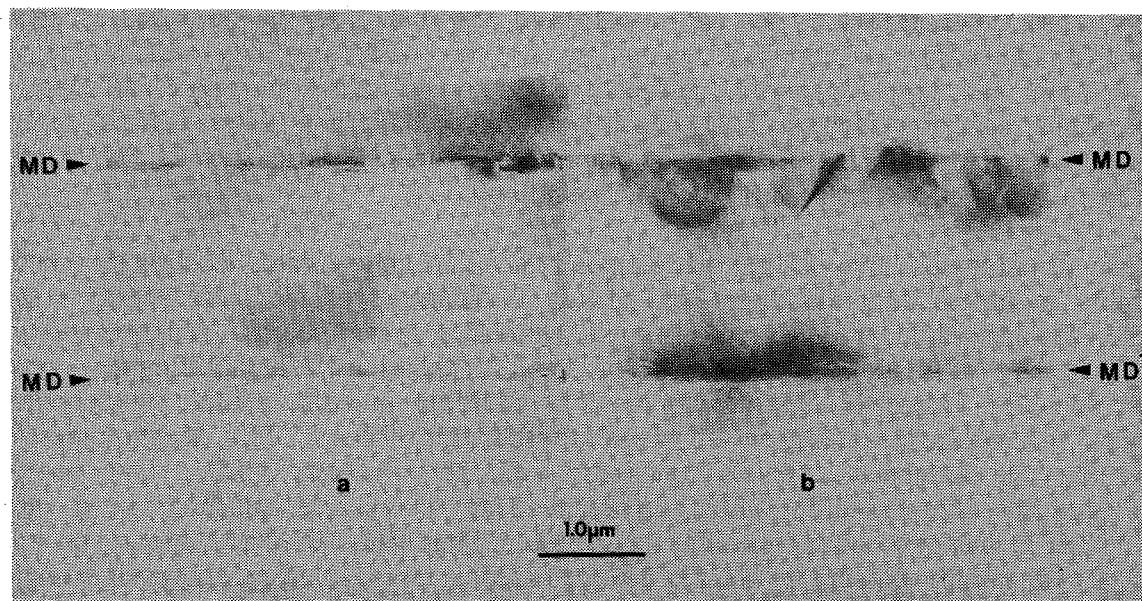


Fig. 5. Bright field image of X-section TEM of $\langle 100 \rangle$ Si with two misfit dislocation (MD) interfaces. (a) before hydrogenation and (b) after hydrogenation, MD decorated with hydrogen-induced defects.

5.0 HIGH-EFFICIENCY CONCEPTS

John Benner, (Manager) and Cecile Leboeuf

The objective of the High Efficiency Concepts Task is to evaluate and develop advanced photovoltaic technologies capable of energy conversion efficiencies in excess of 20% for flat-plate configurations and 30% in concentrator systems. These goals are discussed in the DOE Five-Year Research Plan as technology targets for the late 1990s. Even on this longer term horizon, it is difficult to envision a technology capable of achieving such high efficiencies without incorporating the demonstrated performance of crystalline III-V semiconductors. Thus, the High Efficiency Concepts task has become synonymous with III-V compound semiconductor research.

SERI's program of research in High-Efficiency Concepts has approached the terrestrial photovoltaic goals from the direction of first demonstrating the feasibility of exceeding the efficiency targets to assure that production engineering trade-offs between performance and cost can be accommodated. Recent advancements by the community researching high efficiency technologies provide a high level of confidence that the efficiency goals can readily be met.

The achievement of 25% efficiency in commercial concentrator modules will likely require production cells having more than 29% efficiency. The system cost target for that efficiency corresponds to cell costs less than \$10/cm². At least three organizations have demonstrated single-junction GaAs cell at approximately this efficiency level. Recent successes in multiple-junction technologies show encouraging progress toward fulfilling the theoretical promise of providing commercial cells with more than 35% efficiency. However, a fivefold reduction in processing costs would be needed to meet the cell cost target for concentrator cells. Much of this reduction can be achieved through use of larger wafers and higher through-put deposition systems. Research supported by this program benefits future development efforts by strengthening the understanding of basic mechanisms which affect uniformity of doping, composition, and thickness over large area wafers, from wafer-to-wafer and from run-to-run. Efficient utilization of source materials and evaluation to potentially superior sources (cost, purity, control, safety, and other factors) are also important topics for research. Continued improvement in cell efficiency is also a critical factor in reaching cost-effectiveness for the technology.

Flat-plate technologies have several advantages relative to concentrator technologies because the ability to utilize both the direct and diffuse components of the solar energy resource increases the geographical range of operation, simplifies system design and operation, and opens a variety of market opportunities for small installations. High-efficiency modules can be achieved either through development of multiple junction and/or development of processes for low-cost deposition of single crystal thin films. Two technologies have already reached performance levels consistent with the efficiency goals. One approach, which produces thin-crystalline-films, separated from a reusable substrate in a process called CLEFT, has reached efficiencies of 22.4%. Thin films of GaAs grown on silicon substrates are rapidly closing in on the 20% efficiency target, having improved from 11% to 19.9% efficiency in the last two years.

**Title: High Efficiency Thin-Film GaAs
and Ternary III-V Solar Cells**

**Organization: Kopin Corporation
Taunton, Massachusetts**

**Contributors: Ronald P. Gale and John C. C. Fan,
Coprincipal Investigators;
Robert W. McClelland, Brenda D. King.**

The objectives of this research program are to demonstrate large-areas and high-efficiencies in thin-film III-V solar cells. Kopin's approach is to use a thin-film technique (CLEFT[1]) to produce high-efficiency single-crystal GaAs/AlGaAs cells less than 5 um thick. This very effective use of material coupled with the multiple reuse of the GaAs substrate will allow this approach to meet the Department of Energy's cell cost targets.

Several key advances were achieved in FY89. The area of the thin-film GaAs wafers processed was successfully increased a factor of two to 3" diameter, and our standard process converted to wafers of this large size. Thin-film cell efficiencies were improved to over 21.5% one-sun AM1.5 global on 4 cm² areas, with directions for further improvement identified. Monolithic interconnection with voltage addition of a four thin-film cell string was demonstrated, permitting further scale up of cell size with no loss of efficiency.

Larger Areas

A critical question on our approach was whether or not the CLEFT process can be scaled up to larger areas. In the last year we have doubled the wafer area in this process and found that not only can we scale up the process, but larger wafers are just as easy if not easier to fabricate than the smaller ones. We have observed no fundamental barriers to further increases in wafer size.

The CLEFT process[1] uses mechanical separation of layer from substrate to produce thin films of single-crystal material. Separation is controlled by introducing a carbon layer with low adhesion between the layer and substrate with the lateral epitaxial overgrowth step shown schematically in Figure 1. The carbon layer is patterned on the substrate with seed-line openings, which allow the layer to grow from the substrate through and then over the carbon layer. A continuous, single-crystal layer is produced that is directly connected to the substrate only along the seed lines. The cell is fabricated in the layer and separated from the substrate, leaving the substrate free to be used again and again.

Scale up of the CLEFT process involved the building and shakedown of a larger overgrowth system, and refixturing of the plating and separation operations to handle the larger diameter wafers and layers. The pattern for the overgrowth seed lines did not change

from that indicated in Figure 1, as the number and width of lines per unit area were held constant on the larger wafers. Thus, the per unit-area adhesion of the layer to the substrate remained the same after this scale up and would remain a constant after further increases in wafer size. The overgrowth step therefore can also be held constant for future scale up in terms of thickness of film and distance of lateral overgrowth.

The separation fixturing was scaled in size proportionately to the wafer diameter increase, and no noticeable differences were observed in the separation of 3" and 2" wafers. Since the number of seed lines is constant per unit length, the force to initiate the cleaving does not scale with the wafer area but rather is proportional to the wafer diameter. That the separation of the larger-diameter wafers was as easy to initiate as the 2" wafers indicates the ability to further scale up the wafer size.

Higher Efficiencies

In FY89, thin-film cell efficiencies were improved to 21.5% AM1.5 global on 4 cm² areas, with further improvements made in thin-film cell performance. Initial improvements were made in the adjustment of cell-layer doping, which produced a four-cm² thin-film with 21.5% as measured at SERI. The illuminated I-V curve for this cell is shown in Figure 2. The open-circuit voltage was 0.984 volts, the short-circuit current density was 26.8 mA/cm², and the fill factor was 83.9%.

Several directions for improvement were identified and investigated. Base doping was increased to bring up the cell V_{OC} to over 1 volt. Base thickness was optimized to improve both the red and the blue response, and cell short-circuit currents were obtained between 27 and 28 mA/cm². By the end of FY89, cells were fabricated with efficiencies higher than the 21.5% measured at SERI. As all of these cells used only a single-layer AR coating of silicon nitride, even further improvements in the current and efficiency are possible.

Monolithic Interconnection

One of the key attributes of thin-film cells is their ability to be monolithically interconnected. This ability is especially important in the scaling up of high-efficiency cells, as the use of cell-voltage addition minimizes the cell current and required metallization in order to retain the high fill factors and low shadow losses. Cell grids remain unchanged as the current cell design is duplicated across the entire wafer and interconnected. Thus monolithic interconnection will allow the high efficiency cells to remain high efficiency after scale up.

A schematic cross section of two interconnected cells is shown in Figure 3. The front metallization of one cell is interconnected to the rear metallization of the adjacent cell through a via hole.

Front to back alignment is readily achieved with an infrared aligner, and etching through the GaAs is made easy by the fact that its total thickness is only about 5 μm .

In an initial demonstration, four 1 cm^2 cells were interconnected to produce a 4 cm^2 thin-film submodule. The IV curve for this submodule under one-sun AM1.5 global illumination is shown in Figure 4. The open-circuit voltage was 3.98 volts, the short-circuit current was 27.8 mA, the fill factor was 58.9%, leading to a total area efficiency of 16.3%. The voltage addition is clearly demonstrated, and the total current from the submodule is equivalent to our best current density. The low fill factor has been attributed to a high contact resistance between the front and rear metallization, and can be improved with an added sinter step. This is the first successful demonstration of a CLEFT monolithically interconnected four-cell string, and permits future scale up of cells to many times the current size without significant cell redesign.

Summary

Several key advances were achieved in FY89. The area of the thin-film GaAs wafers processed was successfully increased a factor of two to 3" diameter, and our standard process converted to the 3"-sized wafer. Thin-film cell efficiencies were improved to over 21.5% AM1.5 global on 4 cm^2 areas, with further improvements identified and incorporated. Monolithic interconnection with voltage addition of a four thin-film cell string was demonstrated, permitting further scale up of cell size with no loss of efficiency.

Future work will be centered around improving the cell efficiencies further and addressing process improvements in order to demonstrate lower cost cells. Thin-film cell efficiencies over 25% are achievable, and improvements in deposition, processing, and substrate reuse costs are needed to reach DOE cost goals for these high-efficiency cells.

References

1. R.W. McClelland, C.O. Bozler, and J.C.C. Fan, Appl. Phys. Lett., **37**(1980) 560.
2. Solar Cells paper, R.P. Gale et al... to be published

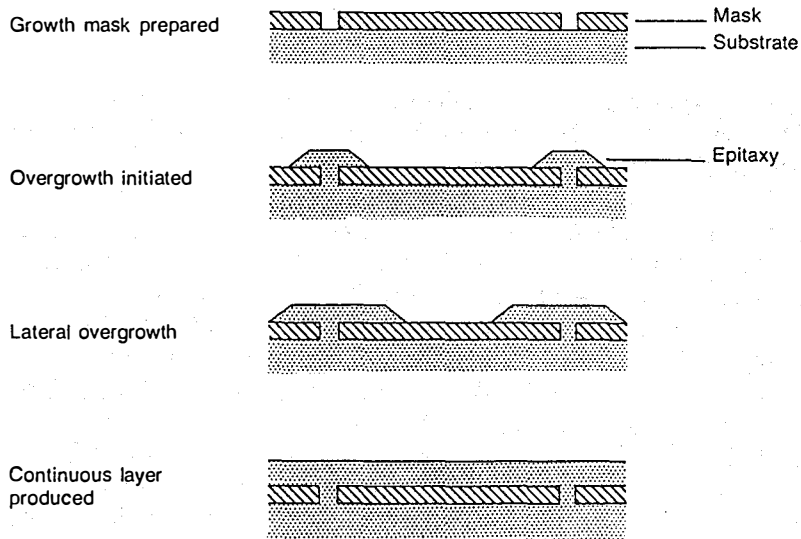


Figure 1. Schematic cross section of the lateral epitaxial growth process.

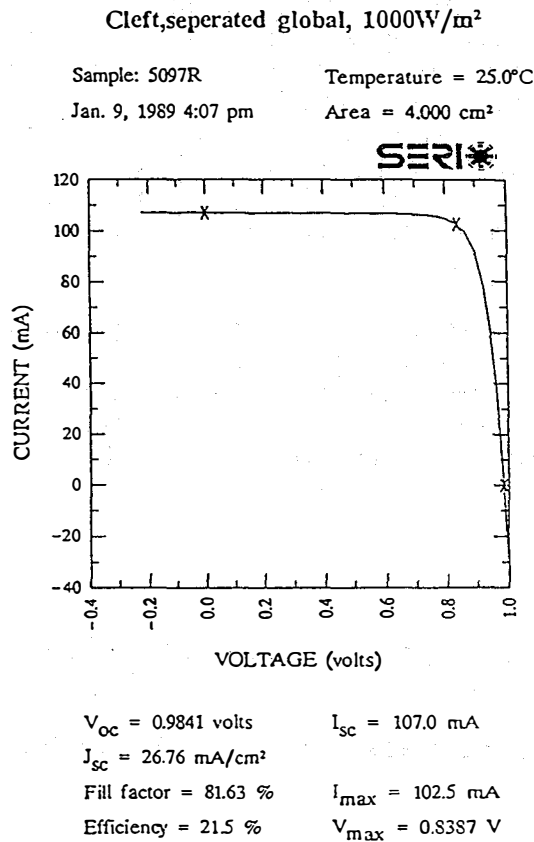


Figure 2. Illuminated I-V of a four-cm² thin-film cell.

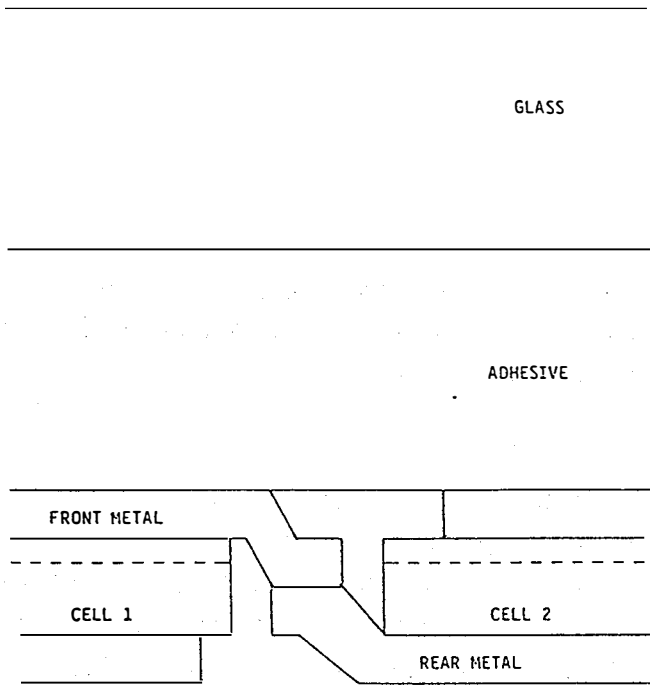


Figure 3.) Schematic cross section of two of the thin-film monolithically interconnected cells.

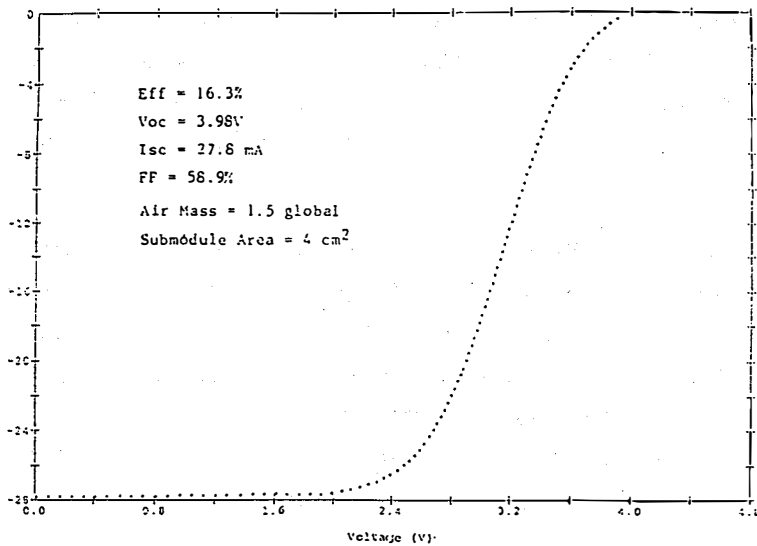


Figure 4. Illuminated I-V of a four-cell string of monolithically interconnected thin-film cells.

Title: Basic Studies of III-V High-Efficiency Cell Components

Organization: Purdue University, School of Electrical Engineering, W. Lafayette, IN 47907

Contributors: M. S. Lundstrom and M. R. Melloch, principal investigators, R. F. Pierret, faculty associate, M. S. Carpenter, A. Keshavarzi, M. E. Klausmeier-Brown, G. B. Lush, and T. B. Stellwag, research assistants

Solar cell efficiencies are determined both by material quality and by device design. As the efficiencies of both single and multiple junction III-V solar cells continue to rise, it is becoming increasingly important to carefully examine the internal device physics of solar cells so that cell designs can be tailored to the material constraints. After a broad program of basic studies in the late 1970's, silicon solar cell designers now understand the internal distribution of photocurrent and dark current losses with a high degree of confidence. In comparison to silicon, there has been relatively little work on basic studies of compound semiconductor solar cells. Our work is directed at meeting this need for an improved understanding of the internal device physics and material parameters of compound semiconductor solar cells. We aim to identify the internal recombination losses that control the performance of state-of-the-art, high-efficiency GaAs-based solar cells and to develop characterization methodologies and approaches that are broadly applicable to compound semiconductor cells. Another goal is to measure for the first time some of the fundamental parameters (such as the effective intrinsic carrier concentration and minority carrier mobility) which control the performance of solar cells. Finally, this evolving device physics knowledge is being used to explore new approaches for enhancing solar cell efficiency. While these basic studies are contributing to the steady progress of III-V cell efficiencies, they may at the same time lead to innovative new approaches for achieving substantial efficiency gains.

During the past year, our activities have focused on: 1) completing work on heavy doping effects in p^+ -GaAs, 2) assessing the importance of analogous effects in n^+ -GaAs, 3) continuing efforts to characterize and control perimeter recombination, 4) work to understand and further develop chemical passivation treatments, 5) conducting a baseline study of loss mechanisms in $Al_{0.2}Ga_{0.8}As$ solar cells, and 6) bringing on-line a new MBE growth facility. Work on these tasks are summarized here and is described more fully in our annual report [1]. Key results include: 1) extension of bandgap narrowing measurements in p^+ -GaAs to one order of magnitude higher in doping, 2) demonstration that effective bandgap shrinkage is not an important factor in n^+ -GaAs, 3) observation of an orientation-dependence to perimeter recombination, 4) demonstration that losses in both MOCVD- and MBE-grown $Al_{0.2}Ga_{0.8}As$ appear to be dominated by similar defects, and 5) successful turn-on and operation of a new MBE growth facility and the subsequent demonstration of GaAs solar cells with 23.8% conversion efficiency under 1-sun, AM1.5 global operating conditions.

Heavy doping effects in GaAs

The heavy impurity doping often employed in GaAs devices such as solar cells and bipolar transistors perturbs the energy band structure thereby affecting both the optical and electronic properties of devices. Because they have important consequences for AlGaAs/GaAs light-emitting diodes and lasers, effects of heavy doping on optical absorption and photoemission have been the subject of much study. Similar effects are well-known to have a profound influence on the electrical performance of silicon solar cells and should also be expected to have correspondingly important consequences for AlGaAs/GaAs solar cells. Our previous work in this area demonstrated that effective bandgap shrinkage in p^+ -GaAs has a substantial effect on the performance of high-efficiency GaAs cells [2]. During the past year, we used a new approach, analysis of the collector current in npn homojunction bipolar transistors [3,4]. Because this approach isolates the current of interest, it offered increased accuracy and enabled us to extend the measurements up to $N_A \approx 10^{20} \text{ cm}^{-3}$. In Fig. 1 we plot the effective intrinsic carrier concentration as deduced from these measurements versus doping density. The results show a much stronger effect than predicted from the perturbed band structure that is commonly used to treat optical effects in heavily doped GaAs. At the same time, the effect in p-GaAs is distinctly weaker than the corresponding effect in p-Si. These results demonstrate that heavy doping effects must be addressed by the GaAs cell designer and that our theoretical understanding of these effects is still inadequate.

Perimeter recombination Losses

Perimeter recombination has usually been neglected in solar cell analysis because it was assumed to be a minor effect in large area diodes. Our recent work demonstrated that perimeter recombination can dominate the $n \approx 2$ dark current for 0.5 cm by 0.5 cm solar cells and even for 2 cm by 2 cm cells [5]. At the one-sun open-circuit voltage point, the $n = 1$ current dominates, but at the maximum power point, the $n \approx 2$ current component is sizeable and degrades the fill factor [5]. As a consequence, perimeter recombination lowers the 1-sun fill factor of high-efficiency cells. Under concentration, the $n = 1$ current typically dominates, and perimeter recombination losses are negligible. But many solar cell diagnostic measurements are done under low current densities and with small area devices.

Our perimeter recombination research is directed at: 1) experimentally characterizing perimeter recombination, 2) exploring approaches to minimize it, and 3) understanding it at a theoretical level. To experimentally characterize perimeter recombination, we analyze test diodes in which the perimeter to area ratio is varied along with other diodes for which the area but not perimeter varies. We're currently examining the dependence of perimeter recombination on the chemical etch employed and on the crystallographic orientation of the diode. As displayed in Fig. 2, we've recently observed a strong (factor of 4-5) dependence of perimeter recombination on the crystallographic orientation of the mesa. We are also beginning to examine aging effects and implications for the long term stability of solar cell performance.

Chemical Passivation of GaAs surfaces

The oxides that form on bare GaAs surfaces produce large surface state densities that often dominate the electrical performance of devices. For solar cells, the consequences are photocurrent losses at the front surface and open-circuit voltage reductions due to recombination at the mesa perimeter. (The front surface is typically passivated by $\text{Al}_{0.9}\text{Ga}_{0.1}\text{As}$, but absorption in the window layer, though small, is now an important loss in the best cells.) Our approach consists of two paths; the first is to explore chemical treatments to passivate GaAs surfaces. Recent work by our group and others has demonstrated that sulfide chemical treatments can reduce recombination losses in solar cells, increase the gain of bipolar transistors, and modify the barrier height of metal-GaAs contacts [6,7]. We are now engaged in work directed at characterizing the electrical effects of ammonium sulfide treatments on front surface and perimeter recombination losses. The work consists of internal quantum efficiency and perimeter recombination analysis of diodes before and after treatment. We are also, in collaboration with W. N. Delgass and colleagues in Purdue's School of Chemical Engineering, performing XPS studies to probe the surface chemistry of treated GaAs [8]. Figure 3 shows XPS spectra of treated and untreated GaAs surfaces which show an absence of oxygen on the treated surface and less than one monolayer of sulfur. Because the passivation benefits of the chemical treatment are temporary, work to increase the stability of the treatment needs to be undertaken. Such work will commence if the treatment shows significant promise for photovoltaic applications. But it should be recognized that even a temporary treatment would prove useful for cell diagnostics.

Conclusions

When we began these basic studies three years ago, we viewed GaAs as a poorly characterized semiconductor when compared with Si. We now understand much more about the fundamental device physics of GaAs and the importance of various loss mechanisms in state-of-the-art cells. With this knowledge, it should now be possible to critically assess, with a high degree of confidence, the potential for innovative GaAs-based solar cell designs. The general features of these results should also apply to other III-V semiconductors. For example, work at other laboratories indicates that effective bandgap shrinkage effects similar to those we observed in p^+ -GaAs appear to be degrading the performance of InP solar cells. For the future, we plan to emphasize two new research directions. First our emphasis is shifting to $\text{Al}_x\text{Ga}_{1-x}\text{As}$, which should serve as a model for the material parameter and device physics issues faced by III-V cells in general. Second, with our new MBE growth facility and the high-quality films now being produced, we plan to place more emphasis on the demonstration of innovative concepts for enhancing the efficiency of III-V solar cells.

References

- [1] M.S. Lundstrom, M.R. Melloch, R.F. Pierret, M.S. Carpenter, H.L. Chuang, A. Keshavarzi, M.E. Klausmeier-Brown, G.B. Lush, and T.B. Stellwag, "Basic Studies of III-V High-Efficiency Cell Components," TR-EE 89-39, Purdue University, School of Electrical Engineering, September, 1989.
- [2] M.E. Klausmeier-Brown, P.D. DeMoulin, H.L. Chuang, M.S. Lundstrom, M.R. Melloch, and S.P. Tobin, "Influence of Bandgap Narrowing Effects in p^+ GaAs on Solar Cell Performance," Conf. Rec, 20th Photovoltaic Spec. Conf., Las Vegas, NV, Sept. 26-30, 1988, p. 503-507.
- [3] M.E. Klausmeier-Brown, M.R. Melloch, and M.S. Lundstrom, "Electrical Measurements of Bandgap Shrinkage in Heavily Doped p-Type GaAs," *J. Electron. Materials*, Jan. 1990.
- [4] M.E. Klausmeier-Brown, M.R. Melloch, and M.S. Lundstrom, "Transistor-Based Measurements of Electron Injection Currents in p-Type GaAs Doped 10^{18} to 10^{20} cm^{-3} ," *J. Appl. Phys.*, Jan. 1990.
- [5] P.D. DeMoulin, S.P. Tobin, M.S. Lundstrom, M.S. Carpenter, and M.R. Melloch, "Influence of Perimeter Recombination on High Efficiency GaAs P/N Heteroface Solar Cells," *IEEE Electron Dev. Lett.*, Vol. EDL-9, pp. 368-370, 1988.
- [6] M.S. Carpenter, M.R. Melloch, M.S. Lundstrom, and S. P. Tobin, "Effect of Na_2S and $(\text{NH}_4)_2\text{S}$ Passivation Treatments on the Dark Current-Voltage Characteristics of GaAs pn Diodes," *Appl. Phys. Lett.*, Vol. 52, pp. 2157-2159, 1988.
- [7] M.S. Carpenter, M.R. Meloch, and T.E. Dungan, "Schottky Barrier Formation on $(\text{NH}_4)_2$ -Treated n- and p-Type (100) GaAs," *Appl. Phys. Lett.*, Vol. 53, pp. 66-68, 1988.
- [8] M.S. Carpenter, M.R. Melloch, B.A. Cowans, Z. Dardas, and W.N. Delgass, "Investigations of Ammonium Sulfide Surface Treatments on GaAs," *J. Vac. Sci. and Tech. B*, Vol. 7, 1989.

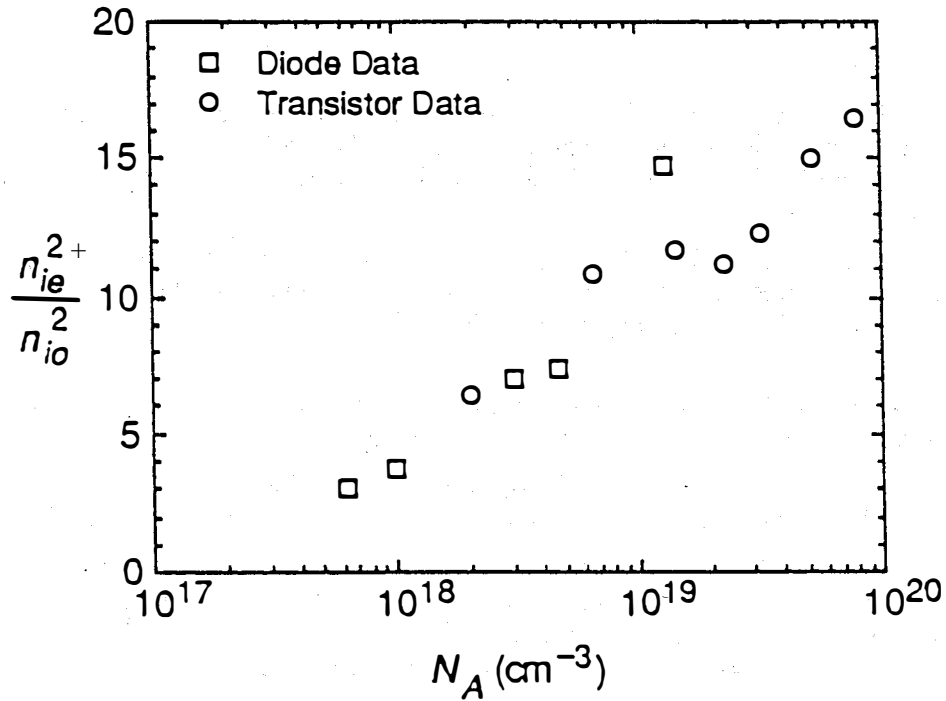


Fig. 1. The np product versus doping density for p-GaAs. (As deduced from the measurements of [3,4].)

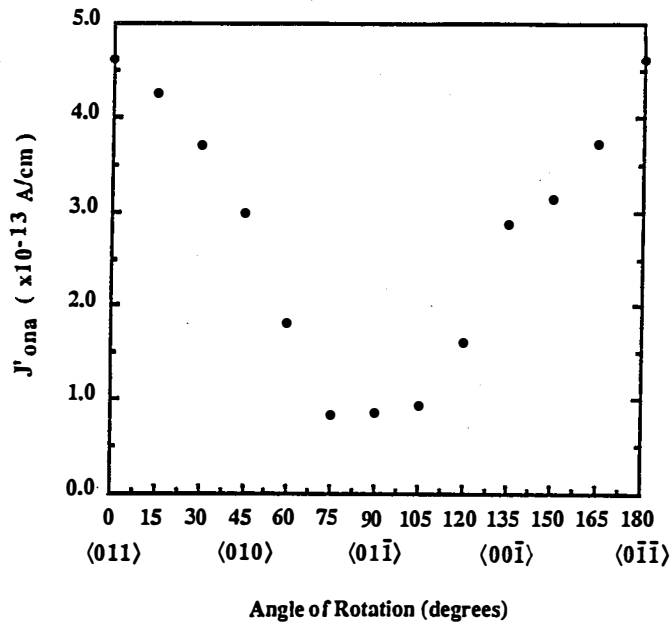


Fig. 2. The saturation current density for a mesa edge as a function of the crystallographic orientation of the edge. (From [1]).

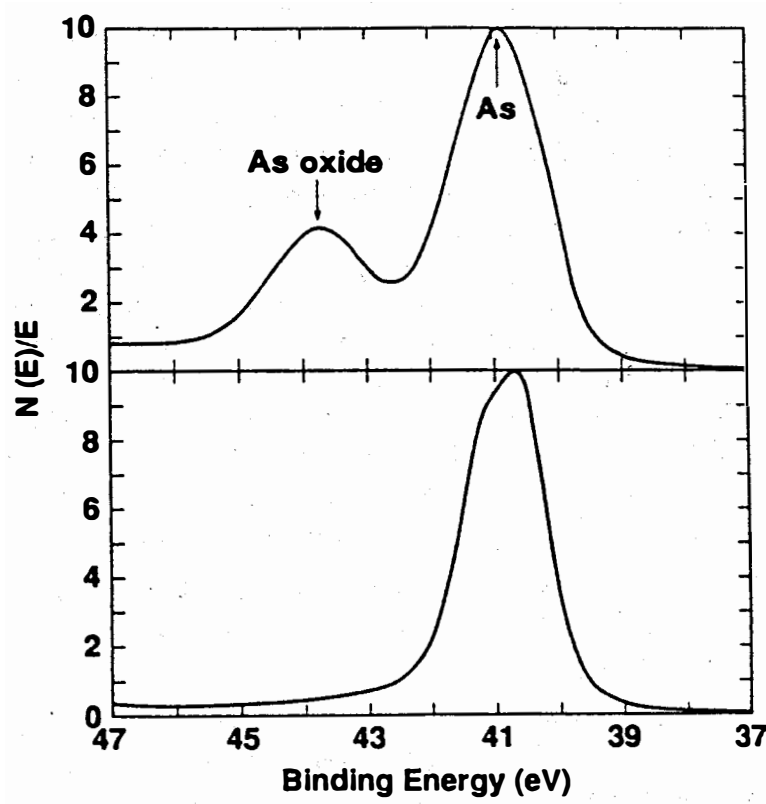


Fig. 3. X-ray photoemission spectra of: (a) bare GaAs surface etched with $\text{H}_2\text{SO}_4:\text{H}_2\text{O}_2:\text{H}_2\text{O}$ and (b) GaAs surface treated with $(\text{NH}_4)_2\text{S}$. (From [8])

Title: **Research on Semiconductors for High Efficiency Solar Cells**

Organization: Department of Electrical, Computer and Systems Engineering,
Rensselaer Polytechnic Institute, Troy, New York

Contributors: J.M. Borrego and S.K. Ghandhi, Co-Principal Investigators

The program objective is to investigate problems which are encountered in the development of high efficiency single and multi-junction solar cells. Specifically, these problems involve issues of materials growth and characterization. A number of separate tasks have been considered, as outlined below.

TASK 1. GROWTH MODELS AND NEW REACTOR CONCEPTS: This task involves the development of computer programs which are specifically directed to OMVPE in practical growth situations, and are capable of experimental verification. A computer program, which gives a direct solution of the Navier Stokes equations in two-dimensional form, has been used to study the effects of convection in epitaxial reactors, and on methods for the elimination of circulation effects. A unique feature of this program is that all wall temperatures are calculated. Thus, it is not necessary to use arbitrary boundary values for this parameter. Results have been directly applied to the growth of GaInAs, which is difficult because TEI and AsH₃ undergo a room temperature, parasitic, gas phase depletion reaction. Excellent material quality and uniformity were achieved at low reactor pressures and steep susceptor slopes. These results can be explained by the presence (or absence) of convection effects. The effect of convection on the temperature field was also studied for growth, with and without recirculation effects. It was shown that operation at low pressures reduces the amount of pre-heating of the gases. In the case of GaInAs growth, this is important in minimizing the effect of gas phase pre-reactions.

Application of the computer program to stagnation point reactors has resulted in the design of a new reaction chamber for growth of solar cell materials with high chemical usage efficiency. This work is in progress.

TASK 2. GROWTH MECHANISMS: A study has been initiated to extend our analysis of growth mechanisms to growth in ternary systems of the II-Va-Vb type, where the sticking coefficient is less than unity for the column V compounds. This task involves both theoretical development as well as experimental verification. One system will be considered initially.

TASK 3. HETEROSTRUCTURE MECHANICS: Most modern solar cell structures call for the heteroepitaxial growth of materials to give an increased photovoltaic conversion efficiency, provided that the resulting layers are of good electrical quality. Thus, there is considerable merit to understanding the problems of mismatched systems.

During mismatched epitaxy, it is observed that the growing layer is tilted with respect to the substrate. This misorientation is an important strain relief mechanism, and we have developed a general theory for this tilt in the last year. A double crystal x-ray diffractometer has been used for quantifying interfacial stress and stress relief in heterostructures with different lattice parameters and thermal expansion characteristics. The GaAs/Si system

is used in this study. The focus of the study is on the reduction of strain by varying the susceptor misorientation, and by the introduction of single and multiple strained layers. In addition to the x-ray techniques, PL, Hall and conventional electrical measurements are being used in this task.

TASK 4. MATERIALS STUDIES AND PHOTOLUMINESCENCE METHODS: A number of studies, of importance to the fabrication of high efficiency solar cells, have been undertaken. Recently, we have studied the use of silicon and sulfur as dopants for heavily doped n^+ -GaAs, since this region represents a "dead layer" in a high efficiency homojunction solar cell. Our work has shown that silicon is an almost ideal dopant for this purpose. We have shown that silicon can be used to dope GaAs to $8 \times 10^{18}/\text{cm}^3$, a value about twice as large as that reported by other OMVPE workers. Moreover, this material is essentially uncompensated ($K = 0.1$) so that this is an ideal dopant for n^+ regions.

A lifetime of 800 nsec. has been measured in n^+ - n - n^+ structures using this dopant, by photoluminescent decay methods (see Fig. 1). This is comparable to the best LPE grown material. Moreover, our results indicate that the surface recombination velocity of the n^+ - n junction is about a factor of 10 lower than that of the AlGaAs-GaAs interface. Using this structure, the classic Haynes-Shockley experiment for ambipolar diffusion has been carried out in GaAs for the first time. This experiment was carried out with a pumped dye laser which produces 8 psec, 800 nm pulses, every 10 μ sec. The resulting data, shown in Fig. 2, indicates spread of the photo-excited carriers as a function of time, and can be used to calculate the diffusion constant and the ambipolar mobility. These values are 14 cm^2/sec and 526 cm^2/Vsec . They are consistent with values determined from electrical measurements of the electron and hole mobilities in high purity bulk GaAs. From these measurements we calculate a diffusion length of 40 μm for this material.

TASK 5. MICROWAVE DIAGNOSTICS: A knowledge of resistivity, mobility and minority carrier lifetime is important in the study of semiconductor materials. Ideally, this should be done without destruction of the material. At present we have developed the use of microwave reflection as the basic technique for non-destructive characterization of these important material parameters. During this year, we have concentrated on the measurement of lifetime, which is perhaps the most direct indicator of solar cell performance. In our system, an AlGaAs laser, with a fall time of 2 nsec, is used for photoexcitation. This limits the minimum value of minority carrier lifetime which can be measured by our system. We emphasize, however, that this is not a limitation in the measurement of solar cell grade material.

A list of papers, written and/or published in FY 1989 now follows.

References

1. Agnello, P.D. and Ghandhi, S.K., J. Electrochem. Soc., 135, 1530, 1988.
2. Ghandhi, S.K. and Ayers, J.E., Appl. Phys. Lett., 53, 1024, 1988.
3. Ghandhi, S.K., Tyagi, S. and Venkatasubramanian, R., Appl. Phys. Lett., 53, 1308, 1988.

4. Chinoy, P., Agnello, P. and Gandhi, S.K., *J. Electron. Mater.*, **17**, 493, 1988.
5. Chinoy, P.B., Agnello, P. and Gandhi, S.K., *Proc. Mat. Res. Soc.*, **144**, 109, 1988.
6. Agnello, P. and Gandhi, S.K., *J. Crys. Growth*, **94**, 311, 1989.
7. Agnello, P., Chinoy, P.B. and Gandhi, S.K., *J. Crys. Growth* (accepted).
8. Venkatasubramanian, R., Patel, K. and Gandhi, S.K., *J. Crys. Growth*, **94**, 34, 1989.
9. Venkatasubramanian, R. and Gandhi, S.K., *J. Crys. Growth* (accepted).
10. Chinoy, P.B., Agnello, P.D. and Gandhi, S.K., *Proc. Mat. Res. Soc.*, **144**, 109, 1988.
11. Venkatasubramanian, R. and Gandhi, S.K., *Proc. Mat. Res. Soc.*, **144**, 67, 1988.
12. Lee, W.I. and Borrego, J.M., *J. Appl. Phys.*, **63**, 5357, 1988.
13. Bothra, S. and Borrego, J.M., *Solar Cells* (accepted).

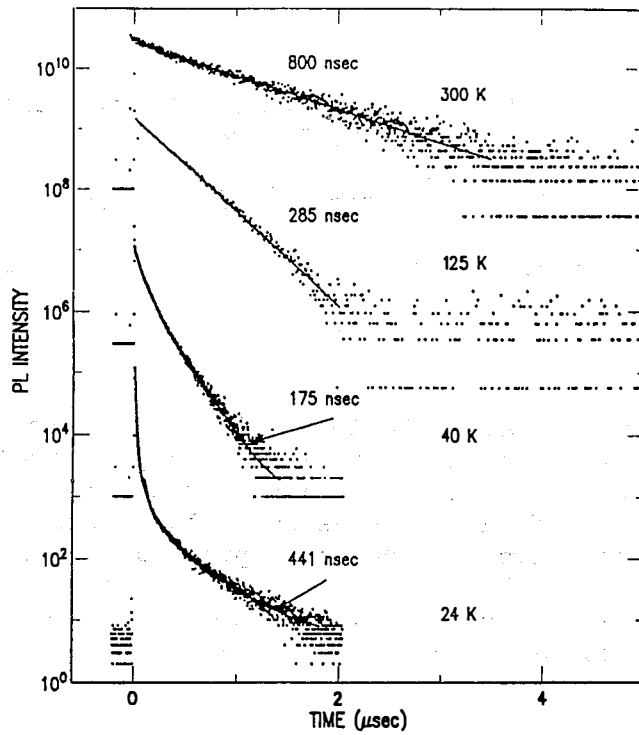


Figure 1.) Transient PL Decay (courtesy D. Wolford, IBM, T.J. Watson Research Center, Yorktown Heights, NY).

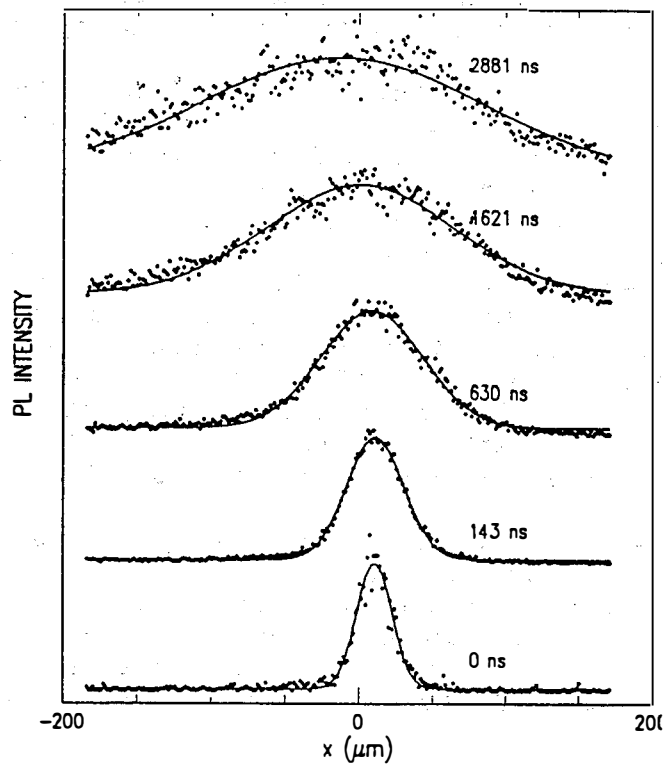


Figure 2. Spatial spread of photoexcited carriers (courtesy D. Wolford, IBM, T.J. Watson Research Center, Yorktown Heights, NY).

Title: Gallium Arsenide Based Ternary Compounds and Multi-bandgap Solar Cell Research

Organization: Spire Corporation, Patriots Park, Bedford, MA 01730

Contributors: S.M. Vernon and S.P. Tobin, Co-principal Investigators

Introduction

The overall goal of this research is to establish a technology for producing very high efficiency solar cells for terrestrial photovoltaic applications using either multijunction or single-junction cell concepts. The approach taken involves the growth of GaAs or GaAs-based ternary materials onto GaAs or Si substrates by the metalorganic chemical vapor deposition (MOCVD) technique. The specific objectives of this past year's research were to improve the performance and understanding of GaAs homoepitaxial cells and of GaAs-on-Si heteroepitaxial cells; successes in both of these areas are described below.

High Efficiency Cell Studies

Our main focus this year has been on concentrator cells. We have achieved the demonstration of a GaAs-on-GaAs concentrator cell having an efficiency of 28.7% at 200X concentration, without the use of a prismatic coverglass; see Figure 1. Our best one-sun efficiency has also climbed to the 24.8% mark. The factors that have led to these efficiency increases include improvements in the areas of cell design and fabrication as well as epitaxial growth.

The improvements in cell design have involved such tasks as optimizing the design of the triple-layer antireflection coating ($\text{MgF}_2\text{-ZnS-Ga}_{.2}\text{Al}_{.8}\text{As}$) and of the concentrator-cell grid pattern and developing an optical-reflectance-modeling characterization technique. Advances in the area of device fabrication include the achievement of tall, narrow grid line ($3\ \mu\text{m}$ wide x $3\ \mu\text{m}$ high); these are the result of our developing processes to do image-reversal photolithography and oxide-assisted liftoff. Epitaxial growth studies have led to increased lifetime in the n-GaAs base and lower recombination velocity at the GaAs-Ga_{.2}Al_{.8}As emitter-window interface; this work has benefitted greatly from collaboration with R.K. Ahrenkiel at SERI. We have also carried out detailed loss analyses on our best cells in order to identify the most important areas on which to concentrate our efforts; Figure 2 graphically displays the result of this analysis for the short-circuit current of our 24.8% solar cell.

Another task undertaken, in collaboration with Profs. M.S. Lundstrom and M.R. Melloch at Purdue University, has been a comparison of MOCVD- and MBE-grown GaAs cells. This has enabled the identification of growth-method-specific losses as well as serving to help establish a source of top-quality epitaxial cell structures at Purdue. Solar cells processed side-by-side at Spire have yielded efficiencies of 23.8% by MBE growth at Purdue and 24.8% by MOCVD growth at Spire.

GaAs-on-Si Studies

Although our major emphasis this year has been on the GaAs homoepitaxial cells, GaAs-on-Si research has continued. One important accomplishment has been the completion of a study, in collaboration with M.M. Al-Jassim of SERI, to quantify the effects of dislocations on individual cell-performance parameters by introducing a controlled number of defects into a GaAs cell. This has been achieved through the use of a lattice-mismatched GaAs_{1-y}P_y layer interposed between a GaAs substrate and the GaAs cell structure. Varying y has enabled us to vary the dislocation density from 10^4 to 10^8 cm⁻². One significant result is shown in Figure 3. From this study it has been determined that, in order for GaAs-on-Si cells to have performance comparable to that of GaAs-on-GaAs cells, a dislocation density of $\leq 5 \times 10^5$ cm⁻² must be reached.

Other GaAs-on-Si work has included continuation of defect-reduction studies employing thermal-cycle growth and strained-layer techniques and preliminary research on the use of the atomic layer epitaxy technique to produce higher quality GaAs-on-Si nucleation layers deposited in a two-dimensional growth mode. Our device studies have led to the achievement of a 19.9%-efficient GaAs-on-Si concentrator cell, as shown in Figure 4.

Future Directions

Our continuing research interests include improving the efficiency of GaAs solar cells as well as reducing the defect level of our GaAs-on-Si "substrates". High-efficiency cell studies may involve the use of alternative window-layer materials and development of two-junction, GaAs-based tandem cells. GaAs-on-Si material improvements can be achieved by continued optimization of thermal-annealing, strained-layer, and two-dimensional-nucleation techniques. Concentrator cell designs will continue to be our major focus in both areas.

Publications

The research conducted in this program has resulted in a number of articles being published in the scientific literature over the course of this past year. These are listed below:

"Assessment of MOCVD- and MBE-Grown GaAs for High-Efficiency Solar Cell Applications," S.P. Tobin, S.M. Vernon, C. Bajgar, S.J. Wojtczuk, M.R. Melloch, A. Keshavarzi, T.B. Stellwag, S. Venkatensan, M.S. Lundstrom, and K.A. Emery, IEEE Trans. Electron Devices, to be published.

"Analysis of AlGaAs/GaAs Solar Cell Structures by Optical Reflectance Spectroscopy," M.M. Sanfacon and S.P. Tobin, IEEE Trans. Electron Dev., to be published.

"Ultra-Long Lifetime Epitaxial GaAs by Photon Recycling," R.K. Ahrenkiel, D.J. Dunlavy, B. Keyes, S.M. Vernon, T.M. Dixon, S.P. Tobin, K.L. Miller, and R.E. Hayes, Appl. Phys. Lett., 55, 1088 (1989).

"Improvement of Minority-Carrier Properties of GaAs on Si," S.M. Vernon, R.K. Ahrenkiel, M.M. Al-Jassim, T.M. Dixon, K.M. Jones, S.P. Tobin, and N.H. Karam, Mater. Res. Soc. Symp. Proc. 145, 349 (1989).

"Efficiency Improvements in GaAs-on-Si Solar Cells," S.M. Vernon, S.P. Tobin, V.E. Haven, C. Bajgar, T.M. Dixon, M.M. Al-Jassim, R.K. Ahrenkiel, K.A. Emery, Proc. of the 20th IEEE PVSC, Las Vegas, September 1988, 481 (1989).

"Minority Carrier Lifetime of GaAs on Silicon," R.K. Ahrenkiel, M.M. Al-Jassim, D.J. Dunlavy, K.M. Jones, S.M. Vernon, S.P. Tobin, and V.E. Haven, Proc. of the 20th IEEE PVSC, Las Vegas, September 1988, 684 (1989).

"Correlation of Material Properties and Recombination Losses in $Al_{0.2}Ga_{0.8}As$ Solar Cells," G.B. Lush, T.B. Stellwag, A. Keshavarzi, S. Venkatesan, M.R. Melloch, M.S. Lundstrom, R.F. Pierret, S.P. Tobin, and S.M. Vernon, to be published in Solar Cells.

"Progress in GaAs Solar Cell Research," S.P. Tobin, Proc. of 4th Intl. Photovolt. Sci. and Eng. Conf., Sydney, Australia, p. 47, Feb. 1989.

"III-V Solar Cell Resesearch at Spire Corp.," S.M. Vernon, S.P. Tobin, S.J. Wojtczuk, C.S. Keavney, C. Bajgar, M.M. Sanfacon, J.T. Daly, and T.M. Dixon, Solar Cells, to be published.

"Influence of Bandgap Narrowing Effects in p^+ -GaAs on Solar Cell Performance," M.E. Klausmeier-Brown, P.D. DeMoulin, H.L. Chuang, M.S. Lundstrom, M.R. Melloch, and S.P. Tobin, Conf. Rec. 20th IEEE Photovoltaic Specialists Conf., pp.503-507, (1988).

"Biaxial and Uniaxial Stress in GaAs on Si: A Linear Polarized Photoluminescence Study," H. Shen, M. Dutta, D.W. Eckart, K.A. Jones, S.M. Vernon, and T.M. Dixon, submitted to Appl. Phys. Lett., Sept. 1989.

"Atomic Layer Epitaxy of GaAs on Si by MOCVD," N.H. Karam, V.E. Haven, S.M. Vernon, J.C. Tram, and N.A. El-Masry, Mat. Res. Soc. Symp. Proc. 145, 331 (1989).

"X-Ray Studies of GaAs/Si and ZnS/Si," H.M. Kim, Y. Choi, S.M. Vernon, P.A. Sekula, and C.R. Wie, Material Research Soc. Symp. Proc. 144 (1988) to be published.

"Electrical Properties of GaAs Homojunctions Grown by MOCVD on GaAs and Si Substrates," K.L. Jiao, A.J. Soltyka, W.A. Anderson, and S.M. Vernon, submitted to Solid State Electronics, 1989.

GaAs CONCENTRATOR CELL

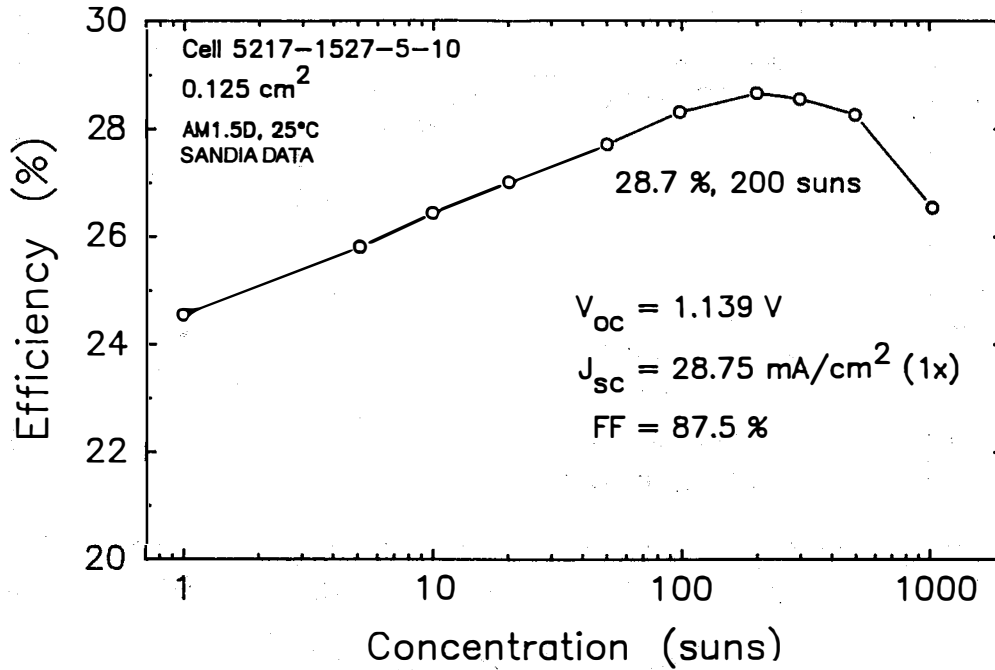


Figure 1. Efficiency vs. Concentration for our Best GaAs Solar Cell.

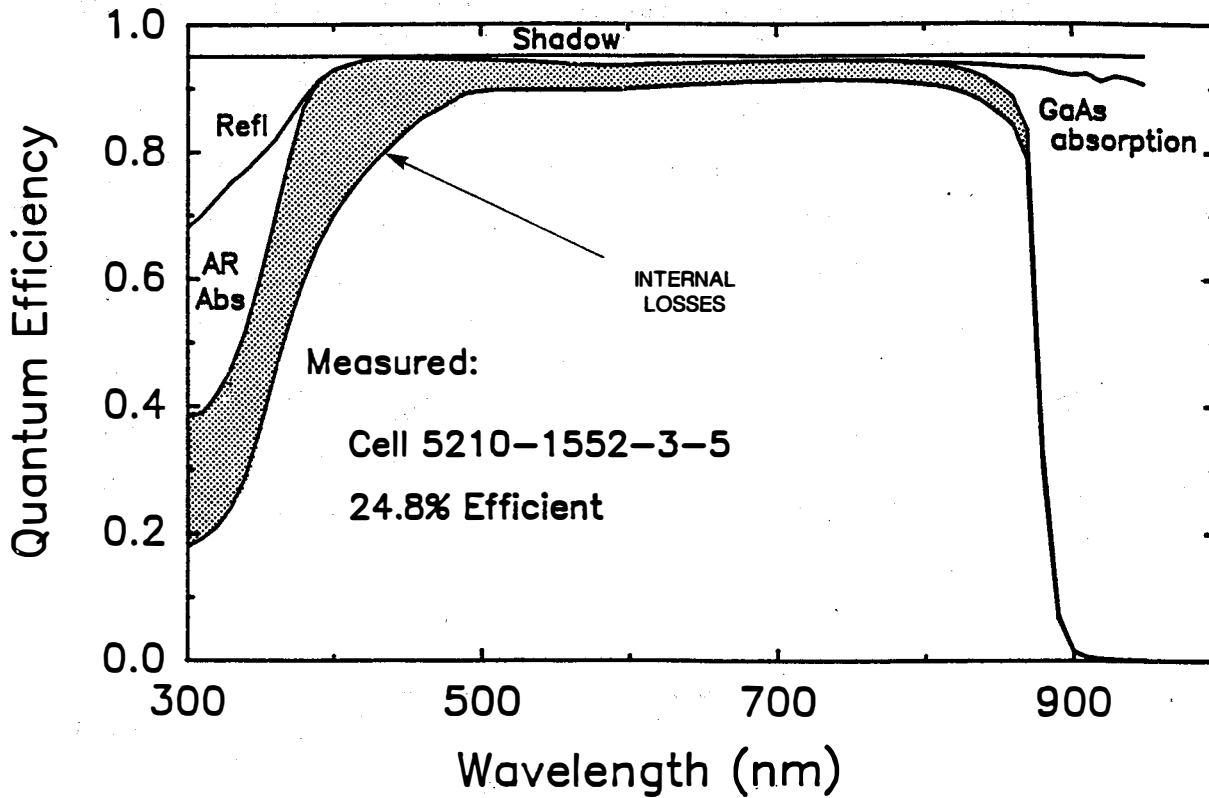


Figure 2. Extrinsic Short-Circuit Current Loss Analysis for 24.8%-Efficient GaAs Cell.

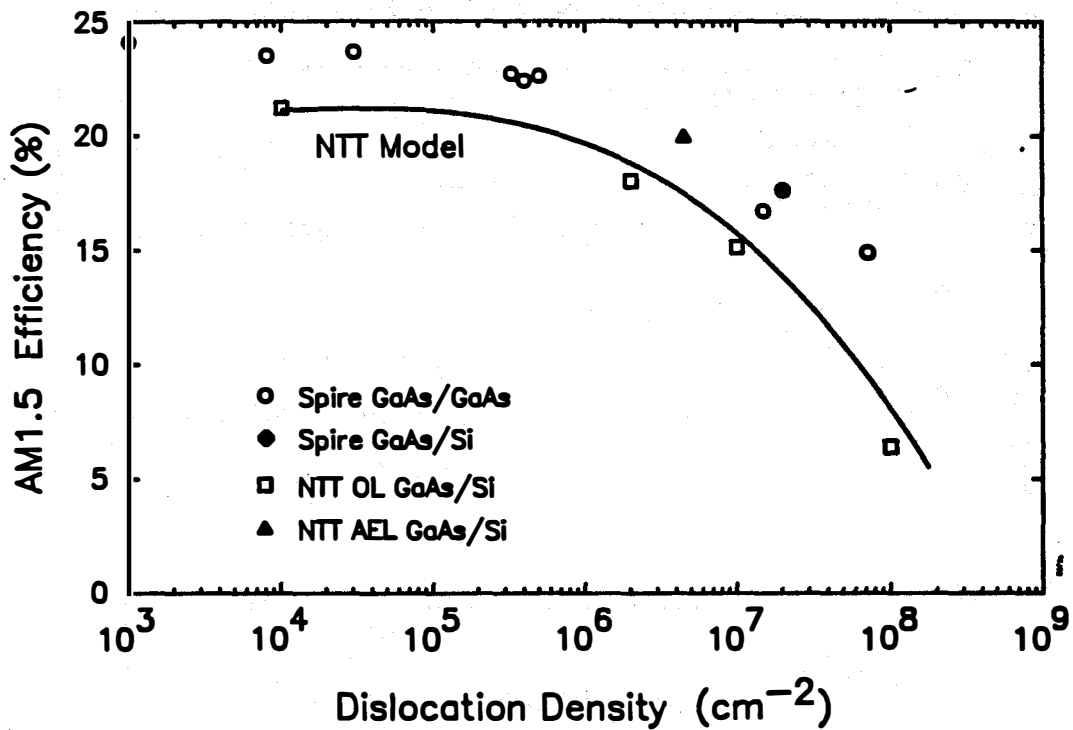


Figure 3. AM1.5 Efficiency as a Function of Dislocation Density for GaAs Cells Grown on GaAsP Buffers. Also shown for comparison are GaAs-on-Si cell results from Spire and NTT.

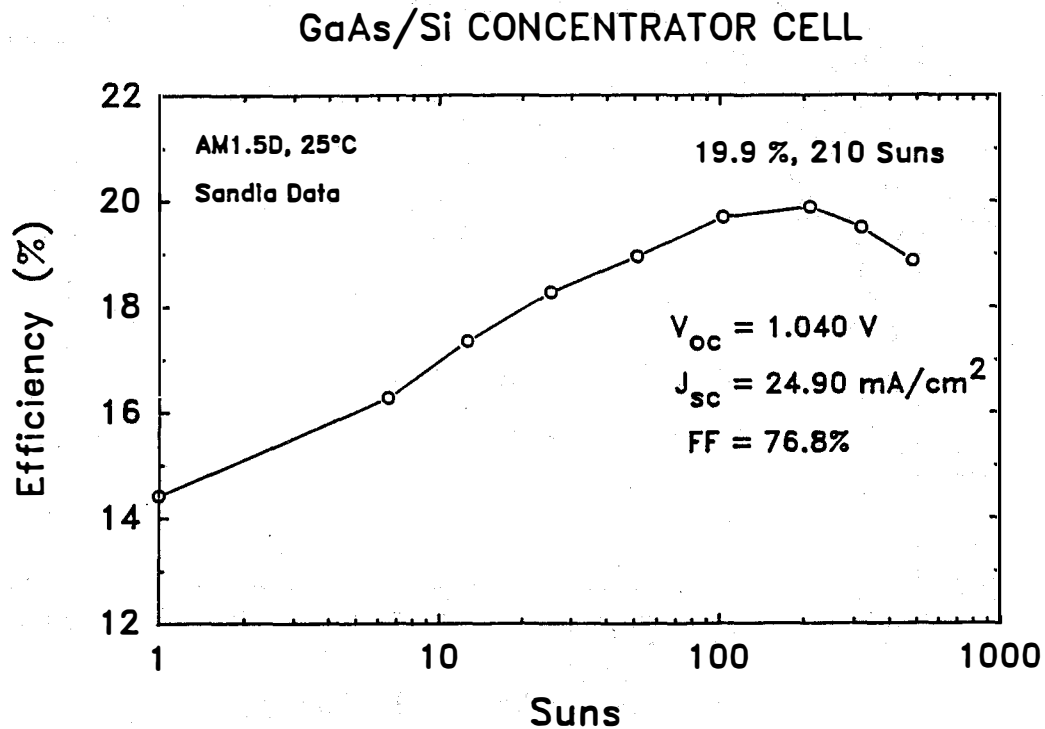


Figure 4. Efficiency vs. Concentration for our Best GaAs-on-Si Cell.

Title: **Advanced High-Efficiency Concentrator Cells**

Organization: **Varian Research Center, Palo Alto, California 94303**

Contributors: **H. F. MacMillan, principal investigator; B-C. Chung,
H. C. Hamaker, N. R. Kaminar, M. S. Kuryla, M. Ladle
Ristow, L. D. Partain, J. C. Schultz, G. F. Virshup and
J. G. Werthen**

The objective of this research program is the development of a multijunction solar cell with a terrestrial power conversion efficiency of 35-40% at solar concentrations of 400 to 1000 AM1.5D. In order to meet the cost goals for utility-scale photovoltaic power systems, the multijunction cells are designed to be monolithic, two-terminal cells.

The approach of this cell development effort encompasses the following key features. First, development strategy and device performance evaluation have been guided by our detailed, realistic computer model [1]. The model predicts total cascade and component cell performance parameters from experimentally established input parameters, i.e., materials properties, device structure and operating conditions. Second, the III-V monolithic multijunction cells and interconnect materials are grown by computer-controlled organometallic chemical vapor deposition (MOCVD) on GaAs substrates. Third, the device fabrication utilizes standard wafer processing procedures for metallization and etching, which can be adapted to high throughput manufacturing. Finally, the development sequence has been to first demonstrate the performance of the component cells and cell interconnects, and then to integrate these into a monolithic multijunction cell, initially for one-sun operation and then for operation under concentrated sunlight.

Using the best available materials data, the modeling of a three-junction cascade predicts an efficiency of 46% under high concentration, as shown in Fig. 1. The efficiencies of the AlGaAs, GaAs and InGaAs component cells are 22%, 15% and 9%, respectively. The modeling predicts that a 1.93-eV AlGaAs/GaAs two-junction cascade can achieve close to 35% efficiency, but a third junction will be necessary to approach or exceed 40% efficiency. In order to minimize the problems due to lattice mismatch and to develop this multijunction in stages, we have adapted the structure shown in Fig. 2. The upper 1.93-eV AlGaAs and GaAs cells are grown on one side of the GaAs substrate. The lower 1.0-eV InGaAs cell is grown on the reverse side of the substrate in a second growth step [2]. While the upper two cells are lattice matched to the substrate, the lower cell is 3% mismatched, which requires development of a high-quality transparent grading layer. The substrate is lightly doped to minimize optical absorption. Also shown in Fig. 2 is an Entech prismatic cover slide, which greatly reduces obscuration of the metal interconnect and permits its use up to 100X concentration [3].

During the past year, we have concentrated on the following areas of development: (1) continued growth and fabrication of high-efficiency component cells, 1.93-eV AlGaAs, GaAs and 1.0-eV InGaAs; (2) continued growth and fabrication of 1.93-eV AlGaAs/GaAs metal-interconnected cascade cells; (3) redesign of the metal interconnect for concentrator operation; and (4) growth of stable tunnel junctions for grown-in cell interconnects.

Summaries of the most significant results of the past year follow.

1. A 1.93-eV AlGaAs/1.42-eV GaAs metal-interconnected cascade cell (MICC) has been fabricated with a one-sun efficiency of 27.6% AM1.5 Global measured at SERI [4]. This performance has improved from 23.9% one year ago and is the highest efficiency at one-sun ever measured. The spectral response and current-voltage characteristics of the MICC are shown in Fig. 3. A detailed cross-section of the MICC highlighting the metal interconnect is shown in Fig. 4.
2. A 1.0-eV InGaAs cell has been fabricated on the reverse side of the substrate with a one-sun efficiency of 1.9% AM1.5D and an efficiency of 2.8% AM1.5D at 100X. The spectral response and current-voltage parameters are shown in Fig. 5. The materials properties of the lattice-mismatched cell must be further improved to increase photocurrent collection and enable current-matching with the upper cells.
3. The metal interconnect has been redesigned to permit operation of the MICC to 100-200X concentrations in conjunction with the Entech prismatic cover slide to reduce obscuration. Development of a transparent, stable, grown-in tunnel junction interconnect using C and Si dopants as on-going, that will enable operation of the AlGaAs/GaAs cascade at 20X and the GaAs/InGaAs cascade at 100X concentration to date. The interconnect resistance-area products are presented in Table I. Further development is required to incorporate these interconnects into cascade cells and to enable their operation at even higher concentrations.
4. Development of a versatile two-layer antireflection coating is complete for single- and multi-junction cells with minimum reflectance over the useful spectral range with or without a prismatic cover slide.
5. Development of a high-resolution process has been completed to produce a thick metallization for concentrator cell front gridlines with low obscuration (<4%).

In preceding years, the focus has been on developing component and cascade cells for one-sun operation. During the past year, the focus has shifted to developing component cells and interconnects for 100X operation. In future work, the emphasis will be on integrating the components for operation at 100X and then on reducing higher concentrations. Portions of this work were supported in part by the Defense Advanced Research Projects Agency and by the Air Force Wright Aeronautical Laboratories.

References

1. H. C. Hamaker, J. Appl. Phys. **58**, 2344 (1985).
2. S. Kamath and R. Loo at Hughes Research Laboratories first proposed this structure.
3. Prismatic cover slide developed by Entech, Inc., Dallas/Fort Worth Airport, TX.
4. B-C. Chung et al., Appl. Phys. Lett. **55**, 15 (1989).
5. H. F. MacMillan et al., Solar Cells (November 1989).

Table I: Interconnect Development Status
(Resistance-Area Products)

<u>Interconnect</u>	<u>Operating Conditions</u>		
	<u>One-Sun</u>	<u>100X</u>	<u>1000X</u>
Goal* (RA) ($\Omega\text{-cm}^2$) _e	5	0.05	0.005
Metal Interconnect (w/Entech cover slide)		0.02	
Upper AlGaAs:C, Si Interconnect Tunnel Junction	0.1		
Lower GaAs:C, Si Interconnect Tunnel Junction		0.02	

* For total loss <1 efficiency point.

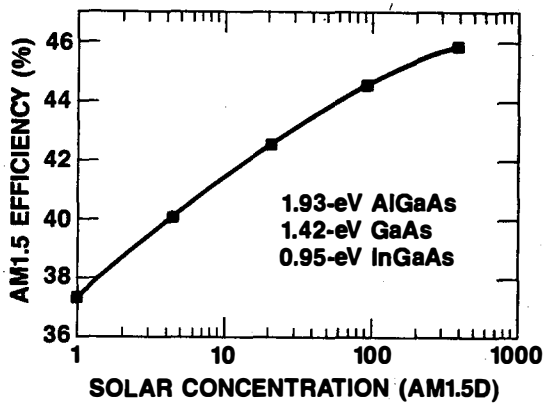


Fig. 1 Predicted efficiency of 1.93-eV AlGaAs-GaAs/0.95-eV InGaAs two-terminal cascade cell under concentrated terrestrial sunlight (25°C).

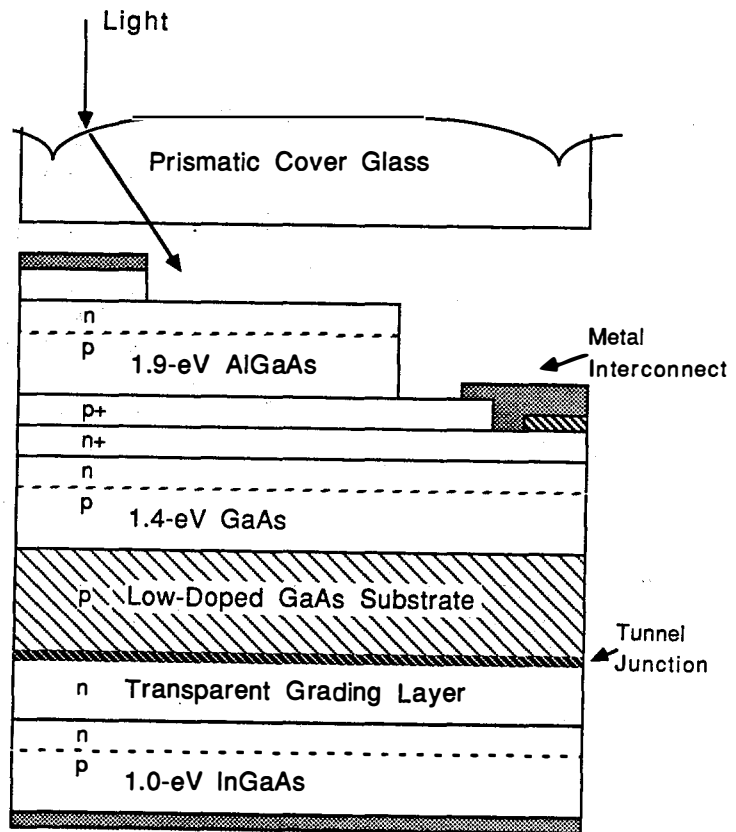


Fig. 2 Three-junction, two-terminal, cascade cell structure.

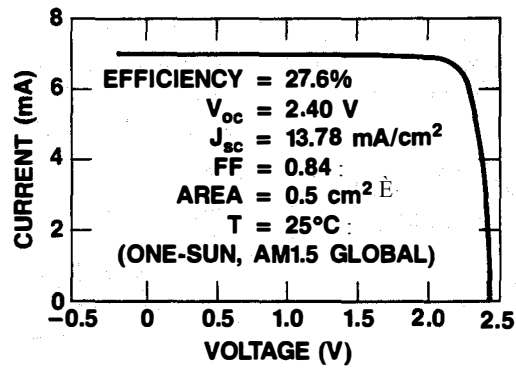
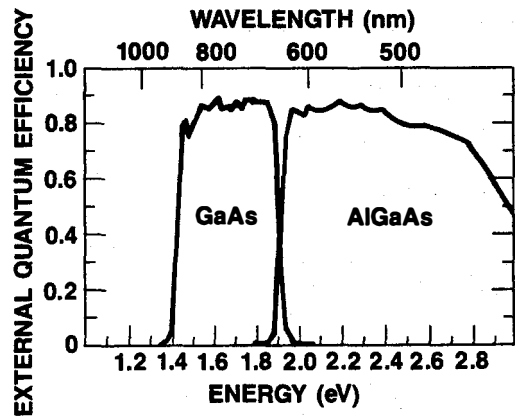


Fig. 3 Spectral response and current-voltage characteristics of a 1.93-eV AlGaAs/GaAs metal-interconnected, two-terminal, cascade cell.

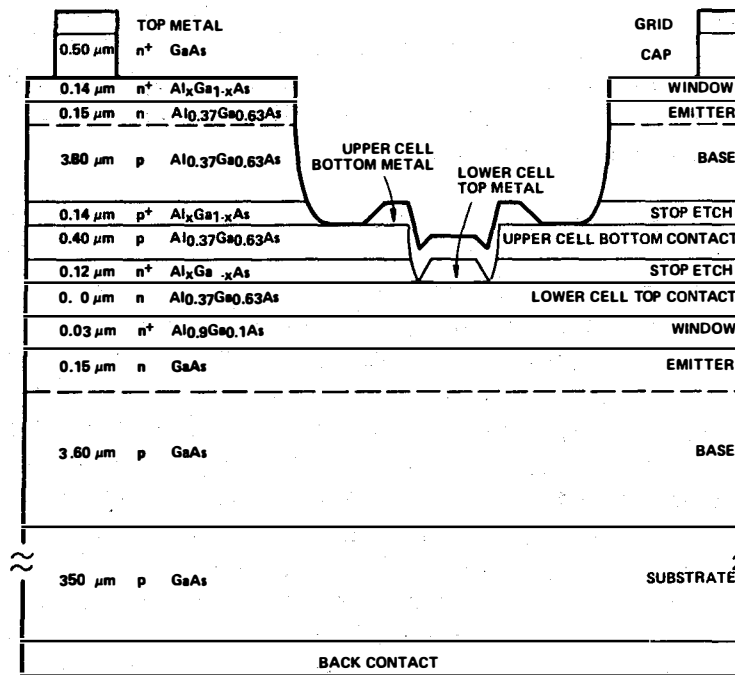


Fig. 4 Cross section of 1.93-eV AlGaAs/GaAs MICC with exaggerated detail of metal interconnect features.

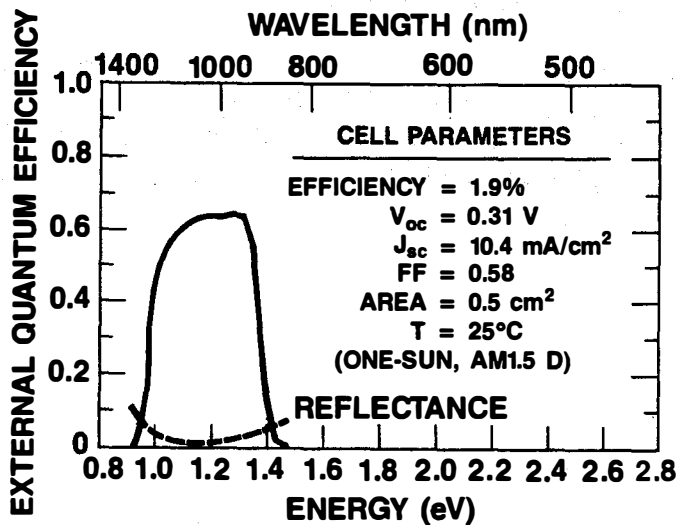


Fig. 5 Spectral response and current-voltage parameters for 1.0-eV InGaAs cell on reverse side of GaAs.

6.0 NEW IDEAS PROGRAM

Richard Mitchell, (Manager)

The objective of the New Ideas Task is to identify new photovoltaic materials, device configurations, and concepts and to conduct preliminary research and development in the areas that show the most promise. Subcontracted research in this task that shows significant potential is transferred into the appropriate major task area within the DOE Photovoltaic Program for continued support.

The New Ideas Task provides public solicitations for new and innovative research ideas that are relevant under the Photovoltaic Advanced Research and Development Project's guidelines to perform high-risk, long-term, and potentially high-payoff research and development. These solicitations for new and innovative research ideas are submitted by universities, business, and nonprofit organizations. Subcontracts are awarded to study the most promising concepts associated with these solicitations. These subcontracts are reviewed, and successful concepts are selected for renewal with a second year of funding. In FY 1988, the program did not have sufficient funding to carry out a renewal of those research efforts funded in FY 1987. However, the remaining research under these programs was continued on the funding originally allotted for this effort. These concepts included the avalanche heterostructure and superlattice solar cell developed by Georgia Tech Research Institute; the low-cost techniques for producing CdZnTe devices for cascade cell applications, researched by International Solar Electric Technology; the hydrogen radical enhanced growth of InP solar cells, investigated by Rensselaer Polytechnic Institute; and the high-efficiency, flat-plate silicon solar cells, investigated by Stanford University.

During FY 1988, the New Ideas Task issued a competitive solicitation for New Ideas for Photovoltaic Conversion. The solicitation received almost 100 Letters of Interest (LOI). Preliminary evaluation and selection of these LOI responses have identified several promising concepts for further evaluation. During FY 1989, expanded proposals from these finalists will be evaluated and several concepts will be chosen for support. Successful subcontracted research efforts under this solicitation will be initiated in the fall of 1989.

Three concepts funded during the FY 1987 solicitation have been selected to receive a delayed second year of funding. During FY 1989, these concepts will be funded for an additional year and monitored. This monitoring and an evaluation will allow selection of successful subcontracts for possible funding by the appropriate major program area.

Title: **The Avalanche Heterostructure and Superlattice Solar Cell**

Organization: Physical Sciences Division, Georgia Tech Research Institute, Atlanta, Georgia

Contributors: C.J. Summers, Program Manager; A. Rohatgi, A. Torabi, D. Rajavel, B.K. Wagner, and R.G. Benz II

The objective of this program is to assess both the potential of new material structures for enhanced solar cell performance, and to develop the technology of semiconductor material systems for testing these concepts. Device structures under study include the avalanche heterostructure and variably spaced superlattice photovoltaic device¹, modulation doped (nipi) superlattices² and heteroface GaAs solar cells.³

Computer Modeling Studies

To predict the performance and characteristics of an ideal avalanche heterostructure photodiode solar cell, the method used by Henry was developed to calculate the solar cell efficiency as a function of bandgap energy and sun concentration.⁴ In this model the smaller (n-side) bandgap energy, E_{G1} , of the cell was assumed to control the I-V characteristics, while the bandgap ratio, g , between it, and the wider p-side bandgap energy, E_{G2} ; and the electron impact ionization rate, ($1 < \gamma < 2$), were assumed to be the principal parameters controlling the increased collection efficiency of the cell. Figures 1 and 2, respectively, show the ideal efficiencies calculated for this structure as a function of the smaller bandgap energy; for $g = 2$ and a range of γ -values; and for $\gamma = 2$ and a range of g -values. Assuming an ideal bandgap ratio of 2 and an impact ionization rate of 2, this calculation shows an optimum efficiency of 35.3% for a bandgap energy of 1.15 eV under unity sun concentration, and an optimum efficiency of 45.4% at a bandgap energy of 0.95 eV for 1000 suns concentration. Thus, this cell design approaches within 5% of the ideal efficiencies predicted for a conventional heterojunction solar cell, 38 and 50%, respectively. Because this performance also depends on a very efficient ionization process, it appears unlikely that this concept can effectively compete with the other structures. For this reason, several other cell designs have also been investigated.

Using a model recently developed for high-efficiency GaAs heteroface solar cells,³ different cell geometries have been designed to investigate the effect of the junction width and doping level on cell efficiency. After extensive material calibration runs, these device structures have been grown by molecular beam epitaxy, and are currently being fabricated.

In addition, a model is also being developed for modulation doped (nipi) superlattice structures whose long-carrier lifetimes and extended absorption characteristics may have the potential to enhance solar cell performance. In this study the equations derived by Dohler² have been solved so that the properties of this structure; effective bandgap, carrier-lifetime, and absorption coefficient spectrum, can be computed as a function of the design parameters of the structure, such as the absolute doping levels, the widths of the n- and p-type doping and intrinsic regions, and also the light excitation level. Once formulated this model will be used to assess the potential of these structures for solar cell applications in a way similar to the other studies.

Material Growth Studies

The range of bandgap energies and material properties required for complex cell designs requires the development of II-VI material systems such as the ZnCdTe and HgCdTe alloys, and the ability to grow sophisticated structures in these material systems. Currently, molecular beam epitaxy is being investigated for this purpose, but the growth of high quality crystals and their reproducible doping is still a problem.⁵ To overcome these limitations, a chemical beam epitaxy system is being developed under this and related programs. The advantage of this technique is that the use of hydride and/or metalorganic sources enables greater flexibility and more precise control to be achieved over the chemical reactions occurring during growth, as monomer, dimer, or tetramer species can be supplied to the growth surface depending on which is found to optimize the nucleation and growth process. To implement this study, extensive modifications have been made to a Varian GEN II MBE system as described below. These consist of the development of a turbomolecular pumping system, new types of gas sources and injectors, and a Hg-vapor source.^{6,7}

Pumping System: Because of the relatively high loads of toxic gases used in CBE, a specially designed pumping system was implemented to handle hazardous and corrosive organometallics, hydrides and Hg vapor. Figure 3 shows a schematic representation of the pumping system, the main component of which is a Balzers MBE Series turbomolecular pump with a pumping speed of 1400 l/s for N₂ and approximately 1000 l/s for Hg.. Gases exhausted from the turbomolecular pump pass into a cold trap operated at -60°C which is designed to condense the Hg vapor and minimize any contamination of the mechanical backing pump. Similarly, to minimize contamination of the turbomolecular pump due to hydrocarbon backstreaming, a micromaze oil vapor trap is included on the inlet of the backing pump.

The backing pump, an Alcatel 50 cfm Corrosion Series Pump, also uses inert gas ballasting to dilute and prevent condensation of the pumped vapors. The Alcatel pump exhausts into an Emcore toxic gas scrubber filled with a sulfur impregnated activated

charcoal capable of absorbing up to 40 percent of its weight in Hg. This feature has no effect on the charcoal's ability to absorb organometallics and hydrides which can then be oxidized and disposed of in a controlled manner. As indicated in Figure 3, an array of valves enable various parts of this system to be isolated for removal of trapped vapors and the atmospheric pressure purging of both the pumping components and gas source lines.

Finally, a Varian cryopump is also attached to the system for removing Hg and organometallics from the growth ambient when needed. Provisions are made for hot gas purging of the cryopump using the gas purging system described above.

Gas Sources: The gas sources utilized in the CBE system are pressure controlled and can operate with inlet pressures on the order of a torr. Hence, the source gases can be directly injected without a carrier gas. This greatly simplifies gas source construction, minimizes the gas load on the pumping system, and makes it easier to maintain the beam fluxes in the molecular flow regime. This is especially important in the growth of Hg-based materials because of the large Hg fluxes required.

The pressure controlled vapor sources operate on the principle of choked viscous flow through an orifice and are similar in concept to a Hg source of this type, which has been designed and implemented in our laboratory.⁷ The Te, Cd, and Zn sources operating on this principle use an MKS Instruments 1150B flow controller and are designed for the following source gases; diisopropyltelluride (DipTe), diethylcadmium (DeCd), and diethylzinc (DeZn). The DipTe (10 sccm f.s.), DeCd, and DeZn (5 sccm f.s.) flow controllers have repeatabilities of 0.2% and are configured to produce growth rates of up to 2 $\mu\text{m/hr}$. The precision of the flow controllers is calculated to produce a stability in the Cd to Te ratio of approximately 0.1%. For $\text{Hg}_{1-x}\text{Cd}_x\text{Te}$ alloys with $x = 0.2$, this stability corresponds to a deviation in the x value of 0.0002, a factor of 5-10 better than is currently available with conventional thermal sources.

Dopant Source: A p-type gas dopant source was also designed which operates on the same principle as the host gas sources. However, the design principles of the dopant source are even more severe as it must be able to accurately regulate flow rates that are four to eight orders of magnitude less than the host gas flow controllers. To achieve this level of control, an absolute pressure regulator is utilized, thus allowing control of the dopant gas at less than atmospheric pressure. The reduced pressure gas is then fed through a stepper motor driven leak valve which maintains the downstream pressure as measured by a high accuracy capacitance manometer. This controlled pressure exits through another leak valve (which acts as a variable orifice) and enters the CBE growth chamber. The sensitivity of the manometer and valve feedback system gives the dopant source a four order of magnitude dynamic range for a fixed orifice setting. Changing the orifice setting obviously allows the

system to achieve an even greater dynamic range. Figure 4 shows a schematic of the dopant gas source. For the initial studies arsine was chosen as the dopant gas although, any of the organometallic As gases could be substituted when more fully developed. The pure arsine is contained in a small volume, low pressure bottle with a built-in flow limiting orifice, thus minimizing the safety hazards usually associated with arsine.

Injectors: To prevent gas phase reactions, separate injectors are used for the group II and group VI elements. This also enables optimization of the cracking conditions for each source gas. The group II injector uses a 3/4 in. o.d. high purity Ta delivery tube while the group VI utilizes a similarly sized pyrolitic boron nitride (PBN) delivery tube to avoid any reaction of Te with Ta. Both injectors are fitted with thermocouples to monitor the hot and cold zone temperatures and have individually designed boron nitride diffuser/nozzle elements to enhance the cracking of the metalorganic gases and increase flux uniformities. In particular, the group VI nozzle was carefully designed to avoid the recombination of monomer Te into its dimer form, once it had been thermally dissociated from the metalorganic complex.

Results: So far preliminary system evaluations and a few test growth runs have been performed. These include a study of the cracking dependence of DipTe and CdTe and HgZnTe growth using solid Cd and Zn sources. From these studies we conclude that monomer Te is produced with reasonably high efficiencies and can be used to grow epitaxial CdTe and HgZnTe films (Figures 5 and 6). From these initial results we believe that CBE has the potential to solve many of the problems currently experienced by conventional growth technologies in obtaining abrupt heterointerfaces, precise stoichiometric adjustment and complex n- and p-type extrinsic doping profiles in II-VI semiconductor systems.

References

1. J Pearsall, T.P., Electronics Lett. 18, 1982, p. 512.
2. J Dolher, G.H., Phys. Stat. Sol. (b) 52, (1972, p. 79.
3. J Ringel, S.A., Rohatgi, A., and Tobin, S.P., IEEE Trans. Elect. Devices 36, 1989, p. 1230.
4. J Henery, C.H., J. Appl. Phys. 51, 1980, p. 4494.
5. J Summers, C.J., Benz II, R.G., Wagner, B.K, Benson, J.D. and Rajavel, D., SPIE 1106, 1989, p. 2.
6. J Benz II, R.G., Wagner, B.K., and Summers, C.J., to be published in J. Vac. Sci. & Technol.
7. J Wagner, B.K., Benz II, R.G., and Summers, C.J., J. Vac. Sci. & Technol. A7, 1988, p. 295.

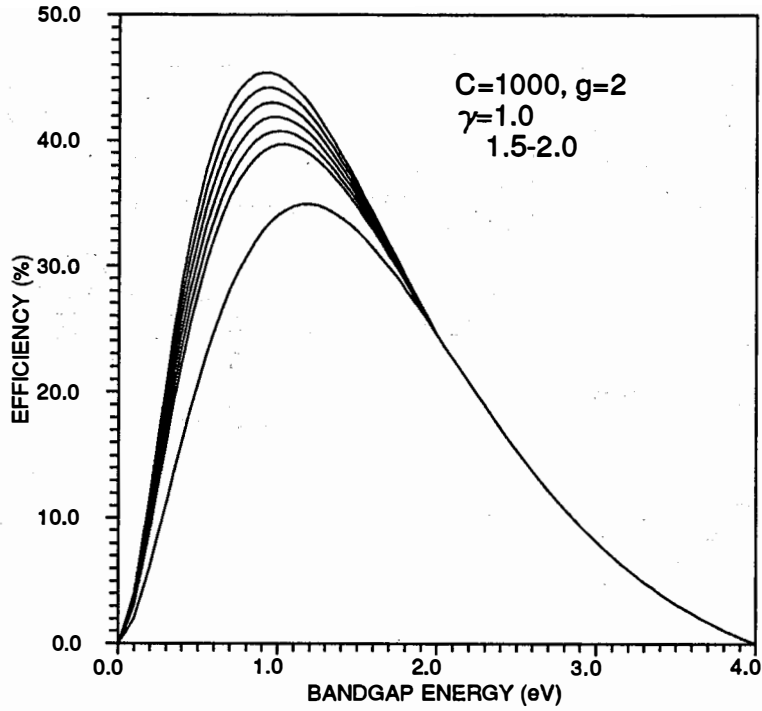


Figure 1. Efficiency of avalanche heterojunction solar cell as a function of bandgap energy, and impact-ionization ratio for ideal bandgap ratio and 1000 suns concentration.

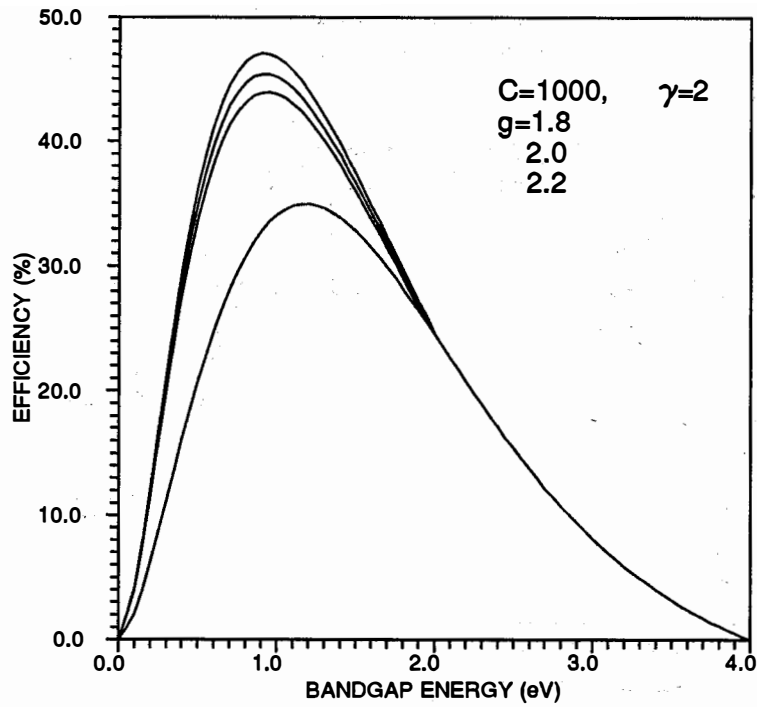


Figure 2. Efficiency of avalanche heterojunction solar cell as a function of bandgap energy, and bandgap ratio for ideal impact-ionization conditions and 1000 suns concentration.

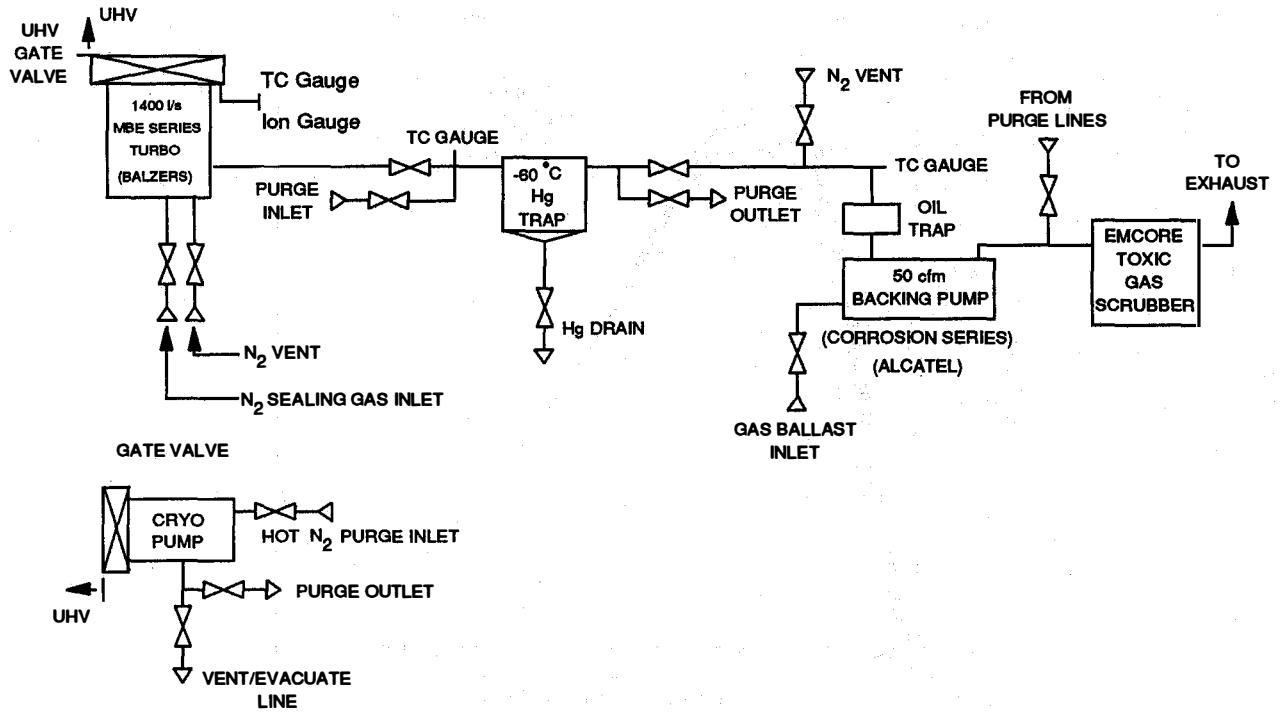


Figure 3. Schematic representation of CBE pumping system.

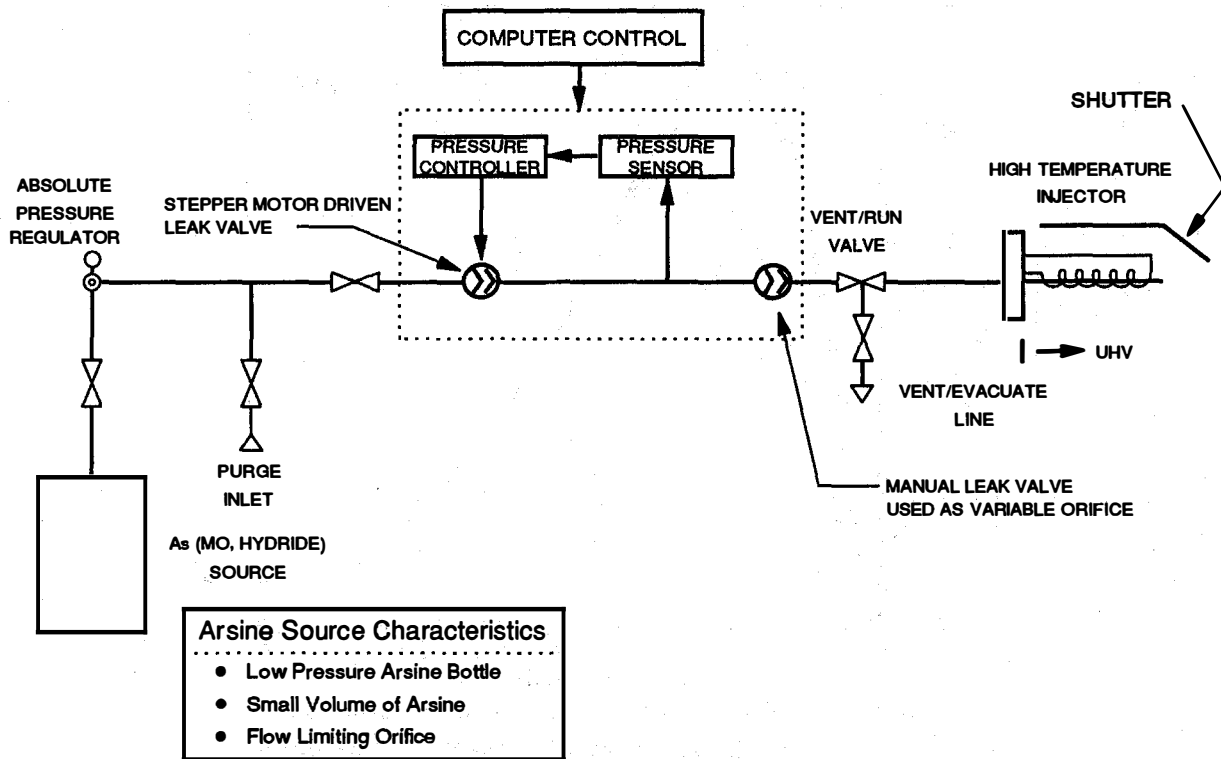


Figure 4. Schematic of arsine gas dopant source.

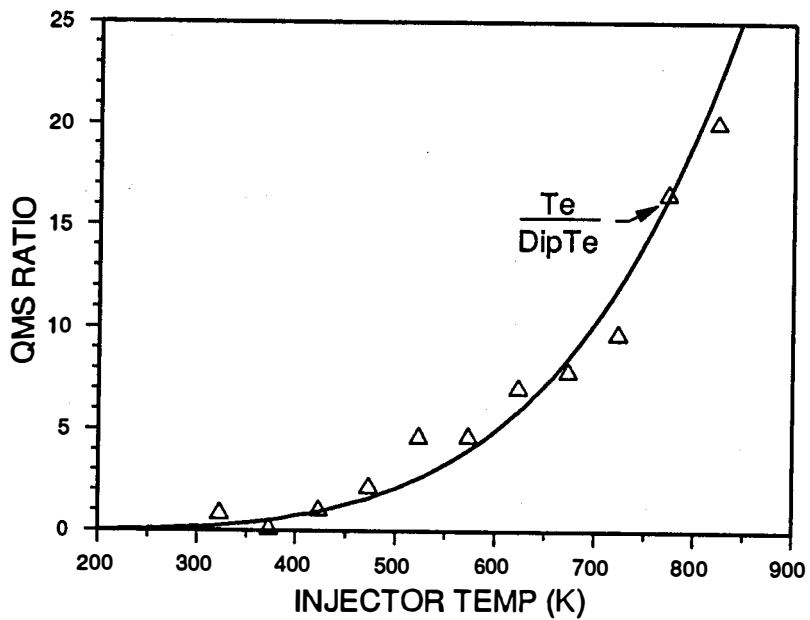


Figure 5. Ratio of QMS Te^+ current to DipTe^+ current as function of injector temperature.

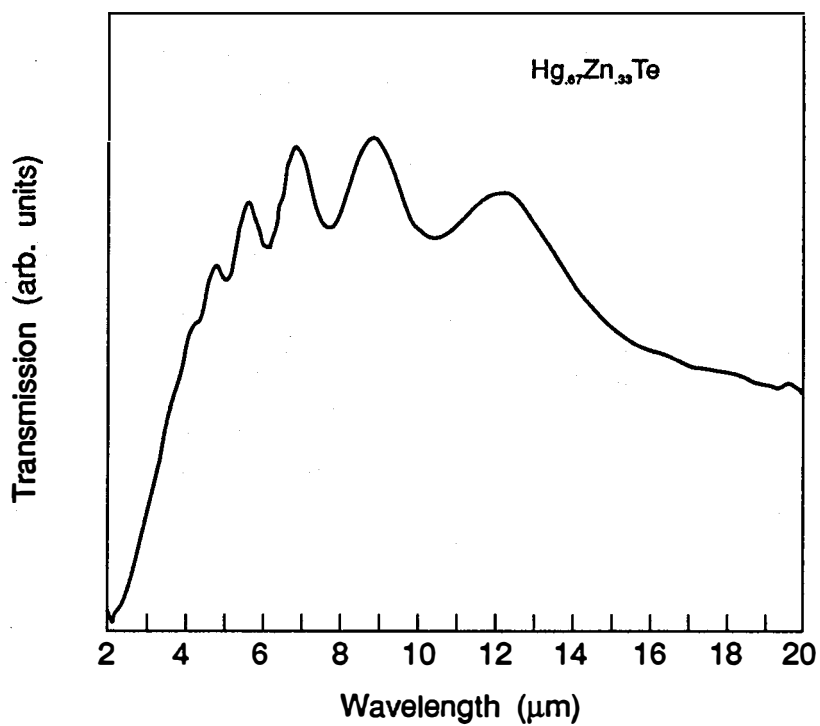


Figure 6. IR transmission spectrum of $\text{Hg}_{0.67}\text{Zn}_{0.33}\text{Te}$ layer.

Title: Low Cost Technique for Producing CdZnTe Devices for Cascade Cell Application

Organization: International Solar Electric Technology (ISET), Inglewood, California

Contributors: B. M. Basol, principal investigator; V. K. Kapur and R. C. Kullberg

The objective of this program is to develop thin film CdZnTe devices with transparent contacts. The ultimate use of such devices will be in high-efficiency tandem structures. The technique used in this program for obtaining the CdZnTe films is the two-stage process. The two-stage process consists of first depositing elemental layers of Cd, Zn and Te on a suitable substrate and then reacting these elemental layers to form the compound. During the first year of this program we had concentrated our efforts on the electrodeposition technique to obtain Cd, Zn and Te films. Plating conditions for each layer were determined and the compound films obtained by reacting these electroplated films were analyzed [1,2,3].

During the present period of the program we have carried out work on evaporated/reacted compound films. The electrodeposition process is limited to the use of Te/Cd/Zn stacked layers due to the values of the plating potentials of these three elements. In evaporation, however, the order of deposition can be changed.

A vacuum system and resistively heated Mo boats were used to deposit the Cd, Zn and Te films on transparent substrates. Both ITO coated glass and CdS/ITO/glass structures were used as substrates. Many of the initial experiments were carried out on CdTe films obtained by reacting Cd and Te films. Reaction temperatures changing from 350 C to 550 C were successfully used to obtain 1-1.5 micron thick CdTe films with smooth morphologies. Good quality ZnTe films were also obtained by reacting Zn and Te layers at temperatures ranging from 400 C to 550 C. In films containing both Cd and Zn, however, Zn was found to be distributed non-uniformly throughout the film. In these films Zn was found to be localized on the surface of the film possibly in the form of an oxide. This is apparent from the Auger depth profiles of two films shown in Figs. 1 and 2. Fig. 1 shows the composition of a film with an intended stoichiometry of $Cd_{0.2}Zn_{0.8}Te$ obtained after 2 hours of annealing at 400 C. The substrate for this sample was ITO coated glass. Fig. 2 is the Auger depth profile for a similarly processed film with an intended composition of $Cd_{0.4}Zn_{0.6}Te$. In both cases the surface is seen to be Zn and oxygen-rich. The order of deposition for the elemental layers of these films was Te/Cd/Zn, i.e Zn was already on the surface. Changing the order of deposition to Te/Zn/Cd did not change the observed phenomena of Zn-rich surface. In fact, in that approach, higher temperature anneals were found to enhance Zn diffusion to the surface. The reasons for this observed non-uniform distribution of Zn in the films is presently under study.

During this period we have also carried out work on reducing the window layer thicknesses for the CdZnTe/CdS cells. The 1-2 micron thick evaporated CdS window layers were replaced by chemically deposited thin CdS films and the two-stage process was modified to allow processing of films and devices

with CdS thicknesses as low as 1000 Å. Devices with glass/ITO/CdS/CdZnTe structure were produced using both thick and thin CdS window layers. The efficiency values of these cells were around 4%. Studies to enhance the grain size of the absorber layers in these devices are in progress.

References

1. Basol, B.M., and V.K. Kapur, Thin Solid Films, vol.54, p.1918, 1989.
2. Basol, B.M., V.K. Kapur, R.C. Kullberg, and R.L. Mitchell, Proc. 20 th IEEE PV Conf., IEEE, N.Y., p. 1500, 1988.
3. Basol, B.M., V.K. Kapur, and M.L. Ferris, J. Appl. Phys., vol.66, p. 1816, 1989.

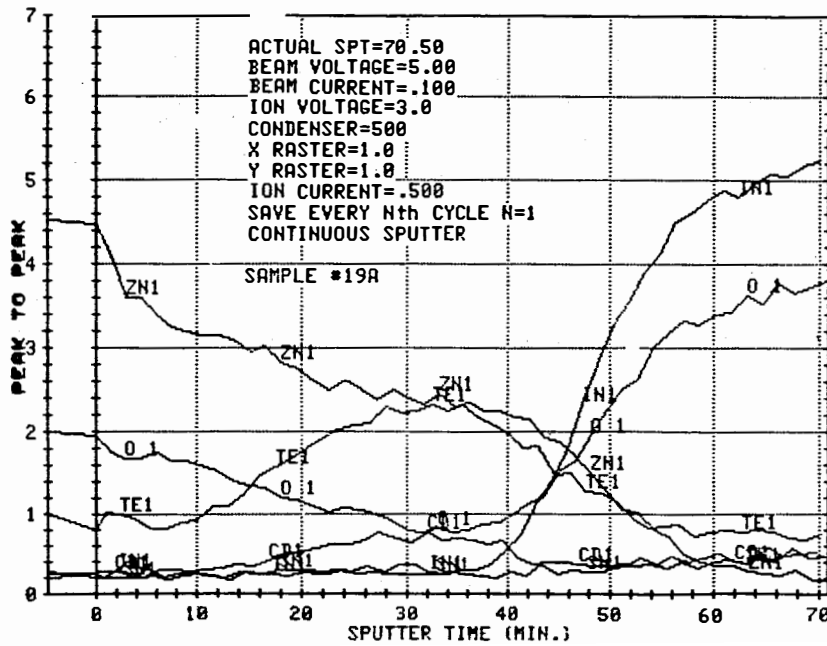


Fig. 1 Auger depth profile of a Cd_{0.2}Zn_{0.8}Te film.

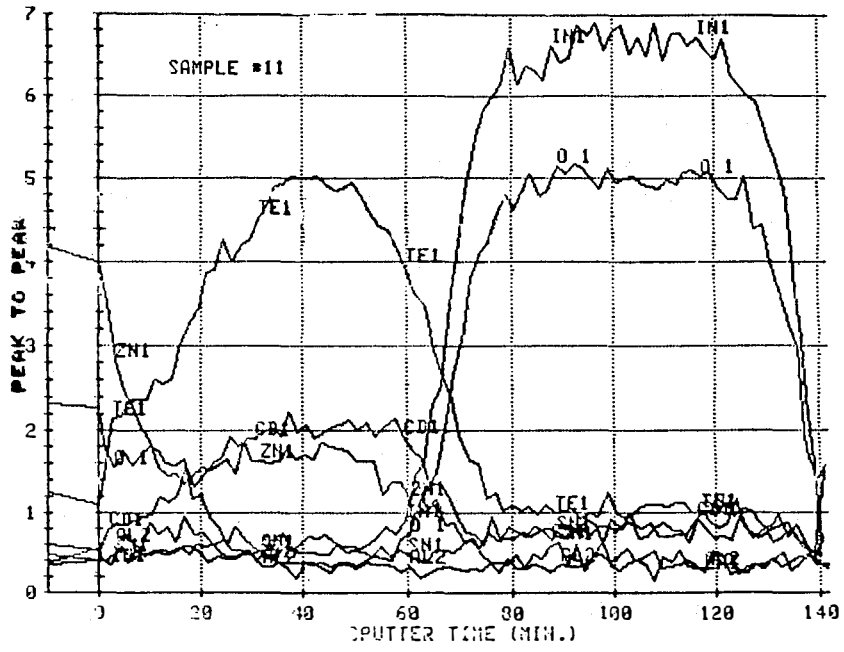


Fig. 2 Auger depth profile of a $\text{Cd}_{0.4}\text{Zn}_{0.6}\text{Te}$ film.

Title: Hydrogen Radical Enhanced Growth of Solar Cells

Organization: Department of Electrical, Computer and Systems Engineering,
Rensselaer Polytechnic Institute, Troy, New York

Contributors: J.M. Borrego and S.K. Ghandhi, Co-Principal Investigators

The objective of this research is to grow InP in the presence of active radical species, and to characterize this material for solar cell applications. This effort falls under the "New Ideas for Photovoltaic Energy Conversion" program. Here, we proposed the use of hydrogen radicals to aid in the organometallic vapor phase epitaxial (OMVPE) growth process, in two ways. First, energy transferred to the alkyl and hydride species would provide a high electron temperature, allowing growth at a reduced thermal temperature. Second, these active species can be used to enhance substrate cleaning prior to growth. This, in turn, would allow growth at lower temperatures than those which are normally encountered in conventional OMVPE growth. The tasks undertaken on this program are outlined below.

TASK 1. REACTOR DESIGN AND CONSTRUCTION: A reactor has been designed for use with these species, and is now in operation. Growth with these species requires operation in the 0.5 to 2 Torr range, in order to reduce collisional losses in the gas phase. Moreover, provision must be made to rapidly deliver these radicals to the growth environment. Thus, low pressure operation is necessary.

A total of five gas lines are provided in this reactor: two bubbler channels, and separate channels for PH_3 , H_2 diluent, and H_2/He through the microwave cavity. One of the channels is trimethylindium (TMI), which is a solid powder at room temperatures, and the other kept as a spare for an alternative In or dopant source. Ultra high purity H_2 was used as a carrier gas through the TMI source. During the course of this program, we recognized that energetic He had unique properties not present in H_2 . Thus, we expanded our effort to include this active species. As a result, the reactor was modified and a UHP He line added as the helium source. Pure PH_3 was used as the phosphorous source, with UHP H_2 to purge its line after use. Operation of this reactor is thus possible in a pure He or pure H_2 mode.

Design of the system required the development of a special cold trap to safely handle pyrophoric species. Effluent scrubbing was carried out after each run, by bringing this trap up to room temperature.

TASK 2. MICROWAVE CAVITY DESIGN: The microwave cavity we are using is not optimized for our work at the present time. It is powered by a microwave generator capable of supplying up to 120W at 2.45 GHz. The gas to be ionized flows in a quartz tube through the microwave cavity, and is ignited by touching a Tesla coil to the tube. Adjustments are provided to tune this cavity to the load, which depends on the type of gas, the flow rate, and the system pressure.

The design of a new cavity has been undertaken. This cavity is shorted at one end and open at the other so that, at resonance, it is approximately a quarter wavelength, i.e., at resonance the wavelength is approximately 12 cms, which corresponds to a resonant

frequency of 2.5 GHz. The cavity is capacitively coupled to a 50 ohm coaxial line connected to the 120 watt microwave generator. Its capacitance coupling is adjustable so as to achieve critical coupling at the optimum operating conditions. This assures that the generator power is dissipated in the production of the microwave plasma with almost no power reflected. One of the tasks is to model the microwave cavity for plasma generation, and to develop guidelines for scaling the plasma generation microwave cavity. This will also allow us to obtain estimates of the plasma concentration and of the parameters which affect its density.

An extensive series of tests have been made to characterize the plasma, by using a Langmuir probe which is located just above the substrate. V-I characteristics of this probe have been taken for a number of different bias conditions. These have been established between a mesh in the plasma line and the substrate. For a typical H[•] plasma, with a flow rate of 50 sccm through the cavity, a microwave power of 100 W and a system pressure of 0.5 Torr, we have measured an electron density of 10^6 cm^{-3} , and an electron energy of about 1.5 eV. This corresponds to an electron temperature of 17,000 K.

TASK 3. CLEANING STUDIES: An in-situ clean step, using radical species, can be beneficial since it can remove surface oxides. In addition, it can remove hydrocarbons which are always present in a laboratory environment, and adsorb strongly on the surface of the substrate before it is introduced into the reactor. Our work on this program has emphasized substrate cleaning studies.

Preferential damage was observed with H radical species, and comes about by the formation of PH₃ (or PH_x). When helium replaced hydrogen in the plasma the damage to the sample is eliminated. The Langmuir probe detects a considerable ion current, indicating that there are He ions present, but they do not damage the sample. This confirms that the etching action is accomplished by the active H species forming a volatile PH_x species, and not by thermal effects. We have changed our emphasis to the use of He species for these reasons, after consultations with our program monitor. System modifications now allow all-He or all-H₂ operation; i.e., the same species is used as the carrier gas, the excited species, and also the pickup gas through the bubbler.

TASK 4. GROWTH: This effort has been initiated during the second phase of our program. Here, growth is being carried out with (and without) active He and H₂ species, and also in the presence (or absence) of an in-situ clean step. Initial results indicate that a He[•] clean step is beneficial for stabilizing the growth process. Growth in either H₂[•] results in damage to the layer. Currently, experiments are underway to quantify this effect, and also to minimize it by suitable bias techniques.

TASK 5. CHARACTERIZATION: This is an important component of any program of research which involves materials growth, since it provides feedback for effecting improvements on the growth process. Our characterization effort is limited to conventional methods which includes optical and Scanning Electron Microscopy, Hall Effect, Double Crystal X-Ray Diffraction, and Photoluminescence. In addition, we hope to use Deep Level Transient Spectroscopy in conjunction with PL, when it is necessary to obtain information concerning non-radiative defects.

Phase 1 of this project has been recently concluded. Much of the groundwork has been laid for the main experiments which will be carried out during Phase 2.

References

1. Iacoponi, J., "A Plasma Enhanced CVD System for OMVPE Growth", Masters Thesis, Rensselaer Polytechnic Institute, Troy, New York, 1989.

7.0 UNIVERSITY PARTICIPATION PROGRAM

John Benner (Manager), and Cecile Leboeuf

The objective of this program is to maximize the contribution of universities to the future of photovoltaic technology by focussing on the traditional needs and strengths of that community. Thus, it provides a forum in which the university researchers identify research topics critical to the advancement of photovoltaic technology with minimal influence from current programmatic interests. The selected participants are then permitted to pursue the proposed basic and applied research ideas in an environment designed to foster creativity by limiting requirements for delivery of reports, samples and achievement of specific goals. Reporting is limited to annual reports and journal publications. Research Symposia organized by the participants, are held periodically and are open to all students, program participants, and outside researchers. The intent of the initiative is to provide continuity of funding over a minimum three-year period which will allow universities to build and support interdisciplinary teams with specialized expertise which can be applied to furthering the technology base of photovoltaics. Such a program is expected to attract the most highly qualified university research teams to the DOE National Photovoltaics Program. The University Participation Program also supports photovoltaic industry through the technology transfer which occurs not only by publication of research results in the technical literature, but also through enhanced student awareness of photovoltaic technology and education of future professionals.

During FY 1989, SERI completed third competitive procurement which resulted in initiating of four new subcontracts in 1989. Existing participants, whose subcontracts were awarded in 1986 and 1987, needed to respond to the competition in order to seek a continuation of their projects. The periods of performance of existing subcontracts were adjusted, as necessary, to permit continuity of funding if successful in the current competition. The technical review and selection process was performed using review teams consisting predominately of other university professors and industrial research scientists. Three of the four new awards were previous awardees in this program, including North Carolina State University, University of Utah, and Stanford University.

Title: Rapid Liquid Phase Epitaxy

Organization: Physics Dept., Brown University
Providence, RI

Contributors: Prof. H.J. Gerritsen (Principal Investigator),
E.E. Crisman, J.T. Daly, D.T. Schaafsma,
S.K.F. Karlsson

ABSTRACT

Single crystal layers of gallium arsenide have been grown on <111> and <100> oriented GaAs substrates using a flowing solution of gallium saturated with GaAs. With this novel technique, growth rates as high as $9.0\mu\text{m}/\text{min}$ have been achieved for 5 minutes, while rates of approximately $4\mu\text{m}/\text{min}$ are typically achieved for 20 minutes of growth. These figures are in good agreement with a previously developed theoretical model and are about two orders of magnitude greater than those for conventional, static solution, liquid phase epitaxy (LPE) for layer thicknesses greater than $1\mu\text{m}$. Undoped, p-doped and n-doped layers of high crystallographic and electronic quality have been grown. A description of the technique and some of the electro-optical properties are presented in this paper.

INTRODUCTION

For many years, liquid phase epitaxy (LPE) was the preferred crystal growth method for producing high perfection single crystal layers of gallium arsenide, as well as other III-V compounds. Due to its relative simplicity, lower capital outlay for equipment, and greater safety, LPE has remained a viable technique despite the recent advances in vapor phase and molecular beam epitaxy. All common epitaxy techniques suffer from rather slow growth rates, with LPE typically on the order of $10\mu\text{m}/\text{hour}$ [1] for layers $>1\mu\text{m}$. Thus, if growth rates can be increased by an order of magnitude or more while maintaining good crystalline perfection and electronic properties, the potential exists for decreasing the cost and optimizing the production of large area, single crystal GaAs wafers for VLSI circuits, microwave devices, and photovoltaic cells. In addition, by trading off growth rate for lower processing temperature, other advantages such as reduced dopant migration and minimized differential expansion (in heterostructures) could be exploited.

Many of the advantages of the technique referred to in this paper as RLPE for rapid liquid phase epitaxy, can be seen in contrast to other LPE techniques. In conventional LPE, the liquid solution is brought into static contact with the substrate and epitaxial growth is induced by causing supersaturation to occur at the melt/substrate interface. The two methods of achieving supersaturation most commonly used are "ramp cooling" the entire system, or "differential cooling" of the substrate relative to the melt; other methods, such as thermoelectric interface cooling [2], can be viewed as variations of the first two. In all of these static methods, the growth rates are time dependent because the width of the solute depletion layer at the liquid/solid interface increases with time; thus increasing the distance that the solute must diffuse to reach the growth interface. Since the driving mechanism for solute diffusion is the concentration gradient between liquid and solid, and since this gradient decreases as the depletion layer grows, it is evident that minimizing the depletion layer thickness and holding it constant in time would increase the growth rate and make it time independent.

One way to minimize the depletion layer thickness is to continually replace the melt that is in contact with the substrate with fresh, saturated solution. A method of doing that is the RLPE flowing solution technique, first described by M. Cook [3] and shown schematically in figure (1). The solution is forced from one reservoir to another, passing through a channel which incorporates the substrate as part of one wall. Epitaxy is promoted as the solution flows across the substrate, by establishing a temperature gradient at the liquid/solid interface. In the system pictured below, gas pressure is used to drive the solution between reservoirs, and the temperature gradient is produced by means of a cool gas jet directed against the bottom of the substrate.

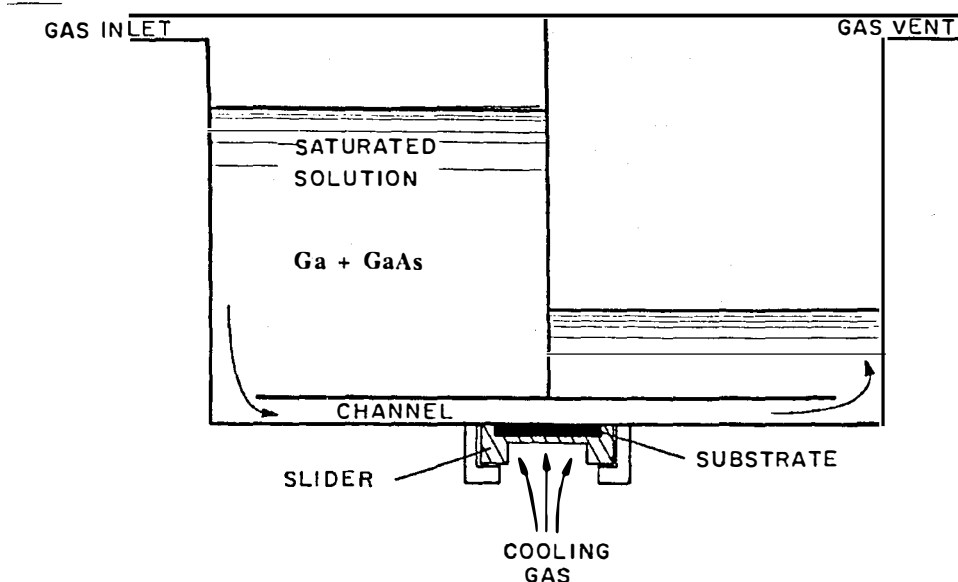


FIGURE 1: Schematic illustration of RLPE flowing solution technique.

A complete mathematical description of the RLPE process was developed and presented in an earlier publication [4]. The salient points of this study were:

- 1) The initial transient time before quasi-steady-state conditions are established would be much less than the duration of the RLPE cycle, i.e., a few seconds out of a growth time of several minutes.
- 2) The steady state growth rate would be largest at the point of initial contact with the substrate (the "upstream" end) and taper nonlinearly with distance downstream to mirror the solute depletion layer profile assuming constant temperature gradient along the flow channel.
- 3) Modest differential hydrostatic pressures, on the order of 15 Torr, would be sufficient to sustain the required laminar flow rates of 5 to 20 *cc/min* in the channel. (It was also shown that laminar flow would be maintained for the projected range of growth parameters, a necessary condition for the original theoretical analysis.)
- 4) Cooling the back of the substrate by 5C° or less would maintain the desired growth rates.
- 5) Under the above conditions, growth rates in excess of 10 *μm/min* could be achieved, with total growth limited only by the amount of solution in the reservoirs. This scheme, however, easily lends itself to large area, high volume production.

EXPERIMENT

Figure 2 shows a drawing of the actual growth crucible, the design of which was based on the theoretical calculations described in [4]. From published values of the surface tension, viscosity and wetting coefficients for gallium, clearances of ± 0.002 inches were calculated to be sufficient to prevent leakage between the pieces of the crucible. The crucible was made from Poco DFP-3-2 high purity, high density graphite.

In the system the maximum flow velocity for a channel height of 2.0mm is 2.5cm/sec at a flow rate of 30cc/min, which is an order of magnitude less than the velocity at which turbulent flow begins. It should be noted, however, that even though the flow is well below the turbulence threshold and care was taken in the design to minimize the channel roughness and edge discontinuities, the flow is not necessarily smoothly laminar. Typical overpressures used to control the flow were ± 9 Torr. The gas handling system was constructed of fluorocarbon and stainless steel parts. The furnace system was constructed with fused silica and stainless steel chamber and a four zone (split center zone) tube furnace.

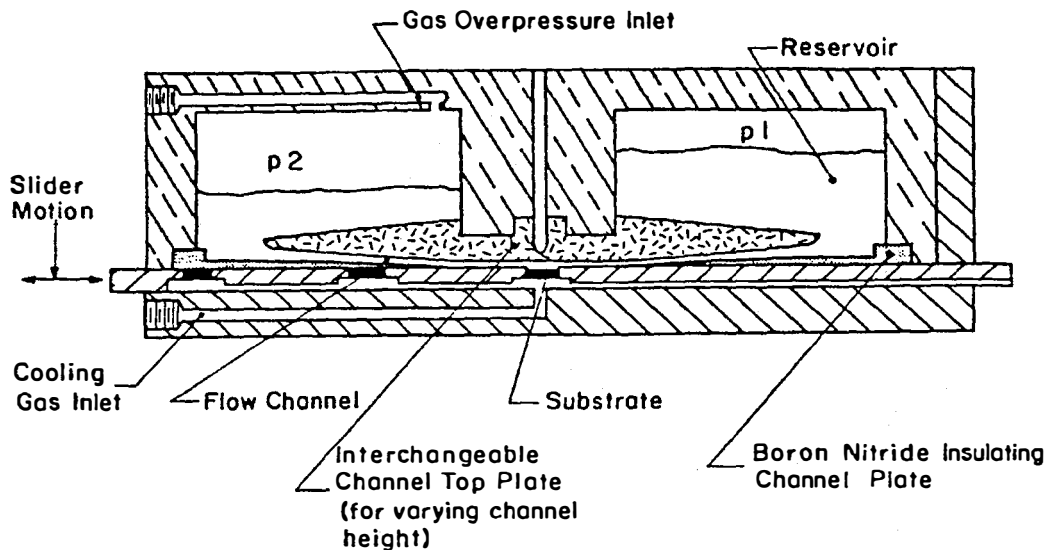


FIGURE 2: Crossection of two well chamber used for RLPE.

Substrates were 1x1 cm cut from bulk single crystal GaAs wafers, either $\langle 111 \rangle$ or $\langle 100 \rangle$ tilted 2° towards $\langle 110 \rangle$ orientation, mostly p-type Cd-doped or semi-insulating Cr-doped. Chemo-mechanical polishing in 0.2-2.0% bromine in electronic grade methanol was used to reduce the thickness of the specimens to the range of 0.4 to 0.5mm, so as to fit the indentation in the wafer carrier. Before the growth cycle, the substrates were cleaned in organic solvents and etched 3 min in 0.1% bromine-methanol to expose a clean surface for growth.

During the time required for the furnace to come to operating temperature (~ 3 hours), the chamber was flushed with palladium-diffused ultrapure hydrogen at approximately $10\ell/\text{min}$. In order to force the liquid gallium through the channel for growth, the pressure in one well was increased relative to the other. One chamber was left open to the furnace tube, at 1/3 psi above atmosphere, while the pressure in the other was varied above and below the tube that of by adding hydrogen and leaking it to the exhaust burn off. The growth was initiated by starting the nitrogen cooling gas flow, and then moving a substrate into position in the channel. According to the calculations, laminar flow, thermal distribution and depletion profiles are established in the channel in less than 10 seconds. Therefore, for the growth times used in this study, typically 3 minutes or greater, these transients can be ignored. At the end of the growth, the specimen was removed from the growth area by pushing the wafer carrier out of the channel flow position.

RESULTS

RLPE layers from three different melts have been evaluated for this study. The first was an undoped solution prepared from 7N pure gallium and undoped single crystal GaAs. The second was doped with high purity silicon at 0.1 atomic percent, which was expected to yield $5 \times 10^{17} \text{cm}^{-3}$ p-type epilayers at 800°C . The third was an n-type melt doped with tellurium from 5N pure Ga_2Te_3 .

The epilayer growth rate is quite sensitive to the cooling of the substrate relative to the liquid that can be induced by undercooling the wafer. The growth velocities in figure 3 were calculated assuming a value of $\Delta T = 5^\circ\text{C}$. Measurements of the actual temperature gradient across the melt/substrate interface have been complicated by two factors. First, the region to be profiled is small, and buried deep within a large volume of graphite with moving parts. Also, metal thermocouples inserted into liquid gallium at 800°C will quickly dissolve. Therefore, direct measurements of the interface temperature gradient are not practical in this system. The initial theoretical study assumed cooling gas blowing on the back of the substrate at room temperature. However, revised calculations of the cooling gas temperature rise that would occur during the transit through the furnace to the substrate (a length of approximately two feet) indicate that even after the addition of a liquid nitrogen precooler, a temperature difference of $\sim 3^\circ\text{C}$ is more likely than the 5°C assumed in. Much of the interface instability and uneven growth morphologies observed to date are attributable to difficulties in maintaining an adequate temperature gradient across the growth interface.

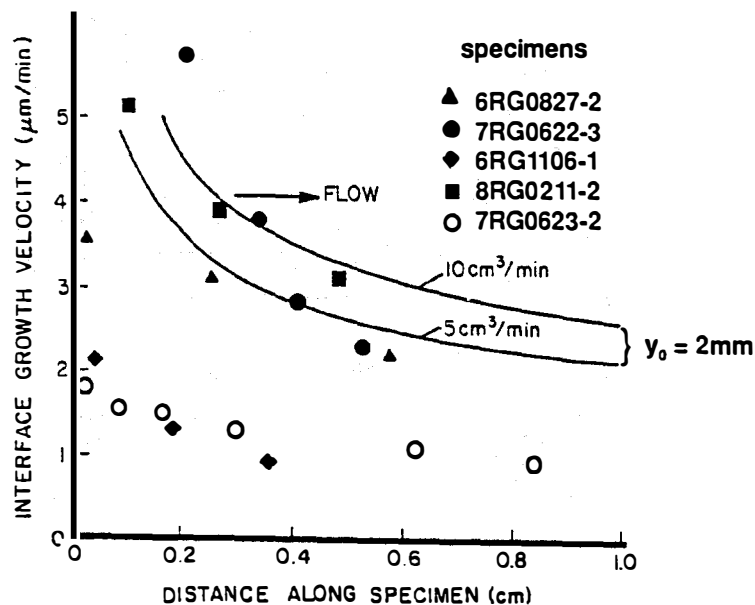


FIGURE 3: Theoretical growth curves compared with measured values (plotted points) for RLPE specimens.

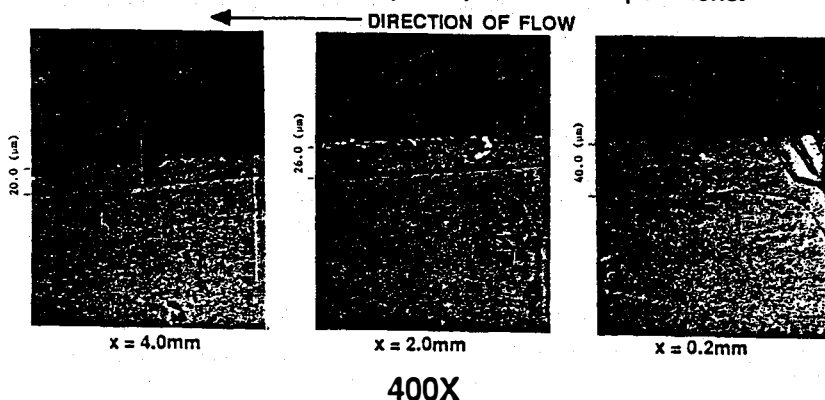


FIGURE 4: Crosssection of RLPE specimen #6RG1106-1 grown on (111) substrate at various positions along the direction of flow [800°C, 5cc/min for 19min with 1.1 l/min].

The solid lines of figure 3 show the theoretical prediction of a tapered growth, highest at the upstream end of the substrate. Figure 4 shows three views along a cleaved section of a typical layer, where the epilayer has been stained to make it stand out from the substrate. The layer is clearly thicker at the upstream end, with a growth profile in good qualitative agreement with the theoretical model. (Note the reverse direction of flows in figures 3 and 4.) Other specimen thicknesses are plotted in figure 3 along with the specimen shown in the photographs of figure 4. The thicknesses reported below were measured using optical or electron microscope "cut-away" photographs of epilayer/substrate profiles, wherein the wafers were sectioned either by cutting, polishing and staining, or by simple cleaving.

To date, experiments have been conducted under varying conditions, with the main objectives being to evaluate the effects of system parameters on growth rate and surface morphology. Although the

majority of layers have shown a great deal of surface structure, a few specularly smooth specimens have been grown. Further experiments are necessary to identify operating parameters for consistently good morphology.

Photoluminescence measurements have been made on several specimens. Two main types of photoluminescence spectra have been identified, as shown in typical traces of figure 5 for undoped and Si-doped specimens. At $\sim 77\text{K}$ the undoped line is very close to the 819 nm predicted for GaAs and no indication of any impurity line is seen. The Te doped n-type material had essentially the same peak position with 20% FWHM increase. The specimens with Si doping however showed consistently reduced band edge recombination coupled with an approximately 6X stronger peak at 888nm as show in figure 5. The only impurity line cited in the literature corresponding to the 33 meV shift indicated by this line is a Si As-vacancy complex [5]. The broadness of the 888nm peak indicates that there is probably another peak overlapping in this vicinity.

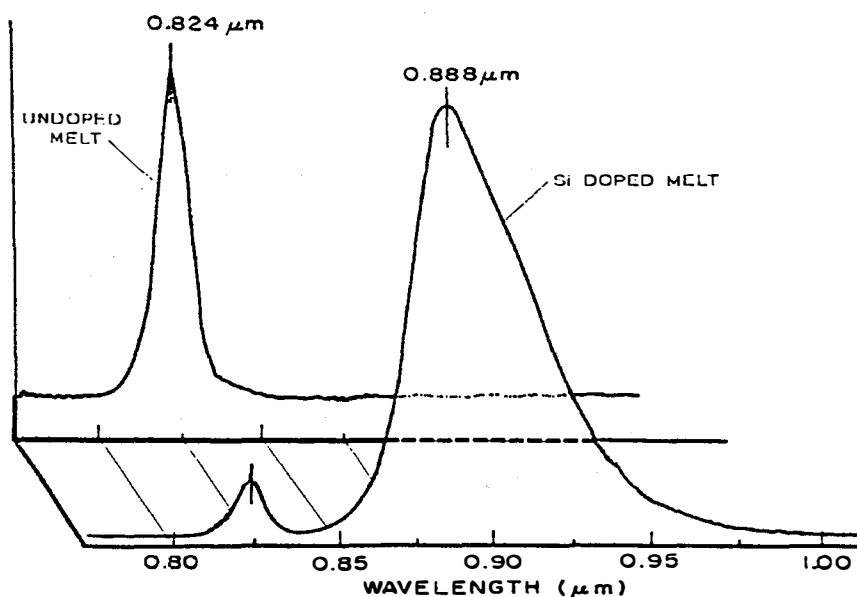


FIGURE 5: Photoluminescent response of undoped and Si doped RLPE GaAs.

A quantitative comparison was made with high quality MBE material obtained from C. Leboeuf at SERI. The MBE specimen was a Be-doped structure with an $\text{Al}_{0.25}\text{Ga}_{0.75}\text{As}$ window layer specifically designed for PL lifetime measurements. The RLPE specimen was a single, Si-doped layer. The two specimens were measured side by side in the same optical set-up, and their photoluminescence peak intensities were compared as a function of excitation wavelength. A plot of the ratio of peak intensities, MBE/RLPE as a function of excitation wavelength is shown in figure 6. At the longest excitation wavelengths, the influence of the window layer is reduced, bringing the ratio of intensities down to 6:1. With the window layer removed from the MBE specimen, the ratio of intensities is less than 2:1. From these data, it is clear that the optical quality and purity of the RLPE layers are of the same order of magnitude as good MBE material. A similar comparison at 300K with an undoped RLPE layer and a moderately doped ($5 \times 10^{17}\text{cm}^{-3}$) MOCVD layer obtained from Spire, Inc. showed the RLPE intensity to be 10x greater with 33% larger FWHM.

The Hall mobility at 300K of both n and p type layers have been measured for specimens of approximately $5 \times 10^{17}\text{cm}^{-3}$ carrier concentrations giving $3480\text{cm}^2/\text{V-s}$ (n) and $280\text{cm}^2/\text{V-s}$ (p). These values are within 10% of published data for high quality material of similar carrier concentration [6].

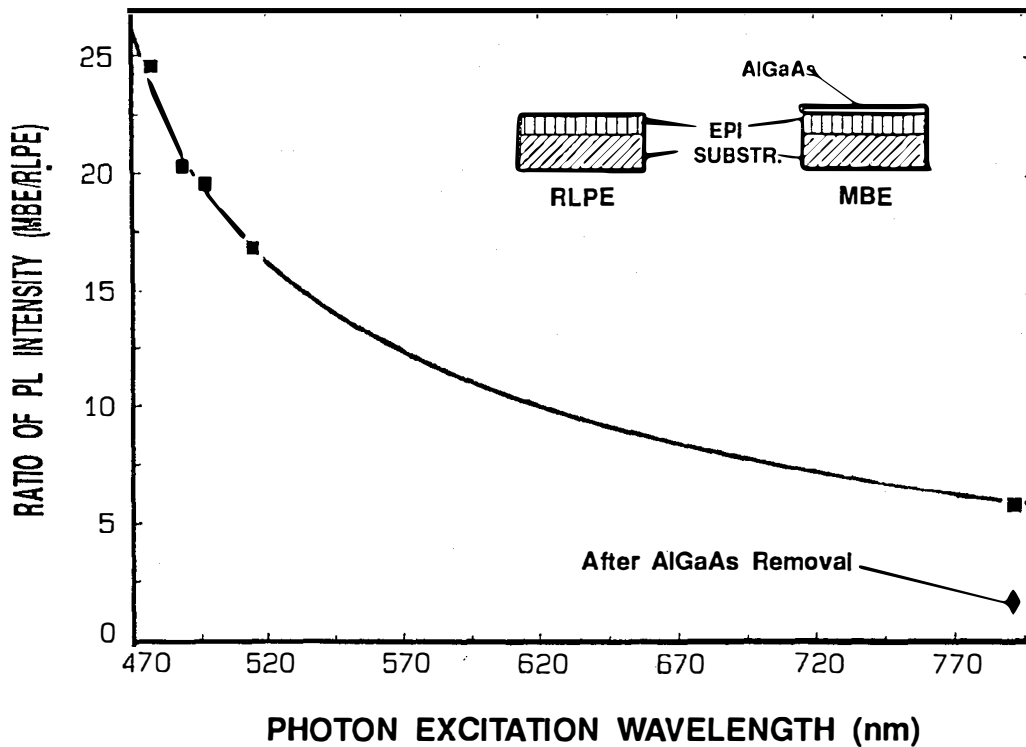


FIGURE 6: Comparison of photoluminescence intensities of MBE and RLPE specimen 7RG1110-2 as a function of excitation wavelength.

SUMMARY

The RLPE technique for producing single crystal GaAs epitaxial layers holds great promise for volume production and improved safety, yet the apparatus requires further improvement, beyond the scope of this study. As will be reported in a subsequent publication, the electronic and optical properties substantiate the good quality of these epilayers. With the high growth rates given above, this preliminary evaluation indicates that RLPE could be an extremely successful research and commercial epitaxy process.

ACKNOWLEDGEMENT

The authors thank the Department of Energy, Solar Energy Research Institute, and the Brown University Laboratory for Interface Science and Engineering for support of this research.

REFERENCES

1. J. J. Hsieh, J. Crystal Growth 27, 49 (1974).
2. D. J. Lawrence, L. F. Eastman, J. Crystal Growth 30, 267-275 (1975).
3. M. Cook, Holobeam, Inc., Ridgewood, NJ 07451, Patent applied for.
4. J. T. Daly et al, J. Crystal Growth 78, (1986) 291-302.
5. Semiconductor Lasers and Heterojunction LED's by H. Kressel and K. Butler, 330, (1977).
6. J. S. Blakemore, J. Appl. Phy. 53 (1982)

Title: Improvement of Bulk and Epitaxial III-V semiconductors for Solar Cells by Creation of Denuded Recombination Zones

Organisation: Department of Electrical and Computer Engineering, Carnegie Mellon University, Pittsburgh, Pennsylvania

Contributors: A. G. Milnes and T. E. Schlesinger, principal investigators, H. F. Pan and D. Wong

The performance of GaAs solar cells is often limited by short minority carrier diffusion lengths in the material. This is especially true of cells fabricated with active regions in bulk substrates, a consideration which has, in the past, necessitated the use of expensive epitaxial processing to achieve high efficiency cells. In FY89 CMU researchers have concentrated efforts on identifying the dominant recombination centers in bulk n-type GaAs and developing a simple process to suppress these recombination centers. The effects of annealing on defect structure and minority carrier diffusion lengths have been extensively characterized and insight has been gained on the anneal conditions which will yield optimal improvement. Zn diffused solar cells were fabricated directly in bulk substrates to demonstrate the impact of enhanced minority carrier diffusion lengths on the performance of solar cells which are made without any epitaxy.

Raising hole diffusion lengths in n-type bulk GaAs

A process involving proximity annealing in high purity quartz ampoules was developed for the purposes of increasing hole diffusion lengths (L_p) in n-type bulk GaAs. Specimens were placed with their polished faces together in the ampoules which were then evacuated to a pressure of about 10^{-5} Torr and sealed. The ampoules were placed in a furnace which had been preheated to the selected anneal temperature. Anneals were terminated with a water quench.

Figure 1 shows the effect of proximity annealing at 950 °C on L_p in $1 \times 10^{17} \text{ cm}^{-3}$ Si-doped horizontal Bridgman (HB) material and $1 \times 10^{17} \text{ cm}^{-3}$ Te-doped liquid encapsulated Czochralski (LEC) material. The two types of material were obtained from different manufacturers; the Te-doped material had been boule annealed by the manufacturer whereas the Si-doped material had not.

It is clear from fig. 1 that the annealing process affects both classes of material in a similar manner, and that substantial increases in L_p can be achieved. The increase in L_p resulting from a 16 hour 950 °C anneal was by nearly a factor of 3, with the best diffusion length obtained being about 2.6 μm . Thus the process appears to be generally effective on bulk n-type GaAs, regardless of the crystal growth method and dopant type, and results in improvements to the material even if it has already been given a boule anneal.

The enhancement of L_p as a result of annealing was found to be associated with the proximity surface. A specimen annealed without its polished face protected by stacking in a proximity arrangement was found to show no improvement in terms of L_p .

Fig. 2 contains plots of photoresponse as a function of depth in specimens given 16 hour proximity anneals at different temperatures. The plots were obtained using a

transparent electrolyte electrochemical cell arrangement [1]. A glass filter was used to remove a substantial proportion of the high energy components of the white light illumination. Specimens were successively etched so that photoresponse as a function of depth could be obtained. Given these experimental conditions, the photocurrent profiles indicate qualitatively the diffusion length profiles in the specimens. The plots of fig. 2 show that the beneficial effect of proximity annealing is largest at the specimen surface and falls off with depth. This result has been quantitatively confirmed with electron beam induced current (EBIC) measurements of diffusion lengths [2].

EBIC measurements on pieces of the specimens characterized with photoresponse yielded L_p values which implied that the hole diffusion length of the specimen given the 900 °C anneal was smaller than the L_p of the specimen given the 950 °C anneal. This is consistent with the data of fig. 2 if account is taken of the fact that EBIC measurements yield an assessment of L_p at a depth of between 5 and 10 μm below the test junction. Since GaAs is a direct bandgap material, the junction depth of a GaAs solar cell is, in an optimal design, a fraction of a μm from the surface. An electrochemical cell photocurrent measurement made at the surface is more representative of the effective L_p value which will be reflected in the solar cell performance, than an L_p value determined by EBIC. Thus EBIC measurements (such as used to obtain the data of fig. 1), while useful in the sense that they yield quantitative information with regard to L_p , will tend to underestimate the beneficial effect of the proximity annealing treatment. Further, EBIC data will not accurately indicate the optimal choice of anneal condition for maximised solar cell performance.

The effect of annealing on the defect structure in GaAs

Deep level transient spectroscopy (DLTS) was used to determine the effect of annealing on the defect structure in bulk n-type GaAs. From fig. 3 it can be seen that in proximity annealed material, L_p is directly proportional to the square root of the concentration of the hole trap HCX ($E_v+0.29\text{eV}$), and the same is true of the square root of the concentration of the electron trap EL2. This association between defect concentration and diffusion length is characteristic of defects which are carrier lifetime limiting recombination centers [3]. There is ample evidence in the literature, however, that EL2 is not an effective recombination center in bulk GaAs [4,5,6]. From this it can be concluded that HCX is the dominant recombination center in bulk n-type GaAs. HCX is believed to be associated with a native defect since it has been found to be present in a several different (Si- and Te-doped, HB and LEC) GaAs wafers obtained from different vendors [7]. The straight line characteristic associated with the EL2 data in fig. 2 is an indication that the suppression of EL2 during proximity annealing occurs at a rate comparable to the suppression of HCX.

The data from the specimen given a 9 hour anneal deviates from the straight line characteristics suggested by the other data points, having an unexpectedly low hole diffusion length. The DLTS spectra from this specimen revealed an additional hole trap which is believed to be associated with an (unidentified) impurity [2]. This was the only respect in which the defect structure of this specimen differed from what might be expected, given the DLTS spectra from the other specimens. From this it can be concluded that if insufficient care is taken to eliminate contamination during processing the full benefit of proximity annealing may not be achieved.

Profiles of defect concentration as a function of depth reveal that the suppression of EL2 and HCX as a result of proximity annealing is associated with the specimen surface, with defect concentrations being lowest at the surface [8]. The variation of HCX concentration with depth in a proximity annealed specimen and the photocurrent profiles of fig. 2 are qualitatively consistent with HCX being the dominant recombination center in the material.

Annealing without proximity protection of the specimen surfaces was found to result in the introduction of a hole trap HCZ ($E_v+0.57\text{eV}$) at the exposed surfaces. Specimens given such a treatment showed a low L_p , indicating HCZ is an effective recombination center. Data published by other workers [9], and our own results [2], suggest that HCZ is associated with arsenic vacancies.

Model to account for the experimental observations

It was found that extending the anneal period beyond 16 hours results in a falloff in the L_p values as measured by EBIC. DLTS measurements on a specimen given a 49 hr anneal at 950 °C showed that this falloff was in part due to the introduction of the defect associated with contamination, and in part due to an apparent rise in the HCX concentration over the corresponding HCX concentration in a specimen given a 16 hr 950 °C anneal. (In contrast, the suppression of the EL2 concentration was found to be monotonic with increasing anneal time.) The defect concentrations were measured at a fixed depth from the surface of 9 μm . This observation, coupled with the profiles of fig. 2, implies that the suppression of recombination centers in the material is associated with a limited source diffusion process [8].

We propose the following model to account for the experiment observations : The suppression of HCX occurs at the immediate surface of the specimen in the early part of the anneal. This is perhaps the result of changes in stoichiometry at the surface due to arsenic loss during the time the ampoule is warming to the anneal temperature, and the equilibrium arsenic overpressure inside the ampoule is being built up. Once this equilibrium overpressure has been attained no further suppression of HCX occurs at the surface. There is a net diffusion of HCX to the surface during the rest of the anneal, driven by the concentration gradient of the defect. The diffusion coefficient of HCX increases with anneal temperature. Thus the higher the anneal temperature, the more complete the redistribution of HCX; the region in which L_p is enhanced extends further into the bulk, while the residual improvement at the immediate surface (0 μm) is reduced. This accounts for the photocurrent profiles of fig. 2. A similar line of reasoning applies to the case of a series of anneals at a fixed temperature for varying lengths of time and offers an explanation of the result that there is an optimal anneal temperature for maximum suppression in HCX (improvement in L_p) at any given depth.

The impact of improving L_p on solar cell performance

Solar cells were fabricated using a sealed ampoule vapour phase Zn diffusion process with a ZnGaAs source. A simple gold grid was used for the front surface metallization pattern. A cell was made using a piece of 1×10^{17} Te-doped GaAs which had been given a 16 hour 950 °C proximity anneal and found to have an L_p value of 2.6 μm (EBIC measurement). A second cell was made using a piece of material from the same crystal,

which had not been subjected to any wafer annealing. The two cells were processed simultaneously, and were placed in the same ampoule for the p^+ layer diffusion. The diffusion anneal was for 15 minutes at 600 °C, corresponding to a junction depth of about 0.2 μm . Mesa etching with a photoresist mask was used to precisely define the 0.5 cm x 0.5 cm cell area in each case. Fig. 4 contains the spectral response curves obtained from these cells. The cell made from the proximity annealed material shows a substantially larger long-wavelength photoresponse.

Conclusions and further work

A simple method of increasing hole diffusion lengths in n-type bulk GaAs by proximity wafer annealing has been developed. Specimens with L_p values of up to 2.6 μm have been obtained by this anneal process, and the impact of improving the material in this manner on the performance of Zn diffused solar cells fabricated without epitaxy has been demonstrated. The dominant recombination center in the material has been identified as a hole trap HCX ($E_v+0.29\text{eV}$). The beneficial effects of the annealing are associated with the specimen surface but extend some tens of μm into the bulk of the material. The spatial variation in the concentration of the dominant recombination center after annealing is characteristic of a limited source diffusion process.

In the final phase of the project improvements to the solar cell fabrication process will allow a quantitative assessment of the effect of improving L_p on solar cell performance. Further efforts will be made to optimise the anneal procedure, and to confirm the physical basis for the effects of annealing which have been observed. The possibility of determining the atomic structure of HCX and the other defects found in the material with positron annihilation measurements is currently being explored.

References

1. Kurtz, S. R., and J. M. Olson, Proc. of the 19th IEEE Photovoltaic Specialists Conf., (IEEE, New York, 1987), p. 823.
2. Wong, D., T. E. Schlesinger and A. G. Milnes, to appear in Solar Cells.
3. Wong, D., T. E. Schlesinger and A. G. Milnes, Proc. of the International Conference on the Science and Technology of Defect Control in Semiconductors, Yokohama, Japan, September 1989 (Elsevier, Amsterdam, 1989).
4. Mitonneau, A., A. Mircea, G. M. Martin, and D. Pons, *Revue de Physique Appliquee* **14**, 853 (1979).
5. Hunter, A. T., Defect Recognition and Image Processing in III-V Compounds II, edited by E. T. Weber, Elsevier, Amsterdam, 1987, pp. 137-145.
6. Fang, Zhao-Qiang, T. E. Schlesinger and A. G. Milnes, *J. Appl. Phys.* **53**, 5047 (1987).
7. Wong, D., H. K. Kim, Z. Q. Fang, T. E. Schlesinger and A. G. Milnes, *J. Appl. Phys.* **66**, 2002 (1989).
8. Wong, D., T. E. Schlesinger and A. G. Milnes, presented at the Fall Meeting of the Materials Research Society, Boston, November 1989.
9. Chiang, S. Y., and G. L. Pearson, *J. Appl. Phys.* **46**, 2986 (1975).

Figure 1 : Hole diffusion length (determined with EBIC measurements) as a function of anneal time for proximity annealed bulk material. The error bars indicate the standard deviation of several measurements made on the same specimen. The lines drawn are intended as guides to the eye, and reflect the similarity between the two data sets.

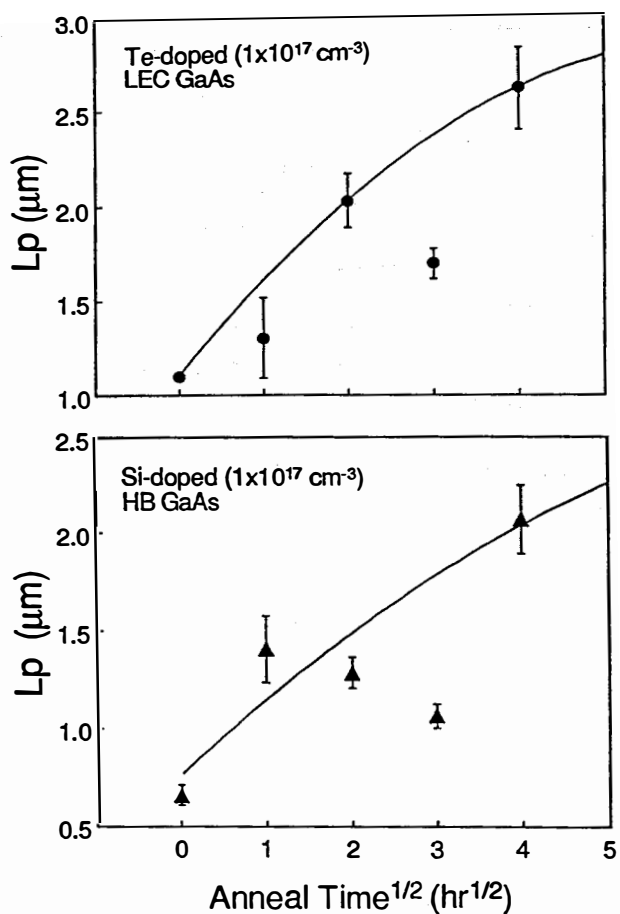


Fig. 2 : Electrochemical cell photocurrent as a function of depth for specimens given 16 hr proximity anneals at different temperatures. The open circles represent data from a control specimen which had not been wafer annealed. The lines drawn are intended as guides to the eye.

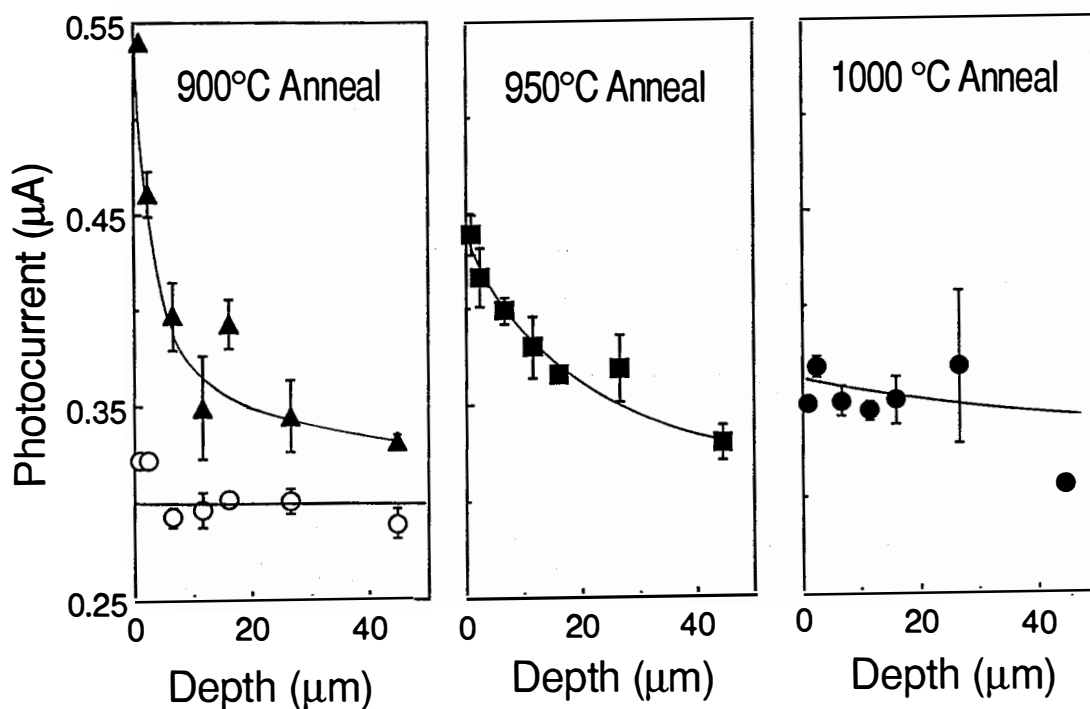


Fig. 3 : Diffusion length as a function of the inverse square root of trap concentration for the defects HCX and EL2. Specimens had been given anneals at 950 °C for durations as indicated in the figure. The error bars indicate the standard deviation of several measurements made on the same specimen. The lines drawn are least squares fits to the data point and the origin. The points associated with the specimen annealed for 9 hours were not considered in computation of these line fits.

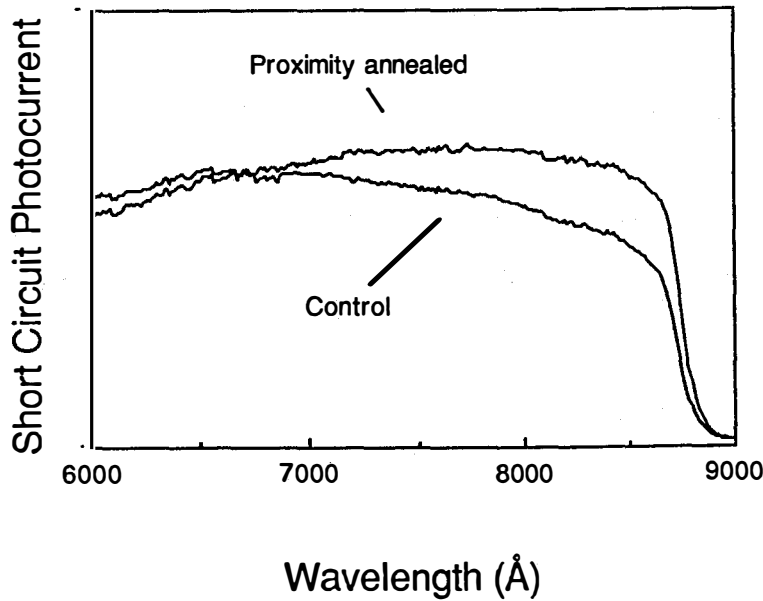
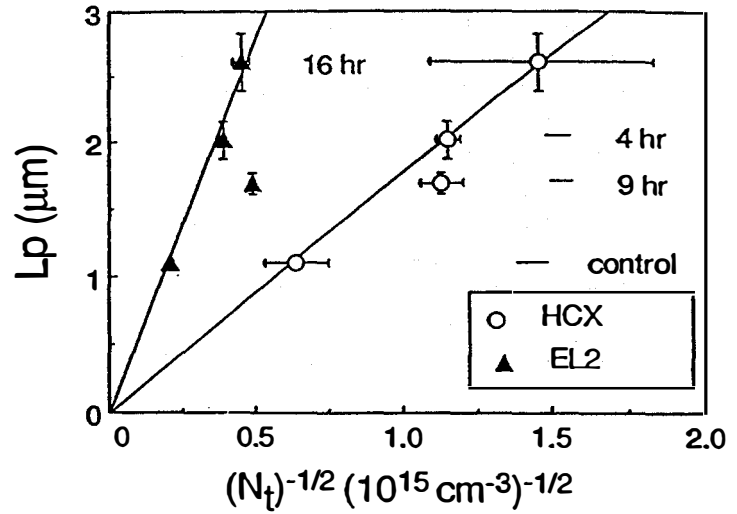


Fig. 4 : Spectral response plots for two solar cells, one fabricated from proximity annealed (16 hr 950 °C) material and the other from material from the same crystal which had not been given any wafer anneal. The vertical axis is plotted in arbitrary current per photon units.

Title: New Approaches for High Efficiency Solar Cell:
Role of Strained Layer Superlattices

Organization: Electrical and Computer Engineering Department
North Carolina State University, Raleigh, North Carolina
27695-7911

Contributors: S.M. Bedair and N.A. El-Masry

Objective

The objective of the research program is to address current problems that are hindering progress towards achieving high efficiency cascade solar cell structures. Problems include proper interconnect between the two cells and the lack of compatible material systems for the optimum bandgap combinations. During the last year we have concentrated our activities on addressing potential techniques that can be used to reduce defects generated when incompatible material systems or poor quality substrates are being used in solar cells.

In order to achieve such goals, we have carried out fundamental studies to understand the behavior of defects and dislocations in strained layer superlattices buffer films and the mechanisms involved in their reductions. These studies were carried out both experimentally and theoretically.

An Energy Model for Blocking Threading Dislocations by Strained Buffer Layers in GaAs Grown on Si Substrates

The misfit strain between a substrate and a growing epilayer can be used to drive threading dislocations to the edge of epitaxial thin films and thus improve the film crystal quality. A threading dislocation bends as a result of the force exerted on it by the misfit strain. We present a model to evaluate the minimum critical thickness based on energy consideration. This approach differs from the previous mechanical equilibrium models⁽¹⁻²⁾ and relies on the change in the total system energy for a threading dislocation due to the presence of a misfit dislocation segment at the strained interface. The energy terms considered in this calculation are (1) the films strain energy E_e , (2) the dislocation self-energy E_D , and (3) the interaction energy between the dislocation segments E_1 .

The threading dislocation configurations considered are shown in Figs. 1(a) and 1(b). The areal strain energy density E_e associated with a films of thickness h is

$$E_e = \left[2\mu(1 + \nu)/(1 - \nu) \right] \epsilon^2 h, \quad (1)$$

where μ is the shear modulus of the thin film taken as 4×10^{11} dyn/cm², ν is Poisson's

ratio, 0.33 is for GaAs, and ϵ is the elastic strain parallel to the film plane. The difference in the strain energy (ΔE_ϵ) between the two configurations in Figs. 1(a) and 1(b) represents the proportion of the strain energy that is relaxed due to the formation of a length L of a misfit dislocation. The area in which the misfit strain has been accommodated by the formation of a length L of misfit dislocation is

$$A = (b_c/2f)L, \quad (2)$$

where b_c is the edge component of Burger's vector on the films plane and f is the misfit strain in the film. In this model, f is taken to equal ϵ .

The difference in the strain energy (ΔE_ϵ) that accompanies the change from the configuration shown in Fig. 1(a) to that in 1(b) is a result of the strain energy relaxation due to the creation of a misfit segment L . ΔE_ϵ is the product of Eqs. (1) and (2), resulting in

$$\Delta E_\epsilon = - \frac{\mu(1 + \nu)b_c L}{(1 - \nu)f} \epsilon^2 h. \quad (3)$$

The negative sign indicates a reduction in the system energy. The change in the self-energy of the dislocation associated with the two configurations in Figs. 1(a) and 1(b) is ΔE_D . It is equal to the self-energy of a length L of misfit dislocation and is given approximately by⁴

$$\Delta E_D \approx \frac{\mu b^2 L}{4\pi(1 - \nu)} (1 - \nu \cos^2 \beta) \ln \left(\frac{\alpha R}{b} \right) \quad (4)$$

where b is Burger's vector ($b = \alpha/2[110]$ type), β is the angle between the dislocation line and its Burger's vector ($\beta = 60^\circ$ for mixed dislocation), and αR is taken to be $4\pi b$ in our calculations².

The difference in the interaction energy of the dislocation segments in the two configurations in Figs. 1(a) and 1(b) is ΔE_1

$$\Delta E_1 = E_1(A,B) + E_1(B,C) + E_1(A,C) - E_1(A,C'). \quad (5)$$

This interaction energy between dislocations has been derived by Hirth⁵.

Therefore, the difference in the system energy ΔE that accompanies the movement of a dislocation line a distance L along the strained interface is the sum of the change in the system strain energy ΔE_ϵ , the dislocation self-energy ΔE_D , and the dislocation interaction energy ΔE_1 :

$$\Delta E = \Delta E_{\epsilon} + \Delta E_D + \Delta E_1. \quad (6)$$

The total energy change in the system depends on both the misfit strain f and the length of the misfit dislocation segment, L . Equation (6) has been used to calculate the total energy change for different misfits and layer thicknesses h . The elastic constants used in these calculations are taken for GaAs. For a given degree of misfit ($f = 0.0135$) between the strained layer and the length of misfit (L) is shown in Fig. 2. From Figure 2, a stable configuration can be achieved when $h > 200 \text{ \AA}$.

Figure 3 illustrates the calculated results for a given film thickness subjected to different values of strain. Increasing the misfit strain f between the film and the substrate also leads to the decrease of the critical misfit dislocation length L^* and the energy barrier ΔE^* .

We redefine the minimum critical thickness for a given degree of misfit f as the thickness at which the critical misfit dislocation length L^* and the energy barrier ΔE^* are equal to zero. For a strained layer with thickness less than the minimum critical thickness, there is an energy barrier to form a critical length of misfit dislocation L^* . This barrier can be decreased by increasing either the films thickness or the misfit string. However, if we provide energy to the system, e.g., in the form of thermal energy, a stable misfit dislocation segment can form.

The above model indicates that the number of bent-over threading dislocations in a given system depends critically on the total energy change ΔE associated with the introduction of misfit dislocations segments. Generally, ΔE is determined by the strained-layer thickness h and the misfit strain f between the strained layer and substrate. On the other hand, ΔE is expected to be small if there is a large misfit and/or a thicker strained layer.

The trend of above model was confirmed experimentally in our studies of the effect of SLS buffer layers in reducing defects in GaAs grown on Si buffer layers substrates⁽⁶⁾. We found that the length of bent segment of dislocation increases with the strain level in the SLS. Also, the combined effect of SLS and annealing was studied. Annealing in this case will enhance the activated process of bending dislocations. We have found that annealing allows better confinement of dislocations to the strained interfaces.

The above model is experimentally confirmed only on the microscopic level, does not however, address the question of how far the bent dislocations stay at the strained interface? For low dislocation density (less than $10^4/\text{cm}^2$), the dislocation-dislocation interactions at the strained interfaces is not very likely, thus a bent dislocation remains at the strained interface. On the other hand for high dislocation density (higher than $10^6/\text{cm}^2$) dislocation-dislocation interactions at the strained interfaces is very likely that will result in the upward threading of some these dislocation.

In summary, the minimum critical thickness in a strained-layer structure for bending threading dislocations is predicted by an energy model. The model indicates that the bending process can be thermally activated. This conclusion agrees with our experimental results, where thermal annealing of SLSs grown on GaAs/Si improved their efficiency in blocking threading dislocations by an order of magnitude. These results allow us to

develop more understanding of the role of SLS in blocking dislocations and improving the quality of epitaxial layers.

References

1. L.W. Mathews and A.E. Blakeslee, *L. Cryst. Growth*, **32**, 265 (1976).
2. 7 L.P. Hirth, *S. Afr. L. Phys*, **9**, 72 (1986).
3. L.H. Van der Merwe and C.A.B. Ball in *Epitaxial Growth*, edited by L.W. Matthews academic, N.Y. 1975.
4. 7 F.R.N. Nabarro in *The Theory of Crystal Dislocation* (Oxford University, Clarendon, 1967).
5. L.P. Hirth and L. Lothe in *Theory of Dislocation*, 2nd ed. (Wiley, N.Y. 1982).
6. 7 N.A. El-Masry, L.C. Tarn and S.M. Bedair, *Appl. Phys. Lett.*, **55**, 1442 (1989).

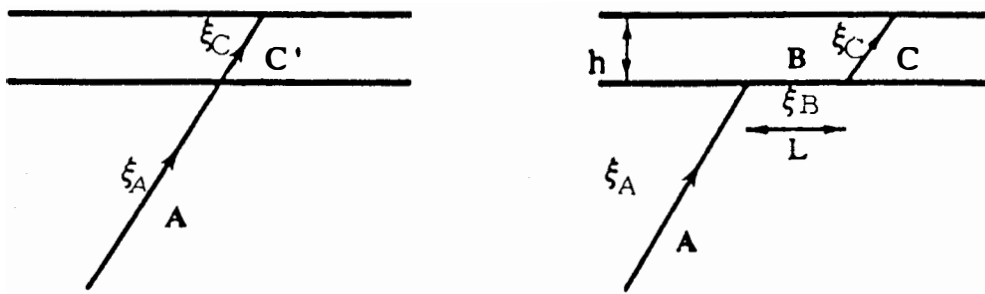


Figure 1. Two configurations of threading dislocations in a strained layer a) without a misfit dislocation segment b) with a misfit dislocation segment.

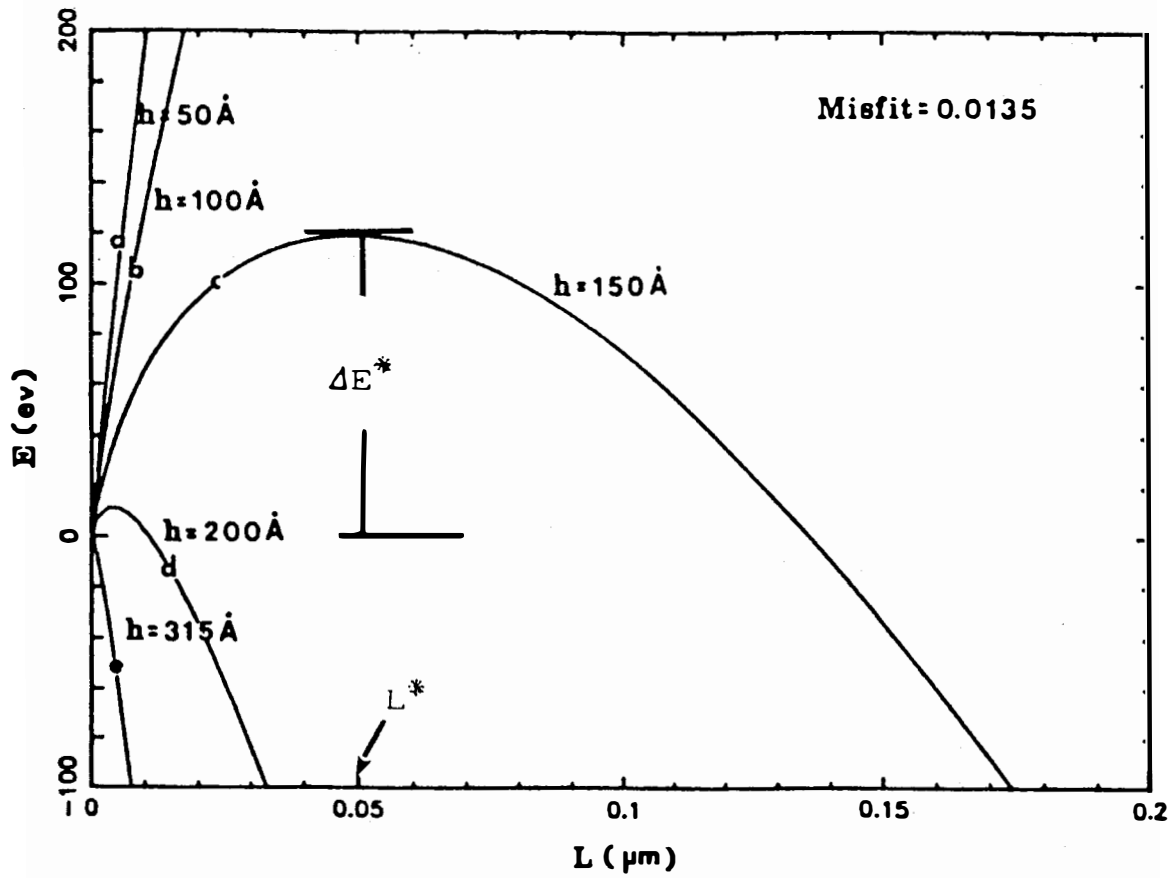


Figure 2. Change of the total energy (ΔE) with the length of the misfit dislocation L for different layer thicknesses.

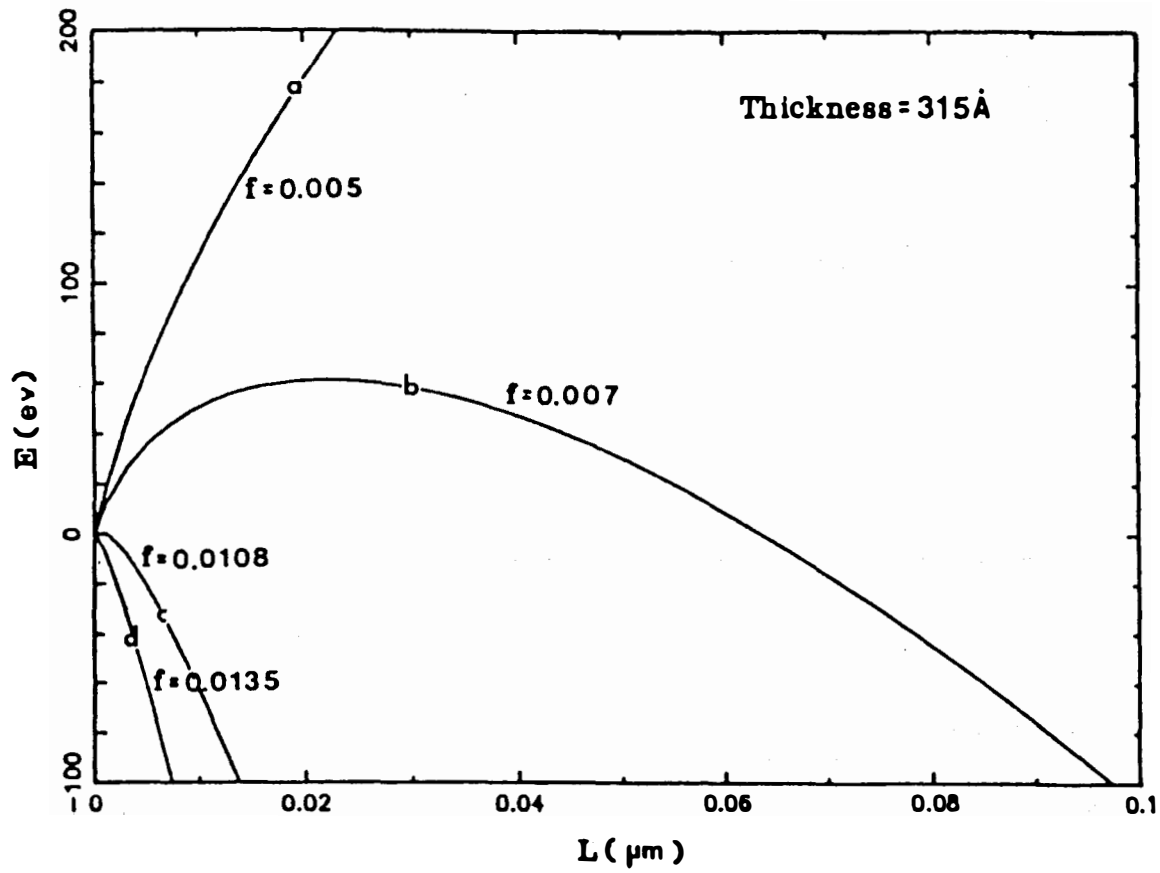


Figure 3. Change of the total energy (ΔE) with the length of the misfit dislocation L for different misfit f .

Title: **Fundamental Studies of Defect Generation in Amorphous Silicon Alloys Grown by Remote Plasma-Enhanced Chemical-Vapor Deposition (Remote PECVD)**

Organization: Departments of Physics, and Materials Science and Engineering,
North Carolina State University
Raleigh, North Carolina 27695-8202

Contributors: Professor Gerald Lucovsky, Principal Investigator;
Professors Robert J Nemanich and Jerzy Berhnolc,
Contributors; Greg Parsons, Cheng Wang, Brian
Davidson and Merideth Williams, Graduate Students

Introduction

Research under this sub-contract, XM-9-18141-2, was begun on 01 July 1989. The research reported below addresses research issues relevant to the tasks that define Phase I of this three-year program. This research has been reported at the 1989 ICALS/ICAST Conferences/Asheville NC, August 1989; and has been submitted for presentation at the MRS Spring 1990-Amorphous Silicon Symposium.

Hydrogen Incorporation in a-Si:H Thin Films

We have shown that if the incorporation of hydrogen in a-Si:H thin films is controlled by a surface reaction, as in the glow-discharge (GD) deposition process, reactive magnetron sputtering (RMS) and Remote PECVD, that: i) the amount of hydrogen incorporated in the film is determined by an availability factor, that is characteristic of the particular deposition process, GD, RMS or Remote PECVD; and ii) the substrate temperature, which determines the fraction of the available hydrogen atoms retained in the the film at a given T_S . The distribution of bonded hydrogen between mono- and polyhydride bonding groups is determined primarily by the fraction of hydrogen incorporated under the particular combination of deposition conditions, and is not an intrinsic function of any of the deposition variables, as for example, the substrate temperature, T_S , the concentration or flow rate of SiH_4 , etc.

This is illustrated in Figs. 1 and 2, which shown the relative concentrations of mono- and polyhydride groups in a-Si:H produced by the GD and Remote PECVD processes as function of T_S , in Figs. 1(a) and (b), and the total hydrogen concentration, [H], in Figs. 2(a) and (b). The solid lines in Figs. 2(a) and (b) are derived from a statistical model that is used to compute the probabilities of isolated and connected Si-H bonding sites. These comparisons between the model calculation and the GD and Remote PECVD data are further reinforced by similar results for a-Si:H deposited by RMS. Taken together they establish that the monohydride/polyhydride ratio, which provides a measure of film quality can be controlled in a given deposition process by controlling the availability of hydrogen for incorporation into the film. The differences between the GD and Remote PECVD curves in Fig. 1(a) and (b) simply derive from different hydrogen availability factors that are determined by different chemical

reaction pathways in the way the silane reactant is utilized. A second factor contributing to electronic quality is a relaxation process that contributes to defect reduction. This can take place during deposition, or afterwards, and is discussed in the next section.

Defect Reduction in a-Si:H via Thermal Relaxation Processes

Incorporation of bonded-hydrogen can result in a reduction of electronic defects in sputtered and plasma-deposited a-Si:H thin-films. Thermal relaxation of metastable photo-induced defects has also been linked to hydrogen motion. We have prepared hydrogenated ([H] = 5-15 at.%) and unhydrogenated a-Si films by magnetron sputtering at a substrate temperature, T_S , = 40°C, and have studied the kinetics of defect reduction by monitoring the dark dc-conductivity, σ_D , for annealing temperatures, T_A , between 150 and 240°C. For hydrogenated a-Si:H with [H]=14 at.%, we find an initial rapid increase in σ_D followed by a slower increase and then saturation; the rate of change of σ_D increases with increasing T_A . A defect reduction process with the same kinetics is found for the annealing of light-soaked films [H=14 at.%] deposited at 240°C. After "complete" annealing, the defect density in a film with [H]=14 at.%, and deposited at 40°C, was $5 \times 10^{15} \text{ cm}^{-3}$ as determined from sub-bandgap absorption, a reduction of >100 compared to the as-deposited state (see Fig. 3). For the annealing of unhydrogenated a-Si, σ_D initially decreases rapidly, followed by a slower decrease. We find that the initial rates of change in σ_D , for times < 20 min, in unhydrogenated a-Si and at T_A = 150°C or 175°C, are the same, at the same T_A 's, as for a-Si:H with [H]~14 at.% (see Fig. 5). This suggests the same annealing process occurs initially in a-Si:H, and is independent of the hydrogen content. For longer annealing times, the change in σ_D is faster in a-Si:H films suggesting that hydrogen plays a role, but only for longer annealing times.

Deposition Process Windows for Electronic-Quality a-Si:H by GD and Remote PECVD

We have found that material produced by the Remote PECVD process for T_S between about 150 and 200°C is superior to GD material deposited in the same range of T_S , and that materials deposited by Remote PECVD in the temperature range between about 225 and 250°C have essentially the same electronic properties as GD materials deposited at the same T_S . These results can be understood in terms of the discussions given above, specifically: 1) the incorporation of bonded hydrogen, and defect relaxation can either be accomplished during film deposition, as in the GD process, or in two separate steps; and 2) that the improved performance of the Remote PECVD films is determined by two factors: (a) the lower bonded hydrogen concentrations, and therefore lower fractions polyhydride bonding groups, which result from the specific nature of the heterogeneous surface reactions in the Remote PECVD process, and (b) the significant amount of annealing and defect relaxation that takes place during film growth at temperatures between 150 and 200°C. Even though a similar amount of annealing may take place in GD films deposited at these same temperatures, the higher bonded hydrogen concentrations, and higher polyhydride bonding fractions, produce too high a concentration of defects for the annealing to be effective.

Doping of Remote PECVD Hydrogen Amorphous Silicon Thin Films

Intrinsic, and doped hydrogenated amorphous silicon (a-Si:H) for device applications are typically produced by glow discharge (GD) deposition, where both the silane and the dopant gases are directly plasma-excited. In the remote PECVD process for intrinsic a-Si:H, silane is introduced downstream from an rf-excited helium plasma, yielding films with a factor of two less hydrogen at substrate temperatures between about 100 and 300°C, but similar electronic properties as device-quality GD films. We have extended the remote PECVD process for the deposition of doped a-Si:H by introducing either the diborane or phosphine dopant source gas downstream with the silane [$B_2H_6/SiH_4=10^{-3}$ to 10^{-1} and $PH_3/SiH_4=10^{-4}$ to 10^{-2}]. We have studied electronic properties of the doped films, including photoconductivity, and the dark conductivity activation energy, E_a . In addition, chemical properties have been studied using infrared and Auger electron spectroscopy, and the relationship between dopant-gas/silane ratios in the gas phase and dopant-atom/silicon-atom ratios in the film bulk will be presented. Doping by P and B-atoms increases the room-temperature dark conductivity by a factors up to 10^7 , and decreases E_a from 0.8 eV for undoped films to <0.2 eV for n-type films [$PH_3/SiH_4=10^{-2}$] and <0.3 eV for p-type films [$B_2H_6/SiH_4=0.1$] (see Figs. 4(a) and 4(b)). The relationship between dopant-gas/silane feed gas ratios, and the room-temperature dark conductivity is the same in the Remote PECVD films as for the n- and p-doped GD films. To demonstrate the electronic quality of the Remote PECVD intrinsic and doped films, we have applied the remote PECVD process to form TFT device structures as is discussed below.

Deposition of μ -Crystalline Silicon by Remote PECVD

We are currently investigating remote PECVD, and RMS as alternative deposition techniques to glow discharge decomposition (GD) for the formation of a-Si devices that include photovoltaics and thin-film transistors. As a part of this effort, we have demonstrated that μ c-Si can be deposited by both RMS and Remote PECVD. We have used Raman scattering and transmission electron microscopy (TEM), specifically differences between bright and dark-field images, to identify and characterize the μ -crystalline character of deposited thin films. For RMS, we find two different conditions for the deposition of μ c-Si. These are: 1) at high substrate temperature, $T_S \geq 540^\circ\text{C}$, independent of the dilution of Ar by H_2 ; and 2) at T_S as low as 200°C , but only for significant H_2 dilution of Ar ($>$ about 2:1). Films of μ c-Si have also been deposited by Remote PECVD with T_S as low as 250°C . This is accomplished by plasma-exciting mixtures of 40% H_2 and 60% He (with a combined flow rate of ~ 280 sccm), and then mixing the active species extracted from the plasma (H-atoms, electrons, He^+ ions, etc.) with down-stream injected silane (flow rate of 1 sccm). TEM imaging shows that there are sometimes significant amorphous regions ($>500\text{\AA}$ thick) between the substrate (crystalline Si or fused silica) and the onset of μ -crystallinity. We are currently investigating the factors that contribute to the formation of these transition regions. Our preliminary results suggest two different mechanisms for μ c-Si formation. The first involves processes in which a combination of high hydrogen dilution and high deposition temperatures leads to a near equilibrium between etching and deposition; this leads to film deposition without a transition region. The other mechanism involves deposition of an amorphous phase, with a solid state crystallization that is driven by a

relatively slow thermal annealing process at the growth temperature, i.e., slow annealing and crystallization with respect to the rate of film deposition. We plan to extend these studies to the optical and electronic properties of boron and phosphorous doped $\mu\text{c-Si}$.

Studies of a-Si:H,O and a-Si:H,N Formed by Remote PECVD

We have established deposition process procedures for the formation of alloys of Si,O,H and Si,N,H with variable concentrations of O and N respectively. Using O_2 and N_2 as the source gases, we find that a higher incorporation of bonded O, relative to bonded N, for the same gas phase ratios of O_2 and N_2 flow relative to silane flow. This is anticipated based on differences in the effectiveness in generating active oxygen and nitrogen precursors.

We now restrict the discussion to the oxides, where we have so far made the most extensive studies of the chemical bonding and electronic properties. We have used the frequency of the Si-O stretching vibration to monitor the film composition, and have found that the relative oxygen concentration (x in the alloy SiO_x) is approximately linear in O_2 gas flow. For x between 0 and 1, there is a relatively slow increase in the band-gap, whereas for $x > 1$ the gap increases more rapidly (our results agree with H. Philipp). For sub-oxides with band-gaps less than about 1.85 eV, the dark conductivity activation energy is less than $E_g/2$, whereas for band-gaps greater than 1.85 eV, it is larger than $E_g/2$. For x between 0.0 and 0.7, the photoconductivity drops by about a factor of two, and then it drops by more than three orders of magnitude between $x = 0.7$ and $x = 1.1$.

Formation of a-Si TFT's

Thin films of intrinsic and doped device-quality hydrogenated amorphous silicon (a-Si:H), as well as device quality SiO_2 and Si_3N_4 can be deposited by remote plasma-enhanced chemical-vapor deposition (Remote PECVD) at substrate temperatures between 200 and 250°C. Inverted staggered TFT's were prepared in a multichamber UHV-compatible system that currently provides: 1) sequential deposition of dielectrics, and intrinsic and doped a-Si:H by Remote PECVD in a single deposition chamber; and 2) in-situ surface analysis by Auger Electron Spectroscopy; and will shortly provide 3) in-situ metallization by magnetron sputtering. A series of a-Si thin-film devices have been fabricated using a 3-mask process. Thin films of a gate dielectric (SiO_2 or Si_3N_4), intrinsic a-Si:H, and P-doped n^+ a-Si:H were deposited onto Cr-patterned fused-silica substrates using Remote PECVD. Cr was sputter-deposited (1000Å) for the ohmic contact to the n^+ a-Si:H, and was also used as an etch mask for the active-area patterning. The Cr and n^+ layers in the channel area were removed by using patterned source and drain Al electrodes (~1 μm thick) as an etch mask. A field-effect electron mobility of 0.74 $\text{cm}^2/\text{V-s}$ and a threshold voltage of 2.5 volts have been measured at room temperature in the TFT's. We plan to compare defect generation by light soaking in bulk a-Si:H, and in p-i-n device structures, and by stress bias in TFT structures.

Deposition of a-Si,Ge:H Alloys by Remote PECVD

We have established that a-Si,Ge:H alloy films can be produced by the Remote PECVD process. Deposition is accomplished by: i) remote plasma excitation of He; ii) extraction of active species from the He discharge; these are mostly He⁺ ions, and electrons; iii) activation of a down-stream injected mixture of He diluted (10:1) silane and germane gases; and iv) film deposition on a heated substrate. We have so far deposited thin films of a-Si:H, a-Si,Ge:H and a-Ge:H, under the same effective flow rates. We find that films the a-Si:H films deposited at approximately 150°C do not show significant polyhydride incorporation, whereas a-Si,Ge:H alloys (about 50-50) display significant polyhydride incorporation. We believe that this results from gas phase reactions between activated silane and gemane species prior to film deposition. This will be investigated in our deposition analysis system using mass spectrometry.

Modelling of Weak Si-Si Bonding Arrangements

High densities of electronic states in the energy gap of a-Si can degrade the transport of the charged carriers. We have used a tight-binding Hamiltonian and Bethe lattice structures, and have investigated the formation of defect states in the gap of a-Si arising from deviations from ideal tetrahedral bond angles. The local density of states (LDOS) for Si atoms in disordered environments is calculated using a cluster-Bethe lattice method (CBLM). We use the tight-binding parameters for a nearest neighbor sp³s* orbital basis set that have been obtained by a fit to the crystalline Si band structure. These same parameters yield a gap of 1.8 eV for an a-Si Bethe lattice with perfect tetrahedral angles, which we use as a reference for an idealized a-Si. The Hamiltonian, for a-Si with bond-angle distortions ($\delta\Theta$) is then taken as an average over configurations associated with a random choice of bond-angles, weighted by Gaussian distributions with average deviations between 5 and 15 degrees. Bond angle deviations in this range generate a density of defect states at the valence band (VB) edge that: i) increases as the average bond angle deviation increases ($\Delta E=0.2$ eV for $\delta\Theta_{av} = 10$ degrees); and ii) is significantly larger (by a factor of at least 3-5) than the density of band tail states generated at the conduction band edge. In addition, a calculation of the LDOS for a distorted tetrahedral cluster embedded in an idealized Bethe lattice yields a threshold bond angle distortion of $\pm 20^\circ$ for the appearance of a discrete state in the gap near the VB edge. We also use the CBLM to determine shifts in the position of a neutral dangling bond associated with bond angle distortions. Our results demonstrate that disorder in a-Si due to bond-angle deviations can generate a density of defect states in the lower half of the gap of the same magnitude as has been detected by a variety of different experimental techniques.

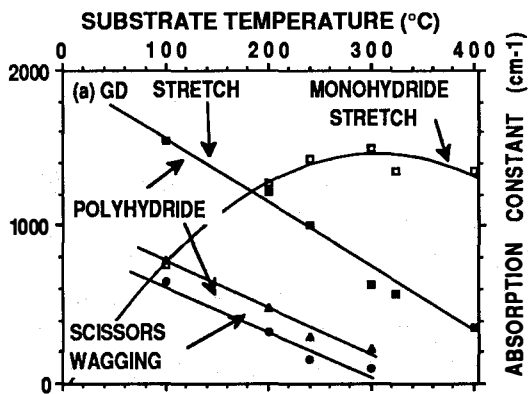


FIG. 1(b) IR Absorption in GD a-Si:H versus Substrate Temperature (°C)

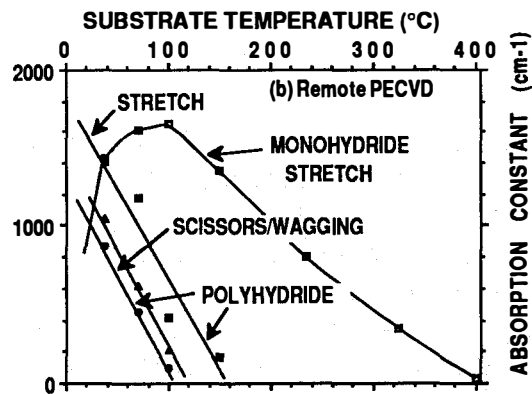


FIG. 1(a) IR Absorption in Remote PECVD a-Si:H versus Substrate Temperature (°C)

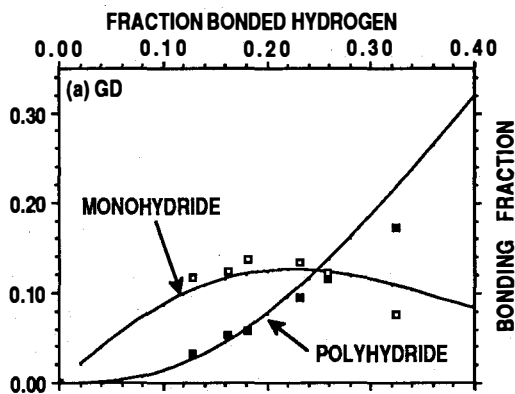


FIG. 2(a) Bonding Fraction Monohydride and Polyhydride versus Total Hydrogen

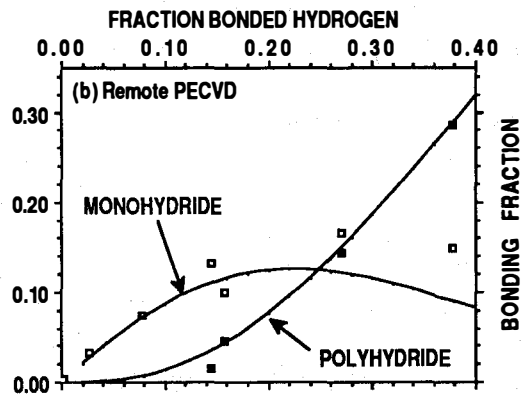


FIG. 2(b) Bonding Fraction Monohydride and Polyhydride versus Total Hydrogen

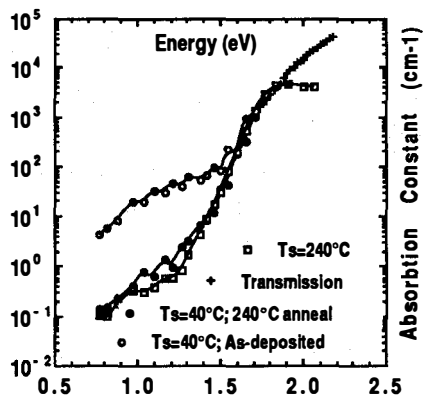


FIG. 3 Optical Absorption Constant versus Photon Energy: Transmission and CPM

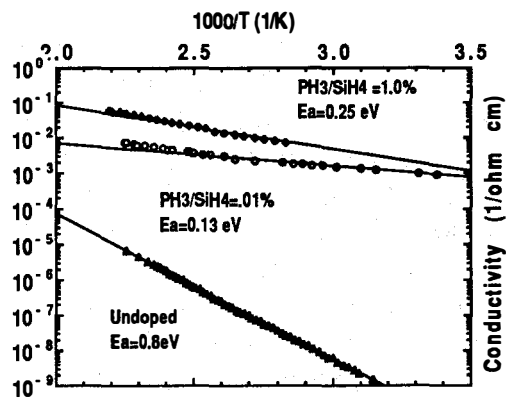


FIG. 4(a) Conductivity versus 1/T(K) Phosphorus Doped a-Si:H

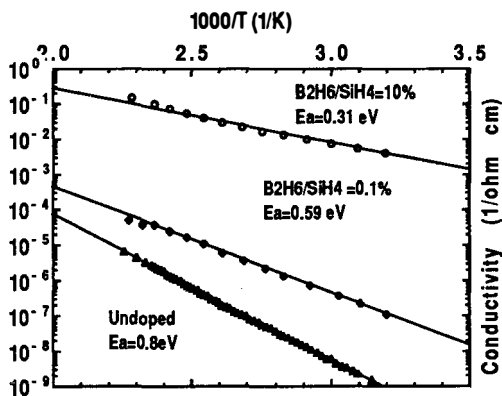


FIG. 4(b) Conductivity versus 1/T(K) Boron Doped a-Si:H

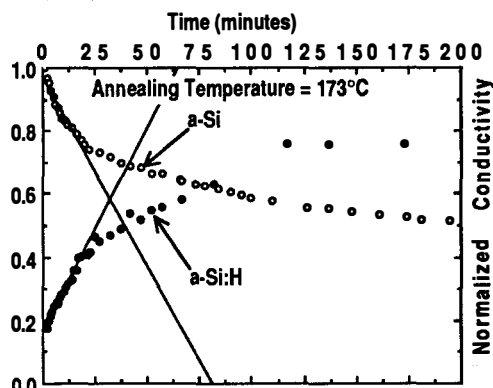


FIG. 5 Conductivity Relaxation in a-Si and a-Si:H versus Annealing Time (minutes)

Title: Ion-Assisted Deposition Doping of p-CdTe

Organization: Department of Materials Science and Engineering, Stanford University
Stanford, CA 94305

Contributors: R.H.Bube (Principal Investigator), A. L. Fahrenbruch, M. Grimbergen,
D. Kim, A. Lopez-Otero, and P. Sharps

The purpose of this work is to investigate ion-assisted physical vapor deposition of p-CdTe and to determine the influence of co-doposition of ionized dopant atoms on the growth, structural, and photoelectronic properties of the deposited films.

Method of Approach

Primary problems for the utilization of polycrystalline p-CdTe based solar cells are those of obtaining sufficiently low series resistance and high V_{oc} . Sufficiently increasing the p-type doping density in the CdTe would lower both bulk and contact resistivity. Control of V_{oc} has been obtained by variation of the relative doping levels in CdS and CdTe [2] for single-crystal based solar cells; thus control of p-type doping promises to be a tool for maximizing V_{oc} in polycrystalline cells as well.

Many of the dopants successfully used in bulk semiconductor growth present problems in the case of film growth from the vapor due to low incorporation probabilities and/or surface segregation. However, impingement of low-energy dopant ions on the growing film during deposition can be used to significantly increase the sticking probability and/or incorporation of the dopant species [1,3].

Our apparatus consists essentially of an ion source, a movable Faraday cup to monitor ion current, an effusion cell for CdTe, and a heated substrate holder, all situated in a vacuum system with a base pressure during deposition of $\approx 6 \times 10^{-8}$ Torr. The ion source uses a BN Knudsen cell to supply the dopant atoms and an ionizer section with a W filament and a graphite anode and grid. Elemental As and P have been used as dopants. Epitaxial CdTe films were grown on single-crystal n- and p-CdTe substrates at typical rates of 0.1-0.3 $\mu\text{m}/\text{min}$ and substrate temperatures $T_{\text{sub}} = 300\text{-}500^\circ\text{C}$. Polycrystalline films on graphite and 7059 glass have also been grown.

Significant Results

Results on junction transport mechanisms for diodes prepared using the epitaxial films, elucidation of the deep states using DLTS, and properties of n-CdS/p-CdTe solar cells were used to characterize the films. For example, for the homoepitaxial layers, using an ion energy of 60 eV, the carrier density (measured using $1/C^2$ vs. V plots) increased smoothly with increasing ion current reaching a plateau of $\approx 10^{17} \text{ cm}^{-3}$ at an ion current of $\approx 0.5 \mu\text{A}/\text{cm}^2$ [4] (e.g., Fig. 1). For ion currents larger than $\approx 2 \mu\text{A}/\text{cm}^2$ the carrier density decreased sharply and the deep level density increased.

The carrier density typically increased sharply with substrate temperature from 350 to 350°C , then decreased slowly with increasing substrate temperature up to 500°C (e.g., Fig. 2). As a function of ion energy E_{ion} , the carrier density remained relatively constant (e.g., Fig. 3), in contrast with previous results which showed a decrease for $E_{\text{ion}} > 100 \text{ eV}$.

Results from n-CdS/p-CdTe solar cells on ion doped material, Fig. 4 [see also 5,6], showed an increase in the quantum efficiency with decreased doping. This is due to (a) increased depletion layer width with lower doping density, which increases the region of junction-field aided collection, and (b) a reduction of

minority carrier diffusion length by doping, possibly by ion damage, even at the relatively low ion energies used.

In related work, the near-surface reduction of carrier density in p-CdTe:P on heat treatment at temperatures above $\approx 400^\circ\text{C}$ is explained by compensation by formation of P_{Cd} anti-site donors, and not by out-diffusion of P [7].

Conclusions

Our results show that controlled doping in p-CdTe epitaxial films up to $\approx 6 \times 10^{16} \text{ cm}^{-3}$ for ion-assisted deposition with As ions and up to $\approx 10^{17} \text{ cm}^{-3}$ for P has been achieved using ion energies of 30-300 eV. For P, using a growth rate of $\approx 0.15 \mu\text{m}/\text{min}$, a substrate temperature of 450°C , and an ion energy of 80 eV, a maximum in carrier density of $2 \times 10^{17} \text{ cm}^{-3}$ is obtained for an ion current of $0.7 \mu\text{A}/\text{cm}^2$, corresponding to $\approx 1.5\%$ of the impinging P ions being electrically active in the deposited film [5,6].

-
1. J.E. Greene and S.A. Barnett, J. Vac. Sci. Technol. **21**, 285 (1982).
 2. C.M. Fortmann, A.L. Fahrenbruch, and R.H. Bube, J. Appl. Phys. **61**, 2038 (1987).
 3. N. Matsunaga, T. Suzuki, and K. Takahashi, J. Appl. Phys. **49**, 5710 (1978).
 4. A. Fahrenbruch, A. Lopez-Otero, P. Sharps, and R.H. Bube, Proc. 19th IEEE Photovoltaic Spec. Conf. (1987) p. 1309.
 5. P. Sharps, A.L. Fahrenbruch, A. Lopez-Otero, and R.H. Bube, presented at Materials Research Society Meeting, Boston, 11/29-12/2/88. To be published, Vol. 28A, MRS Symposium Proceedings.
 6. P. Sharps, A.L. Fahrenbruch, A. Lopez-Otero, and R.H. Bube, Proc. 20th IEEE Photovoltaic Spec. Conf. (1988).
 7. D. Kim, A.L. Fahrenbruch, and R.H. Bube, Proc. 20th IEEE Photovoltaic Spec. Conf. (1988).

Also see: Final Report, "Ion-Assisted Doping of II-VI Compounds During Physical Vapor Deposition," 9/1/'85 to 8/30/89. Draft dated 9/22/89.

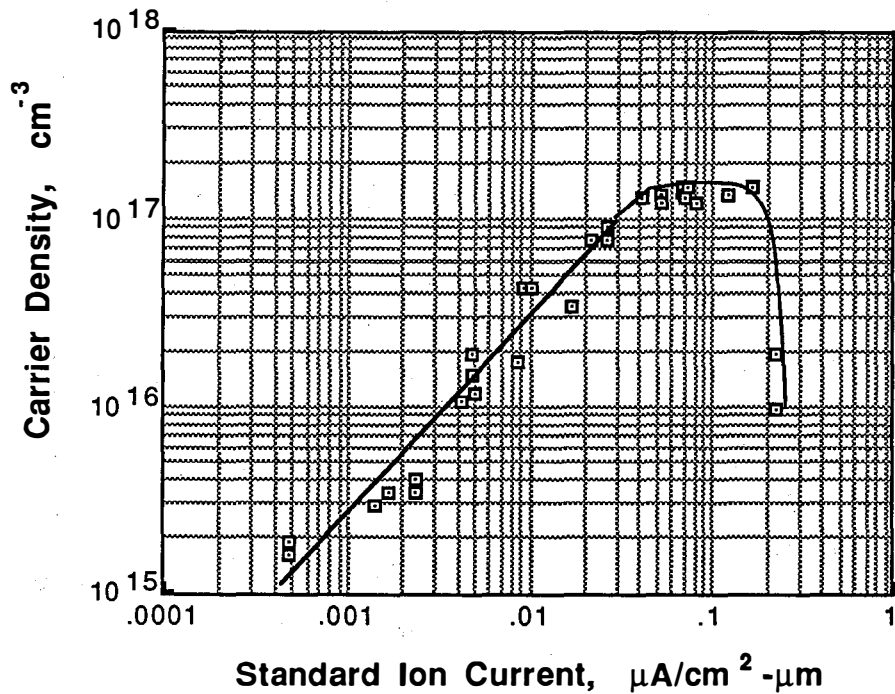


Figure 1. Carrier density as a function of "standard" ion current for an ion energy of 60 eV and a growth temperature of 400°C. [Because of variability in the thickness of the films, the ion current was divided by the film thickness ($\approx 10 \mu\text{m}$) to standardize it.]

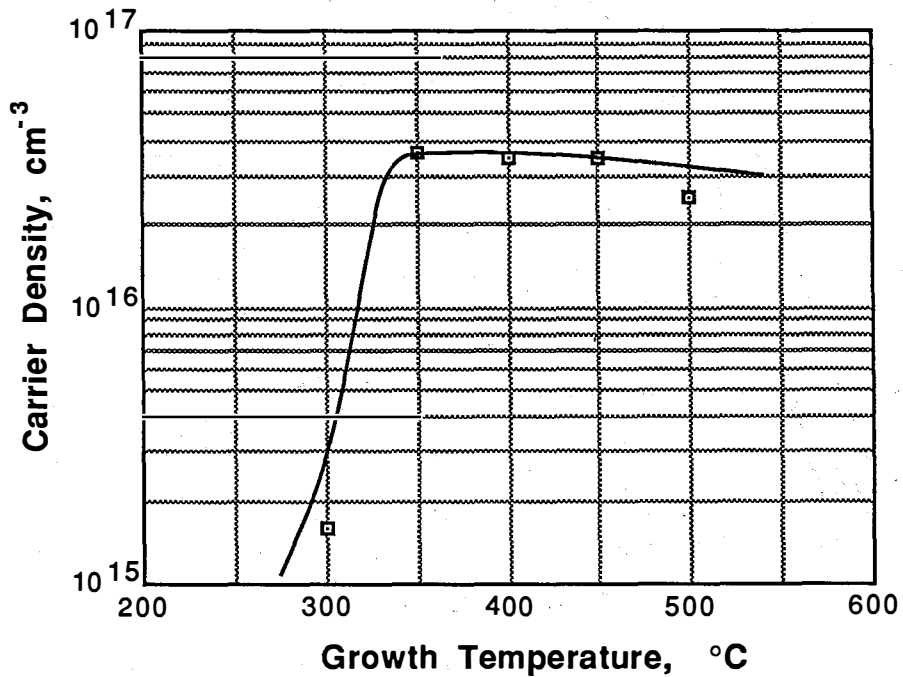


Figure 2. Carrier density as a function of substrate temperature for an ion energy of 60 eV, and a "standard" ion current of $\approx 0.02 \mu\text{A}/\text{cm}^2\text{-}\mu\text{m}$.

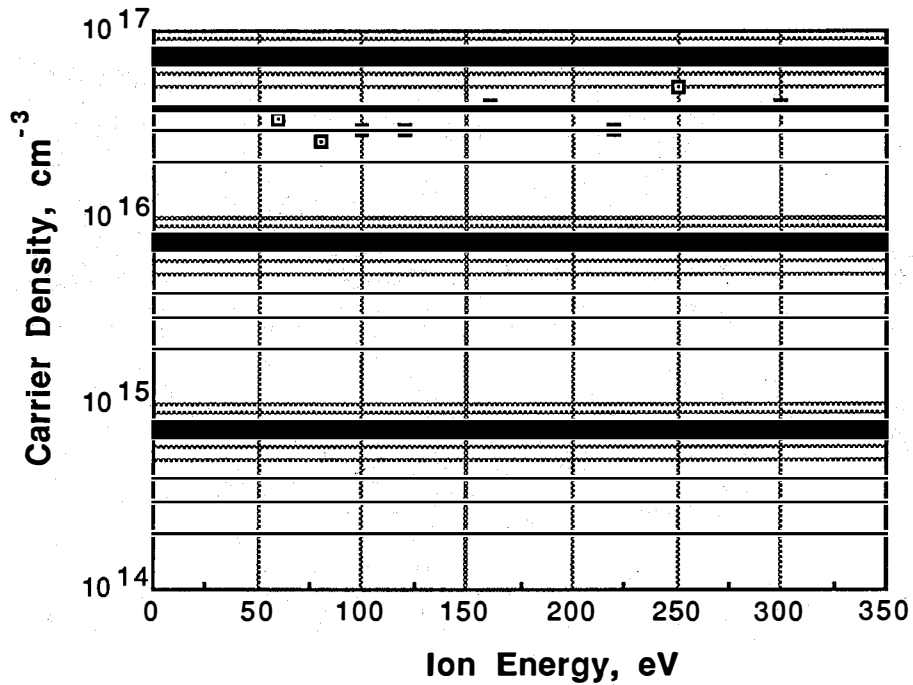


Figure 3. Carrier density as a function of ion energy for a substrate temperature of 400°C, and a "standard" ion current of $\approx 0.02 \mu\text{A}/\text{cm}^2\text{-}\mu\text{m}$.

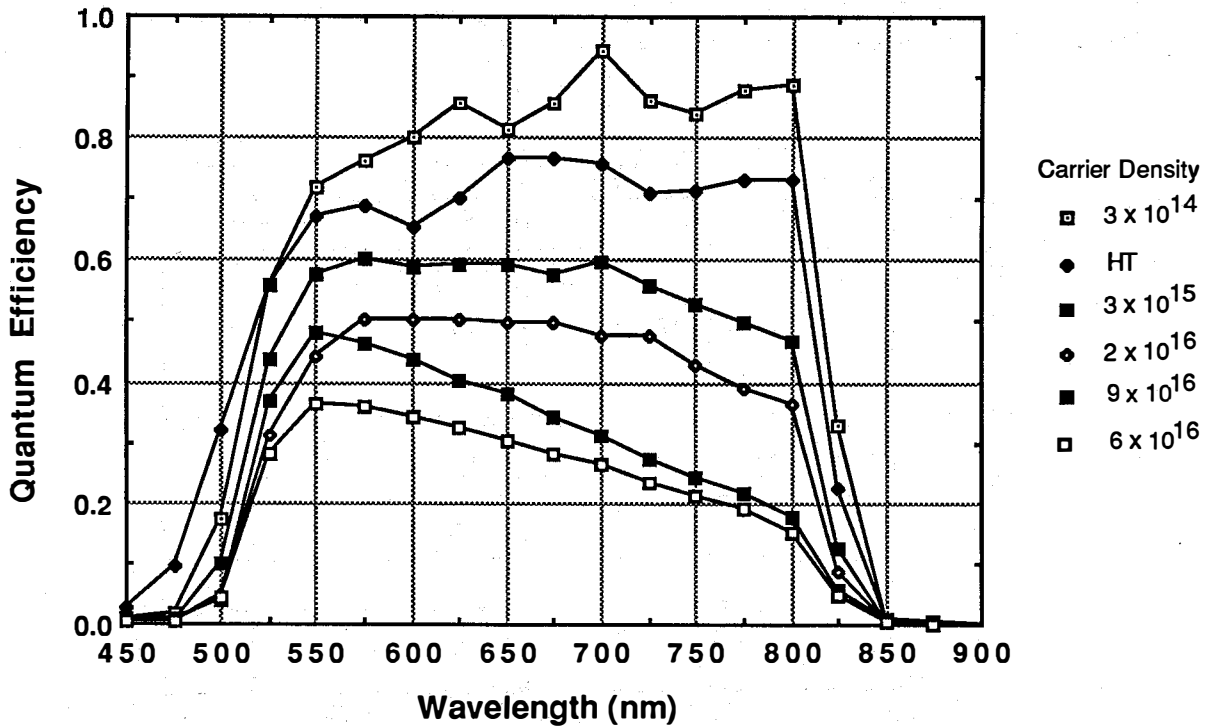


Figure 4. Quantum efficiency spectra for n-CdS/p-CdTe solar cells with an ion doped CdTe layer adjacent to the CdS. The carrier density of the ion-doped CdTe layer is given in the legend. The device marked "HT" was made using an ion-doped layer grown simultaneously with the $9 \times 10^{16} \text{ cm}^{-3}$ layer but heat-treated at 425°C in H_2 for 5 min prior to CdS deposition.

Title: Carrier Processes in Hydrogenated Amorphous

Organization: Department of Physics, Syracuse University, Syracuse, NY 13244

Contributors: Eric A. Schiff, principal investigator; Homer Antoniadis, Steven Hotaling, Jung-Keun Lee, and Sufi Zafar.

Project Objectives and Research Approaches

The materials studied in this project are hydrogenated amorphous silicon-germanium alloys. The project aims to identify the defects which limit photovoltaic applications to of these materials and to determine the origins of these defects. It is our intention that this work will either suggest strategies for improvement of these materials or establish that the defect densities are fundamental. The two principal research approaches are:

- (i) **Studies the D -center defect in $a\text{-Si:H}$ and $a\text{-Si}_{1-x}\text{Ge}_x\text{:H}$.** Although it is generally accepted that there is a good correlation between the density of " D -centers" and the electron properties of these materials, there is as yet no satisfactory explanation for the processes which lead to defect creation during growth of hydrogenated amorphous alloys, nor for the subsequent degradation processes which have limited the efficiency of single-junction and tandem solar cells fabricated from these materials.

The experimental research associated with this objective primarily involves electron spin resonance of the D -center; our silicon-germanium alloys have also been studied using infrared *photomodulation spectroscopy* by Tauc' group at Brown University. These measurements have led us to investigate *hydrogen-mediated defect density models* for $a\text{-Si:H}$. At present our view is that hydrogen is involved in defect reactions in $a\text{-Si:H}$; our future research will attempt to better establish this view and to explore strategies for materials improvement based upon it.

- (ii) **Studies of photocarrier transport and recombination.** We seek to establish a complete picture for the evolution of photocarriers from photogeneration until recombination, and to relate this picture to deep level information obtained from electron spin resonance and other measurements.

The experimental research associated with this objective primarily involves measurements of *photocarrier drift* in an electric field as a function of time following generation. These measurements have now been carried out over a time range of 10^{14} (from 1 ps to 100 s); the picosecond domain measurements were executed at Prof. Tauc' laboratory at Brown University. Our measurements show that electron deep-trapping on the microsecond time scale does *not* limit electron transport; electrons are re-emitted at about 1-10 ms at 300 K. We have also better established the correlation between electron & hole transport and the D^0 density. Future research will study the relationship between hole deep-trapping and recombination.

In the remainder of this document we present summaries of our research in four areas:

Temperature dependent spin density in $a\text{-Si:H}$
Hydrogen-mediated models for defect metastability in $a\text{-Si:H}$
ESR defect lineshape in $a\text{-Si}_{1-x}\text{Ge}_x\text{:H}$
Electron photocarrier drift in $a\text{-Si:H}$

Temperature-dependent spin density measurements in a-Si:H.

It has proven difficult to determine the origin of illumination-induced defects in a-Si:H by direct study of this process. Smith and Wagner [1] suggested an alternate approach to the general problem of defect metastability in a-Si:H when they observed that the electronically active density of defects might be in thermal equilibrium with a *defect pool*. This line of research has the advantage that thermal equilibrium models are simpler to formulate and test than the non-equilibrium models required to account for illumination effects. Smith, *et al* also offered limited experimental evidence supporting their view. Several more elaborate experimental studies of this effect have now been executed. In general these studies find significant temperature-dependence above about 200 C, which is a characteristic "freezing" temperature. Some of the work of this project is summarized in Fig. 1 [2], which shows the temperature-dependent spin density for several specimens of a-Si:H. We find for specimens with moderate to low spin densities ($< 10^{18} \text{ cm}^{-3}$) that the spin density is simply activated ($E_a \cong 0.3 \text{ eV}$). Our measurements are comparable to results reported by researchers at Xerox PARC [3] and at Kanazawa University [4]; there are differences in detail, in particular regarding the accuracy of the thermally activated form.

A Two-phase Model for Hydrogen-Mediated Defect Metastability.

The defect pool idea is not microscopically specific regarding the identity of its constituents or the mechanism through which thermal equilibrium is established. Several experiments by the Xerox PARC group correlating the relaxation kinetics of excess defect densities with hydrogen diffusion have suggested that hydrogen diffusion is the mechanism for establishment of equilibrium, and thus that the varying states of the defects in a-Si:H are hydrogen bonding states; the view is that a-Si:H is a *hydrogen glass* [5]. In our research we assumed the broad validity of the hydrogen-glass model as a description for the *D*-center density in a-Si:H. We have constructed [6] a specific version of this model based upon the two hydrogen phases found by nuclear magnetic resonance: a *clustered* phase consisting of clusters of about six bonded hydrogen atoms, and a *dilute* phase consists of isolated bonded hydrogen atoms [7].

We assumed that the observed spins are unhydrogenated sites (dangling bonds) in the dilute phase, and that unhydrogenated sites in the clustered phase are not detected by ESR because of a *negative hydrogen correlation energy* property. This property would result if the first hydrogen bound to a site in the clustered phase is more weakly bound than the second; the configuration coordinate diagram we proposed is presented in Fig. 2.

This model was originally devised to account for the fact that only a single paramagnetic site seems to be associated with defect metastability. Our calculations showed that the model is compatible with the thermally activated spin density; the activation energy is interpreted as the difference in the average hydrogen binding energy of the two phases. Perhaps the most significant success of this model is that it provides insight into hydrogen evolution measurements of Biegelsen, *et al* [8]. Roughly, these authors found that for every 1000 hydrogen atoms evolved from a-Si:H during extended thermal treatment only a single spin is created. We found that a calculation based on the two-phase model which utilized the known densities of sites from NMR and the known activation energy of the spin density gives fair agreement with the densities measured in the hydrogen evolution experiment. We are unaware of any other model which accounts for these observations; this success may be important support for the hydrogen glass view of a-Si:H.

D-Center ESR Lineshape Measurements in a-Si_{1-x}Ge_x:H.

For this project we deposited a series of specimens of a-Si_{1-x}Ge_x:H of varying composition x and conducted a thorough study of the D -center lineshape; similar research has been conducted previously, although with a rather different analytical approach [9]. Originally our intention had been simply to improve techniques for distinguishing the spectra of D -centers associated with Si and Ge atoms (Si-D and Ge-D). The identification of the D -center with a highly localized, dangling bond defect suggests that the alloy lineshape should simply be a superposition of the lineshapes observed in unalloyed a-Si:H and a-Ge:H, but this approach has proved inadequate. We unexpectedly discovered [10] a simple deconvolution of the alloy lineshape. We used a straightforward procedure of assuming that an alloy specimen's lineshape has three components: unshifted Si-D and Ge-D lines (the lineshapes measured in unalloyed materials), and an "alloy line" (GeSi-D) for which three lineshape parameters were selected by nonlinear least squares fitting.

The results for the relative contributions of these three components to the lineshape as a function of the alloy composition x are illustrated in Fig. 3, which shows that for $x > 0.3$ the Ge-D density declines essentially linearly, while the GeSi-D rises linearly. We also obtained estimates of the principal g -tensor components for these three lines. These fitting results may be rationalized if the alloy line is primarily localized on a Ge-atom, but with part of the wavefunction on a *single* Si atom; we have not been able to account for these results using the *three* backbonds of a dangling bond. One possibility is that the *top* atom to which a dangling bond points (the "top bond") may be a more important perturbation than the backbonds.

Electron Photocarrier Drift Measurements in a-Si:H

Photocarrier drift experiments measure the average displacement $x(t)$ of a carrier following its photogeneration as a function of electric field E ; since this relationship is often linear, this displacement can be written in terms of a *transient mobility-lifetime product* $\mu\tau(t)$:

$$x(t) = \mu\tau(t) \cdot E$$

The usual steady-state mobility-lifetime product is $\mu\tau(\infty)$. $x(t)$ was estimated from our measurements using two procedures. The first is conventional electrical detection technique based on the expression $x(t) = (Q(t)/Q_0) \cdot d$, where $Q(t)$ is the photocharge induced in external bias circuit, d is the interelectrode spacing, and Q_0 is the charge launched by photogeneration. The second was an equivalent optical detection technique based on the electroabsorption effect in a-Si:H [11]; optical detection permits picosecond domain measurements where electrical detection would be cumbersome or impossible.

At room-temperature and above electrons move with a well defined drift velocity [11,12] until they "deep-trapped." In present materials deep-trapping is complete before 10 μ s. Deep-trapping may be characterized by the magnitude $\mu\tau(10 \mu$ s), since the transient mobility-lifetime product is only weakly dependent upon time in this domain. $\mu\tau(10 \mu$ s) exhibits a fair inverse correlation with the spin density determined by electron spin resonance [13,14] which suggests the identification of the deep-trap with the D -center.

Remarkably, it was not until 1987 that it was noted in the literature that the steady-state value of $\mu\tau$ exceeded $\mu\tau(10 \mu$ s) in a given specimen by two orders of magnitude or more [15,16]. This discrepancy has an obvious resolution if electrons are re-emitted and re-captured by the deep traps many times prior to recombination. Although this resolution was consistent with the many reports of transient photocurrents following 10 μ s, no unequivocal measurement of the characteristic emission time was presented.

We have recently succeeded in measuring charge displacement parallel to the specimen surface over nine decades of time; these data apparently exhibit the emission process [17]. The transient photocharge is plotted for four specimens of widely varying quality are presented in Fig. 4; the data are normalized to yield the transient mobility–lifetime product. For the two better specimens there is a linear displacement at short times which corresponds to a drift–mobility of $0.6 \text{ cm}^2/\text{V}\cdot\text{s}$. This linear rise is terminated at a broad plateau during which little displacement occurs; the magnitude of the plateau is roughly inversely proportional to the spin density, in adequate absolute agreement with the original reports on deep–trapping. At about 1 – 10 ms the displacement again rises, and increases by over two orders of magnitude by 100 s. The emission time suggests a mean trap depth of about 0.5 – 0.6 eV based upon a nominal attempt–to–escape frequency of 10^{12} s^{-1} .

We have also conducted a study of the isotropy of the electron mobility–lifetime product up to 10^{-4} s using displacements parallel and perpendicular to the specimen surface. The majority of measurements are *isotropic*; we apparently misinterpreted our data when we previously claimed intrinsic electron mobility anisotropy in a–Si:H [18].

References

1. Z. E. Smith and S. Wagner, in *Amorphous Silicon and Related Materials Vol. A*, edited by H. Fritzsche (World Scientific, Singapore, 1989), p. 409.
2. Sufi Zafar and E. A. Schiff, *J. Non–Cryst. Solids*, *in press*.
3. R. A. Street and K. Winer, *Phys. Rev. B* **40**, 6236 (1989).
4. X. Xu, A. Morimoto, M. Kumeda, and T. Shimizu, in *Amorphous Silicon Technology – 1989*, edited by A. Madan, *et al* (Materials Research Society, Pittsburgh, 1989), p. 143. ž
5. James Kakalios and Warren B. Jackson, in *Amorphous Silicon and Related Materials Vol. A*, edited by H. Fritzsche (World Scientific, Singapore, 1989), p. 207.
6. Sufi Zafar and E. A. Schiff, *Phys. Rev. B* **40**, 5235 (1989).
7. Jeffrey A. Reimer and Mark A. Petrich, in *Amorphous Silicon and Related Materials Vol. A*, edited by H. Fritzsche (World Scientific, Singapore, 1989), p. 3.
8. D. K. Biegelsen, R. A. Street, C. C. Tsai, and J. C. Knights, *Phys. Rev.* **B20**, 4839 (1979).
9. F. Finger, W. Fuhs, G. Beck, and R. Carius, *J. Non–Cryst. Solids* **97&98**, 1015 (1987).
10. J.–K. Lee and E. A. Schiff, *J. Non–Cryst. Solids*, *in press*.
11. E. A. Schiff, R. I. Devlen, H. T. Grahn, J. Tauc, and S. Guha, *Appl. Phys. Lett.* **54**, 1911 (1989).
12. T. Tiedje, in *Hydrogenated Amorphous Silicon II*, edited by J. D. Joannopoulos and G. Lucovsky (Springer–Verlag, New York, 1984), p.
13. R. A. Street, *Phil. Mag. B* **49**, L15 (1984) and references therein.
14. S. Hotaling, H. Antoniadis, and E. A. Schiff, *J. Non–Cryst. Solids*, *in press*.
15. E. A. Schiff, *Phil. Mag. Lett.* **55**, 87 (1987).
16. K. D. MacKenzie and W. Paul, *J. Non–Cryst. Solids* **97&98**, 1055 (1987).
17. H. Antoniadis and E. A. Schiff, unpublished.
18. M. A. Parker and E. A. Schiff, *Phys. Rev.* **B37**, 10426 (1988).

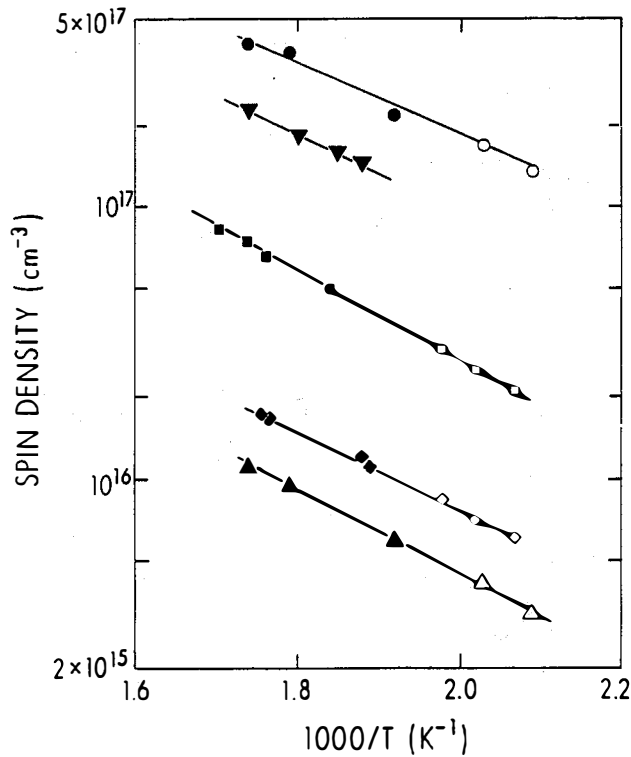


Fig. 1: Temperature dependence of the spin density in several specimens of undoped a-Si:H prepared at differing substrate temperatures; filled symbols reflect *in situ* measurements, whereas open symbols are measured following quenching to room-temperature. The activation energy and its standard deviation for these measurements are 0.30 and 0.03 eV. From *Zafar and Schiff* [2].

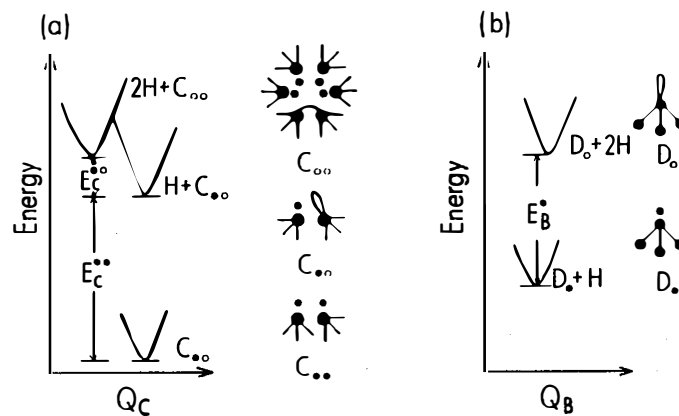


Fig. 2: Proposed structures and configuration coordinate diagrams for the two hydrogen phases observed by NMR. (a) A site of the clustered phase is envisioned as a weak Si-Si bond when unhydrogenated. Most sites are doubly hydrogenated in a-Si:H. Singly hydrogenated sites are rare in thermal equilibrium because the second bonding energy (E_C) of the site significantly exceeds the first (E_C). (b) The unhydrogenated site of the clustered phase is the *D*-center found in ESR. From *Zafar and Schiff* [14].

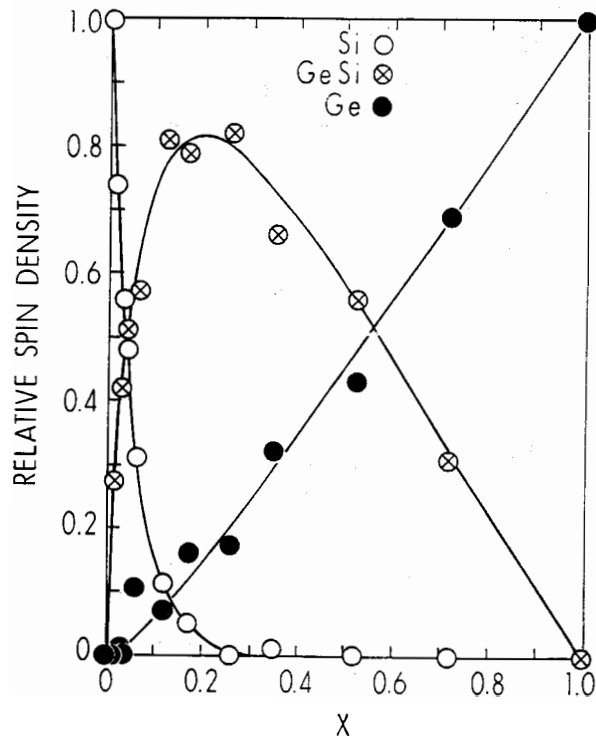


Fig. 3: Relative densities of the unshifted Si and Ge *D*-centers and the shifted alloy line (GeSi). For the range $x > 0.3$ the linear rise of the GeSi-*D* and the decline of the Ge-*D* suggests that a dangling bond wavefunction is primarily perturbed by a single atom instead of by three backbonds. *Unpublished.*

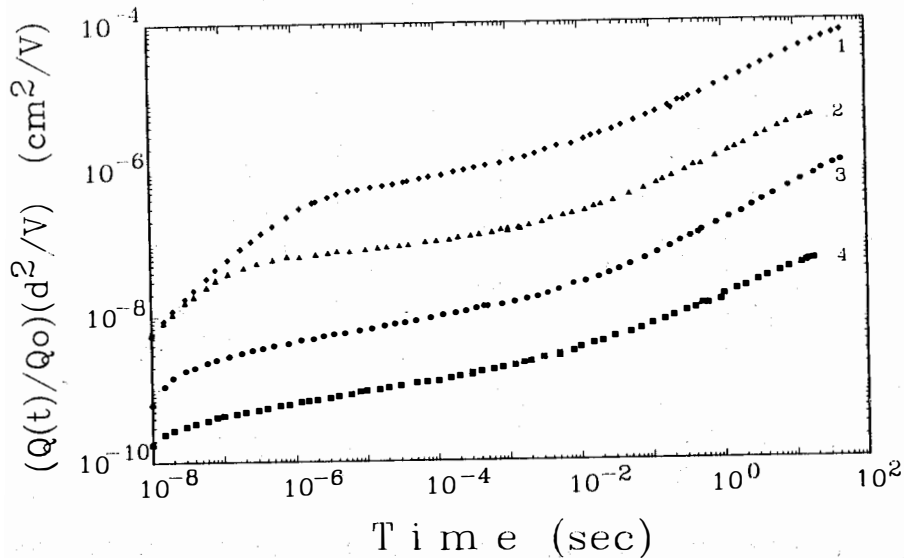


Fig. 4: Transient photocharge measurements following a 3 ns laser illumination impulse for four specimens of undoped a-Si:H measured using coplanar electrodes. The measurements have been normalized by the interelectrode spacing d and the generated charge Q_0 ; the normalized measurements estimate the transient mobility-lifetime $\mu\tau(t)$.

Title: Low Temperature MOCVD Processes for High Efficiency Solar Cells

Organization: University of Southern California, Los Angeles, CA 90089-0483

Contributors: P. Daniel Dapkus, Principal Investigator, B. Y. Maa, W. G. Jeong, Q. Chen, S. G. Hummel

Introduction

Metalorganic chemical vapor deposition (MOCVD) is widely used to fabricate high efficiency III-V solar cells. The process has produced the highest efficiency solar cells to date and is unique in its ability to be scaled to large volumes. Despite these inherent advantages, MOCVD suffers certain disadvantages. Chief among these are that it is carried out at relatively high temperatures and that it inefficiently utilizes highly toxic precursors (ASH₃ and PH₃). These characteristics frustrate attempts to fabricate multijunction solar cells and create added hazard and cost. This program is directed to resolve these difficulties by providing a better understanding of the gas phase and surface kinetics of MOCVD, by exploring techniques for low temperature growth of III-V materials and device structures, and by exploring photoenhanced MOCVD processes.

Summary of Previously Reported Work

The activities of the previous three years of work have included basic studies of gas phase chemistry of organometallic III and V compounds, empirical studies of the reactions of organometallics on III-V surfaces in a dense gas phase medium, and empirical studies of the low temperature growth of III-V compounds by alternate supply of the III and V reactants -- atomic layer epitaxy (ALE). The results of these studies can be summarized as follows:

(1) The decomposition of TMGa to atomic Ga and CH₄ is complete at temperatures as low as 450°C with an contact time of ~6 sec. Hydrogen as a carrier gas plays an active chemical role in the decomposition process by reacting, as atomic hydrogen, directly with the TMGa and reaction products and by scavenging CH₃ radicals from the gas phase. The apparent activation energy of the decomposition is reduced in H₂ (50.9 kcal/mole) as compared to N₂ (64.6 kcal/mole). (References 1-3)

2.) ALE growth of AlAs, GaAs, InAs, and InP using organometallic precursors has been accomplished at low temperatures and thoroughly characterized with respect to growth parameters. (References 4-17)

3.) Photoassisted ALE of GaAs using organometallic precursors has been accomplished at temperatures below 400°C (as low as 200°C) and has been thoroughly characterized with respect to growth parameters. (References 6-13)

4.) Low temperature (<340°C) ALE growth rate of InAs has been shown to be limited by steric hindrance effects. Photoexcitation with visible light at intensities near 100-200 W/cm² increases the surface reaction times by more than 200 fold as measured by the time necessary to form one monolayer of GaAs (~10nsec compared with 5sec). (References 14-17)

5.) The optical and electrical properties of ALE grown GaAs have been studied. Under the best conditions studied to date, the net carrier concentration in ALE grown GaAs is estimated to be $p \sim 2-5 \times 10^{16} \text{cm}^{-3}$. The photoluminescence quality and carrier concentration are affected by the relative exposure times of III and V reactants. PL intensity increases with increasing V exposure and decreasing III exposure. (References 4-7, 10, 11)

Role of Surface and Gas Phase Processes in ALE

The ALE growth mechanism at atmospheric pressure involves both gas phase and surface reactions. At the lower temperatures surface reactions dominate while gas phase reactions dominate at higher temperatures and begin to frustrate the surface saturation phenomena upon which the benefits of ALE depend. This latter trend is exemplified in virtually all ALE growth data that we or others have accumulated by a distinct lack of complete saturation at one monolayer for increasing exposure and by greater than one monolayer deposition at temperatures slightly higher than the optimum. At temperatures above 450°C, significant homogeneous decomposition of TMGa occurs. For all higher temperatures we expect that a significant fraction of the species impinging on the surface during ALE growth of GaAs will be atomic Ga. Under these conditions, we expect and, in fact, observe weak saturation of the growth under these conditions. At temperatures above 500°C homogeneous decomposition dominates and no saturation is observed.

The data obtained in this program and recent data on the decomposition of AsH₃ in the presence of GaAs substrates indicates that the decomposition of the organometallic will limit the growth rate of III-V's at low temperatures. Surface reactions play a dominant role in atmospheric pressure ALE at temperatures below which there is no significant gas phase decomposition of the III alkyl. We have investigated the ALE growth of both InAs and GaAs under such conditions. At temperatures above 400°C, the rates of gas phase decomposition and surface reactions are accelerated. Some fraction of the TMGa is partially decomposed in the gas phase. The surface adsorbates formed under these conditions will likely be a mixture of species that exhibit different surface reaction rates. The effect of these species are that some surface sites are hindered by the presence on the surface of unreacted or partially reacted TMGa. These sites become available for adsorption only when the adsorbate fully reacts to produce atomic Ga. If the source of TMGa molecules is removed before this takes place less than one monolayer is formed during the cycle. For long exposure times the adsorbates fully react and one monolayer is formed. Fig. 1 shows the dependence of GaAs growth rate at 400°C on TMGa exposure for various exposure times. The fact that monolayer saturation requires ~10sec of exposure independent of the TMGa concentration is indicative of steric hindrance effects and slow surface reactions.

Based upon these observations it is interesting to speculate whether true monolayer ALE can be achieved with metal alkyls at atmospheric pressure. The surface decomposition rates of TMGa (and TMIn) seem to be in the practical range for ALE growth in the same temperature range as that in which homogeneous decomposition rates become significant. This precludes achieving a perfectly saturated growth process. There are at least two that can be taken to solve this dilemma. The first strategy involves increasing the surface reaction rates by photoexcitation. A comparison of thermally driven ALE growth of GaAs with photo-assisted ALE has been described previously. The second strategy for achieving saturated ALE growth is to reduce the homogeneous gas phase reaction rates. This can be done by reducing the reactor pressure, the extreme limit of which is UHV conditions, or by changing the carrier gas to an inert species such as N₂. In either case, it is expected that surface reactions will dominate and saturated ALE will occur.

To investigate vacuum ALE (VALE) and to study the surface reactions and reaction rates in ALE, we have established a UHV surface analysis/deposition system based upon XPS and RHEED analysis techniques. The schematic of the system is shown in Fig.2. We combined both XPS and RHEED to study adsorption processes of TMGa on GaAs (001) surfaces under conditions which simulated actual ALE growth. XPS was used to identify adsorbed chemical species and RHEED was used to reveal surface reconstruction. Both analyses also provided important information about surface stoichiometry and chemical bonding of surface atoms. Through this study we elucidate the growth mechanisms involved in TMGa based GaAs ALE. The reaction chamber provides for exposure to As₄ and TMGa. Arsenic metal contained in a quartz effusion cell is used to create As-stabilized surfaces. After sample preparation a clean surface showed no evidence of

carbon as measured by the XPS C1s spectrum. A well defined RHEED 2x4 As-stabilized surface also was observed.

Fig.3 shows the intensity ratio of Ga 2p_{3/2} to As 3d at various temperatures and exposure levels. At T_s=320°C with exposure time of either 10 or 15 seconds and TMGa pressures of P_{TMGa} = 2x10⁻⁶~5x10⁻⁶ Torr no change in the Ga intensity can be observed. The surface still shows a 2x4 RHEED pattern after TMGa exposures. When the substrate temperature is increased to higher than 370°C, we observe both a gradual increase of Ga 2p_{3/2} and decrease of As 3d intensities with increasing exposures to TMGa and finally their ratio reaches a saturation level. These data clearly show that The surface reactions are inherently self limiting. Furthermore no evidence of carbon is seen on the surface suggesting that atomic Ga and not GaCH₃ is the surface species.

Under UHV conditions, monolayer saturation of Ga atoms is obtained over a broad temperature range of 370°C to 530°C. This contrasts with most published atmospheric or low-pressure ALE growth data which show monolayer saturation over a relatively narrow temperature regime. In these reports, more than one ML per exposure cycle and unsaturated Ga atom deposition was observed when the substrate temperature was higher than ~450°C, depending on individual reactor design. We believe that gas phase reactions involving TMGa decomposition cannot be excluded from the overall deposition processes in these high pressure experiments as compared with pure surface reactions in our case. Most likely some Ga atoms are produced in the gas phase and transported to the surface.

In our VALE experiments, TMGa must first adsorb on As sites long enough to undergo further surface reaction and decompose to atomic Ga. At 320°C, we did not observe any Ga atom deposition up to a relatively high TMGa exposure of 200L. We believe that surface desorption plays a dominant role at this temperature and that TMGa does not remain on the surface long enough for decomposition reactions to occur. A 2x4 As-stabilized surface is observed even after a 200L TMGa exposure. Above 370°C, however, Ga deposition occurs and the deposition rate increases with increasing substrate temperature due to a rapidly increasing TMGa decomposition rate. We are further investigating these trends to understand surface reaction kinetics.

No evidence of methylgallium species after TMGa adsorption is observed in the substrate temperature range of 320°C to 530°C. The decomposition activation energy of TMGa on GaAs surface from all reported data is much less than that in the gas phase. This could be due to the formation of Ga-As and/or Ga-Ga bonds on the surface with the simultaneous breaking of the Ga-CH₃ bond. Most released CH₃ radicals desorb into vacuum but some are adsorbed on surface Ga atoms and are later incorporated into the grown film as acceptors. It is worthwhile to point out the different hybridization of the surface Ga and As dangling orbitals. Arsenic dangling orbitals tend to have nondirectional s-like characters that are filled and lie well below the Fermi level. For Ga, the dangling orbitals have directional p-like characters that are empty above the Fermi level and can provide more overlap when bonding to a carbon atom. As a result, the chemisorption of carbon or hydrocarbon radicals on Ga dangling orbitals is significantly stronger than on As dangling bonds. Less carbon incorporation can occur by removing CH₃ radicals at higher substrate temperatures but not so high as to create arsenic vacancies on the surface which then expose more Ga atoms for further carbon incorporation. In ALE growth, insufficient arsenic supply during AsH₃ or As₄ injection period has the same effect on carbon incorporation. AsH_x (x=1,2,or 3) may react with CH₃ radical species and form CH₄ which then evaporates rapidly and the carbon impurity level is therefore reduced in the grown film.

We have thus demonstrated VALE using TMGa and a solid arsenic source instead of AsH₃. This demonstrates As₄ can react on the Ga-covered surface after TMGa exposure to revert it to the As-

stabilized surface. Thus, an AsH_x species is not required to react with the Ga adsorbate. This further suggests that the Ga adsorbate is primarily atomic Ga and not GaCH_3 .

We have also found that an As-stabilized surface can be converted to a Ga-stabilized surface by exposure of the surface to TMGa in the temperature range 450°C-530°C with exposures of less than a few seconds. The Ga surface coverage saturates at one monolayer in this temperature range. There is no appreciable C surface species indicating that the surface adsorbate does not involve a bonded methyl radical. The Ga-stabilized surface is largely unreactive to the TMGa molecule and no further Ga adsorption occurs with prolonged exposure. At temperatures below 370°C no apparent reaction takes place even with the As-stabilized surface. These studies continue with emphasis being placed on the measurement of the surface reaction kinetics.

Conclusions and Future Work

Photoassisted ALE appears to be a practical means to grow GaAs at low temperatures. The inherent uniformity of the process and the potential for scale up are motivation to study further the limits to the achievable growth rate and the fundamental growth mechanisms.

References and Publications

1. S. P. DenBaars, B. Y. Maa, P. D. Dapkus, H. C. Lee and A. D. Danner, *J. Crystal Growth* **68** 155 (1986).
2. < S. P. DenBaars, P. D. Dapkus, and A. Melas, *J. Electrochem. Soc.*, **136**, 89 (1989).
3. Qisheng Chen and P. Daniel Dapkus, "Decomposition Kinetics of Trimethylgallium." Submitted to *J. Electrochemical Society*.
4. < S. P. DenBaars, C. A. Beyler, A. Hariz, P. D. Dapkus, *Appl. Phys. Lett.* **51**, 1530 (1987).
5. < S.P. Denbaars, A. Hariz, C. Beyler, B.Y. Maa, Q. Chen and P.D. Dapkus, *Mat. Res. Soc. Symp. Proc.* **120**, 527 (1988).
6. < S.P. Denbaars, P.D. Dapkus, C.A. Beyler, A. Hariz and K.M. Dzurko, *J. Crystal Growth* **93**, 195 (1988)
7. S. P. DenBaars, P. D. Dapkus, J. S. Osinski, M. Zandian, C. A. Beyler, and K. M. Dzurko, "Thermal and Laser Assisted Atomic Layer Epitaxy of Compound Semiconductors." *Proceedings of International Symposium on GaAs and Related Compounds*, *Inst. Phys. Conf. Ser.*, **96**, 89 (1989). Also S.P. Denbaars, P.D. Dapkus, J.S. Osinski, M. Zandian, C.A. Beyler and K.M. Dzurko, presented at International Conference on GaAs and Related Materials, Atlanta, Ga (1988).
8. P. D. Dapkus and S. P. DenBaars, "Atomic Layer Epitaxy for Heterostructure Devices," IEDM Invited Talk, December, 1988.
9. P.D. Dapkus, S.P. DenBaars, Q. Chen, W.G. Jeong, and B.Y. Maa, *Progress in Crystal Growth and Characterization* **19**, 137 (1989).
10. P. D. Dapkus, S. P. DenBaars, Q. Chen, W. G. Jeong, and b. Y. Maa, "The Role of Surface and Gas Phase Reaction in Atomic Layer Epitaxy of Compound Semiconductors," in Mechanisms of Reactions of Organometallics Compound with Surfaces. NATO ASI Series, Vol. **B198**, Plenum Publishing Corp., New York, pp 257 - 266.
11. S. P. DenBaars and P. D. Dapkus, "Atomic Layer Epitaxy of Compound Semiconductors with Metalorganic Precursors," *J. Crystal Growth* (1989) (in Press). also, P. D. Dapkus and S. P. DenBaars, "Atomic Layer Epitaxy of Compound Semiconductors with Metalorganic Precursors." Presented at US-Japan Conference on Compound Semiconductor Alloys, Honolulu, HI, October 1988.
12. S.P. DenBaars, Ph.D. Thesis, University of Southern California.
13. P. Daniel Dapkus, Weon G. Jeong, Bang Y. Maa, Qisheng Chen, and Steven. P. DenBaars, "Atmospheric Pressure Atomic Layer Epitaxy Using Metal Alkyls." Invited talk Presented at International Conference on Crystal Growth, Sendai, Japan, August 1989. Submitted to *Journal of Electronic Materials*

14. ^g W. G. Jeong, E. P. Menu, and P. D. Dapkus, "Steric Hindrance Effects in Atomic Layer Epitaxy of InAs," *Appl. Phys. Lett.*, **55**, 245 (1989).
15. W. G. Jeong, E. P. Menu, and P. D. Dapkus, "Comparison of the Growth of InP and InAs by Atomic Layer Epitaxy." *Proceedings of First International Conference on InP and Related Components*, SPIE-1141, 86 (1989).
16. W. G. Jeong, E. P. Menu, and P. D. Dapkus, "Atomic Layer Epitaxy of GaAs and InAs," *Materials Research Society Symposium Proceedings Vol. 145*, 163 (1989). Also W. G. Jeong, E.P. Menu, and P.D. Dapkus, presented at Materials Research Society Symposium, San Diego, CA, April 24-29, Spring 1989
17. Weon G. Jeong and P. Daniel Dapkus, "Surface Kinetics and Contributions of Gas Phase Decomposition in Atomic Layer Epitaxy of GaAs." Submitted to *J. Crystal Growth*.
18. B. Y. Maa and P. D. Dapkus, "RHEED and XPS Observations of Trimethylgallium Adsorption on GaAs (001) Surfaces - Relevance to Atomic Layer Epitaxy." Presented at Fourth Biennial Workshop on Organometallic Vapor Phase Epitaxy, Monterey, CA, October 1989. To be published *Journal of Electronic Materials* (1990).
19. ^{nc} B. Y. Maa and P. D. Dapkus, "Kinetics of Surface Reactions of TMGa with GaAs Surfaces," presented at International Conference on CBE, Houston, TX, December 1989.

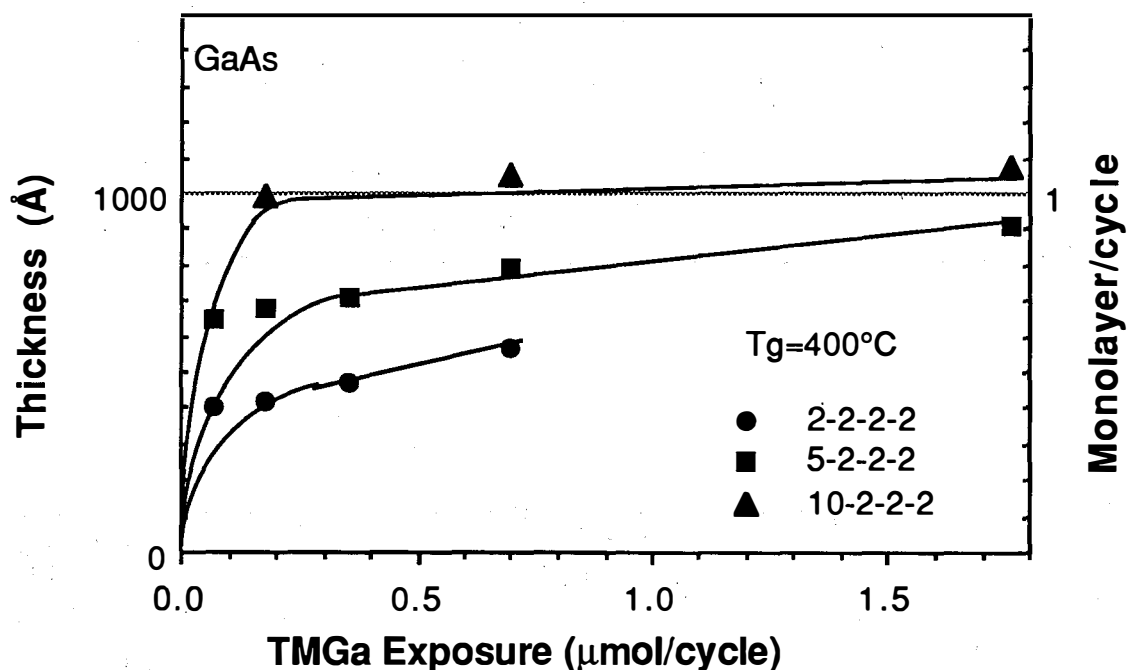


Fig. 1 ALE growth rate of GaAs at 400°C showing pronounced effects of steric hindrance. An exposure time of 10 seconds is required to achieve one monolayer/cycle growth rate.

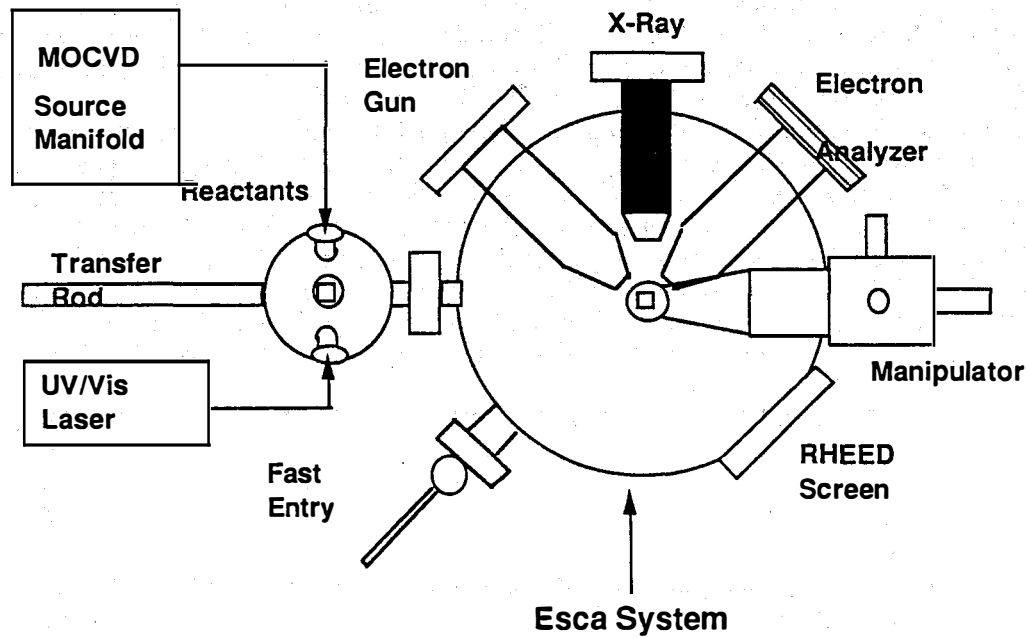


Fig.2 Schematic diagram of XPS/deposition system used for surface reaction studies.

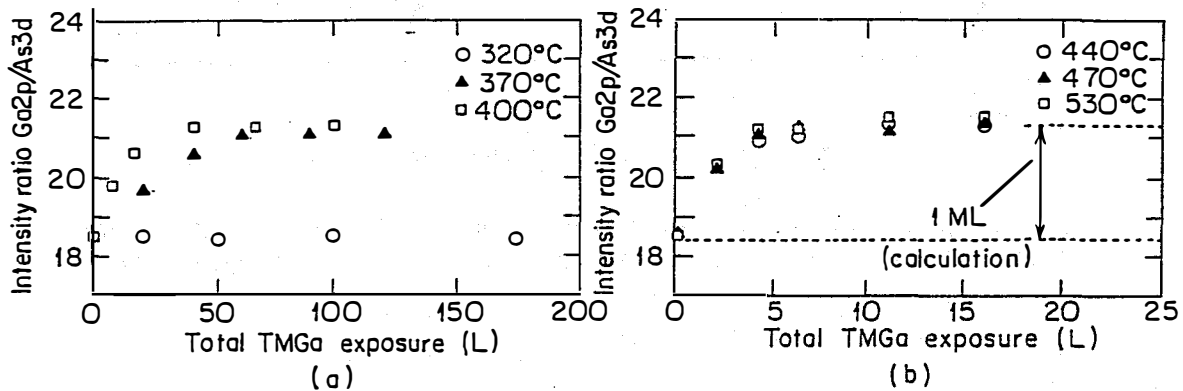


Fig. 3 Ga_{2p}_{3/2} to As 3D intensity ratio for GaAs surface exposed to TMGa under several different conditions.

Title: Electronic Processes in Thin Film PV Materials

Organization: Department of Physics, University of Utah, Salt Lake City, Utah

Contributors: P.C. Taylor, principal investigator, G.A. Williams, W.D. Ohlsen, S. Nitta, C. Lee, S. Gu, I. Viohl

In photovoltaic devices, especially those involving hydrogenated amorphous silicon (a-Si:H), the effects of defects, impurities and interfaces are very important in determining ultimate device performance. Knowledge of these three topics is particularly important for the optimization of PV devices. A second very important problem for PV devices employing a-Si:H is the stability of the optical and electronic properties. One must be able at least to characterize these metastabilities before devices can be effectively optimized. Under this subcontract optical and magnetic resonance techniques have been used to probe these significant questions.

In addition to a-Si:H, There are several amorphous alloy systems which are potentially important for PV applications. These alloys include a-Si_xGe_{1-x}:H and A-Si_xC_{1-x}:H which are used for producing narrower gap materials for tandem cells and wider gap materials for top-surface p-layers, respectively. There are still significant problems with a detailed understanding of the defects and impurities which, among other effects, create enhanced densities of electronic states in the gap in these films. Perhaps of more immediate importance is the fact that all of these alloys exhibit both optically- and electronically-induced metastable changes in their important PV properties. Projections of ultimate device efficiencies and device lifetimes are difficult as long as these metastabilities remain.

Objectives

This subcontract has involved four major scientific objectives. The first objective has been to understand the thermally- and optically-induced metastabilities in a-Si:H and related alloys using primarily electron spin resonance (ESR), nuclear magnetic resonance (NMR), optical absorption and photoluminescence (PL) as the experimental probes. The second and third objectives are to characterize both the defects which lie deep in the gap, such as Si dangling bonds, and the general density of electronic states (DOS) throughout the gap in a-Si:H and related alloys. The fourth major objective involves the understanding of interfacial effects in a-Si:H and related alloys, especially as they relate to interfaces which are potentially important in PV devices.

Discussion

In order to accomplish these objectives we have employed several experimental probes of local order, such as magnetic resonance or optical spectroscopy or a combination of the two techniques, to characterize defects, impurities and other localized electronic states in thin films of a-Si:H and related alloys. We have concentrated on materials which are of particular interest for PV devices and on sample geometries which are most appropriate for devices.

The contract is divided into six tasks. The first task involves the training of graduate students. Three students have been trained directly under the support of this subcontract and three are currently being trained. In addition, several postdoctoral research associates have benefited from training received under this program.

The second task concerns studies of the metastabilities in a-Si:H and related alloys. Our ESR experiments of dangling bonds induced in a-Si:H using white light exhibit a time dependence which is weaker than $t^{1/3}$ over any extended period of illumination times up to 10^5 min. We have observed this behavior on device-quality samples from several different sources. Inducing curves where the time dependence is weaker than $t^{1/3}$ have also been observed by Yokomichi et al.¹

We have also discovered a metastable paramagnetism,² in a-Si:H which can be altered by rapid quenching from elevated temperatures (~ 483 K). These measurements are not necessarily consistent with the most common models for the dominant electronic states which are deep in the gap in a-Si:H. Also we have³ shown that there is a correlation between the thermally quenched metastabilities observed in ESR and optical absorption as measured by photothermal deflection spectroscopy (PDS) and that⁴ the optically induced ESR observed on device quality films obtained from ARCO Solar, Inc. is identical to that observed in films supplied by Solarex.

The third task involves the characterization of defects in a-Si:H and related alloys. Of the defects which are most important in a-Si:H and related alloys perhaps the best studied is the so-called Si dangling bond. This defect (regardless of whether it is a three-coordinated dangling bond or a five-coordinated floating bond) shows up in ESR experiments as a characteristic lineshape, in optical absorption or PDS experiments as a characteristic below-gap absorption, in PL experiments as a characteristic PL peak near 0.8 eV, and in various other experiments such as optically detected magnetic resonance (ODMR). During the present contract⁵ we have investigated these defects using PL in a-Si_xGe_{1-x}:H alloys, using PDS in doping modulated multilayers, and using ESR and PDS following rapid thermal quenching in a-Si:H.

Another important defect, which is perhaps better described as an "impurity" in device quality a-Si:H, is molecular hydrogen (H₂). It is well known that molecular hydrogen is trapped in microvoids in most samples of a-Si:H. We have recently measured the presence of H₂ in silicon-germanium alloys⁶ as shown in Fig. 1. Alloys of hydrogenated amorphous silicon and germanium are of potential use in multijunction solar cells, but currently their use is limited by a marked degradation in the electronic properties as the germanium content is increased. For compositions of the form a-Si_{1-x}Ge_x:H, most solar cell applications require $x \geq 0.3$ while many important electronic properties deteriorate rapidly for $x \geq 0.2$. For example the densities of deep-gap defects, as measured by ESR or PDS, increase by more than an order of magnitude for $x \sim 0.2$.

A study of gap states in a-Si:H and related alloys constitutes the fourth task of the subcontract. The absorption well below the band gap in hydrogenated amorphous silicon (a-Si:H) and related alloys is a very important property for gauging the quality of these materials for use in solar cells. There is known to be a correlation between the magnitude of this absorption and the density of paramagnetic deep-gap states as measured by ESR. It is also well known that

both of these quantities correlate inversely with such properties of importance to solar cells as electron and hole lifetimes and mobilities for the doped and undoped a-Si:H.

Unfortunately, because a-Si:H is only made in thin-film form where the thicknesses are typically less than a few μm , standard measurement techniques for estimating absorption well below the band gap cannot be employed. For this reason several novel techniques are often used in order to extract these important data. During the course of this subcontract we have developed a new technique,⁵ which we have called photoluminescence absorption spectroscopy (PLAS), where the self-absorption of the PL is measured for light traveling in a wave guide mode along the length of the thin-film sample. Because this technique uses the PL generated within the film as a convenient "broad-band" light source, the optical path length in the sample can be greatly increased. If d is the length that the light travels in the films and α the absorption coefficient, then αd can be on the order of unity for $\alpha \sim 1 \text{ cm}^{-1}$. These conditions can be easily met using this technique.

Using the PLAS technique we have found a bump in the absorption spectrum of the undoped a-Si:H near 1.15 eV. This bump, which is only apparent in the 77 K spectrum, has been observed at low temperatures ($\leq 77 \text{ K}$) in all films of intrinsic a-Si:H which have been measured to date. Earlier measurements have shown that this type of below gap absorption is independent of the thickness of the film.⁵

Another way of measuring the below gap absorption, in principle, is to measure the intensity of the PL as a function of the energy of the exciting light. This so-called PL excitation spectrum (or PLE spectrum) can in many cases map out the absorption spectrum, and when it does not, one can often learn important details concerning the transitions which produce the PL processes. We have examined the PLE spectrum in a-Si:H at energies which are well below the optical band gap (see Fig. 2) and have shown that the absorption processes are very different from those which occur near the band gap.⁷

The fifth task concerns the characterization of interfacial effects in a-Si:H and related alloys. ESR and PDS have proved to be useful techniques for measuring interface or surface defects in many thin films including a-Si:H. For example, in good quality a-Si:H films the bulk spin density is $\leq 3 \times 10^{15} \text{ cm}^{-3}$, but there also exists a surface contribution on the order of $10^{12} \text{ spins cm}^{-2}$. This surface spin contribution appears to have the same lineshape as the bulk signal and is thus related to a silicon "dangling bond" on the surface. In addition, PDS experiments have shown a strong surface or interface contribution to the below-gap absorption in a-Si:H and related alloys.

We have found the analog of the E' center at some a-Si:H/a-SiO₂ interfaces. We have also investigated interface states in doping modulated superlattices and surface states in samples of a-Si:H which have been rapidly thermally quenched.⁵

Two recent experiments indicate the potential importance of interface states in a-Si:H. In the first experiment we have examined low temperature, transient, optically-induced ESR measurements (LESR) using below gap light.⁸ In the second experiment we have examined the absorption of photoluminescence (PL) which travels along the length of the a-Si:H film (PLAS).⁷

The final task (number 6) is the construction and testing of an in-house glow-discharge deposition facility. During this subcontract we have developed our own growth capabilities with a glow discharge system originally purchased from Plasma Technology and modified by us. This system, which exists in the Microelectronics Laboratory run by the College of Engineering at the University of Utah, is currently making state-of-the-art i-layers of a-Si:H. We have characterized these films with ESR ($< 10^{16}$ dark spins/cm³), PDS, photoconductivity ($\sigma_{pc}/\sigma_{dark} > 10^4$) and several other techniques. We are now using our own samples for optically-induced ESR, ODMR, PLAS and other on-going experiments. We have made preliminary samples of doped layers and multilayers (Si-Ge and Si-N).

We currently have active collaborative efforts with Solarex Corp., Plasma Technology, North Carolina State University, the University of Chicago, Iowa State University, Harvard University, Gifu University and the University of Marburg. All of these institutions have provided well characterized samples to use for various research purposes.

Conclusions

The tasks proposed at the outset of this subcontract have generally been accomplished. Major accomplishments include (1) an understanding of the kinetics of light-induced defects in device quality films of a-Si:H and in p-i-n structures; (2) an identification of trapped molecular hydrogen in a-Si:H and some alloys (a-Si_{1-x}Ge₂:H) and a discovery of diffusion of molecular hydrogen along microvoids in device-quality a-Si:H; (3) an investigation of the behavior of the defect PL band at 0.8 eV in silicon germanium alloys; (4) the discovery of an E'-type defect at some a-Si:H/SiO₂ interfaces; (5) an initial characterization of some paramagnetic defects induced by rapid thermal quenching in device-quality a-Si:H; (6) the development of a new technique for measuring low levels of absorption in thin films (PLAS) and the discovery of a peak in the below-gap absorption spectrum at 1.15 eV which may be interface related; (7) the use of subgap excitation of ESR and PL to probe deep defects, such as dangling bonds, and other gap states; and, (8) the development of a bistable optical switch bases on thermal modulation of the index of refraction in a-Si:H films.

References

1. H. Yokomichi, M. Kumeda, A. Morimoto, and T. Shimizu, *Jpn. J. Appl. Phys.* **24**, L569 (1985).
2. C. Lee, W.D. Ohlsen, and P.C. Taylor, *Phys. Rev. B* **36**, 2965 (1987); C. Lee, W.D. Ohlsen, and P.C. Taylor, in *Proc. Conf. on Stability of a-Si:H*, E. Sabisky, ed. (SERI, Golden, CO, 1987), p. 223.
4. C. Lee, W.D. Ohlsen, and P.C. Taylor, in *Proceedings of the International Conference on Hydrogenated Amorphous Silicon Devices* (November 1988), in press.
5. P.C. Taylor, G.A. Williams and W.D. Ohlsen, *Annual Technical Status Reports* (1986, 1987, 1988), unpublished.
6. E.J. VanderHeiden, G.A. Williams, P.C. Taylor, F. Finger and W. Fuhs, in *Mat. Res. Soc. Symp. Proc.*, Vol. 149 (1989), p. 503.
7. J. Ristein, B. Hooper and P.C. Taylor, *J. Opt. Soc. Am.* **B6**, 1003 (1989).
8. J. Ristein, J. Hautala and P.C. Taylor, *Phys. Rev. B* **40**, 88 (1989).

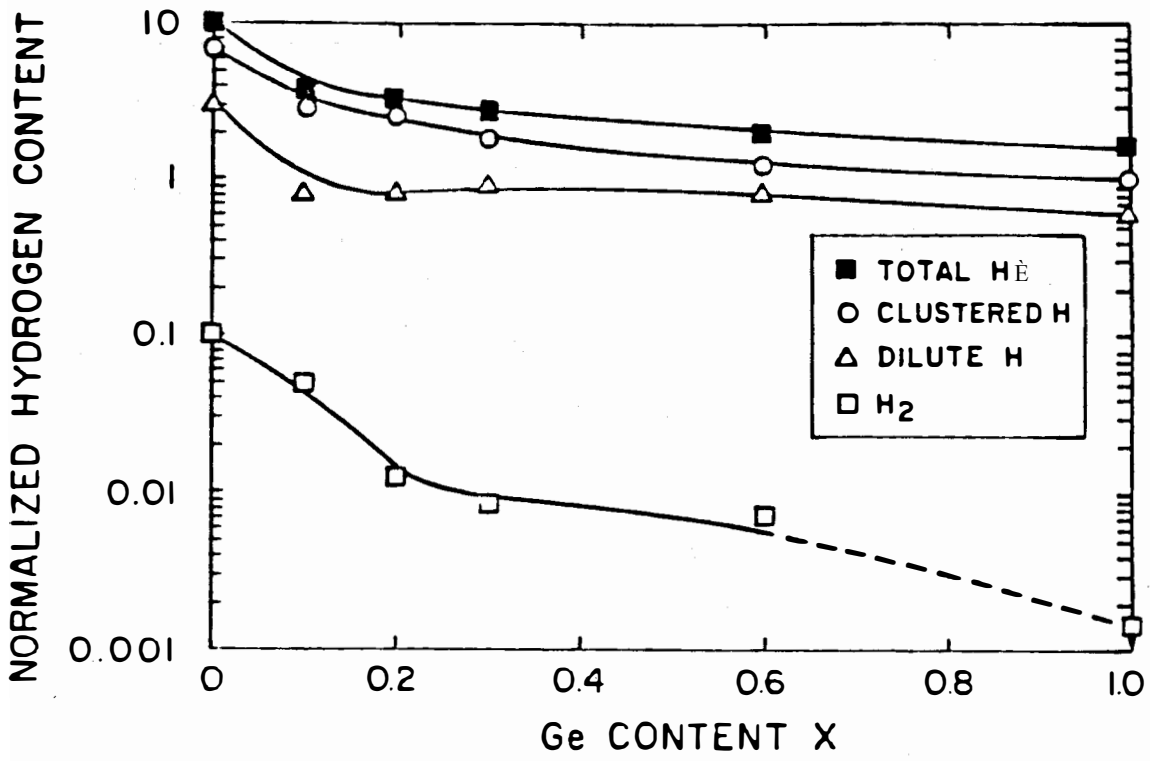


Fig. 1. Normalized hydrogen concentration in $a\text{-Si}_{1-x}\text{Ge}_x\text{:H}$ alloys as a function of x . Solid squares, open circles and open triangles represent total bonded hydrogen, hydrogen bonded in clusters and bonded hydrogen essentially randomly distributed, respectively. Open squares represent trapped molecular hydrogen (H_2). The open square for $x = 1$ is only an upper bound. The normalized scale can be approximately interpreted as at. %.

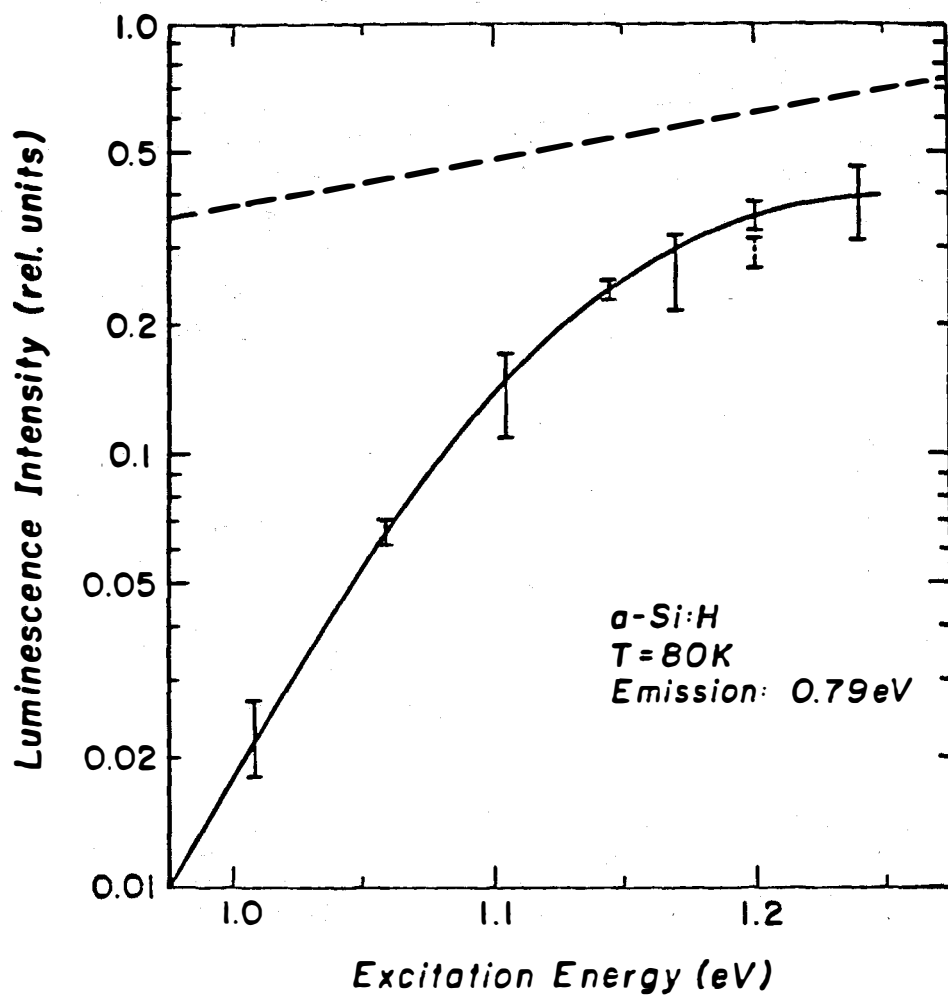


Fig. 2. PLE spectrum for α -Si:H at ~ 80 K. The PL emission energy is 0.79 eV. Experimental points are indicated by error bars. The dashed error bar indicates errors due to long term drift between the first and last points taken. The solid curve is an aid to the eye. The dashed curve shows the energy dependence of the optical absorption (arbitrary units).

8.0 LIST OF ACTIVE SUBCONTRACTS
Active Contract List

Contractor, Principal Investigator, Address	Work Title (Research Activity)	Contract Number	Total Funding (\$K)	FY 1989 Funding (\$K)	Start/End Dates
AMORPHOUS SILICON FY1989					
ARCO Solar K. Mitchell Chatsworth, CA 91311	Res. on Stable Hi-Eff. Large Area a-Si Based Submodules	06003-3	2622.8	599.3	7/89 11/90
Cal Tech. M. Nicolet Pasadena, CA 91125	Stable Contact to a-Si Thin Film & CuInSe ₂ Thin Film & Contacts	07133	60.0	30.0	9/87 10/89
Chronar Corporation A. Delahoy Princeton, NJ 08540	Res. on Stable Hi-Eff. Large Area a-Si Based Submodules	06003-1	4193.0	1399.8	3/87 6/90
ECD S. Guha Troy, MI 48084	Res. Hi-Eff. Multigap Multijunction a-Si Based Submodules	06003-4	4049.3	1350.0	3/87 5/90
Glass Tech Solar P. Bhat 12441 W. 49th Ave. Wheat Ridge, CO 80033	Res. on Material Properties & Device Quality a-Si Deposited at Hi-Deposition Rates Using Higher Order Silanes	06002	606.1	171.2	7/89 8/91
Harvard R. Gordon Cambridge, MA 02138	Characterization & Comparison of Optically Transparent Conducting Films	18148	110.0	55.0	10/88 11/89
Harvard W. Paul 1350 Mass. Ave. Cambridge, MA 02138	Structural & Electronic a-SiGe:H Alloys	18131	210.0	145.0	7/88 1/90
National Institute of Standards & Technology A. Gallagher Boulder, CO 80303	Diagnostics/Glow Discharges Used for a-SiGe:H Alloy Deposition	04078	531.7	99.9	4/84 11/89
Solarex Corp. D. Carlson Newtown, PA 18940	Res. on Hi-Eff. Area a-Si Based Submodules	06003-2	4570.6	1618.9	2/87 4/90

Contractor, Principal Investigator, Address	Work Title (Research Activity)	Contract Number	Total Funding (\$K)	FY 1989 Funding (\$K)	Start/End Dates
<u>AMORPHOUS SILICON FY1989</u>					
Univ. of Delaware J. Meaken Newark, DE 19716	MOCVD of a-Si Alloy Materials & Devices	18092-1	635.0	380.0	5/88 6/90
U. North Carolina M. Silver Chapel Hill, NC 27599	Relative Effects of Charged & Neutral Defects in a-Si:H Research	07183	61.9	30.0	10/87 12/89
Univ. of Oregon J. Cohen Eugene, OR 97403	Research on Origin of Metastable Light-Induced Changes in a-Si:H	18061-1	118.9	69.5	4/89 3/90
Washington University R. Norberg St. Louis, MO 63130	Research into the Structures of a-Si Alloy Films	06055-1	164.9	60.0	1/87 3/90
Xerox Corporation R. Street 3333 Coyote Hill Rd. Palo Alto, CA 94304	Research on Electronic & Structural Properties of a-Si Silicon Alloys	06056-1	1302.8	168.0	11/86
3M F. Jeffrey/M. Weber 3M Center St. Paul, MN 55144	Improvement of Area a-Si Thin Film PV on Polymer Substrate	07271	300.0	170.0	3/88 5/89
<u>POLYCRYSTALLINE THIN FILMS FY1989</u>					
Ametek P. Meyer Harleysville, PA 19438	Polycrystalline Thin Film CdTe Solar Cells	06031-2	554.6	49.0	6/87 9/89
Boeing AeroSpace R. Mickelson Seattle, WA 98124	Hi-Eff. CuInSe ₂ & CuInGaSe ₂ Based Cells & Materials Research	06031-8	447.9	150.0	11/87 12/89
Colorado State Univ. J. Sites Fort Collins, CO 80503	Analysis of Loss Mechanisms in Poly Thin Film Solar Cells	18080	80.0	40.0	4/88 12/89

Contractor, Principal Investigator, Address	Work Title (Research Activity)	Contract Number	Total Funding (\$K)	FY 1989 Funding (\$K)	Start/End Dates
<u>POLYCRYSTALLINE THIN FILMS FY1989</u>					
Georgia Tech. A. Rohatgi Atlanta, GA 30384	Hi-Eff. CdTe & ZnTe Thin Film Cells	06031-1	459.6	85.9	6/87 5/90
ISET V. Kapur Inglewood, CA 90301	Hi-Eff. CuInSe ₂ & CuInSe ₂ Alloy Films	06031-6	889.1	198.9	3/87 7/89
Photon Energy S. Albright El Paso, TX 79924	Hi-Eff. Large Area CdTe & CdHgTe Panels	06031-3	857.0	338.0	6/87 7/90
Univ. Arkansas A. Hermann Fayetteville, AR 72701	Novel Thin Film CuInSe ₂ Fabrication	18017	34.5	19.5	1/88 2/90
Univ. Delaware B. Baron Newark, DE 19716	Fundamentals Polycrystalline Thin Film Materials & Devices	19032	567.0	567.0	1/89 3/90
Univ. of Delaware B. Baron IEC Newark, DE 19716	Two-Terminal CuInSe ₂ Based Cascade Cells	06031-7	425.7	213.9	1/87 3/89
Univ. of Delaware B. Baron Newark, DE 19716	Materials Analysis & Optimization Solar Cells	06031-5	688.9	353.0	1/87 3/89
Univ. of Illinois A. Rockett 809 S. Wright St. Champaign, IL 61820	Alternate Fabrication Techniques for Hi-Eff. CuInSe ₂ Alloy Films & Cells	06031-9	190.1	190.1	9/87 10/90
Univ. of S. Florida T. & S. Chu Tampa, FL 33620	Thin Film CdTe, ZnTe, & Hg _{1-x} Zn _x Te Solar Cells	18091	499.9	200.0	7/88 8/90

Contractor, Principal Investigator, Address	Work Title (Research Activity)	Contract Number	Total Funding (\$K)	FY 1989 Funding (\$K)	Start/End Dates
<u>CRYSTALLINE SILICON MATERIALS RESEARCH FY1989</u>					
Duke Univ. U. Göesele Dept. of Mech. Engin. Durham, NC 27706	Point Defects & Their Influence on Solar Cell Related Elec. Properties of Crystalline Silicon	18097-1	99.3	99.3	7/88 8/89
Georgia Tech A. Rohatgi Atlanta, GA 30332	Impurity Characterization Support for Silicon	18155	25.0	25.0	10/88 12/89
N. Carolina St. Univ. G. Rozgonyi Box 7214 Raleigh, NC 27695	The Effectiveness & Stability of Impurity/Defect Interactions & Their Impact on Minority Carrier Lifetime	18097-2	140.0	140.0	6/88 7/89
Suny/Albany J. Corbett Albany, NY 12201	Passivation & Gettering in Solar Cell Silicon	18097-3	126.7	126.7	7/88 8/89
Univ. of Southern CA S. Forrest University Park Los Angeles, CA 90089	Electric Characterization Support for Crystalline Silicon	18154	25.0	25.0	10/88 12/89
<u>ADVANCED HIGH EFFICIENCY FY1989</u>					
Kopin Corp. J. Fan Taunton, MA 02980	Hi-Eff. Thin Film GaAs & Ternary III-V Solar Cells	18083	769.0	435.0	4/88 2/90
Purdue Lundstrom/Mellock W. Lafayette, IN 47907	Basic Studies of III-V Hi-Eff. Cell Components	05018-1	710.4	101.2	8/85 8/89
Rensselaer Ghandhi/Borrenco Troy, NY 12180	Research on Semiconductors for Hi-Eff. Cell Components	05018-2	995.0	200.0	9/85 1/90
Spire Corporation J. Daly Patriots Park Bedford, MA 01730	Research on Large Scale MOCVD Deposition	18042	297.7	297.7	5/88 7/89

Contractor, Principal Investigator, Address	Work Title (Research Activity)	Contract Number	Total Funding (\$K)	FY 1989 Funding (\$K)	Start/End Dates
<u>ADVANCED HIGH EFFICIENCY FY1989</u>					
Spire Corp. S. Vernon Bedford, MA 01730	GaAs Based Ternary Compounds & Multibandgap Solar Cell Research	18063	651.2	359.9	4/88 2/90
Univ. of Colorado R. Hayes Boulder, Colorado 80309	Device Modeling & Analysis of III-V Solar Cells	07198	55.9	14.8	8/87 3/89
Varian Assoc. H. MacMillan 611 Hansen Way Palo Alto, CA 94303	Advanced High Efficiency Concentrator Cells	18103	400.6	210.6	10/88 11/89
<u>NEW IDEAS FY1989</u>					
Georgia Tech. C. Summers Atlanta, GA 30332	Avalanche Heterostructural & Superlattice Solar Cells	19056	100.0	100.0	5/89 5/90
ISET V. Kapur 8635 Aviation Blvd. Inglewood, CA 90301	Low Cost Technique for Producing CdZnTe Devices for Cascade Cell Application	06074-02	199.1	99.8	6/87 2/90
Rensselaer Office of Grants Troy, NY 12180	Hydrogen Radical Enhanced Growth of Solar Cells	06074-03	200.1	100.0	6/87 4/90
<u>UNIVERSITY PROGRAM FY1989</u>					
Carnegie/Mellon Univ. Milnes/Schlesinger Pittsburgh, PA 15213	Improvement of Bulk Epitaxial III-V Semiconductors	06005-3	369.3	57.4	9/86 11/89
No. Carolina St. Univ. S. Bedair Box 7003 Raleigh, NC 27695	New Approaches to Hi-Eff. Solar Cells by MOCVD	05009-1	615.8	113.8	9/85 7/89

Contractor, Principal Investigator, Address	Work Title (Research Activity)	Contract Number	Total Funding (\$K)	FY 1989 Funding (\$K)	Start/End Dates
<u>UNIVERSITY PARTICIPATION PROGRAM FY1989, (continued)</u>					
Brown University J. Gerritsen Box 1929 Providence, RI 02912	Rapid Liquid Phase Epitaxy of Ternary III-V Semiconductors for Tandem Solar for Tandem Cell Applications	05009-5	509.4	82.4	9/85 12/88
No. Carolina St. Univ. G. Lucovsky Raleigh, NC 27695	Fundamental Studies of Defect Generation in a-Si Alloy Grown by Remote Plasma Enhanced CVD	18141-2	124.7	124.7	7/89 8/90
Stanford University R. Bube 660 Arguello Way Stanford, CA 94305	Ion Beam Doping of II-VI Compounds During Physical Vapor Deposition	05009-4	819.7	228.7	9/85 12/88
Syracuse University E. Schiff Syracuse, NY 13244	Defects & Photo Carrier Processes in a-Si:H Alloys	06005-2	411.4	58.5	9/86 11/89
Univ. of So. Ca D. Dapkus University Park Los Angeles, CA 90089	Low Temperature MOCVD Growth Process for Hi-Eff. Solar Cells	05009-3	616.0	100.0	9/85 7/89
Univ. of Utah C. Taylor 309 Park Bldg. Salt Lake City, UT 84112	Electronic Processes in Thin Film PV Materials	18141-3	169.3	168.3	7/89 8/92

9.0 PHOTOVOLTAIC PROGRAM BRANCH FY 1989 BIBLIOGRAPHY

Subcontractor Reports and Publications

- Abou-Elfotouh, F.A.; Kazmerski, L.L.; Coutts, T.J.; Dunlavy, D.J.; Almassari, M.; Chaudhuri, S.; Birkmire, R.W. (1989). "Characterization of CuInSe₂ Single Crystals for Solar Cell Modeling Studies." *Conference Record of the Twentieth IEEE Photovoltaic Specialists Conference - 1988; September 26-30, 1988; Las Vegas, Nevada.* New York: The Institute of Electrical and Electronics Engineers, Inc.; pp. 1520-1524.
- Ahrenkiel, R.K.; Dunlavy, D.J.; Timmons, M.L. (1989). "III-V Compound Process Development Using Photoluminescence Lifetime." *Conference Record of the Twentieth IEEE Photovoltaic Specialists Conference - 1988; September 26-30, 1988; Las Vegas, Nevada.* New York: The Institute of Electrical and Electronics Engineers, Inc.; pp. 611-615.
- Ahrenkiel, R.K.; Dunlavy, D.J.; Keyes, B.; Vernon, S.M.; Dixon, T.M.; Tobin, S.P.; Miller, K.L.; Hayes, R.E. (11 September 1989) "Ultralong Minority-Carrier Lifetime Epitaxial GaAs by Photon Recycling." *Applied Physics Letters* (55:11); pp. 1088-1090. Work performed by Solar Energy Research Institute, Golden, Colorado; Spire Corporation, Bedford, Massachusetts; Department of Electrical and Computer Engineering, University of Colorado, Boulder, Colorado.
- Ahrenkiel, R.K.; Al-Jassim, M.; Dunlavy, D.J.; Jones, K.M.; Vernon, S.M.; Tobin, S.P.; Haven, V.E. (1989). "Minority Carrier Lifetime of GaAs on Silicon." *Conference Record of the Twentieth IEEE Photovoltaic Specialists Conference - 1988; September 26-30, 1988; Las Vegas, Nevada.* New York: The Institute of Electrical and Electronics Engineers, Inc.; pp. 684-688.
- Arya, R. R. (1988). "High Efficiency Amorphous Silicon Based Solar Cells: A Review." *Amorphous Silicon Technology, Materials Research Society Symposium Proceedings, Volume 118*, Madan, A. et al., eds. Pittsburgh, PA: Materials Research Society; pp. 569-580. Presented at the MRS Spring Meeting, Reno, Nevada, April 5-8, 1988. Work performed by Thin Film Division, Solarex Corporation, Newtown, Pennsylvania.
- Arya, R.R.; Newton, J.L. (1989). "Phosphorous and Boron Doping of a-SiGe:H Alloys and Its Effect on p-i-n Solar Cells." *Conference Record of the Twentieth IEEE Photovoltaic Specialists Conference - 1988; September 26-30, 1988; Las Vegas, Nevada.* New York: The Institute of Electrical and Electronics Engineers, Inc.; pp. 85-90.
- Balberg, I.; Delahoy, A.E.; Weakliem, H.A. (1989). "Light Intensity Dependence of the Ambipolar Diffusion-Length in Hydrogenated Amorphous Silicon." *Conference Record of the Twentieth IEEE Photovoltaic Specialists Conference - 1988; September 26-30, 1988; Las Vegas, Nevada.* New York: The Institute of Electrical and Electronics Engineers, Inc.; pp. 352-356.
- Basol, B.M.; Kapur, V.K.; Kullberg, R.C.; Mitchell, R.L. (1989). "Cd_{1-x}Zn_xTe Thin Films Prepared by a Two-Stage Process Utilizing Electrodeposition." *Conference Record of the Twentieth IEEE Photovoltaic Specialists Conference - 1988; September 26-30, 1988; Las Vegas, Nevada.* New York: The Institute of Electrical and Electronics Engineers, Inc.; pp. 1500-1504.
- Bennett, M.S.; Rajan, K. (1989). "Stability of Multi-Junction a-Si Solar Cells." *Conference Record of the Twentieth IEEE Photovoltaic Specialists Conference - 1988; September 26-30, 1988; Las Vegas, Nevada.* New York: The Institute of Electrical and Electronics Engineers, Inc.; pp. 67-72.
- Bhat, P.K.; Marshall, C.; Sandwisch, J.; Chatham, H.; Schropp, R.E.I.; Madan, A. (1989). "Preparation and Properties of High Deposition Rate A-Si:H Films and Solar Cells Using Disilane." *Conference Record of the Twentieth IEEE Photovoltaic Specialists Conference - 1988; September 26-30, 1988; Las Vegas, Nevada.* New York: The Institute of Electrical and Electronics Engineers, Inc.; pp. 91-96.

FY 1989 BIBLIOGRAPHY (continued)

- Birkmire, R.W.; Phillips, J.E.; Shafarman, W.N. (June 1989) *Materials Analysis and Device Optimization of CuInSe₂ Solar Cells: Annual Subcontract Report 16 January 1987 - 15 January 1988*. SERI/STR-211-3523. Work performed by Institute of Energy Conversion, University of Delaware, Newark, Delaware.
- Birkmire, R.W.; McCandless, B.E.; Phillips, J.E. (May 1989) *Two-Terminal CuInSe₂-Based Cascade Cells: Annual Subcontract Report 16 January 1987 - 15 January 1988*. SERI/STR-211-3511. Work performed by Institute of Energy Conversion, University of Delaware, Newark, Delaware.
- Bottenberg, W.R.; Blaker, K.; Reinker, D. (1989). "Optical Considerations in the Performance of Hybrid, Four-Terminal Tandem Photovoltaic Modules." *Conference Record of the Twentieth IEEE Photovoltaic Specialists Conference -1988; September 26-30, 1988; Las Vegas, Nevada*. New York: The Institute of Electrical and Electronics Engineers, Inc.; pp. 97-101.
- Bottenberg, W.R.; Reinker, D. (1989). "Outdoor Performance of Hybrid, Four-Terminal Tandem Photovoltaic Modules Based on Thin Film Silicon: Hydrogen and Copper Indium Diselenide." *Conference Record of the Twentieth IEEE Photovoltaic Specialists Conference - 1988; September 26-30, 1988; Las Vegas, Nevada*. New York: The Institute of Electrical and Electronics Engineers, Inc.; pp. 1230-1235.
- Bottenberg, W.; Mitchell, K. (March 1989). *Research on Amorphous-Silicon-Based, Thin-Film Photovoltaic Devices, Task B, Annual Subcontract Report 1 January 1988-31 August 1988*. SERI/STR-211-3446. Work performed by ARCO Solar, Inc., Camarillo, California under Subcontract No. ZB-7-06003-3.
- Branz, H.M.; Silver, M. "Charged Dangling Bonds: Key to Electronic Transport, Recombination and Metastability in Hydrogenated Amorphous Silicon." Thirteenth International Conference on Amorphous and Liquid Semiconductors (ICALS 13), Asheville, North Carolina, August 21-25, 1989.
- Catalano, A.; Wood, G. (1988). "Short Wavelength Response in a-Si:H p-i-n Diodes: A Simple Method to Minimize Interface Recombination." *Amorphous Silicon Technology, Materials Research Society Symposium Proceedings, Volume 118*, Madan, A. et al., eds. Pittsburgh, PA: Materials Research Society; pp. 581-586. Presented at the MRS Spring Meeting, Reno, Nevada, April 5-8, 1988. Work performed by Thin Film Division, Solarex Corporation, Newtown, Pennsylvania.
- Chatham, H.; Bhat, P.K. (September 1989) *Preparation and Properties of High Deposition a-Si:H Films and Solar Cells Using Disilane, Final Subcontract Report, 1 May 1988 - 30 April 1989*. SERI/STR-211-3562. 35 pp. Work performed by Glasstech Solar, Inc., Wheatridge, Colorado. Available NTIS: Order No. DE89009467.
- Chatham, H.; Bhat, P. K. (1988). "Comparative Discharge Diagnostic Study of Silane, Disilane, and Germane RF Discharges Using Optical Emission Spectroscopy and Mass Spectrometry." *Amorphous Silicon Technology, Materials Research Society Symposium Proceedings, Volume 118*, Madan, A. et al., eds. Pittsburgh, PA: Materials Research Society; pp. 31-36. Presented at the MRS Spring Meeting, Reno, Nevada, April 5-8, 1988. Work performed by Glasstech Solar, Inc., Wheat Ridge, Colorado.
- Chu, T.L.; Chu, S.S.; Han, K.D.; Mantravadi, M. (1989). "Mercury Telluride as an Ohmic Contact to Efficient Thin Film Cadmium Telluride Solar Cells." *Conference Record of the Twentieth IEEE Photovoltaic Specialists Conference -1988; September 26-30, 1988; Las Vegas, Nevada*. New York: The Institute of Electrical and Electronics Engineers, Inc.; pp. 1422-1425.
- Ciszek, T. F.; Wang, T.; Schuyler, T.; Rohatgi, A. (January 1989). "Some Effects of Crystal Growth Parameters on Minority Carrier Lifetime in Float-Zoned Silicon." *Journal of the Electrochemical Society* (136:1); pp. 230-234. Work performed by Solar Energy Research Institute, Golden, Colorado, and Georgia Institute of Technology, Atlanta, Georgia.

FY 1989 BIBLIOGRAPHY (continued)

- Crandall, R. S.; Kalina, J.; Delahoy, A. (1988). "Simplified Approach to Solar Cell Modeling." *Amorphous Silicon Technology, Materials Research Society Symposium Proceedings, Volume 118*, Madan, A. et al., eds. Pittsburgh, PA: Materials Research Society; pp. 593-598. Presented at the MRS Spring Meeting, Reno, Nevada, April 5-8, 1988. Work performed by Chronar Corporation, Princeton, New Jersey.
- Delahoy, A.E.; Eser, E.; Kampas, F. (March 1989). *Research on Amorphous-Silicon-Based, Thin-Film Photovoltaic Devices, Task B, Annual Subcontract Report 16 March 1987-15 March 1988*. SERI/STR-211-3487. Work performed by Chronar Corporation, Princeton, New Jersey under Subcontract No. ZB-7-06003-1.
- Delahoy, A.E.; Kampas, F.J. (June 1989). *Research on Stable, High-Efficiency, Large-Area, Amorphous-Silicon-Based Submodules, Task B, Semiannual Subcontract Report 16 March 1988 - 15 September 1988*. SERI/STR-211-3528. 59 pp. Work performed by Chronar Corporation, Princeton, New Jersey. Available NTIS: Order No. DE89009439.
- DeMoulin, P.D.; Lundstrom, M.S. (1989). "Assessment of Design Approaches for High-Efficiency GaAs Solar Cells." *Conference Record of the Twentieth IEEE Photovoltaic Specialists Conference - 1988; September 26-30, 1988; Las Vegas, Nevada*. New York: The Institute of Electrical and Electronics Engineers, Inc.; pp. 497-502.
- Devaney, W.E.; Chen, W.S.; Stewart, J.M. (June 1989) *High Efficiency CuInSe₂ and CuInGaSe₂ Based Cells and Materials Research: Annual Subcontract Report 1 November 1987 - 31 October 1988*. SERI/STR-211-3238. Work performed by Boeing Electronics High Technology Center, Seattle, Washington.
- Eberspacher, C.; Ermer, J.; Tanner, D. (May 1989). *Research on Stable, High-Efficiency, Large-Area Amorphous-Silicon-Based Submodules, Task B, Semiannual Subcontract Report, 1 September 1988 - 28 February 1989*. SERI/STR-211-3512. 74 pp. Work performed by ARCO Solar, Inc., Camarillo, California. Available NTIS: Order No. DE89009430.
- Fortmann, C. M. (1988). "Role of Structural Inhomogeneities on the Transport Properties of a-SiGe:H." *Amorphous Silicon Technology, Materials Research Society Symposium Proceedings, Volume 118*, Madan, A. et al., eds. Pittsburgh, PA: Materials Research Society; pp. 691-696. Presented at the MRS Spring Meeting, Reno, Nevada, April 5-8, 1988. Work performed by Thin Film Division, Solarex Corporation, Newtown, Pennsylvania.
- Fortmann, C.M.; Tu, J.C. (1989). "Defects in a-SiGe:H." *Conference Record of the Twentieth IEEE Photovoltaic Specialists Conference - 1988; September 26-30, 1988; Las Vegas, Nevada*. New York: The Institute of Electrical and Electronics Engineers, Inc.; pp. 139-142.
- Gale, R.P.; McClelland, R.W.; King, B.D.; Gormley, J.V. (1989). "High-Efficiency Thin-Film AlGaAs-GaAs Double Heterostructure Solar Cells." *Conference Record of the Twentieth IEEE Photovoltaic Specialists Conference - 1988; September 26-30, 1988; Las Vegas, Nevada*. New York: The Institute of Electrical and Electronics Engineers, Inc.; pp. 446-451.
- Gallagher, A.; Doughty, D.A.; Doyle, J.; He, M.; Lin, G.H. (March 1989). *Diagnostics of Glow Discharges Used to Produce Hydrogenated Amorphous Silicon Films, Annual Subcontract Report 15 June 1987-30 November 1988*. SERI/STR-211-3473. Work performed by National Institute of Standards and Technology and University of Colorado under Subcontract No. DB-4-04078-1.
- Gordon, R.G.; Proscia, J.; Gustin, K.; Chappel-Sokol, J.; Strickler, D.; McCurdy, R.; Hu, J. (June 1989). *Optimization of Transparent and Reflecting Electrodes for Amorphous Silicon Solar Cells, Final Subcontract Report, 1 October 1987 - 30 November 1988*. SERI/STR-211-3524. 160 pp. Work performed by Department of Chemistry, Harvard University, Cambridge, Massachusetts. Available NTIS: Order No. DE89009435.

FY 1989 BIBLIOGRAPHY (continued)

- Gruenbaum, P.E.; Sinton, R.A.; Swanson, R.M. (1989). "Stability Problems in Point Contact Solar Cells." *Conference Record of the Twentieth IEEE Photovoltaic Specialists Conference - 1988; September 26-30, 1988; Las Vegas, Nevada.* New York: The Institute of Electrical and Electronics Engineers, Inc.; pp. 423-428.
- Guha, S.; Yang, J.; Pawlikiewicz, A.; Glatfelter, T.; Ross, R.; Ovshinsky, S.R. (1989). "Novel Design for Amorphous Silicon Alloy Solar Cells." *Conference Record of the Twentieth IEEE Photovoltaic Specialists Conference -1988; September 26-30, 1988; Las Vegas, Nevada.* New York: The Institute of Electrical and Electronics Engineers, Inc.; pp. 85-90.
- Guha, S.; Yang, J.; Pawlikiewicz, A.; Ross, R.; Glatfelter, T.; Burdick, J.; Banerjee, A. (1989) *Progress in High-Efficiency, Multiple-Gap, Multijunction Amorphous Silicon-Based Alloy Thin Film Solar Cells.* SERI/CP-211-3514, p. 119.
- Gustin, K. M.; Gordon, R. G. (November 1988). "Study of Aluminum Oxide Thin Films Prepared by Atmospheric-Pressure Chemical Vapor Deposition from Trimethylaluminum + Oxygen and/or Nitrous Oxide." *Journal of Electronic Materials* (17:6); pp. 509-517. Work performed by Department of Chemistry, Harvard University, Cambridge, Massachusetts.
- Hegedus, S.S. (1989). "Open Circuit Voltage of Amorphous Silicon p-i-n Solar Cells." *Conference Record of the Twentieth IEEE Photovoltaic Specialists Conference - 1988; September 26-30, 1988; Las Vegas, Nevada.* New York: The Institute of Electrical and Electronics Engineers, Inc.;pp. 102-107.
- Hegedus, S.S.; Rocheleau, R.E.; Tullman, R.M.; Albright, D.E.; Saxena, N.; Buchanan, W.A.; Schubert, K.E.; Dozier, R.D. (1989). "Photo-Assisted CVD of a-Si:H Solar Cells and a-SiGe:H Films." *Conference Record of the Twentieth IEEE Photovoltaic Specialists Conference - 1988; September 26-30, 1988; Las Vegas, Nevada.* New York: The Institute of Electrical and Electronics Engineers, Inc.; pp. 129-134.
- Hegedus, S.S.; Cebulka, J.M. (1989). "Characterization of Defects in a-Si:H Solar Cells Using Sub-Band Gap Photocurrent Spectroscopy." *Conference Record of the Twentieth IEEE Photovoltaic Specialists Conference - 1988; September 26-30, 1988; Las Vegas, Nevada.* New York: The Institute of Electrical and Electronics Engineers, Inc.; pp. 186-190.
- Jackson, W.B. (1989) "The Connection Between Dispersive Hydrogen Motion and the Kinetics of Light-Induced Defects in Hydrogenated Amorphous Silicon." *Phil. Mag. Lett.* 59(2), p. 103.
- Johnson, N. M.; Wolff, S. H.; Doland, C. D.; Walker, J. (1988). "Dependence of Hydrogen Incorporation in Undoped a-Si:H and uc-Si:H on Hydrogen Dilution during PECVD." *Amorphous Silicon Technology, Materials Research Society Symposium Proceedings, Volume 118*, Madan, A. et al., eds. Pittsburgh, PA: Materials Research Society; pp. 85-90. Presented at the MRS Spring Meeting, Reno, Nevada, April 5-8, 1988. Work performed by Xerox Palo Alto Research Center, Palo Alto, California.
- Johnson, N.M.; Walker, J.; Doland, C.M.; Winer, K.; Street, R.A. (May 1989) "Hydrogen Incorporation in Silicon Thin Films Deposited with a Remote Hydrogen Plasma." *Applied Physics Letters* 54(19), p. 1872.
- Johnson, N.M.; Walker, J.; Doland, C.M.; Winer, K.; Street, R.A. (8 May 1989). "Hydrogen Incorporation in Silicon Thin Films Deposited with a Remote Hydrogen Plasma." *Applied Physics Letters* (54:19); pp. 1872-1874. Work performed by Xerox Palo Alto Research Center, Palo Alto, California.
- Kaminar, N.R.; Virshup, G.F.; Ristow, M.L.; Liu, D.D.; MacMillan, H.F.; Partain, L.D.; Gee, J.M. (1989). "Concentrator Efficiencies of 29.2% for a GaAs Cell and 24.8% for a Mounted-Cell-Lens Assembly." *Conference Record of the Twentieth IEEE Photovoltaic Specialists Conference - 1988; September 26-30, 1988; Las Vegas, Nevada.* New York: The Institute of Electrical and Electronics Engineers, Inc.; pp. 766-768.

FY 1989 BIBLIOGRAPHY (continued)

- Kim, D.; Fahrenbruch, A.L.; Bube, R.H. (1989). "Effects of Heat Treatment on the Surface Carrier Density In p-type CdTe." *Conference Record of the Twentieth IEEE Photovoltaic Specialists Conference - 1988; September 26-30, 1988; Las Vegas, Nevada.* New York: The Institute of Electrical and Electronics Engineers, Inc.; pp. 1487-1490.
- King, R.R.; Sinton, R.A.; Swanson, R.M. (1989). "Front and Back Surface Fields for Point-Contact Solar Cells." *Conference Record of the Twentieth IEEE Photovoltaic Specialists Conference - 1988; September 26-30, 1988; Las Vegas, Nevada.* New York: The Institute of Electrical and Electronics Engineers, Inc.; pp. 538-544.
- Klausmeier-Brown, M.E.; DeMoulin, P.D.; Chuang, H.L.; Lundstrom, M.S.; Melloch, M.R.; Tobin, S.P. (1989). "Influence of Bandgap Narrowing Effects in p⁺-GaAs on Solar Cell Performance." *Conference Record of the Twentieth IEEE Photovoltaic Specialists Conference - 1988; September 26-30, 1988; Las Vegas, Nevada.* New York: The Institute of Electrical and Electronics Engineers, Inc.; pp. 503-507.
- Krieger, G.; Cambridge, R. (1988). "Medical Surveillance and Biologic Monitoring of Personnel in Semiconductor Research Facilities." *Photovoltaic Safety Conference; Denver, Colorado; January 19-20, 1988, AIP Conference Proceedings 166.* New York: American Institute of Physics; pp. 67-72.
- Langford, A.A.; Bender, J.; Fleet, M.L.; Stafford, B.L. (May/June 1989). "Window Cleaning and Flourine Incorporation by XeF₂ in Photochemical Vapor Deposition." *Journal of Vacuum Science and Technology. B, Microelectronics, Processing and Phenomena (7:3);* pp. 437-442.
- MacMillan, H.F.; Hamaker, H.C.; Kaminar, N.R.; Kuryla, M.S.; Riston, M.J.; Liu, D.D.; Virshup, G.F.; Gee, J. M. (1989). "28% Efficient GaAs Concentrator Solar Cells." *Conference Record of the Twentieth IEEE Photovoltaic Specialists Conference - 1988; September 26-30, 1988; Las Vegas, Nevada.* New York: The Institute of Electrical and Electronics Engineers, Inc.; pp. 462-468.
- MacMillan, H.F.; Hamaker, H.C.; Virshup, G.F.; Werthen, J.G. (1989). "Multijunction III-V Solar Cells: Recent and Projected Results." *Conference Record of the Twentieth IEEE Photovoltaic Specialists Conference - 1988; September 26-30, 1988; Las Vegas, Nevada.* New York: The Institute of Electrical and Electronics Engineers, Inc.; pp. 48-54.
- McCandless, B.E.; Birkmire, R.W.; Buchanan, W.A.; Phillips, J.E.; Rocheleau, R.E. (1989). "Fabrication of Monolithic a-Si:H-CuInSe₂/CdS Tandem Solar Cells." *Conference Record of the Twentieth IEEE Photovoltaic Specialists Conference - 1988; September 26-30, 1988; Las Vegas, Nevada.* New York: The Institute of Electrical and Electronics Engineers, Inc.; pp. 381-384.
- McCandless, B.E.; Birkmire, R.W. (1989). "Control of Deposition and Surface Properties of CuInSe₂ Thin Films for Solar Cells." *Conference Record of the Twentieth IEEE Photovoltaic Specialists Conference - 1988; September 26-30, 1988; Las Vegas, Nevada.* New York: The Institute of Electrical and Electronics Engineers, Inc.; pp. 1510-1514.
- McConnell, R.D.; Wolf, S.A., eds. (1989). *Science and Technology of Thin Film Superconductors.* New York: Plenum Press; 557 pp. Work performed by Solar Energy Research Institute, Golden, Colorado, and Naval Research Laboratory, Washington, DC.
- McCurdy, R. J.; Gordon, R. G. (1988). "Effects of Substrate Temperature and Gas Phase Chemistry on the APCVD of a-Si:H Films from Disilane." *Amorphous Silicon Technology, Materials Research Society Symposium Proceedings, Volume 118,* Madan, A. et al., eds. Pittsburgh, PA: Materials Research Society; pp. 97-102. Presented at the MRS Spring Meeting, Reno, Nevada, April 5-8, 1988. Work performed by Department of Chemistry, Harvard University, Cambridge, Massachusetts.

FY 1989 BIBLIOGRAPHY (continued)

- Meyers, P.V.; Liu, C.H.; Russell, L.; Ramanathan, V.; Phillips, J.E.; McCandless, B.E.; Birkmire, R.W. (1989). "Polycrystalline CdTe on CuInSe₂ Cascaded Solar Cells." *Conference Record of the Twentieth IEEE Photovoltaic Specialists Conference - 1988; September 26-30, 1988; Las Vegas, Nevada*. New York: The Institute of Electrical and Electronics Engineers, Inc.; pp. 1448-1451.
- Meyers, P.V. (June 1989) *Polycrystalline Cadmium Telluride n-i-p Solar Cell: Annual Subcontract Report 1 June 1989 - 31 August 1988*. SERI/STR-211-3519. Work performed by Ametek Applied Materials Laboratory, Harleysville, Pennsylvania.
- Misiakos, K.; Lindholm, F.A. (1989). "Computer Simulation of Transient Experiments for Determining the Transport Parameters in Amorphous Silicon Solar Cells." *Conference Record of the Twentieth IEEE Photovoltaic Specialists Conference - 1988; September 26-30, 1988; Las Vegas, Nevada*. New York: The Institute of Electrical and Electronics Engineers, Inc.; pp. 171-175.
- Mitchell, K.W.; Pollock, G.; Mason, A.V. (1989). "7.3% Efficient CuInS₂ Solar Cell." *Conference Record of the Twentieth IEEE Photovoltaic Specialists Conference - 1988; September 26-30, 1988; Las Vegas, Nevada*. New York: The Institute of Electrical and Electronics Engineers, Inc.; pp. 1542-1544.
- Mitchell, K.; Eberspacher, C.; Ermer, J.; Pier, D. (1989). "Single and Tandem Junction CuInS₂ Cell and Module Technology." *Conference Record of the Twentieth IEEE Photovoltaic Specialists Conference - 1988; September 26-30, 1988; Las Vegas, Nevada*. New York: The Institute of Electrical and Electronics Engineers, Inc.; pp. 1384-1389.
- Mitchell, K.; Liu, H.I. (1989). "Device Analysis of Copper Indium Diselenide Solar Cells." *Conference Record of the Twentieth IEEE Photovoltaic Specialists Conference - 1988; September 26-30, 1988; Las Vegas, Nevada*. New York: The Institute of Electrical and Electronics Engineers, Inc.; pp. 1461-1468.
- Mon, G.; Wen, L.; Meyer, J.; Ross, R., Jr.; Nelson, A. (1989). "Electromechanical and Galvanic Corrosion Effects in Thin-Film Photovoltaic Modules." *Conference Record of the Twentieth IEEE Photovoltaic Specialists Conference - 1988; September 26-30, 1988; Las Vegas, Nevada*. New York: The Institute of Electrical and Electronics Engineers, Inc.; pp. 108-113.
- Mon, G.; Wen, L.; Ross, R., Jr. (1989). "Water-Module Interaction Studies." *Conference Record of the Twentieth IEEE Photovoltaic Specialists Conference - 1988; September 26-30, 1988; Las Vegas, Nevada*. New York: The Institute of Electrical and Electronics Engineers, Inc.; pp. 1098-1102.
- O'Dowd, J.G.; Wilkins, G.F.; Willing, F.S.; McVeigh, J.J.; Jansen, K.W.; Cunningham, D.W.; Poplawski, C.B.; Steiger, R.P.; Kloss, T.J. (1989). "Engineering Approach to Reduction of Direct Costs in the Manufacture of a-Si Photovoltaic Modules." *Conference Record of the Twentieth IEEE Photovoltaic Specialists Conference - 1988; September 26-30, 1988; Las Vegas, Nevada*. New York: The Institute of Electrical and Electronics Engineers, Inc.; pp. 1357-1359.
- Overhof, H.; Silver, M. (15 May 1989). "Comment on "Electron Drift Mobility in Doped Amorphous Silicon"." *Physical Review. B, Condensed Matter* (39:14); pp. 10426-10428. Work performed by Department of Physics, University of Paderborn, Paderborn, Federal Republic of Germany, and Department of Physics and Astronomy, University of North Carolina at Chapel Hill, Chapel Hill, North Carolina.
- Pang, S.K.; Rohatgi, A.; Cizek, T.F. (1989). "Doping Dependence of Minority Carrier Lifetime in Ga-Doped Silicon." *Conference Record of the Twentieth IEEE Photovoltaic Specialists Conference - 1988; September 26-30, 1988; Las Vegas, Nevada*. New York: The Institute of Electrical and Electronics Engineers, Inc.; pp. 435-440.

FY 1989 BIBLIOGRAPHY (continued)

- Parsons, G. N.; Tsu, D. V.; Lucovsky, G. (1988). "Growth of a-Si:H Films by Remote Plasma Enhanced CVD (RPECVD)." *Amorphous Silicon Technology, Materials Research Society Symposium Proceedings, Volume 118*, Madan, A. et al., eds. Pittsburgh, PA: Materials Research Society; pp. 37-42. Presented at the MRS Spring Meeting, Reno, Nevada, April 5-8, 1988. Work performed by Department of Physics, North Carolina State University, Raleigh, North Carolina.
- Pawlikiewicz, A.H.; Guha, S. (1989). "Numerical Modeling of Amorphous Silicon Based p-i-n Solar Cells." *Conference Record of the Twentieth IEEE Photovoltaic Specialists Conference - 1988; September 26-30, 1988; Las Vegas, Nevada*. New York: The Institute of Electrical and Electronics Engineers, Inc.; pp. 251-255.
- Pawlikiewicz, A.H.; Guha, S. "Numerical Modeling of Multijunction Amorphous Silicon-Based p-i-n Solar Cells." *Conference Proceedings of the 20th IEEE Photovoltaic Specialists Conference, Las Vegas, Nevada, September 26-30, 1988*.
- Pawlikiewicz, A. H.; Guha, S. (1988). "Effect of Dominant Junction on the Open Circuit Voltage of Amorphous Silicon Alloy Solar Cells." *Amorphous Silicon Technology, Materials Research Society Symposium Proceedings, Volume 118*, Madan, A. et al., eds. Pittsburgh, PA: Materials Research Society; pp. 599-604. Presented at the MRS Spring Meeting, Reno, Nevada, April 5-8, 1988. Work performed by Energy Conversion Devices, Inc., Troy, Michigan.
- Phillips, J.E.; Roy, M. (1989). "Resistive and Photoconductive Effects in Spectral Response Measurements." *Conference Record of the Twentieth IEEE Photovoltaic Specialists Conference - 1988; September 26-30, 1988; Las Vegas, Nevada*. New York: The Institute of Electrical and Electronics Engineers, Inc.; pp. 1614-1617.
- Ramanathan, V.; Russell, L.; Liu, C.H.; Meyers, P.V.; Ullal, H.S. (1989). "Characterization of CdTe Thin Film Solar Cells." *Conference Record of the Twentieth IEEE Photovoltaic Specialists Conference - 1988; September 26-30, 1988; Las Vegas, Nevada*. New York: The Institute of Electrical and Electronics Engineers, Inc.; pp. 1417-1421.
- Ristein, J.; Hautala, J.; Taylor, P.C. (July 1989) "Excitation-Energy Dependence of Optically Induced ESR in a-Si:H." *Physical Review B* 40 (1), p. 88.
- Ristein, J.; Hautala, J.; Taylor, P.C. (1 July 1989) "Excitation-Energy Dependence of Optically Induced ESR in a-Si:H." *Physical Review B, Condensed Matter* (40:1); pp. 88-92. Worked performed by Department of Physics, University of Utah, Salt Lake City, Utah.
- Rocheleau, R. E.; Tullman, R. M.; Albright, D. E.; Hegedus, S. S. (1988). "Amorphous Silicon-Germanium Deposited by Photo-CVD: Effect of Hydrogen Dilution and Substrate Temperature." *Amorphous Silicon Technology, Materials Research Society Symposium Proceedings, Volume 118*, Madan, A. et al., eds. Pittsburgh, PA: Materials Research Society; pp. 653-658. Presented at the MRS Spring Meeting, Reno, Nevada, April 5-8, 1988. Work performed by Institute of Energy Conversion, University of Delaware, Newark, Delaware.
- Rockett, A.; Lommasson, T.C.; Talieh, H. (July 1989) *Alternative Fabrication Techniques for High-Efficiency $CuInSe_2$ and $CuInSe_2$ -Alloy Films and Cells, Annual Subcontract Report, 10 November 1987 - 31 December 1988*. SERI/STR-211-3539. 49 pp. Work performed by University of Illinois, Urbana, Illinois. Available NTIS: Order No. DE89009451.
- Rockett, A.; Lommasson, T.C.; Yang, L.C.; Talieh, H.; Campos, P.; Thornton, J.A. (1989). "Deposition of $CuInSe_2$ by the Hybrid Sputtering and Evaporation Method." *Conference Record of the Twentieth IEEE Photovoltaic Specialists Conference - 1988; September 26-30, 1988; Las Vegas, Nevada*. New York: The Institute of Electrical and Electronics Engineers, Inc.; pp. 1505-1509.

FY 1989 BIBLIOGRAPHY (continued)

- Rohatgi, A.; Sudharsanan, R.; Ringel, S.A.; Meyers, P.V.; Liu, C.H. (1989). "Wide Bandgap Thin Film Solar Cells from CdTe Alloys." *Conference Record of the Twentieth IEEE Photovoltaic Specialists Conference - 1988; September 26-30, 1988; Las Vegas, Nevada.* New York: The Institute of Electrical and Electronics Engineers, Inc.; pp. 1477-1481.
- Roy, M.; Damaskinos, S.; Phillips, J.E. (1989). "Diode Current Mechanism in CuInSe₂/(CdZn)S Heterojunctions." *Conference Record of the Twentieth IEEE Photovoltaic Specialists Conference - 1988; September 26-30, 1988; Las Vegas, Nevada.* New York: The Institute of Electrical and Electronics Engineers, Inc.; pp. 1618-1623.
- Schiff, E.A.; Devlen, R.I.; Grahn, H.T.; Tauc, J. (8 May 1989). "Picosecond Electron Drift Mobility Measurements in Hydrogenated Amorphous Silicon." *Applied Physics Letters* (54:19); pp. 1911-1913. Work performed by Department of Physics and Division of Engineering, Brown University, Providence, Rhode Island, and Energy Conversion Devices, Inc., Troy, Michigan.
- Shafarman, W.N.; Birkmire, R.W. (1989). "Characterization of Window Layers in CuInSe₂ Thin-Film Solar Cells." *Conference Record of the Twentieth IEEE Photovoltaic Specialists Conference - 1988; September 26-30, 1988; Las Vegas, Nevada.* New York: The Institute of Electrical and Electronics Engineers, Inc.; pp. 1515-1519.
- Sharps, P.; Fahrenbruch, A.L.; Lopez-Otero, A.; Bube, R.H. (1989). "Solar Cells Made From p-CdTe Films Grown with Ion-Assisted Doping." *Conference Record of the Twentieth IEEE Photovoltaic Specialists Conference - 1988; September 26-30, 1988; Las Vegas, Nevada.* New York: The Institute of Electrical and Electronics Engineers, Inc.; pp. 1641-1645.
- Shing, Y.H.; Perry, J.W.; Allevato, C.E. (1989). "Silane and Germane Plasma Diagnostics for Depositing Photosensitive a-SiGe:H Films." *Conference Record of the Twentieth IEEE Photovoltaic Specialists Conference - 1988; September 26-30, 1988; Las Vegas, Nevada.* New York: The Institute of Electrical and Electronics Engineers, Inc.; pp. 224-228.
- Silver, M.; Branz, H.M.; Pautmeier, L.; Bassler, H. "Exponential Bandtails, Optoelectronic Properties and Metastability in Hydrogenated Amorphous Silicon: A Unified Model Based on Charged Dangling Bonds." Thirteenth International Conference on Amorphous and Liquid Semiconductors (ICALS 13), Asheville, North Carolina, August 21-25, 1989.
- Silver, M.; Branz, H. (1988). "Potential Fluctuation and Charged Defects in Hydrogenated Amorphous Silicon." *Conference Record of the International Topical Conference on Hydrogenated Amorphous Silicon Devices and Technology; IBM Thomas J. Watson Research Center, Yorktown Heights, New York; November 21-23, 1988, RC 14189*, Kanicki, J., ed. Yorktown Heights, NY: IBM Thomas J. Watson Research Center; pp. 10-13. Work performed by University of North Carolina, Chapel Hill, North Carolina, and Solar Energy Research Institute, Golden, Colorado.
- Singh, R.; Radpour, F.; Chou, P.; Nelson, A.J.; Ullal, H.S. "Oxidation of Tin-on-Silicon Substrate by Rapid Isothermal Processing." *Journal of Applied Physics*, 66 (6), 2381, (1989).
- Singh, R.; Chou, P.; Radpour, F.; Nelson, A.J.; Ullal, H.S. (15 September 1989) "Oxidation of Tin on Silicon Substrate by Rapid Isothermal Processing." *Journal of Applied Physics* (66:6); pp. 2381-2387. Work performed by School of Electrical Engineering and Computer Science, University of Oklahoma, Norman, Oklahoma, and Solar Energy Research Institute, Golden, Colorado.
- Sites, J.R. (July 1989) *Analysis of Loss Mechanisms in Polycrystalline Thin-Film Solar Cells, Annual Subcontract Report, 1 April 1988 - 31 March 1989.* SERI/STR-211-3545. Work performed by Colorado State University, Fort Collins, Colorado.

FY 1989 BIBLIOGRAPHY (continued)

- Sites, J.R. (July 1989) *Analysis of Loss Mechanisms in Polycrystalline Thin-Film Solar Cells, Annual Subcontract Report, 1 April 1988 - 31 March 1989*. SERI/STR-211-3545. 33 pp. Work performed at Colorado State University, Fort Collins, Colorado. Available NTIS: Order No. DE89009454.
- Sites, J.R. (1989). "Separation of Voltage Loss Mechanisms in Polycrystalline Solar Cells." *Conference Record of the Twentieth IEEE Photovoltaic Specialists Conference - 1988; September 26-30, 1988; Las Vegas, Nevada*. New York: The Institute of Electrical and Electronics Engineers, Inc.; pp. 1604-1607.
- Street, R. A.; Kakalios, J.; Hack, M. (1988). "Doping Dependence of the Drift Mobility in n-Type a-Si:H." *Amorphous Silicon Technology, Materials Research Society Symposium Proceedings, Volume 118*, Madan, A. et al., eds. Pittsburgh, PA: Materials Research Society; pp. 495-500. Presented at the MRS Spring Meeting, Reno, Nevada, April 5-8, 1988. Work performed by Xerox Palo Alto Research Center, Palo Alto, California.
- Sugimura, R.; Mon, G.; Wen, L.; Ross, R., Jr. (1989). "Electrical Isolation Design and Electrochemical Corrosion in Thin-Film Photovoltaic Modules." *Conference Record of the Twentieth IEEE Photovoltaic Specialists Conference -1988; September 26-30, 1988; Las Vegas, Nevada*. New York: The Institute of Electrical and Electronics Engineers, Inc.; pp. 1103-1109.
- Tavakolian, H.; Sites, J.R. (1989). "Effect of Interfacial States on Open-Circuit Voltage." *Conference Record of the Twentieth IEEE Photovoltaic Specialists Conference - 1988; September 26-30, 1988; Las Vegas, Nevada*. New York: The Institute of Electrical and Electronics Engineers, Inc.; pp. 1608-1613.
- Thompson, S. (1988). "Role of Unusual Occurrence Reports in Incident Analysis in the Photovoltaic Industry." *Photovoltaic Safety Conference; Denver, Colorado; January 19-20, 1988, AIP Conference Proceedings 166*, Luft, W., ed. New York: American Institute of Physics; pp. 73-78.
- Thornton, J.A.; Rockett, A.; Lommasson, T.C.; Talieh, H. (July 1989) *CuInSe₂ Solar Cell Research by Sputter Deposition, Final Subcontract Report, January 1985 - November 1987*. SERI/STR-211-3540. Work performed by University of Illinois, Urbana, Illinois.
- Thornton, J.A.; Rockett, A.; Lommasson, T.C.; Talieh, H. (July 1989) *CuInSe₂ Solar Cell Research by Sputter Deposition*. SERI/STR-211-3540. 69 pp. Work performed at University of Illinois, Urbana, Illinois. Available NTIS: Order No. DE89009450.
- Tobin, S.P.; Vernon, S.M.; Bajgar, C.; Haven, V.E.; Geoffroy, L.M.; Sanfacon, M. M.; Lillington, D.R.; Hart, R.E., Jr.; Emery, K.A.; Matson, R.J. (1989). "High Efficiency GaAs/Ge Monolithic Tandem Solar Cells." *Conference Record of the Twentieth IEEE Photovoltaic Specialists Conference - 1988; September 26-30, 1988; Las Vegas, Nevada*. New York: The Institute of Electrical and Electronics Engineers, Inc.; pp. 405-410.
- Tsai, C.T.; Dillon, O.W., Jr.; DeAngelis, R.J. (1989). "Thermal Buckling of Silicon Sheet." *Conference Record of the Twentieth IEEE Photovoltaic Specialists Conference - 1988; September 26-30, 1988; Las Vegas, Nevada*. New York: The Institute of Electrical and Electronics Engineers, Inc.; pp. 1545-1550.
- Turner, G.B.; Schwartz, R.J.; Gray, J.L. (1989). "Band Discontinuity and Bulk Vs. Interface Recombination in CdS/CuInSe₂ Solar Cells." *Conference Record of the Twentieth IEEE Photovoltaic Specialists Conference - 1988; September 26-30, 1988; Las Vegas, Nevada*. New York: The Institute of Electrical and Electronics Engineers, Inc.; pp. 1457-1460.

FY 1989 BIBLIOGRAPHY (continued)

- Venkatasubramanian, R.; Bothra, S.; Ghandhi, S.K.; Borrego, J.M. (1989). "Interface Recombination Velocity and Diffusion Constant in Hi-Lo and p+n GaAs Junctions Measured by a Microwave Technique." *Conference Record of the Twentieth IEEE Photovoltaic Specialists Conference - 1988; September 26-30, 1988; Las Vegas, Nevada.* New York: The Institute of Electrical and Electronics Engineers, Inc.; pp. 689-694.
- Verlinden, P.; Swanson, R.M.; Sinton, R.; Kane, D. (1989). "Multilevel Metalization for Large Area Point Contact Solar Cells." *Conference Record of the Twentieth IEEE Photovoltaic Specialists Conference - 1988; September 26-30, 1988; Las Vegas, Nevada.* New York: The Institute of Electrical and Electronics Engineers, Inc.; pp. 532-537.
- Vernon, S.M.; Tobin, S.P.; Haven, V.E.; Bajgar, C.; Dixon, T.; Al-Jassim, M.; Ahrenkiel, R.K.; Emery, K. (1989). "Efficiency Improvements in GaAs-on-Si Solar Cells." *Conference Record of the Twentieth IEEE Photovoltaic Specialists Conference - 1988; September 26-30, 1988; Las Vegas, Nevada.* New York: The Institute of Electrical and Electronics Engineers, Inc.; pp. 481-485.
- Viner, J. M.; Lee, C.; Ohlsen, W. D.; Taylor, P. C. (1988). "Metastable Optical Absorption and Paramagnetism in Hydrogenated Amorphous Silicon." *Amorphous Silicon Technology, Materials Research Society Symposium Proceedings, Volume 118*, Madan, A. et al., eds. Pittsburgh, PA: Materials Research Society; pp. 309-313. Presented at the MRS Spring Meeting, Reno, Nevada, April 5-8, 1988. Work performed by Department of Physics, University of Utah, Salt Lake City, Utah.
- Virshup, G.F.; Chung, B.C.; Werthen, J.G. (1989). "23.9% Monolithic Multijunction Solar Cell." *Conference Record of the Twentieth IEEE Photovoltaic Specialists Conference - 1988; September 26-30, 1988; Las Vegas, Nevada.* New York: The Institute of Electrical and Electronics Engineers, Inc.; pp. 441-445.
- Wang, F.F.; Fahrenbruch, A.L.; Bube, R.H. (1989). "Properties of Metal-Semiconductor and Metal-Insulator-Semiconductor Junctions on CdTe Single Crystals." *Conference Record of the Twentieth IEEE Photovoltaic Specialists Conference - 1988; September 26-30, 1988; Las Vegas, Nevada.* New York: The Institute of Electrical and Electronics Engineers, Inc.; pp. 1635-1640.
- Wen, L.; Mon, G.; Jetter, E.; Ross, R., Jr. (1989). "Electromigration in Thin-Film Photovoltaic Module Metallization Systems." *Conference Record of the Twentieth IEEE Photovoltaic Specialists Conference - 1988; September 26-30, 1988; Las Vegas, Nevada.* New York: The Institute of Electrical and Electronics Engineers, Inc.; pp. 364-369.
- Werthen, J.G.; Arau, B.A.; Ford, C.W.; Kaminar, N.R.; Kuryla, M.S.; Ristow, M.L.; Lewis, C.R.; MacMillan, H.F.; Virshup, G.F.; Gee, J.M. (1989). "Recent Advances in High-Efficiency InGaAs Concentrator Cells." *Conference Record of the Twentieth IEEE Photovoltaic Specialists Conference - 1988; September 26-30, 1988; Las Vegas, Nevada.* New York: The Institute of Electrical and Electronics Engineers, Inc.; pp. 640-643.
- Winborne, G.; Xu, L.; Silver, M. (1988). "Comparison between Forward Bias Currents in P/I/N and P/C(B/P)/N Hydrogenated Amorphous Silicon Diodes." *Amorphous Silicon Technology, Materials Research Society Symposium Proceedings, Volume 118*, Madan, A. et al., eds. Pittsburgh, PA: Materials Research Society; pp. 501-506. Presented at the MRS Spring Meeting, Reno, Nevada, April 5-8, 1988. Work performed by Department of Physics and Astronomy, University of North Carolina at Chapel Hill, Chapel Hill, North Carolina.
- Winborne, G.; Xu, L.; Silver, M. (April 1989). "Experiments and Discussion on the Electron Mobility in Amorphous Silicon." *Philosophical Magazine Letters* (59:4); pp. 197-203. Work performed by Department of Physics and Astronomy, University of North Carolina, Chapel Hill, North Carolina.

FY 1989 BIBLIOGRAPHY (continued)

- Yang, C.L.; Shing, Y.H.; Allevato, C.E. (1989). "Optical Emission Diagnostics of Electron Cyclotron Resonance & Glow Discharge Plasmas for a-Si:H and a-SiC:H Film Depositions." *Conference Record of the Twentieth IEEE Photovoltaic Specialists Conference - 1988; September 26-30, 1988; Las Vegas, Nevada.* New York: The Institute of Electrical and Electronics Engineers, Inc.; pp. 202-206.
- Yang, J.; Ross, R.; Glatfelter, T.; Mohr, R.; Guha, S. (1988) "Improvement on Narrow Bandgap Amorphous Silicon-Based Alloys and Multijunction Solar Cells." Presented at PVSEC-4, Sydney, Australia.
- Yang, J.; Ross, R.; Glatfelter, T.; Mohr, R.; Hammond, G.; Bemotaitis, C.; Chen, E.; Burdick, J.; Hopson, M.; Guha, S. (1989). "High Efficiency Multijunction Solar Cells Using Amorphous Silicon and Amorphous Silicon-Germanium Alloys." *Conference Record of the Twentieth IEEE Photovoltaic Specialists Conference - 1988; September 26-30, 1988; Las Vegas, Nevada.* New York: The Institute of Electrical and Electronics Engineers, Inc.; pp. 241-246.
- Yoo, J.-B.; Fahrenbruch, A.L.; Bube, R.H. (1989). "Preparation and Properties of CuInSe₂ Solar Cells with a ZnSe Intermediate Layer." *Conference Record of the Twentieth IEEE Photovoltaic Specialists Conference - 1988; September 26-30, 1988; Las Vegas, Nevada.* New York: The Institute of Electrical and Electronics Engineers, Inc.; pp. 1431-1436.

PV Program Branch Reports and Publications

- Annan, R.H.; Stone, J.L. (February 1989). "U.S. National Photovoltaics Program - Investing in Success." *Solar Cells* (26:1-2); pp. 135-148. Work performed by U.S. Department of Energy, Washington, DC, and Solar Energy Research Institute, Golden, Colorado.
- Clausen, T. (1988). "Trends in Workers Compensation in the United States." *Photovoltaic Safety Conference; Denver, Colorado; January 19-20, 1988, AIP Conference Proceedings 166*, Luft, W., ed. New York: American Institute of Physics; pp. 219-228.
- Hulstrom, R.L.; Ohi, J.M. (1989). "Results of the SERI Multijunction Device Efficiency Measurement Task Force." *Conference Record of the Twentieth IEEE Photovoltaic Specialists Conference - 1988; September 26-30, 1988; Las Vegas, Nevada.* New York: The Institute of Electrical and Electronics Engineers, Inc.; pp. 385-388.
- Department of Energy Review of the U.S. Photovoltaic Industry.* (1989) SERI/SP-211-3488.
- Leboeuf, C.M.; Kurtz, S.R.; Olson, J.M. (1989). "Hydrogen Passivation of AlGaAs and GaInP for High Efficiency Solar Cells." *Conference Record of the Twentieth IEEE Photovoltaic Specialists Conference - 1988; September 26-30, 1988; Las Vegas, Nevada.* New York: The Institute of Electrical and Electronics Engineers, Inc.; pp. 644-648.
- Luft, W. (1989). "Characteristics of Hydrogenated Amorphous Silicon-Germanium Alloys." *Applied Physics Communications* (9:1&2); pp. 43-63.
- Luft, W. (1989). "Characteristics of Hydrogenated Amorphous Silicon-Germanium Alloys." *Conference Record of the Twentieth IEEE Photovoltaic Specialists Conference - 1988; September 26-30, 1988; Las Vegas, Nevada.* New York: The Institute of Electrical and Electronics Engineers, Inc.; pp. 218-223.
- Luft, W. (1989) "Characteristics of Hydrogenated Amorphous Silicon-Germanium Alloys." *Applied Physics Communications* (9:1&2); pp. 43-63.
- Mitchell, R. L.; Surek, T. (1988). "SERI's Photovoltaic Research Project: A Foundation for Tomorrow's Utility-Scale Electricity." *Proceedings of the 23rd Intersociety Energy Conversion Engineering Conference; Denver, Colorado; July 31-August 5, 1988.* New York: American Society of Mechanical Engineers; Vol. 3, pp. 107-115.

FY 1989 BIBLIOGRAPHY (continued)

PV Program Branch Reports and Publications

- Proceedings of the 1989 Amorphous Silicon Subcontractor's Review Meeting.* (June 1989). SERI/CP-211-3514. 308 pp. Available NTIS: Order No. DE89009423.
- Proceedings of the Polycrystalline Thin Film Program Meeting, August 16-17, 1989, Lakewood, Colorado.* (August 1989) SERI/CP-211-3550. 218 pp. Available NTIS: Order No. DE89009457.
- Sabisky, E.S.; Stone, J.L. (1989). "Odyssey of Thin Film Amorphous Silicon Photovoltaics." *Conference Record of the Twentieth IEEE Photovoltaic Specialists Conference - 1988; September 26-30, 1988; Las Vegas, Nevada.* New York: The Institute of Electrical and Electronics Engineers, Inc.; pp. 39-47.
- Sopori, B. L. (15 November 1988). "Backside Hydrogenation Technique for Defect Passivation in Silicon Solar Cells." *Journal of Applied Physics* (64:10, Part I); pp. 5264-5266.
- Sopori, B.L. (1989). "Influence of Oxygen on the Performance of Silicon Solar Cells." *Conference Record of the Twentieth IEEE Photovoltaic Specialists Conference - 1988; September 26-30, 1988; Las Vegas, Nevada.* New York: The Institute of Electrical and Electronics Engineers, Inc.; pp. 591-596.
- Sopori, B.L. (15 November 1988). "Use of Optical Scattering to Characterize Dislocations in Semiconductors." *Applied Optics* (27:22); pp. 4676-4683.
- Sopori, B. L.; Hughes, J. L. (January 1989). "Rapid Wax Mounting Technique for Cross-Sectioning and Angle Polishing Metallographic Samples." *Journal of the Electrochemical Society* (136:1); pp. 287-291. Work performed by Solar Energy Research Institute, Golden, Colorado, and Solavolt International, Tempe, Arizona.
- Sopori, B.L. (1989). "Influence of Substrate Resistivity on the Degradation of Silicon Solar Cell Performance due to Crystal Defects." *Conference Record of the Twentieth IEEE Photovoltaic Specialists Conference - 1988; September 26-30, 1988; Las Vegas, Nevada.* New York: The Institute of Electrical and Electronics Engineers, Inc.; pp. 1412-1416.
- Sopori, B. L. (October 1988). "Reflection Characteristics of Textured Polycrystalline Silicon Substrates for Solar Cells." *Solar Cells* (25:1); pp. 15-26.
- Wallace, W.; Sabisky, E.; Stafford, B.; Luft, W.; Ohi, J. (1989). "Advances in Material/Cell/Submodule Research in the DOE/SERI Amorphous Silicon Research Project." *Conference Record of the Twentieth IEEE Photovoltaic Specialists Conference - 1988; September 26-30, 1988; Las Vegas, Nevada.* New York: The Institute of Electrical and Electronics Engineers, Inc.; pp. 328-334.
- Zweibel, K. (1989). "Solar Cell." *McGraw-Hill Yearbook of Science and Technology.* pp. 367-370. McGraw-Hill Book Company, New York.
- Zweibel, K.; Ullal, H.S.; Mitchell, R.L. (1989). "DOE/SERI Polycrystalline Thin Film Subcontract Program." *Conference Record of the Twentieth IEEE Photovoltaic Specialists Conference - 1988; September 26-30, 1988; Las Vegas, Nevada.* New York: The Institute of Electrical and Electronics Engineers, Inc.; pp. 1469-1476.
- Zweibel, K.; Ullal, H.S. (May 1989) *Thin Film Photovoltaics.* SERI/TP-211-3501.

Document Control Page	1. SERI Report No. SERI/TP-211-3643	2. NTIS Accession No. DE90000318	3. Recipient's Accession No.
4. Title and Subtitle Annual Report, Photovoltaic Program Branch, FY 1989		5. Publication Date March 1990	
		6.	
7. Author(s) Photovoltaic Program Branch, SERI		8. Performing Organization Rept. No.	
9. Performing Organization Name and Address Solar Energy Research Institute 1617 Cole Blvd. Golden, CO 80401-3393		10. Project/Task/Work Unit No. PV940101	
		11. Contract (C) or Grant (G) No. (C) (G)	
12. Sponsoring Organization Name and Address		13. Type of Report & Period Covered Annual Progress Report	
		14.	
15. Supplementary Notes SERI Editor: K. Summers (303) 231-1395			
16. Abstract (Limit: 200 words) This report summarizes the progress of the Photovoltaic (PV) Program Branch of the Solar Energy Research Institute (SERI) from October 1, 1988, through September 30, 1989. The branch is responsible for managing the subcontracted portion of SERI's PV Advanced Research and Development Project. In fiscal year (FY) 1989, this included nearly 50 subcontracts, with a total annualized funding of approximately \$13.1 million. Approximately two-thirds of the subcontracts were with universities, at a total funding of nearly \$4 million. The six technical sections of the report cover the main areas of the subcontracted program: Amorphous Silicon Research, Polycrystalline Thin Films, Crystalline Silicon Materials Research, High-Efficiency Concepts, New Ideas, and University Participation. Technical summaries of each of the subcontracted programs provide a discussion of approaches, major accomplishments in FY 1989, and future research directions.			
17. Document Analysis a. Descriptors Photovoltaic cells ; amorphous state ; silicon solar cells ; thin films ; deposition ; copper selenide solar cells ; cadmium telluride solar cells ; gallium arsenide solar cells ; efficiency ; semiconductor materials b. Identifiers/Open-Ended Terms Solar Energy Research Institute c. UC Categories 270			
18. Availability Statement National Technical Information Service U.S. Department of Commerce 5285 Port Royal Road Springfield, VA 22161		19. No. of Pages 290	
		20. Price A13	